UNIVERSITÀ DEGLI STUDI DELL'AQUILA

Dipartimento di Scienze Fisiche e Chimiche

Dottorato di ricerca in Scienze Fisiche e Chimiche

XXXII ciclo

Titolo della tesi

The paradox of conserving plastics: a *contemporary* challenge

SSD CHIM/12

Dottoranda

Natalia Macro

Coordinatore del corso:
Prof. Antonio Mecozzi

Tutor:
Prof. Giorgio Cerichelli

Co-tutor:
Dott.ssa Marcella Ioele

ANNO ACCADEMICO 2018-2019

One word: *Plastics*

The Graduate, 1967

Abstract

Plastic objects nowadays surround us in many ways, enough to consider these materials as modern par excellence. Plastics can be defined as semi or fully synthetic polymers modified with various typologies of additives designed to improve several properties of the final product. Additives, as well as polymerization and processing processes, have great influence on the resulting products, making possible to produce extremely versatile materials which can be shaped as three-dimensional objects, films, foams, fibers and much more.

Aside from the environmentally non-friendly heritage, which disastrous consequences are well known, another kind of heritage made of plastics has been recently drawing the scientific community attention: the cultural one. As a matter of fact, artists worldwide have been choosing plastics to express their creativity since the beginning of XX century, thanks to the incredible adaptability of these modern materials. Nowadays, objects made of synthetic polymers are present in numerous art collections worldwide. However, differently from traditional ones, these manmade materials have not yet been extensively studied regarding their long-term durability in outdoor and indoor museum environments.

It is indeed well known how plastics, especially the semi-synthetic ones, are susceptible of fast weathering processes which often have dramatical consequences, even when the artworks are not exposed to extreme environmental conditions. Moreover, the juxtaposition of different materials is often part of the artist's design and contributes to the fast deterioration of plastics and surrounding components.

Collecting and caring for contemporary artworks made of plastics are today marked as priorities for museums and conservators. Indeed, it is nowadays recognized by conservators and scientists worldwide how the conservation intervention must come along with a deep knowledge of materials and techniques chosen by the artists, in order to identify the best strategies for the restoration and conservation of cultural heritage. The lack of comprehension of materials and their degradation patterns may, in fact, easily lead to inaccurate or even wrong conservative interventions which can affect, often irremediably, the artworks.

The aim of this PhD work was to study different plastics as constituents of contemporary artworks dated between 1966 and 1997 to understand materials and ageing pathways. One of the goals of this work was to provide the conservators with a complete overview about the ageing behaviors of

synthetic and semi-synthetic polymers in order to support the restoration and to identify suitable conservation conditions. To achieve this purpose, the Physical and Chemical Sciences department of L'Aquila University has started a fruitful collaboration with the *Istituto Centrale per la Conservazione ed il Restauro* (ISCR) of Rome, the *Scuola ENAIP of Botticino* (Br) and several museum institutions as well as the Center for Research in Biological Chemistry and Molecular Materials (CIQUS) of Santiago de Compostela.

The astonishing versatility of plastics often corresponds to complex compositions, which required a multi-analytical approach in order to obtain a complete set of information. Such approach was mostly based of molecular spectroscopy, as both FTIR (Fourier transformed infrared) and Raman spectroscopy allowed to get qualitative data and to determine functional groups in the molecules studied. At the same time, optical and scanning electron microscopy (SEM) in conjunction with energy dispersive spectroscopy (EDS) and portable XRF were used to study both macro and micro morphology of the surfaces and to get fundamental information on the inorganic components.

All these analytical techniques were applied successfully to the study of the materials composing the artworks investigated, providing an interesting insight on the conservative conditions and often highlighting degradation products and inaccurate conservation interventions.

Table of Contents

List of abbreviations

Analytical techniques

CS: cross section

DSC: differential scanning calorimetry

FTIR: Fourier transformed infrared spectroscopy

OM: optical microscopy

SEM-EDS: scanning electron microscopy coupled with energy dispersive spectroscopy

TGA: thermo gravimetric analysis

XRF: X-ray fluorescence

Polymers

CA: cellulose acetate

CN: cellulose nitrate

HDPE: high-density polyethylene

LDPE: low-density polyethylene

LLDPE: linear low-density polyethylene

MF: melamine-formaldehyde

PE: polyethylene

PET: polyethylene terephthalate

PMMA: polymethyl methacrylate

PUR: polyurethane

PVAc: polyvinyl acetate

PVC: polyvinyl chloride

Chapter 1. Introduction

1.1. The Plastic era

Since prehistory, our species felt the need to express creativity through art, using simple tools such as fingers and colored earths to paint scenes of everyday life.

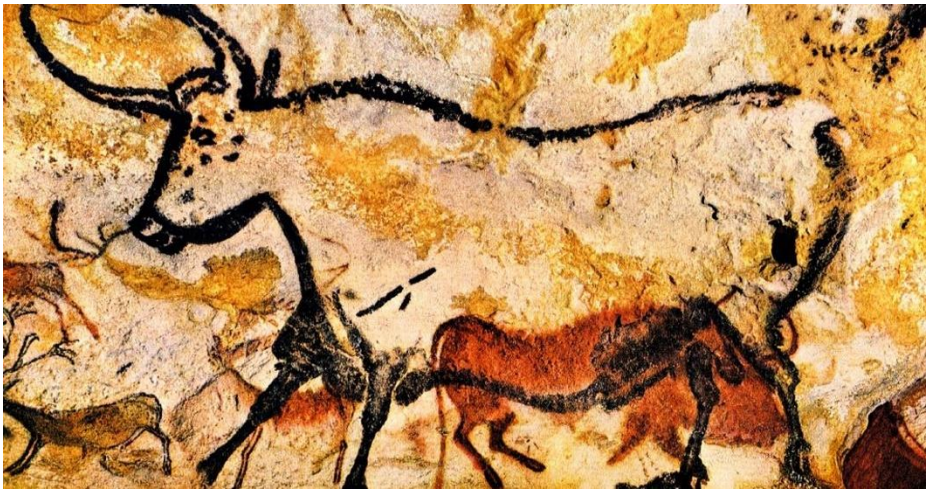

Figure 1: Cro-Magnon cave Art from the Upper Paleolithic period, picture from https://eu.usatoday.com/story/travel/destinations/2015/04/22/cave-paintings/26120059/

During thousands of years, as other skills, art evolved according to the historical time and to the instruments humanity found available. Quoting a meaningful parallelism [1] as historians defined time periods according to the materials used by humanity (Stone, Iron, Bronze ages) we may call our age the "*Plastic era*" since we cannot deny how plastics are, nowadays, an important part of our life. The love-hate relationship we share with plastics is driven by the

Figure 2: single use plastics polluting the oceans, on the right a seahorse grabbing a plastic cotton swab (Justin Hofman Photo). From https://act.wemove.eu/campaigns/eu-single-use-plastic

awareness of these materials being widespread and essential for us, but at the same time we cannot refuse to admit how the whole “single use” habit is severely polluting our environment. However, even if our biggest concern now is to deal with plastic pollution, there is one specific area of use in which it is mandatory to study how to preserve plastics: cultural heritage.

1.2. Plastics as -fragile- art tools

Being incredibly versatile materials, plastics have been in fact used since the first decades of the XX century to create sculptures and artworks. First examples are the Cubist-inspired works realized by the Russian brothers Naum Gabo and Antoine Pevsner [2]. Gabo used early plastics such as celluloid or Rhodoid (respectively cellulose nitrate and acetate) in order to embrace the modernity of industrial culture with its brand-new materials. According to this mentality, plastics were only tools to express creativity and esthetic purposes, therefore, as soon as new and better materials were released, Gabo started using them to make replicas of his old works like *Square Relief* in Figure 3, which is made of polymethyl methacrylate.

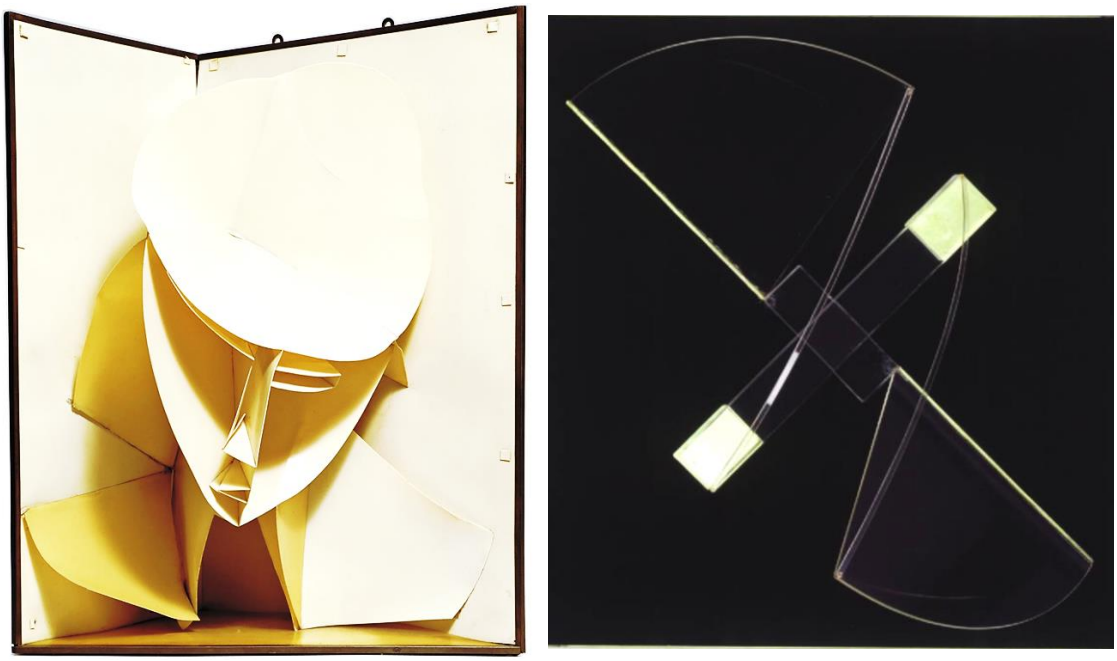

Figure 3: Naum Gabo, Head of a Woman 1917-20 from https://www.moma.org/collection/works/81440 on the right *Square Relief*, original from 1920 from https://www.ivam.es/en/coleccion/

Even strongly denying the intrinsic fragility of some of his works [3] Gabo somehow acknowledged the struggle of museums and collectors in conserving artworks made of plastics. As a matter of fact, he used to restore and make templates of his works in order to produce replicas when the originals were no longer in condition to be exposed [4]. The

abstract sculpture *Construction in space: two cones* is a meaningful example of how the lack of knowledge on the materials may lead to disastrous consequences. Conceived in 1928, the artwork was realized in 1936 using the -at that time- modern, transparent and easily foldable cellulose acetate. Acquired by Philadelphia Museum of Art, in 1960 the statue started showing signs of extended deterioration, enough to drive Gabo to make a replica, not without blaming the museum for being responsible of the damage. The replica, made in 1968, was then donated in 1977 to the Tate Museum, which exposed it for years, until the early 2000's when the artwork started to become brittle and eventually ended up in shards (Figure 4) [5].

Figure 4: Construction in Space "Two cones", on the left as seen in 1990 and on the right in 2007 The work of Naum Gabo © Nina and Graham Williams

In general, this rapid degradation phenomenon concerns more early plastics such as cellulose acetate, nitrate or vulcanized rubber which may start showing signs of deterioration after few decades [2], [6]. Another dramatic example of this fragility is the cubist sculpture *Portrait of Marcel Duchamp* made by Anton Pevsner using celluloid sheets and metal in 1926. Cellulose nitrate is made modifying the natural polymer cellulose reacting it with a mixture of nitric and sulfuric acid in order to obtain a transparent, flexible and thermoplastic[1] substance, which, once plasticized makes an incredibly versatile material for that time. Cellulose nitrate is, however, highly unstable and tends to lose plasticizer shrinking and becoming brittle. Moreover, cellulose nitrate spontaneously undergoes hydrolysis, virtually going back to cellulose and releasing nitric acid which can attack materials close to it [7], [8].Nowadays the

[1] A thermoplastic polymer can be shaped through heating to solidify after cooling maintaining the shape. Virtually this process can be infinite

artwork shows extended signs of degradation. In fact, as visible in Figure 5, the conservation conditions of the Portrait of Marcel Duchamp are extremely precarious, as the nitrocellulose sheets have lost most of their original flexibility and transparency, appearing warped, cracked and severely discolored. Moreover, the nitric acid released by nitrocellulose has attacked, corroding, the copper support, generating a diffuse greenish patina.

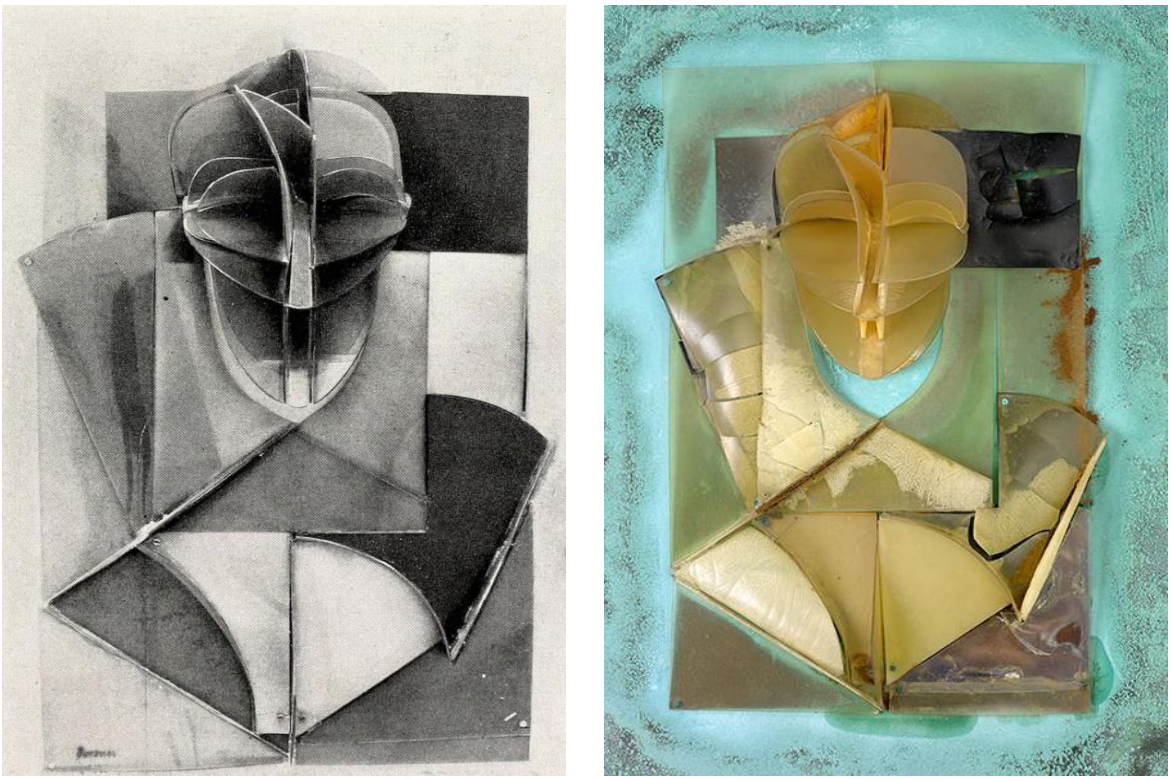

Figure 5: On the left, Portrait of Marcel Duchamp, made in 1926, on the right the artwork nowadays. Photo: charnelhouse https://thecharnelhouse.org/2015/02/22/naum-gabo-and-antoine-pevsner/antoine-pevsner-portrait-of-marcel-duchamp-1926-celluloid-on-zinc-37-x-25/

Contemporary art is meant to communicate feelings to the observer. Sometimes the whole "picture" may look hard to understand, as usually may happen with abstract artworks; just think about Jackson Pollock, modern action artist whose works, now sold for millions of dollars (Figure 6) were the results of completely casual dripping of paint on canvas.

Aside from the economic value of some modern and contemporary pieces, we should protect our cultural heritage for the following generations. To quote the English academic Simon Thurley [9], by enjoying art we may experience a "thirst to understand" it, which leads to the moral imperative of valuing and caring about it. Clearly the artist's first intention, or idea, is what should be preserved. Usually the artist's design and the actual artwork coincide, but when working with unstable materials like plastics, this may represent a real challenge. Eva Hesse's sculpture *Expanded Expansion*, made in 1969 (just one year before her premature death) using fiberglass, polyester resin and latex infused cheesecloth embodies how extremely aged materials may lead to the complete loss of artist's message. Forty years after the realization of the artwork, Expanded Expansion was no longer the "translucent and ethereal sculpture" [10] designed by the artist, appearing dramatically altered, yellowed and brittle (Figure 7).

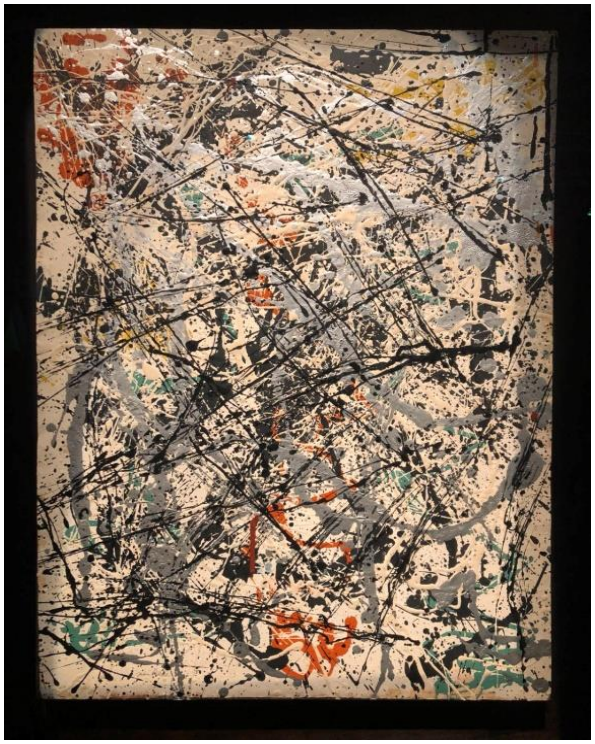

Figure 6: Number 32, 1949 by Jackson Pollock sold for 30 milions of dollars https://www.artmarketmonitor.com/2018/03/29/sothebys-brings-30m-pollock-to-new-york/

The damages were so extended to make impossible exposing the artwork, and made the art world wonder if the second picture in Figure 7 was still able to represent Eva Hesse's original intention or if the transformation of the material was so radical to have caused the loss of every artistic value from the object itself.

Figure 7: Eva Hesse, Expanded Expansion, top 1969. Bottom, 2010 © The Estate of Eva Hesse. Courtesy Hauser & Wirth

Indeed, these modern materials, albeit usually seen as eternal, are way less resistant than the ones traditionally used in art (marble, bronze, even wood and canvas). From these examples, it emerges clear the necessity of studying plastics and their degradation patterns, in order to understand how to preserve and restore artworks made of them.

1.3. But what are plastics?

To better understand the whole plastic revolution, and the variability of these materials, it is mandatory to define them. Plastics are man-made materials produced modifying natural polymers (semi-synthetic plastics) or creating completely synthetic polymers. In both cases, the properties of this kind of materials are generally improved adding various typologies of additives. The final product can be shaped as fiber, film, three-dimensional object, foam [1].

The first stage of the "plastic era" probably started in 1839 when the American self-taught chemist Charles Goodyear discovered how natural rubber (polyisoprene) properties of elasticity and resistance were significantly improved by heating it with sulfur. The discovery, called by William Brockendon "vulcanization" was patented by Goodyear in 1844 [11] and set the bases for modern rubber industries.

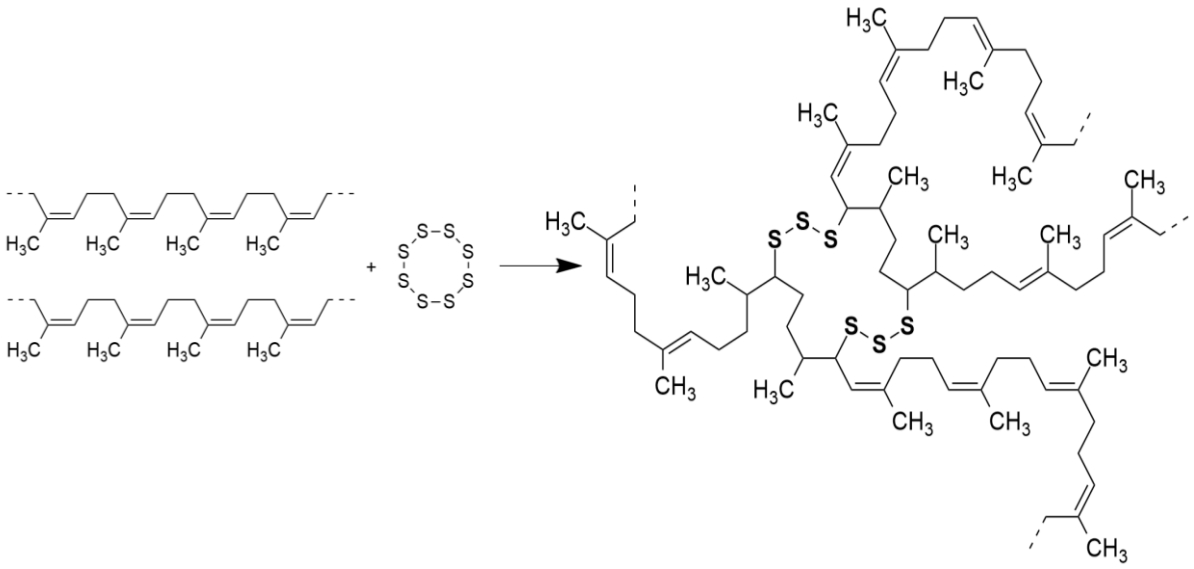

Figure 8: vulcanization of polyisoprene

Further researches led to the discovery of ebonite, natural rubber vulcanized with larger amounts of sulfur (with a proportion about 50:100). Ebonite, also known as vulcanite, was patented in 1851 by Nelson Goodyear (brother of Charles), and marked a huge step in plastics technology as it was the first thermosetting[2] man-made material [1]. While the Goodyear brothers were working on vulcanization of rubber, in 1847 the German chemist Schönbein "accidentally" perfected the synthesis of nitrocellulose, discovered in 1832 by the French chemist and pharmacist Henri Braconnot [1]The product was initially used as explosive and for the production of collodion, a syrupy solution of nitrocellulose in ether and alcohol used as an alternative to albumen in glass photographic plates [1].

[2] A thermosetting material is usually a highly crosslinked polymer which is irreversibly shaped and hardened by curing. The high degree of crosslinking makes molecular movements hard so this kind of materials cannot be re-shaped by further heating, as with thermoplastic polymers

Plastics history is full of peculiar, self-taught, creative characters. The most famous one is probably the English inventor Alexander Parkes, who in 1862 presented at the London Great International Exhibition his brand-new creation, the Parkesine. Parkesine, nowadays known as the first plastic, was obtained dissolving cellulose nitrate in a small amount of solvent, to get a moldable, jelly mixture which was possible to shape by "dies or pressure"[1]. However, aside from a bronze medal at the Great International Exhibition, Parkes struggled getting real recognition and solid earnings from his discovery and, despite his great creativity, his *Parkesine Company* failed after few years from the foundation. The biggest problems were, in fact, the excessive cost of production processes and the fact parkesine made objects suffered severe shrinkage after some time. In 1870 the American brothers John Wesley and Isaiah Hyatt patented a product made plasticizing cellulose nitrate with camphor [12] creating celluloid and prospering through the creation of Celluloid Manufacturing Company.

Figure 9: plaque in Parkes honor in Newhall Street (Birmingham)


Figure 10: "Philadelphia bracelet" made of Bakelite

During the first thirty years of XX century, different kinds of plastics were invented, and one of the most important is surely Bakelite, patented by Leo Baekeland in 1909. Bakelite, produced reacting phenol with formaldehyde through multi-step condensation, is the first fully synthetic resin. The invention of bakelite paved the way for the development of various thermosetting resins produced reacting formaldehyde with thiourea, urea and melamine. Nowadays, objects made of bakelite, especially jewelry, are collected and sold as “vintage”; in 1998 a “Philadelphia bracelet” similar to the one in Figure 10 was sold for 17000 dollars at Treadway/Toomey auction [13].

Between 30-40’s the syntheses of four of the nowadays most important thermoplastics were perfected. One of these is polystyrene, which was casually discovered in 1839 by the German apothecary Eduard Simon who was experimenting distillation of storax, a natural resin

extracted from the tree *Liquidambar styraciflua*. The oily distillation product obtained, after some days at air thickened becoming harder. Simon explained the transformation presuming oxidation occurred [14]. Almost one century later, in 1930 the German pharmaceutical I.G Farben was finally able to successfully produce polystyrene, while Styrofoam, a popular closed-cell extruded polystyrene foam, used mostly for insulation, was patented in 1944 by the American Dow Chemical Company [1]. Meantime, polyethylene was accidentally discovered at Imperial Chemical Industries (ICI) in 1931 while experimenting with high pressure ethylene in organic systems. Scientists immediately realized the high potentialities (above all the excellent chemical resistance and the low electric and thermal conductivity) and production of polyethylene started already in 1939 [1]. The temporal distance between the discovery and the industrial production of polyvinylchloride (PVC) was not so short. Firstly, patented by the Russian chemist Ostromislensky in 1912, PVC was not successfully produced, due to high decomposition rate when heated, before 1926. In fact, only almost 15 years later, the discovery of suitable plasticizing system made possible to lower the processing temperature of PVC. Finally, polymethyl methacrylate (PMMA) was produced in the early 30's by chemists of Imperial Chemical Industries, but the commercial and famous name "plexiglass" was given to the polymer by the German apothecary Otto Röhm, founder of Rohm and Haas, today Dow Chemical. Today, PMMA is used for multiple purposes when a transparent, robust and economic plastic is needed [15]. The years before and immediately after the World War II saw intense development and production of new plastics such as Nylon, polytetrafluoroethylene (PTFE) and isotactic polypropylene, which delivered the chemistry 1963 Nobel prize in the hands of Giulio Natta and Karl Ziegler and was successfully commercialized with the name "Moplen" by the Italian company Montecatini Edison.

Figure 11: different pictures representing the importance of isotactic polypropylene (branded Moplen) during the 70's from https://www.mudeto.it/moplen_giulio_natta_karl_ziegler_montecatini.htm

1832	Discovery of **nitrocellulose** (CN)	1918	Invention of **urea-formaldehyde resin**
1844	**Vulcanized rubber** patent	1926	First plasticized **PVC**
1846	Schönbein accidentally perfects **CN** synthesis	1928	Invention of **polymethyl methacrylate** (PMMA)
1856	**Parkesine** (CN) patent	1931	Accidental discovery of **polyethylene** (PE)
1862	**Parkesine** at the Great International Exhibition	1933	**Plexiglass** (PMMA) trademark
1865	First successful synthesis of **cellulose acetate** (CA)	1935	Invention of **nylon 6.6**
1869	Spill creates **Xylonite** (CN)	1938	Invention of **nylon 6** (polycaprolactam)
1869	Hyatt invents **celluloid** (CN)	1938	First nylon-bristled toothbrush
1872	Accidental synthesis of **polyvinyl chloride** (PVC)	1938	Accidental synthesis of **polytetrafluoroethylene** (PTFE)
1897	Invention of **Galalith**	1941	**Polyethylene terephthalate** (PET) patent
1898	Accidental synthesis of **polystyrene** (PS)	1944	**Styrofoam** (PS) patent
1908	First safety films made of **CA** by Kodak	1953	Invention of **polycarbonate** (PC)
1909	Baekeland invents **Bakelite**	1954	First synthesis of isotactic **polypropylene** (PP)
1912	**Cellophane** patent	1963	Nobel prize to Natta and Ziegler for isotactic PP
1912	**PVC** patent	1973	PET bottle patent

Table 1: brief history of plastics timeline

1.4. The challenge of conserving plastics

In spite of the fact that plastics in art collections are nowadays object of interest from scientists and conservators worldwide, there is still a lot we do not know about the long-term ageing behavior of synthetic polymers. We know they often degrade way faster than expected, even when conserved in not extreme conditions such as the ones found in museums and galleries [6]. The purpose of this thesis was to investigate plastics used in contemporary artworks dated between 1966 to 1997, highlighting the fragilities of these materials and how conservation science may provide information that is fundamental to the proper conservation of contemporary art.

This work was possible only thanks to the collaboration between the University of L'Aquila (AQ, Italy), the *Istituto Superiore per la Conservazione ed il Restauro* di Roma (ISCR) (RM, Italy), the *Scuola di restauro ENAIP of Botticino* (BR, Italy), the *MAMbo - Museo d'Arte Moderna di Bologna* (BO, Italy) and the *MAGA – Museo di Arte di Gallarate* (VA, Italy). Furthermore, part of the experimental work was performed at CiQUS-Center for Research in Biological Chemistry and Molecular Materials of Santiago de Compostela. Moreover, some of the results presented in this thesis were motivated by the MIUR (Ministry of Education, University and Research) founded project "Smart Cities And Communities", which involved several different institutions, between universities and industries[3].

The results on the seven contemporary artworks studied for this thesis are showed in different chapters, trying to point out the peculiar characteristics of the different materials. To help the understanding of the singular complexity of polymers degradation patterns, a short introduction for each material is provided before discussing the results regarding each single artwork.

[3] Project "*innovazione di prodotto e di processo per una manutenzione, conservazione e restauro sostenibile e programmato del patrimonio culturale"* , D.D n.2057 31th October, Cultural Heritage scn_00520 Smart Cities And Communities- MIUR D.D.391/ric 5 July 2012

References

[1] J. A. Brydson, *Plastics materials*. Butterworth-Heinemann, 1999.

[2] Y. Shashoua, *Conservation of Plastics 1st Edition*. 2008.

[3] N. Gabo, M. Hammer, and C. Lodder, *Gabo on Gabo : texts and interviews*. Artists Bookworks, 2000.

[4] C. Lodder, "Naum Gabo and the Quandaries of the Replica," *Tate Pap.*, vol. 8, 2007.

[5] J. Mundy, *Lost art : missing artworks of the twentieth century*. .

[6] M. Lazzari, A. Ledo-Suárez, T. López, D. Scalarone, and M. A. López-Quintela, "Plastic matters: an analytical procedure to evaluate the degradability of contemporary works of art," *Anal. Bioanal. Chem.*, vol. 399, no. 9, pp. 2939–2948, Mar. 2011.

[7] C. Selwitz, *Cellulose nitrate in conservation*. 1988.

[8] M. A. Robson, "The degradation of cellulose nitrate in composite museum artefacts: isolation, replica cellulose replacement and regular inspection in storage and on display," *Cellul. Cellul. Deriv.*, pp. 245–248, Jan. 1995.

[9] S. Thurley, "Into the Future Our strategy for 2005 – 2010," *Conserv. Bull.*, 2005.

[10] F. Domínguez Rubio, "Preserving the unpreservable: docile and unruly objects at MoMA," *Theory Soc.*, vol. 43, no. 6, pp. 617–645, 2014.

[11] C. Goodyear, "Improvement in India-rubber fabrics," US3633A, 15-Jun-1844.

[12] J. W. Hyatt and I. S. Hyatt, "Improvement in treating and molding pyroxyline," US105338A, 12-Jul-1870.

[13] "Plastic Timeline - From First to Modern Plastic." [Online]. Available: http://www.historyofplastic.com/plastic-history/plastic-timeline/. [Accessed: 10-Oct-2019].

[14] J. . Simon, "Üeber den flüssigen Storax (Styrax liquidus)," *Ann. der Pharm.*, vol. 31, no. 3, pp. 265–277, Jan. 1839.

[15] U. Ali, K. J. B. A. Karim, and N. A. Buang, "A Review of the Properties and Applications of Poly (Methyl Methacrylate) (PMMA)," *Polym. Rev.*, vol. 55, no. 4, pp. 678–705, Oct. 2015.

Chapter 2. Materials and Methods

Conservation science is a complex matter and requires different kinds of expertise to work together. The final goals of this thesis were to better understand the materials used in the artworks and their degradation patterns as well as to plan the conservation intervention and setting the best storage conditions for each artwork. To fulfill these needs, several analytical techniques have been chosen as the complexity of the task required to collect multiple information.

2.1. Analytical Techniques

Optical and portable microscopy, XRF, FTIR, colorimetry, DSC, TGA, SEM-EDS

All the samples were preliminary observed through optical microscopy, using a Leica M125 microscope, equipped with a Leica DFC 420C camera. For the artworks studied at *ISCR* of Rome, portable microscopy (dino-lite) and portable XRF were also employed. All XRF measurements were performed with X-MET8000 handheld X-ray fluorescence (HHXRF) analyzer equipped with a silicon-drift detector (SDD); excitation of X-ray tube: 40 kV, acquisition time: 16 sec, 8 μA. Excitations were performed at 40 and 8 kV.

One of the most important part of this work is surely infrared spectroscopy, as it provides fundamental qualitative data about polymers and their degradation products. The regular approach, as normally the amount of material collectable from the artworks is small, consisted in using a micro-FTIR. The measurements were performed using a Thermo Scientific™ Nicolet™ iN™10 Infrared Microscope equipped with an MCT detector, liquid nitrogen cooled. In most cases transmission modality on diamond cell was preferred, but in some specific case a germanium ATR crystal was used. All the samples were examined in the region 4000–670 cm^{-1} at a resolution of 4 cm^{-1}.

The artificial ageing and all the measurements on the melamine formaldehyde reference sample[1] were performed at USC Center for Research in Biological Chemistry and Molecular Materials (CIQUS) in Santiago de Compostela, thanks to Professor Massimo Lazzari. FTIR analysis

[1] Formica ColorCore® CC7940 spectrum yellow matte 58

were carried out using a Nicolet 7600 Spectrophotometer equipped with a diamond ATR crystal.

It may perhaps be useful to highlight some advantages and disadvantages of this technique. In fact, ATR allows to acquire fast and reliable measurements without requiring any particular sample preparation, but it requires the contact of the sample with a crystal characterized by a higher refractive index than the sample itself. At proper conditions the IR beam undergoes internal reflection creating an evanescent wave which penetrates the sample, being absorbed. Since ATR is based on internal reflectance of the IR beam, the depth of penetration (given in the equation below) is particularly significative.

$$DP = 1/[2\pi W n_c(\sin^2\theta - n^2_{sc})^{1/2}]$$

Where:

DP = Depth of penetration

W = Wavenumber

n_c = Refractive index of ATR crystal

θ = Angle of incidence

$n_{sc} = n_{sample}/n_{crystal}$

Differently from transmission modality, where the IR beam passes through the sample, when using ATR several factors must be considered to perform a good analysis, and the refractive index of the ATR crystal is one of them.

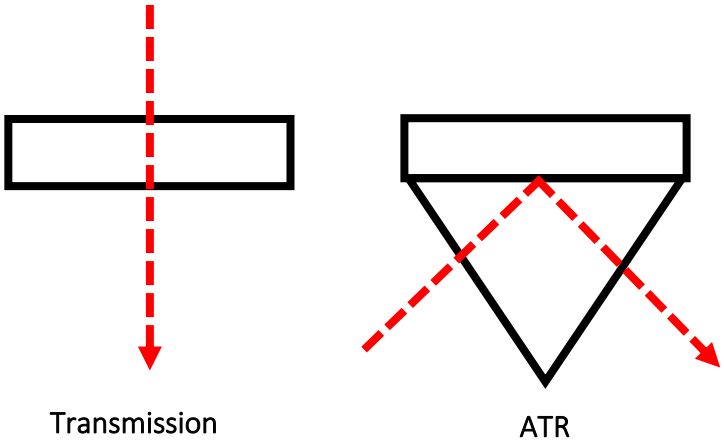

Figure 1: schematic representations of transmission and ATR acquisition modalities

Nowadays, the most used materials for ATR crystals are diamond and germanium. Diamond is chemically inert, extremely hard and has a relatively low refractive index (2.40) which allows, controlling other conditions, a good penetration depth. Germanium, on the contrary, has a high refractive index (4.01) which makes it more suitable for the analysis of highly absorbing samples (such as dark colored ones). The refractive index of most organic substances is about 1.5 [1], therefore it is reasonable to assume that the depth of penetration is sample independent for the majority of polymeric materials. However, this assumption cannot be made for inorganics (often added as fillers in polymers) where the refraction index can vary significantly from substance to substance. Since the depth of penetration depends on wavenumbers, the peaks relative intensity changes in comparison with a transmission spectrum. Figure 2 reports a comparison between spectra obtained, on the same sample (the laminate "Spectrum yellow"), in transmission and in ATR, and shows how the peaks relative intensity change is particularly evident at high wavenumbers, influencing the N-H, O-H and C-H stretching region. Furthermore, the refractive index of some samples can vary in proximity of absorbance bands giving raise to the anomalous dispersion phenomena and causing some bands to shift from their corresponding position in a transmission spectrum [1]. All these differences between transmission and ATR spectra make better to avoid comparisons [2], especially when monitoring ageing behaviors. Finally, ATR allows surface analyses but requires good contact between the sample and the crystal. The contact can be improved by applying more pressure on the crystal, making possible to investigate deeper layers in the sample, but excessive pressure may damage delicate materials [3].

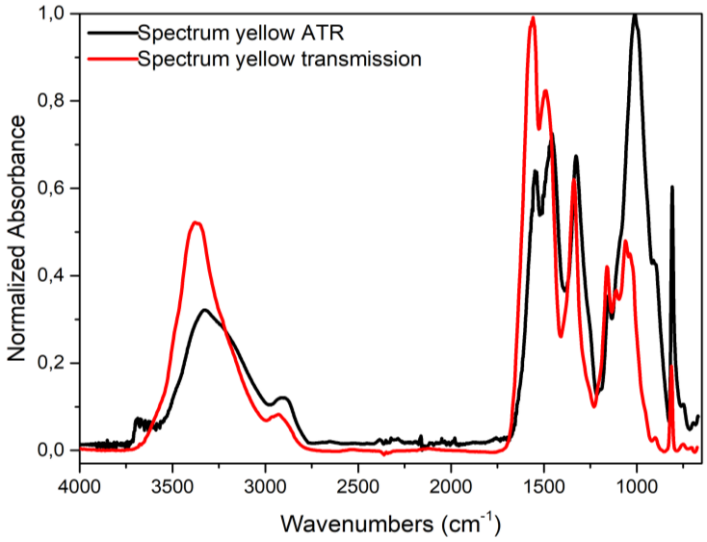

Figure 2: Comparison between spectra acquired in transmission and in ATR of the same laminate sample

Aiming to study and preserve cultural heritage, color is a particularly important parameter to consider as a significative feature in an artwork. Multiple ageing phenomena can be held responsible of changes which may alter dramatically the color of a surface. Studying the ageing behavior of melamine formaldehyde laminates (Chapter 7), color changes were monitored

using a CM-600d Chroma Meter colorimeter (Konica Minolta Sensing), according to L*a*b* color space[2]. The L*a*b system recognizes red/green and yellow/blue as opposite colors and defines the following variables as follows:

- L* is the lightness, from complete black (0) to perfect white (100)
- a* is the redness, tends to red for positive values and to green for negative ones
- b* is the yellowness, tends to yellow for positive values and to blue for negative ones

To represent the cumulative variations in an artificially aged sample, it is common to use the total color change ΔE^*_{ab}, which is the Euclidean distance (in the CIELAB diagram) between the reference and the measured color:

$$\Delta E^*_{ab} = [(\Delta L^*)^2 + (\Delta a^*)^2 + (\Delta b^*)^2]^{1/2}$$

Where:

$\Delta L^* = L^* - L_{ref}$

$\Delta a^* = a^* - a_{ref}$

$\Delta b^* = b^* - b_{ref}$

Surface conditions of an object can influence how the light is reflected on it, and both specular and diffuse reflections can affect the way human eye perceives colors.

Modern colorimeters give values in SCI (specular component included) including both specular and diffused reflected light and SCE (specular component excluded) which excludes any specular reflected component (although including the diffused reflected ones). According to what is the purpose of a study, it is possible to choose how to express the data obtained by colorimetry, as SCI for instance is not affected by any surface condition, while SCE is more sensitive to local rugosities or glossy surfaces. Normally, specular component excluded data are preferred since only the diffusely reflected components of light is responsible for the perceived color of the object [4]. Modern instruments such as the one used for the experimental work of this thesis give values of reflectance % which is another important parameter to take into account when studying the color variations of an object, as showed in Chapter 7.

[2] Also called CIELAB, defined in 1976 by the International Commission of Illumination (CIE)

Thermal analyses such as DSC (Differential scanning calorimetry) and TGA (thermo gravimetric analysis) are also useful to study polymeric materials and their degradation behaviors. In particular, DSC measures temperatures and heat flows associated with thermal transitions in the polymer, hence it is useful to study glass transitions, phase changes and melting temperatures. DSC data were acquired using a Q200 Differential Scanning Calorimeter from TA Instruments under a nitrogen flow (50.0 ml/min) equilibrating at -80.00 °C, with a ramp of 20.00 °C/min to 200.00 °C. Each measurement was repeated two times in order to erase the thermal history of the samples.

TGA registers variations of mass of the sample while the temperature is raised, and it is particularly useful to study thermal decomposition of polymers and to monitor changes before and after artificial ageing. Thermal analyses were performed with a thermo gravimetric analyzer from TA Instruments Q5000 using a platinum-HT pan under nitrogen flow (25.0 ml/min), equilibrating at 40.00 °C with a ramp of 10.00 °C/min to 1000.00 °C.

Scanning electron microscopy (SEM) coupled with energy dispersion spectroscopy (EDS) is a powerful technique which allows to investigate the micro-morphology while getting information on the elemental composition of a sample. All the samples were analyzed under low pressure conditions, a methodology which allows to analyze non-conductive surfaces without requiring any sputtering or further preparation. The samples were analyzed glued on a conductive adhesive on an aluminum stub or in resin block cross section when the study of the stratigraphy was particularly significative.

SEM-EDS analysis were executed with a Zeiss EVO 60, equipped with a micro probe OXFORD Inca Pentaflex EDS for semi-quantitative analysis. All the samples were analyzed in low pressure, without any treatment or in resin block cross section.

Finally, Raman spectroscopy was employed to investigate the possible occurrence of unsaturation due to chemical degradation of a polyolefin (Chapter 3). The instrument used for the measurement is a RENISHAW Raman model “InVia Reflex” equipped with a CCD detector, and a 785 nm laser.

References

[1] J. M. Chalmers, “Mid-Infrared Spectroscopy: Anomalies, Artifacts and Common Errors,” *Handb. Vib. Spectrosc.*, 2006.

[2] B. C. Smith, *Fundamentals of Fourier Transform Infrared Spectroscopy*. CRC Press, 2011.

[3] J. C. Lindon, G. E. Tranter, and J. L. (John L. Holmes, *Encyclopedia of spectroscopy and spectrometry*. Academic Press, 2000.

[4] D. Malacara, *Color vision and colorimetry: Theory and applications*, vol. 28, no. 1. 2003.

Chapter 3. Polyethylene (PE)

It is somehow expected to start this thesis with polyethylene, since it is the simplest of the synthetic polymers, being virtually formed only by an "endless" methylene groups chain, and at the same time is probably the most studied synthetic polymer ever [1].

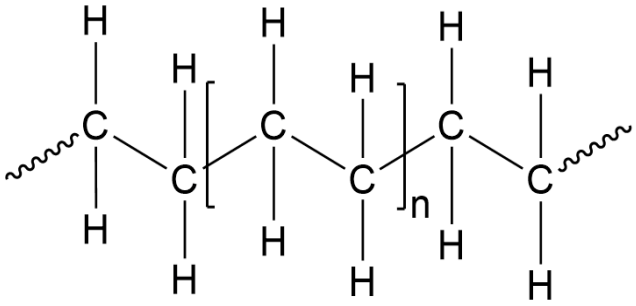

Figure 1: molecular structure of polyethylene

Industrially produced from ethylene the first time in 1933, nowadays polyethylene is the second most important plastic in the word, in terms of production and consumption, right after polypropylene [2]. The first patent, obtained in 1937, described a high-pressure process which allowed to obtain a low molecular weight and branched final product. Such way was the preferred one until the first half of the 50's, when two different pathways were introduced: the Phillips and the Ziegler processes[1], allowing the production of more linear types of polyethylene and lowering the pressure and the temperature during the synthesis [1]. The final product obtained through these news modalities is called high density polyethylene (HDPE) while the first obtained is called low density (LDPE).

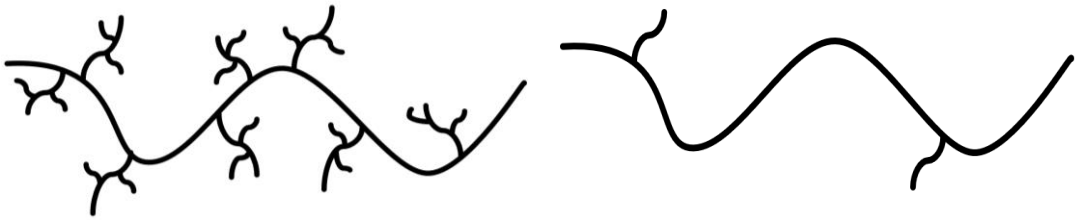

Figure 2: schematic representations of LDPE (on the left) and HDPE (on the right)

At the present days, several typologies of polyethylene are commercially available, according to the degree of branching and some physical properties such as melting point or stiffness, which are significatively higher for linear polymers [3]. Linear low-density polyethylene (LLDPE) for instance, is produced using mechanisms similar to the one for HDPE but adding small

[1] The Phillips process uses metal oxide catalysts while the Ziegler one involves the use of aluminium alkyl and similar compounds

amount of α-olefin (such as 1-butene-1 or 1-octene) to increase the degree of branching to the desired level [4]. For such reason LLDPE structure can be considered as in between HDPE (highly crystalline) and LDPE (mostly amorphous). Controlling the branching allows, therefore, to influence the density, passing from LDPE with ρ < 0.930 g cm^{-3}, to linear low density (LLDPE) (ρ ca 0.915-0.940 g cm^{-3}) to high density (HDPE) (ρ ca 0.940-0.965 g cm^{-3}) [5].

3.1. Degradation phenomena

Being virtually representable as a long chain aliphatic hydrocarbon, polyethylene should be extremely resistant to environmental factors such as light and atmospheric oxygen. In reality, Both HDPE and LDPE usually contain already oxidized chromophoric moieties and/or residual unsaturation that can lead to the formation of allylic hydroperoxides, which in turn may act as initiators during oxidative processes [6],[7].

In general, the most important degradative process for polyethylene is oxidation [8], [9] whose mechanism is based on the one described by Bolland & Gee for rubbers [10] and follows a free-radical chain reaction mechanism in which an alkyl radical, most likely formed during processing [1], reacts with molecular oxygen to form an alkyl-peroxy radical [2]. This peroxy radical is highly unstable and may abstract a hydrogen inter- or intra-molecularly forming a hydroperoxide [1]. Such hydroperoxide may act as photo-initiator, undergoing photolysis to give an alkoxy radical and a hydroxy radical [4]. The alkoxy radical can abstract a hydrogen from another polymer molecule to form an alcohol and an alkyl radical [5], which, reacting rapidly with oxygen, acts

$$R - R \rightarrow R \cdot + R \cdot \quad [1]$$

$$R \cdot + O_2 \rightarrow ROO \cdot \quad [2]$$

$$ROO \cdot + RH \rightarrow R \cdot + ROOH \quad [3]$$

$$ROOH \rightarrow RO \cdot + \cdot OH \quad [4]$$

$$RO \cdot + RH \rightarrow ROH + R \cdot \quad [5]$$

$$RO \cdot \rightarrow R'R''C = O \quad [6]$$

as new initiating radical as in [1]. Another possible mechanism involves the formation of carbonyl containing moieties, predominantly ketones [6],[11] but also, in secondary steps, esters,

carboxylic acids and γ-lactones [12], [6]. Such mechanisms are schematically represented in Figure 3.

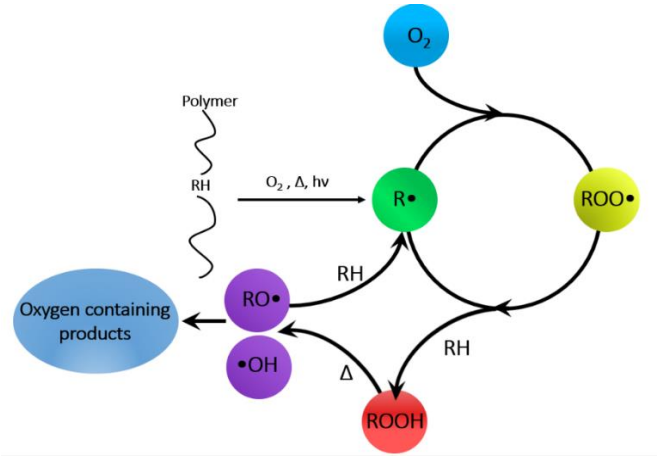

Figure 3: schematic representation of the oxidation processes of polymers such as polyethylene

Oxidized products can then undergo further degradation when exposed to environmental conditions (in particular to UV radiation) following Norrish I and II mechanisms illustrated in Figure 4 these mechanisms have equally catastrophic consequences. In fact, Norrish I leads to the formation of two free radicals which can take part of the vicious circle illustrated in Figure 3, while following Norrish II two light absorbing (and highly instable) moieties are produced [7].

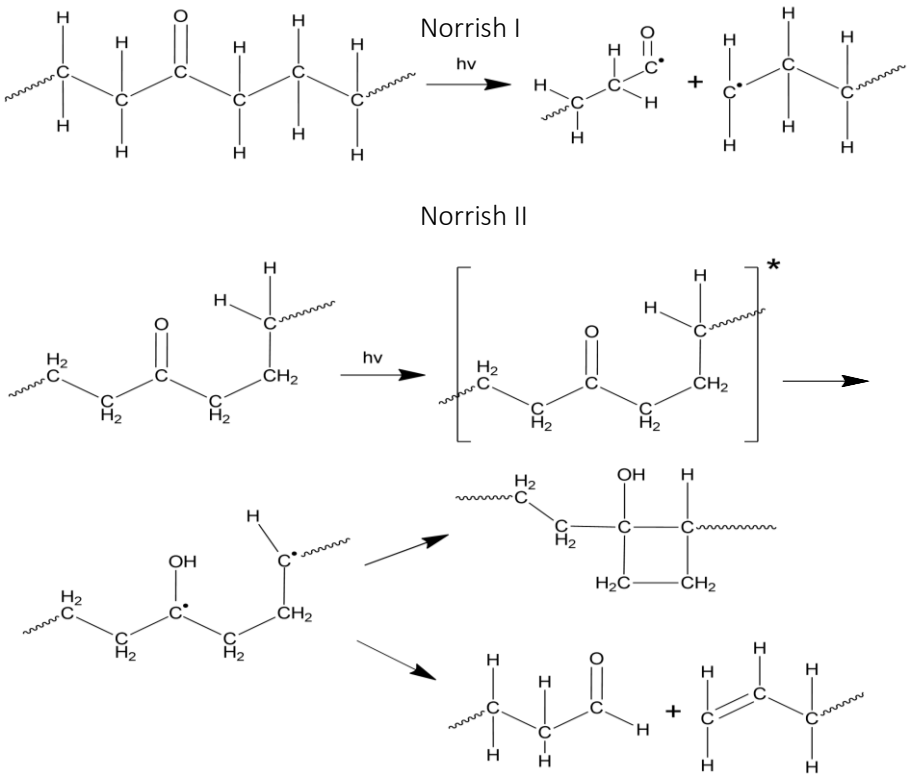

Figure 4: Norrish I and II mechanisms

References

[1] J. A. Brydson, *Plastics materials*. Butterworth-Heinemann, 1999.

[2] R. Geyer, J. R. Jambeck, and K. L. Law, "Production, use, and fate of all plastics ever made," *Sci. Adv.*, vol. 3, no. 7, p. e1700782, Jul. 2017.

[3] F. A. Mohamed and A. S. Abbas, "Production and Evaluation of Liquid Hydrocarbon Fuel from Thermal Pyrolysis of Virgin Polyethylene Plastics," *Iraqi Journal of Chemical and Petroleum Engineering*, 2015. [Online]. Available: https://www.iasj.net/iasj?func=article&aId=99238. [Accessed: 30-Sep-2019].

[4] H. Lobo and J. V. Bonilla, *Handbook of plastics analysis*. Marcel Dekker, 2003.

[5] M. Satkowski, "The crystallization and morphology of polyethylene and its blends," 1990.

[6] M. Gardette *et al.*, "Photo- and thermal-oxidation of polyethylene: Comparison of mechanisms and influence of unsaturation content," *Polym. Degrad. Stab.*, vol. 98, no. 11, pp. 2383–2390, Nov. 2013.

[7] G. Wypych, *Handbook of material weathering*. .

[8] J. V. Gulmine, P. R. Janissek, H. M. Heise, and L. Akcelrud, "Degradation profile of polyethylene after artificial accelerated weathering," *Polym. Degrad. Stab.*, vol. 79, no. 3, pp. 385–397, Mar. 2003.

[9] J. V. Gulmine and L. Akcelrud, "FTIR characterization of aged XLPE," *Polym. Test.*, vol. 25, no. 7, pp. 932–942, Oct. 2006.

[10] J. L. Bolland and G. Gee, "Kinetic studies in the chemistry of rubber and related materials. II. The kinetics of oxidation of unconjugated olefins," *Trans. Faraday Soc.*, vol. 42, no. 0, p. 236, Jan. 1946.

[11] C. H. Chew, L. M. Gan, and G. Scott, "Mechanism of the photo-oxidation of polyethylene," *Eur. Polym. J.*, vol. 13, no. 5, pp. 361–364, 1977.

[12] J. V. Gulmine, P. R. Janissek, H. M. Heise, and L. Akcelrud, "Polyethylene characterization by FTIR," *Polym. Test.*, vol. 21, no. 5, pp. 557–563, 2002.

Chapter 4. Massimo Zuppelli, *Teca con Frutta*, 1967

Teca con Frutta ("Case with fruit") was realized in 1967 by the Italian artist Massimo Zuppelli, famous exponent of the Italian neorealism movement and well known for his painting style, able to merge realism with surrealism.

The artwork is a multi-material piece, resembling a three-dimensional still-life painting: a black painted wood case containing different kinds of plastic fruit shaped objects, spray painted with different layers of metallic colors (Figure 1).

Figure 1: "Teca con frutta", on the left case closed, on the right case open without the glass

During 2018 *Teca con Frutta* was object of conservation thesis of the student Alessia Sturari under the supervision of Giovanna Scicolone at the *Scuola di Restauro ENAIP Botticino*[1], in this occasion it was possible to remove the glass sheet on top of the frame and to study the materials used by the artist and to assess their conservation state. In general, the artwork was showing extended signs of degradation, worsened by long-term unsuitable conservation conditions in a very humid environment.

[1] A. Sturari "*Teca con Frutta: installazione-opera tridimensionale complessa statica*", Scuola di Restauro ENAIP Botticino 2019

Many of the objects being part of the artwork showed an extended degree of degradation, in Figure 2 it is possible to notice cracked apple and pineapple.

Figure 2: details of the fruit elements samples, on the left the apple, on the right the pineapple

4.1. Sampling

Sample from both apple and pineapple were taken and preliminary observed by optical microscopy and then analyzed through different techniques to study the composing materials and assessing the conservation conditions.

Sample	Description	Analyses
1 (apple)	Fragment of an apple	OM, FTIR, Raman, DSC, SEM-EDS
2 (pineapple)	Fragment of a pineapple	OM, FTIR

Table 1: samples taken from the artwork and analyses performed

4.2. Polymer characterization

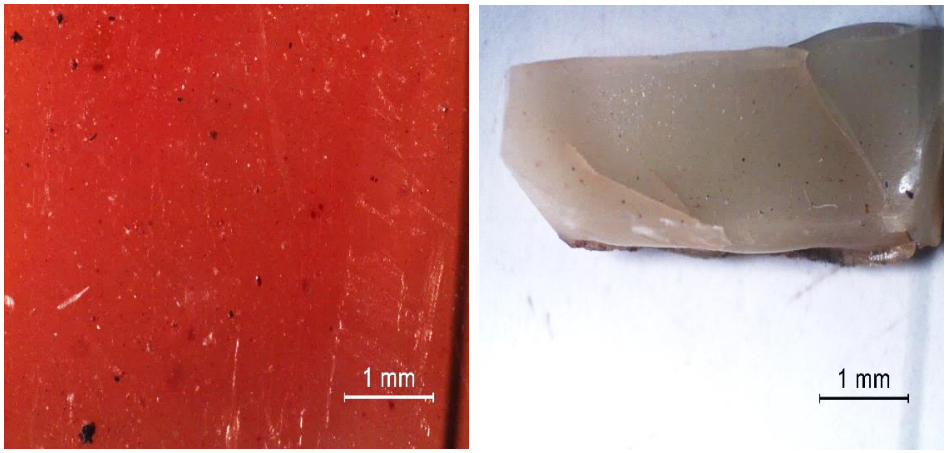

Figure 3: optical microscopy pictures of the two samples, on the left the apple, on the right the pineapple

Observation with optical microscopy of the internal zone of sample apple highlighted diffused presence of scratches and dark colored inclusions inside a reddish matrix, while the sample pineapple, dark yellow colored, showed a cracked surface with black inclusion here too (Figure 3).

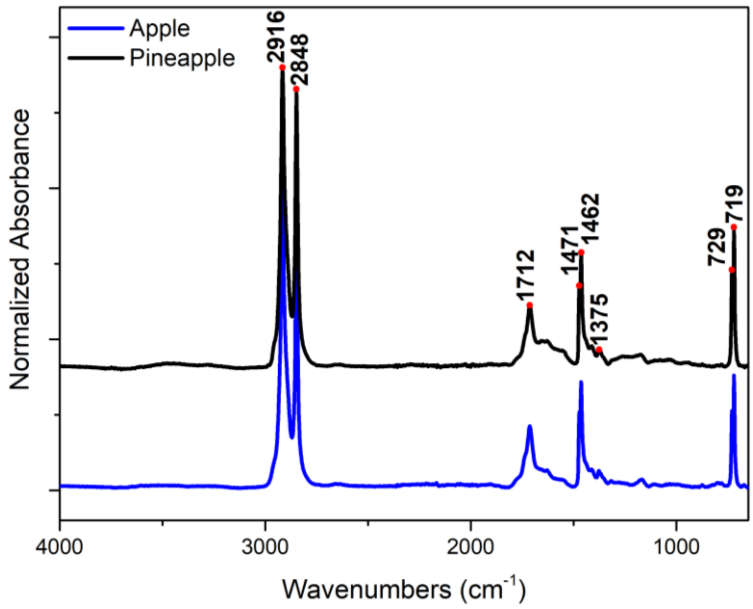

Wavenumber (cm^{-1})	Assignment
2916	ν C-H (CH_2)
2848	ν C-H (CH_2)
1712	ν C=O
1471	δ C-H (CH_2)
1462	δ C-H (CH_2)
1375	δ C-H (CH_3)
729	δ C-H (CH_2)
719	δ C-H (CH_2)

Figure 4: FTIR spectra of both samples, on the right tables with IR absorptions

The non-painted surface of the samples apple and pineapple was analyzed using ATR method, which allows analysis of thin surfaces [1] without requiring any further sampling or preparation.

Both samples showed almost identical spectral features (Figure 4) addressable to polyethylene. Typical features of polyethylene are, in fact, the signals at 2916 and 2848 cm^{-1} due to asymmetrical

and symmetrical stretching of methylene group, the absorptions at 1473 and 1462 cm^{-1} (methylene scissoring), and 729 and 719 cm^{-1} (CH_2 rocking). The appearance of doublet for the bending modes is typical of solid-state linear alkanes samples [2] and may be linked to the crystalline nature of the sample [3]. The absorption centered at 1712 cm^{-1} is due to oxidation phenomena of the polymer and will be discussed later (paragraph 4.4).

Fourier transformed Infrared spectroscopy may also be useful to distinguish between low-density polyethylene (LDPE), linear low-density polyethylene (LLDPE) and high-density polyethylene (HDPE). In fact, the presence of signals due to CH_3 groups, as terminals of chain branching, may help to better understand the structure of the studied polyethylene. In this case, the appearance of a small absorption at 1375 cm^{-1} (bending of methyl group) may be linked to the presence of branching, typical of LDPE and LLDPE.

Moreover, both the samples show three small peaks in the spectral range between 1400-1330 cm^{-1}, as common in LDPE (HDPE normally presents only two small absorptions in this area, as showed in Figure 5).

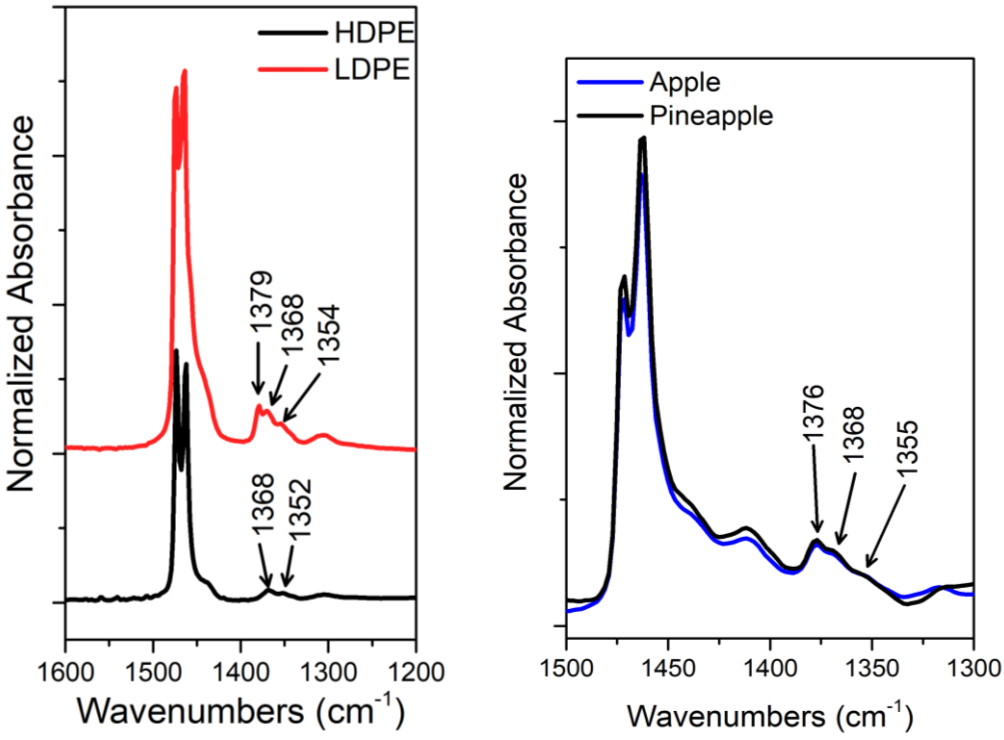

Figure 5: spectral comparison between HDPE and LDPE, on the right same spectral region for both samples taken from "Teca con Frutta"

The absence of bands around 1000-890 cm^{-1}, attributable to residual unsaturation present in LLDPE, suggests the polymer used in *Teca con Frutta* may be LDPE[2].

4.3. Paint characterization

As showed in Figure 6 on both samples it was possible to notice the presence of different layers of painting, apparently applied using spray colors. To better understand the chemical nature of the painting, small portions of the different layers were sampled and analyzed via micro-FTIR, separating the different components according to the colors and pressing each of them to obtain thin films deposited on a diamond cell for transmission analysis. On heterogeneous surfaces, this sampling technique allowed to get better results compared to ATR ones.

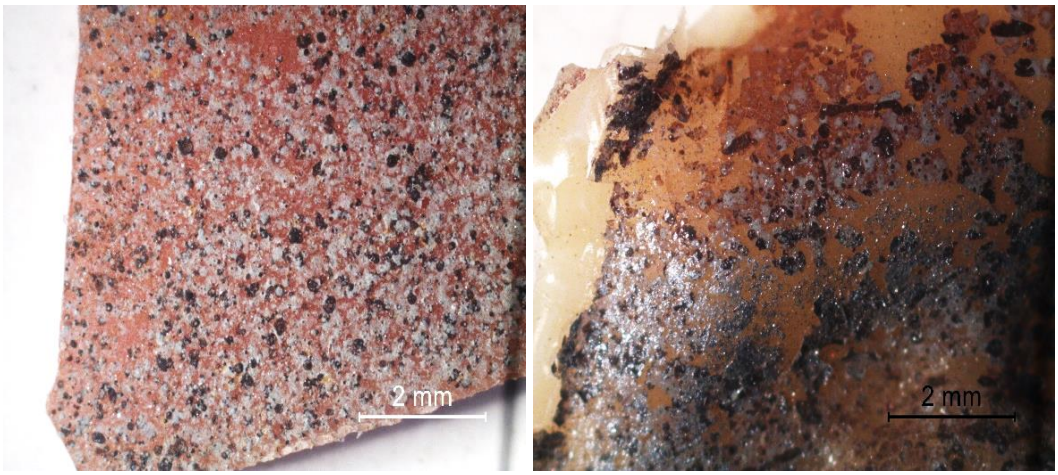

Figure 6: optical microscopy pictures of the painted surfaces of both samples (apple on the left, pineapple on the right)

Two colors of paint, silver and black, were recognized on the sample pineapple and apple. Since the FTIR spectra of both the colors (and for both pineapple and apple) are perfectly comparable, it is possible to assume that the artist sprayed the same colors after the fruits were secured on the support.

[2] These considerations cannot lead to unambiguous conclusions since often two samples of the same polymer can exhibit slightly different spectral features according to several factors such as synthesis conditions, additives or fillers.

FTIR analysis showed that the paints used were formulated containing cellulose nitrate and alkyd resin (Figure 7).

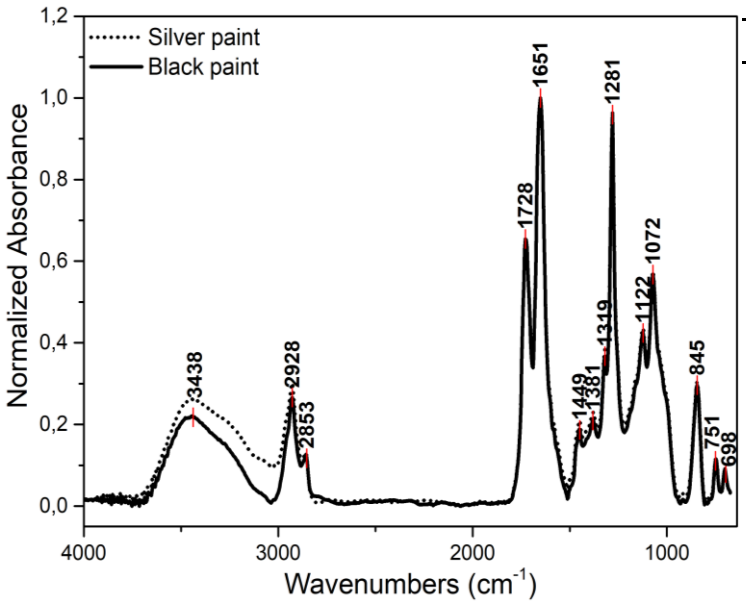

Wavenumber (cm^{-1})	Assignment
3438	ν O-H
2928	ν C-H (CH_2) alkyd
2853	ν C-H (CH_2) alkyd
1728	ν C=O alkyd
1651	ν NO_2 nitrocellulose
1449	δ C-H (CH_2 alkyd)
1381	δ C-H
1319	ν C-O-C alkyd ester
1281	ν NO_2
1122	ν C-O-C alkyd ester
1072	δ C-H aromatic
845	ν NO_2
751	γ NO_2 + δC-H aromatic
698	δ C-H aromatic

Figure 7: spectral comparison between two paint colors on the pineapple sample, on the right the table with IR bands assignments

It is indeed possible to notice the presence of the cellulose nitrate's typical absorptions, such as the NO_2 stretching (asymmetric at 1651 cm^{-1} and symmetric at 1281 cm^{-1}). Alkyd resins are usually added to nitrocellulose coating products such as spray paints in order to improve their flexibility acting as plasticizer [4]. Typical coating formulations include cellulose nitrate mixed with aromatic polyesters (commonly produced from phthalic anhydride and a glycol , Figure 8) modified with castor, linseed or cottonseed oils, to obtain medium oil alkyd resins[3] [5].

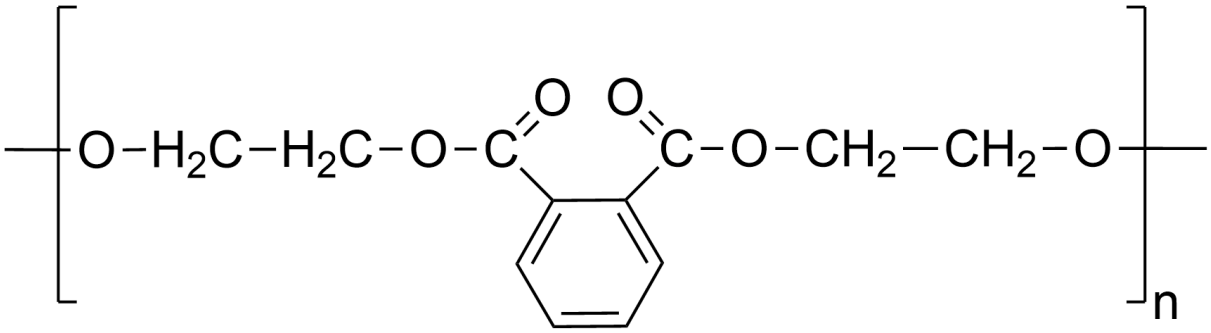

Figure 8: typical structure of an alkyd resin produced from phthalic anhydride or phthalic acid

[3] Alkyd resins are usually grouped, according to the percentage of fatty acid added to the polyester, in short oil (35-45% of oil), medium oil (46-55%), long oil (56-70%) [6].

Important spectral features related to alkyd resins are the C-H methylene stretching (2928 and 2853 cm^{-1}), the strong carbonyl stretching at 1728 cm^{-1} and the C-O-C stretching (asymmetric at 1319 cm^{-1} and symmetric at 1122 cm^{-1}) [2]. The broad absorptions centered at 1651 cm^{-1} appears to cover the sharp doublet (usually located at 1600-1580 cm^{-1}) useful for the detection of the aromatic component, however the in-plane deformation (1072 cm^{-1}) and the out-of-plane deformation (751 and 698 cm^{-1}) of the aromatic ring are clearly visible [6], [2].

4.4. Chemical degradation

As for other polyolefins, oxidation of polyethylene can be monitored and studied via FTIR spectroscopy, observing the formation and evolution of the carbonyl band as result of degradation phenomena of the polymer [7], [8], [9].In the spectrum in Figure 9 is possible to see different contributions in the range 1800-1600 cm^{-1} (C=O stretching). In particular, at 1712 cm^{-1} due to the ketone group (it is also possible to see the band at 1411 cm^{-1} attributed to scissoring of methylene adjacent to ketone carbonyl [10], 1734 cm^{-1} (esters), 1772 and 1781 cm^{-1} (γ-lactones) [7], [8], [11].

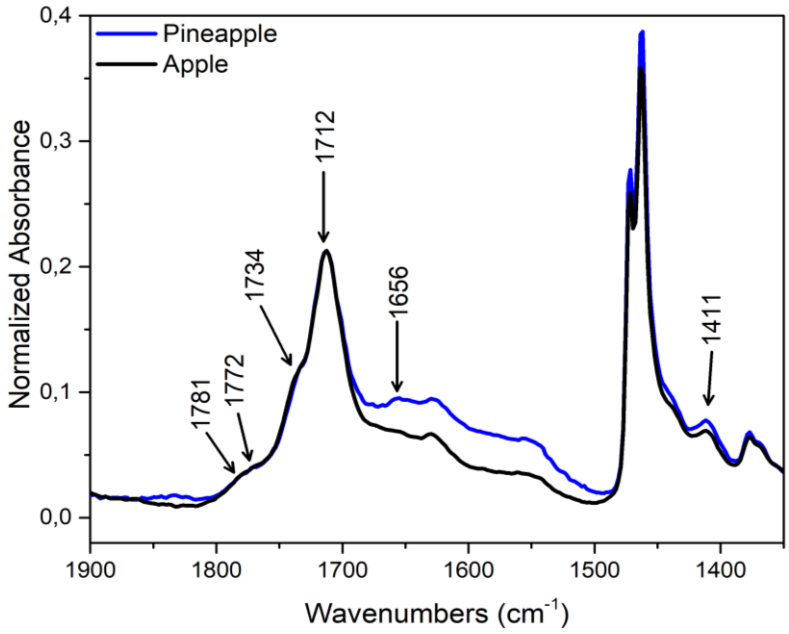

Figure 9: carbonyl stretching region spectral comparison of the two samples

4.4.1. Cristallinity

Crystallinity of the polymer may influence the degradation patterns and vary during ageing on the polymer. Initially, chain scission appears to be the prevailing phenomenon, producing smaller fragments of polymer chains which are more free to move and thus more susceptible to secondary crystallization. The absorption at 1656 cm^{-1} may be related to the formation of double bonds with *cis*- configuration [10]. Oxidated species can further react when exposed to sunlight by Norrish II

mechanism leading to the formation of vinyl compounds and it is well known how the presence of insaturations can weaken the strenght of C-H stabilizing the formed radical [12].

Differential scanning calorimetry measurements allow to investigate some important thermal properties of polymers such as glass transition and melting temperatures (for semi-crystalline polymers). To study the different constituents, the sample apple was taken as representative for both specimina and analyzed via DSC both with and without the paint layer (Figure 10). While the two endothermic peaks are significative of low density polyethylene melting[4] , the slight hump visible at around 44°C (pointed out by the arrow in Figure 10) is related to the presence of the paint layer and it is due to the glass transition temperature of nitrocellulose, calculated to be around 44°C. Zhanning [13] signaled an inconsistency in the found glass transition values of nitrocellulose, however the value of 44°C is coherent with the one reported by Crompton [14].

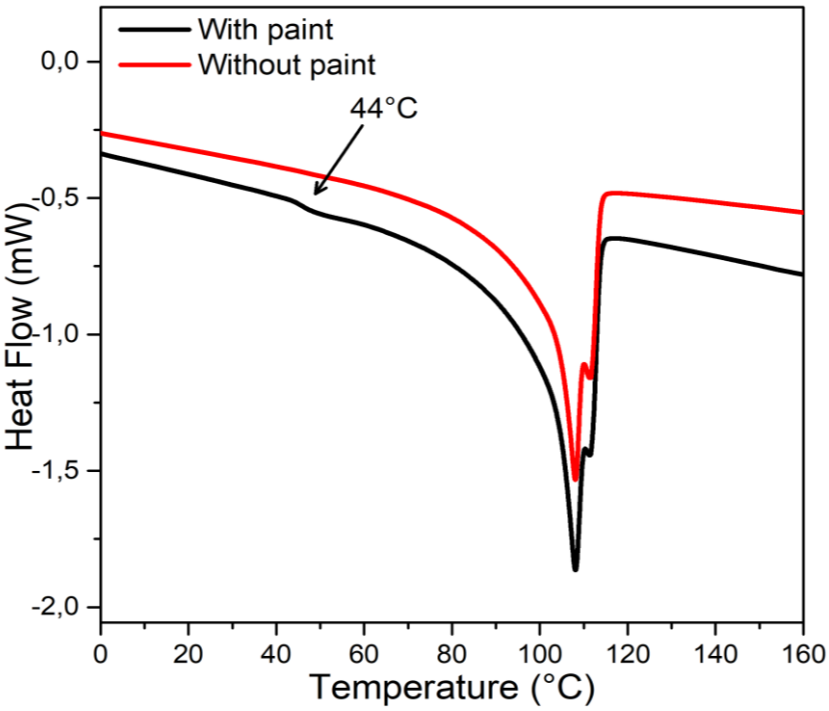

Figure 10: DSC curves for the sample apple with and without paint

DSC analysis allowed also to estimate the melting temperature and degree of crystallinity of the polymer, which can be particularly significative when studying the weathering of polymers considering secondary crystallization is a common phenomenon [15].

The degree of crystallinity α may be calculated according to the formula:

$$\alpha = \frac{\Delta H_f}{\Delta H_f^0} \cdot 100$$

[4] The melting peaks are at 108°C and 112°C coherently with LDPE regular melting points (between 105 and 115°C). HDPE exhibits higher melting points (up to 180°C) [32]

Where ΔH_f is the enthalpy of fusion of the sample determined from the endothermic peak of fusion as 103.2 J/g while ΔH^0_f is a stardard value of the enthalpy of fusion for a perfectly crystalline material (293 J/g) [14], [16], [17] it is possible to calculate the approximated crystallinity of the studied material as 36%.

Satkowski [18] reports as standard values of α for HDPE and LDPE respectively up to 90% and 50% or lower; Sato [19] studied via Raman spectroscopy different kind of polyethylene exhibiting α from 66.6 to 68.3% for HDPE and from 33.1 to 26.1% for LDPE. Lin [20] obtained with Raman spectroscopy an average crystalline percentage between 55.9% and 61% for HDPE and between 31.1 and 32.4 % for LDPE.

4.4.2. Possible unsaturation in the polymer

Raman spectroscopy has widely been used to study the three components system exhibited by polyethylene: an ortorhombic crystalline phase, an amorphous phase and a third, intermediate phase which appears to be semi-crystalline [21].

The wide shoulder between 797-920 cm^{-1} (highlighted in Figure 11 by a green circle) is indicative of high levels of side short branches, tipical of LLDPE or LDPE [19], confirming FTIR and DSC data.

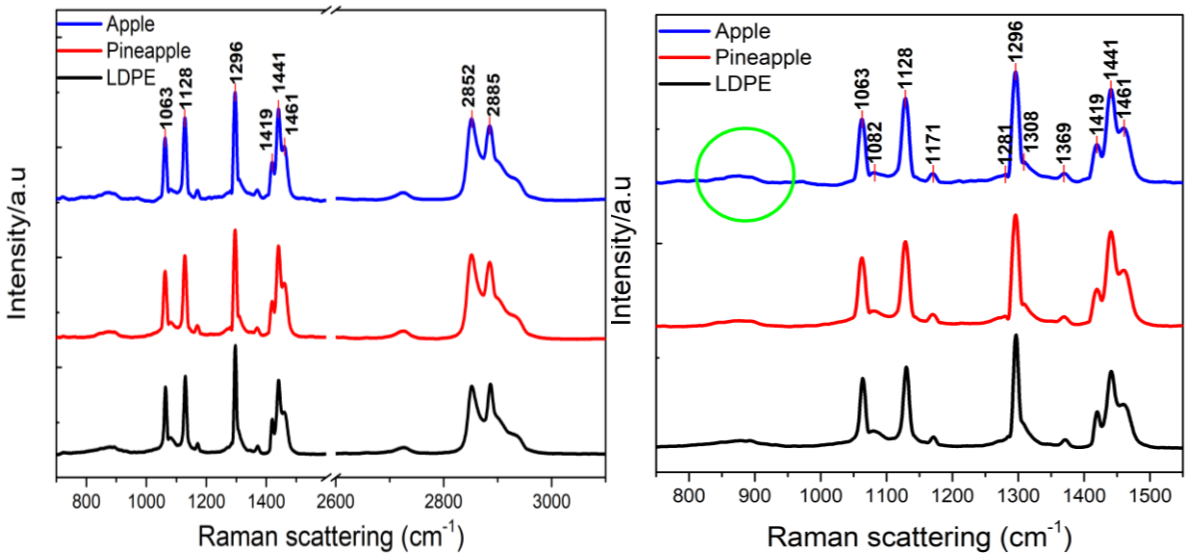

Figure 11: Raman spectra of the two samples compared to LDPE

The band at 1419 cm^{-1} is associated with CH_2 bending in orthorhombic crystalline phase [19], [22] and may appear split in two peaks (in this case 1419 and 1440 cm^{-1}) indicating the presence of two

molecules occupying each unit cell [23]. The spectral region between 1350-1250 cm^{-1} (CH_2 twisting) is independent from the polymer chain conformation [15].

The lack of absorptions between 1600-1650 cm^{-1} suggests the degradation pathways for the polymers do not involve the formation of C=C in sufficient concentration to be detected by Raman spectroscopy.

4.5. Biological attack

On the surface of pineapple was visible a brown thin layer (highlighted by a yellow arrow in Figure 12) initially attributed to the aged paint binder. The FTIR analysis, instead, revealed the presence of altered polyethylene. Comparing the spectrum of the internal surface of the sample pineapple with the darker external layer[5], it is possible to notice the more intense absorption due to the carbonyl stretching, but also the appearance of some other bands not characteristic of the polymer itself.

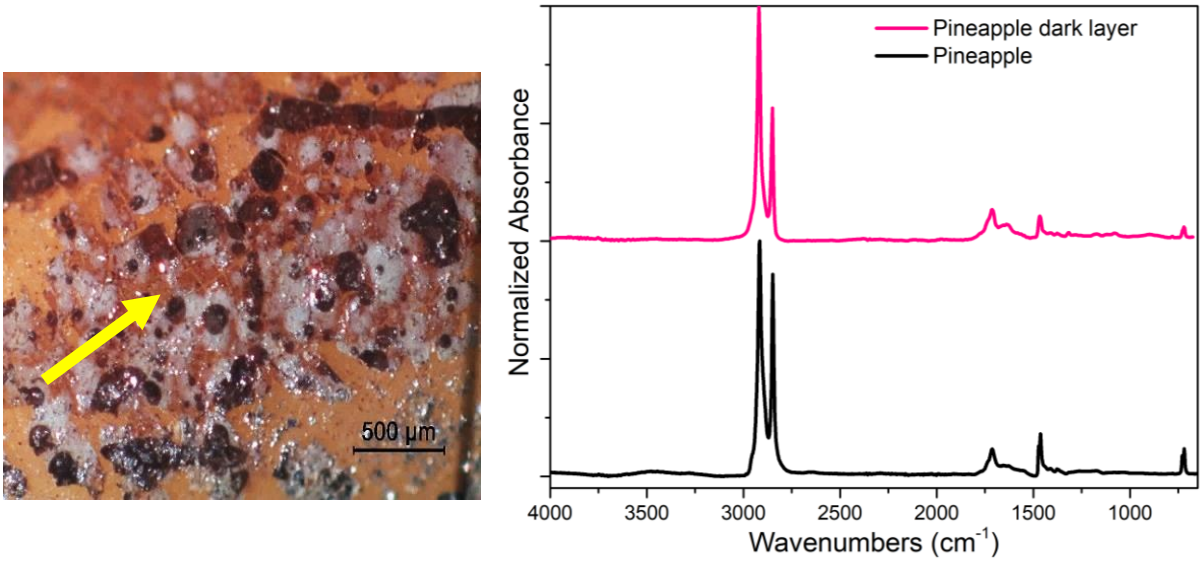

Figure 12: optical microscopy picture of the painted surface on pineapple, on the right spectral comparison between the dark layer and the lower surface

[5] Since spectra obtained with ATR sampling technique are strongly influenced by the refractive index of both the sample and the crystal and by the dept of penetration of the evanescent wave generated in the crystal, it was necessary to apply a correction factor in order to compare the two spectra in Figure 12 and following

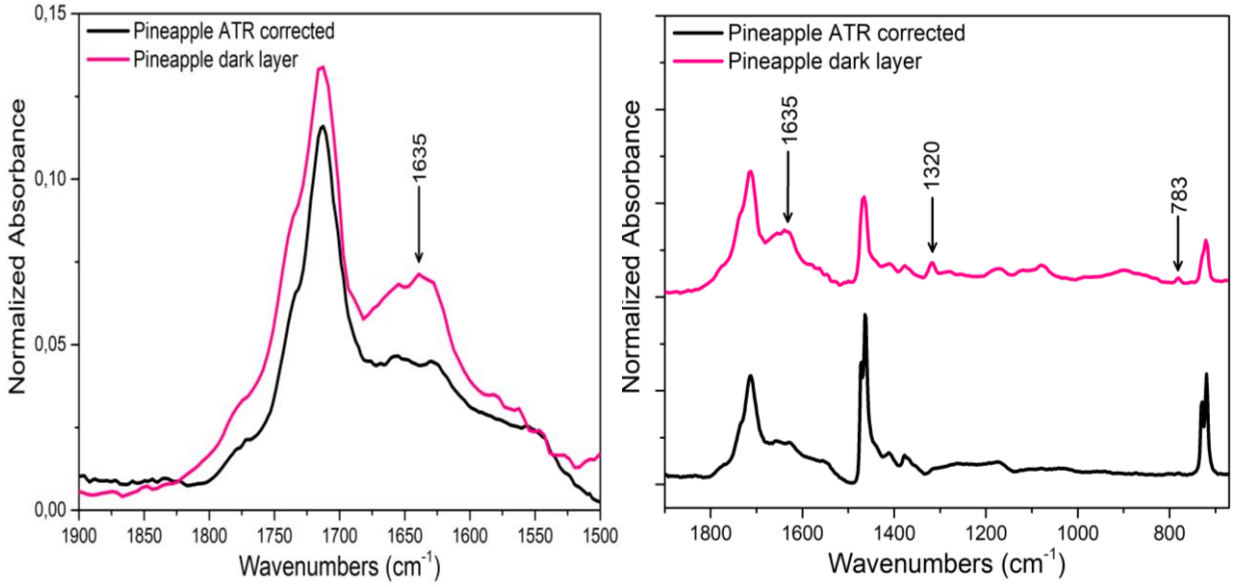

Figure 13: spectral comparisons between the dark layer on the sample pineapple and the lower surface

Signals at 1635, 1320 and 783 cm^{-1} have been attributed to C-O vibrational modes in calcium salts of oxalic acid [24], [25]. Oxalic acid salts are found in sediments, soils, plant tissues, kidney stones [24] and as products of fungi metabolism [26]. Fungi are heterotroph organisms able to secrete extracellular enzymes to digest organic materials like polysaccharides and proteins decomposing them into sugars and amino acids [27]. Calcium oxalate is usually associated with hyphal structures, mostly in mono and dihydrate phase (whewellite CaC_2O_4 H_2O and weddellite $Ca(C_2O_4)\cdot 2(H_2O)$ [26]. The production of oxalic acid by fungi requires sources of carbon and nitrogen and it has been proven that nitrocellulose may provide an available source of nitrogen for fungal metabolism [28].

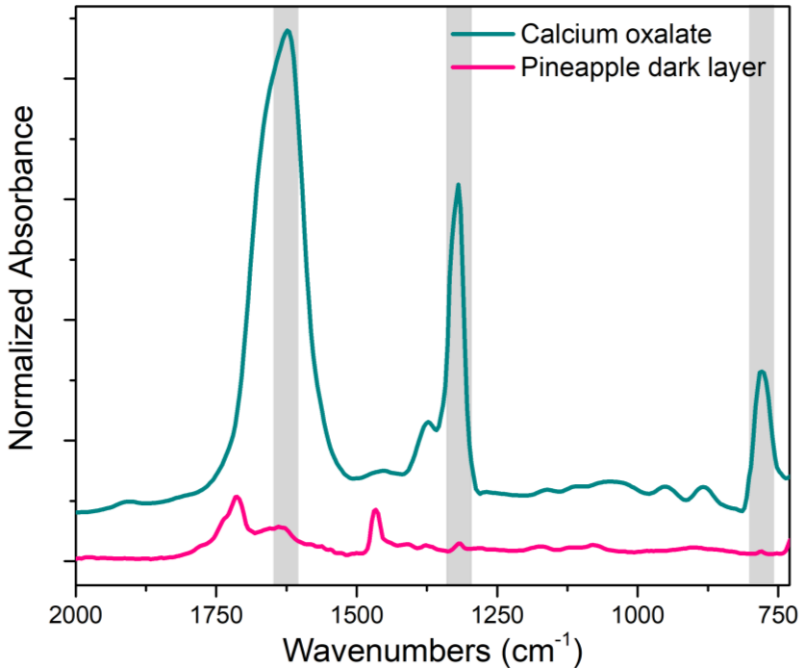

Figure 14: spectral comparison between calcium oxalate and the dark layer on the sample pineapple

Mechanistically, the enzymatic degradation of cellulose nitrate caused by fungi appears to be sterically hindered by nitration of the glucose ring (Figure 15), but this ability is strongly influenced by the degree of substitution of the hydroxyl group [29] . In fact, Auer [28] reported that degradation of nitrocellulose by microorganism may involve the cleavage of the β-1,4 glucoside bond, forming nitro-oligosaccharides of various molecular weights, pathway normally carried on by fungi. Denitration, with loss of nitric acid, may be another mechanism followed out by fungi [28]. It has been also reported that cellulolytic fungus *Chaetomium elatum* and the lignocellulolytic *Coprinus cinereus* can degrade nitrocellulose. *Chaetomium elatum* can attack nitrocellulose causing autocatalytic hydrolysis with release of nitric acid [28]. Cappitelli [30] showed how different strains of fungi can attack paint binders, in particular alkyd resins, highlighting how it is not easy to address the microbial activity to a specific component of commercial paints.

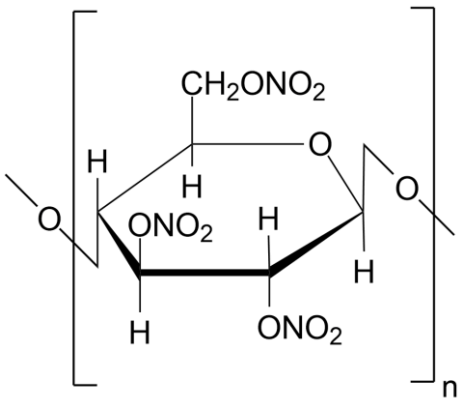

Figure 15: chemical structure of cellulose nitrate

To better investigate the presence of biological attack on the surface of the samples, small portions of both were analyzed through SEM-EDS in variable pressure, fixing the pieces on an aluminum stub covered in conductive adhesive. The results shown below are relative only to the apple fragment, which, thanks to its natural flat surface, allowed to obtain optimal results both in SEM microscopy and in EDS mapping. However, the shown specimen can be considered representative of both samples. SEM analysis confirmed the presence of fungal elements namely hyphae and spores on the surface of the samples (Figure 16). The typical fungal network is composed by filamentous elongated elements called hyphae, tubular cell walls that sorround the cytoplasmic membrane (signaled by yellow arrows in following figure). Hyphae associate togheter to form a mycelium which holds the conidia, asexual spores often responsible of the dusty or colored appeareance of fungal structures [27]. Spores are reproductive cells produced by fungi and other microorganism, recognizable in Figure 16 as the rounded elements highlighted by the yellow circles.

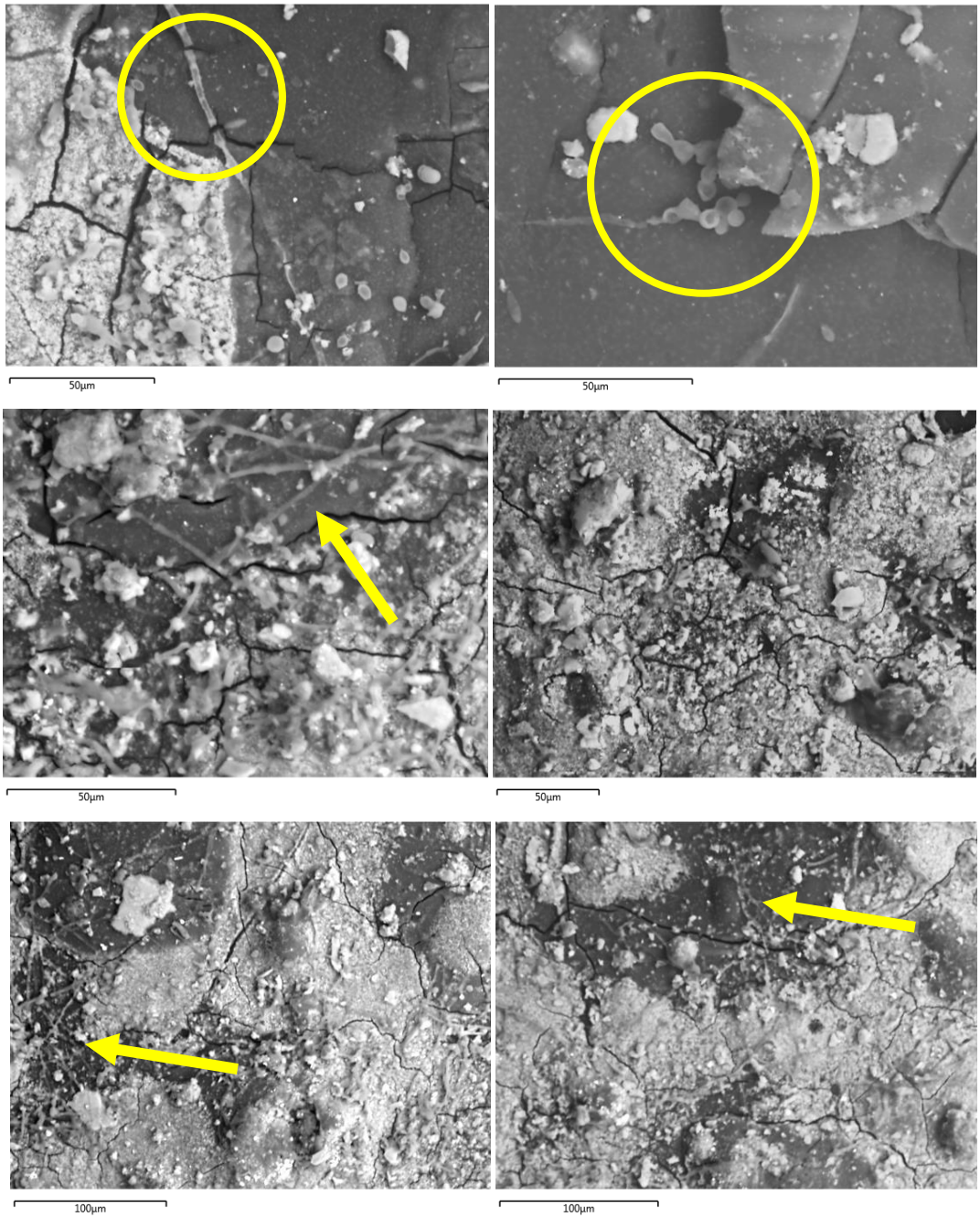

Figure 16: SEM BSD images of the apple sample on the painted surface showing hyphae and spores

4.6. EDS characterization

EDS mapping of elements on one area of the same sample (Figure 17) revealed diffused presence of titanium, plausibly as dioxide, widespread industrial white pigment (Figure 18) [31]. Titanium is not present in the black painted areas, and the scarcity of elements normally associated with black

pigments such as iron or manganese, is coherent with the use of carbon black[6] as main dark pigment [31]. Iron is actually located only on some spots and associated with magnesium. Calcium associated with sulfur is significative of calcium sulphate (gypsum), while aluminum, silicon and potassium together could be addressed to aluminosilicate; both are commonly added as filler in industrial varnishes. In fact, aluminosilicates such as micas can be added in metallic industrial colors, so they can be responsible for the silver metallic paint sprayed on the fruit elements of *Teca con Frutta*.

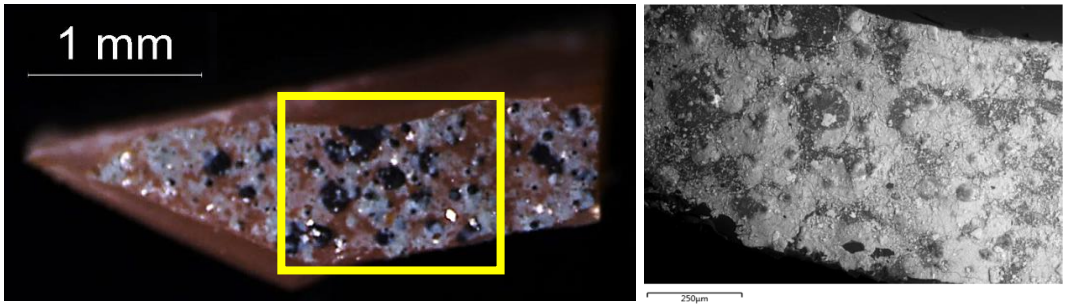

Figure 17: optical microscopy and SEM BSD image of the apple sample. SEM-EDS investigated area is highlighted by a yellow rectangle

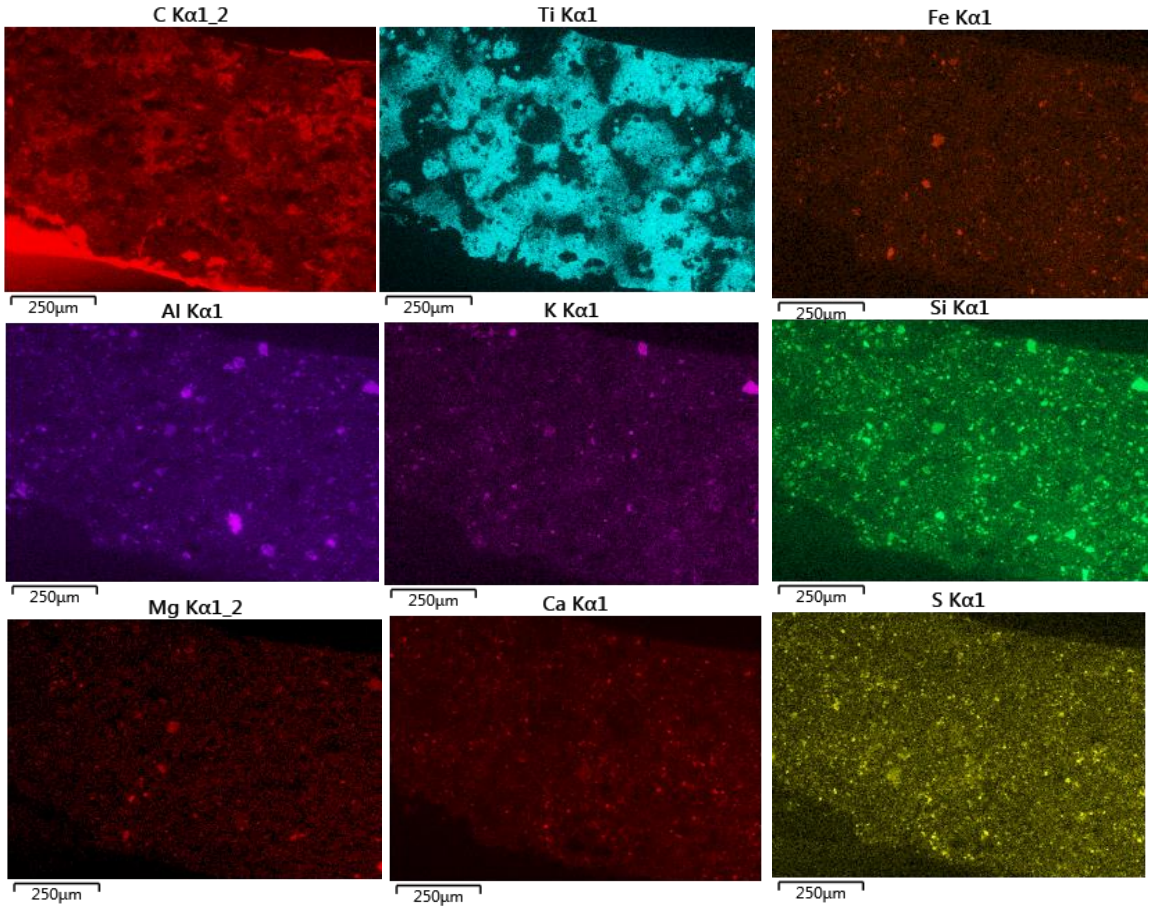

Figure 18: EDS maps of elements on the sample apple

[6] Carbon black is composed up to 99.5% by carbon [31].

4.7. Conclusions

Two samples taken from *Teca con Frutta* were studied to investigate the materials used by the artist and to assess their conservation conditions. *Teca con Frutta* is composed by several fruit plastic object, sewed to the support using a thick wire. Once the objects were secured to the support, the artist sprayed different colors on the whole surface of the artwork. The samples were taken from two different parts of the artwork, and both were covered in different layers of spray paint. The support polymer was identified, thanks to FTIR, Raman and DSC analysis, as low-density polyethylene (LDPE). For its branched structure, LDPE is generally more exposed to oxidation phenomena in comparison with the more linear high-density polyethylene. Oxidation signs were observed by the appearance of a complex carbonyl band in the infrared spectrum of both the samples. One of the degradation pathways of polyethylene involves the formation of unsaturation in the polymer chain, however Raman spectroscopy did not show the appearance of C=C related absorptions. DSC analysis allowed to study the degree of crystallinity of the polymer, confirming values coherent with LDPE.

FTIR analysis also highlighted on the external surface of both the samples signals typical of oxalic acids salts. Further observation through scanning electron microscopy discovered diffused presence of fungal elements on both samples. Since infrared spectroscopy revealed the binder of the spray paints is, for all colors, composed by a mixture of nitrocellulose and alkyd resin, it is plausible to assume the biological attack started at the expensed of such paint medium.

The inorganic components of the paint were studied through EDS mapping, recognizing elements typical of industrial spray paints, such as titanium dioxide (used as white pigment) and aluminum silicates (plausibly clay materials) with gypsum (both used as fillers).

This study allowed to obtain data particularly significant for the restoration of *Teca con Frutta*. In fact, the conservators applied an antifungal treatment, using Ketoconazole 1% in deionized water, to clean all the surfaces of the artwork, in order to inhibit further fungal colonization. The assessment of conservative conditions, severely worsened by extended oxidation signs, led the conservators to suggest avoiding direct light and high temperatures during the storage and exhibition.

References

[1] J. Grdadolnik, "ATR-FTIR spectroscopy: Its advantages and limitations," *Acta Chim. Slov.*, vol. 49, no. 3, pp. 631–642, 2002.

[2] R. M. Silverstein and G. C. Bassler, *Spectrometric identification of organic compounds*, vol. 39, no. 11. 1962.

[3] H. Lobo and J. V. Bonilla, *Handbook of plastics analysis*. Marcel Dekker, 2003.

[4] J. H. Stoner, "Conservation of Easel Paintings," *Conserv. Easel Paint.*, 2013.

[5] W. K. Moffett, "Cellulose nitrate coating compositions," US2498091A, 14-Jun-1947.

[6] R. Ploeger and O. Chiantore, "Characterization and Stability Issues of Artists' Alkyd Paints," *New*, no. November 2010, pp. 89–95, 2013.

[7] M. Gardette *et al.*, "Photo- and thermal-oxidation of polyethylene: Comparison of mechanisms and influence of unsaturation content," *Polym. Degrad. Stab.*, vol. 98, no. 11, pp. 2383–2390, Nov. 2013.

[8] J. V. Gulmine and L. Akcelrud, "FTIR characterization of aged XLPE," *Polym. Test.*, vol. 25, no. 7, pp. 932–942, Oct. 2006.

[9] A. A. Cuadri and J. E. Martín-Alfonso, "The effect of thermal and thermo-oxidative degradation conditions on rheological, chemical and thermal properties of HDPE," *Polym. Degrad. Stab.*, vol. 141, pp. 11–18, Jul. 2017.

[10] F. Carrasco, P. Pagès, S. Pascual, and X. Colom, "Artificial aging of high-density polyethylene by ultraviolet irradiation," *Eur. Polym. J.*, vol. 37, no. 7, pp. 1457–1464, 2001.

[11] F. Gugumus, "Physico-chemical aspects of polyethylene processing in an open mixer. Part 32: Formal kinetics of γ-lactone formation from secondary products. Heterogeneous kinetics," *Polym. Degrad. Stab.*, vol. 92, no. 4, pp. 703–719, 2007.

[12] B. Baum, "The Mechanism of Polyethylen Oxidation," vol. 11, no. 6, pp. 1–2, 2008.

[13] J. Zhanning, "The glass transition temprature measurement of nitrocellulose by torsional braid analysis," *Propellants, Explos. Pyrotech.*, vol. 17, no. 1, pp. 34–37, 1992.

[14] T. R. (Thomas R. Crompton and Rapra Technology Limited., *Polymer reference book*. Rapra Technology Ltd, 2006.

[15] F. Rull, A. C. Prieto, J. M. Casado, F. Sobron, and H. G. M. Edwards, "Estimation of crystallinity in polyethylene by Raman spectroscopy," *J. Raman Spectrosc.*, vol. 24, no. 8, pp. 545–550, 1993.

[16] E. Földes, G. Keresztury, M. Iring, and F. Tüdős, "Crystallinity of polyethylene measured by density, DSC, and raman spectroscopy. A comparison," *Die Angew. Makromol. Chemie*, vol. 187, no. 1, pp. 87–99, 1991.

[17] H. Hagemann, R. G. Snyder, A. J. Peacock, and L. Mandelkern, "Quantitative Infrared Methods for the Measurement of Crystallinity and Its Temperature Dependence. Polyethylene," *Macromolecules*, vol. 22, no. 9, pp. 3600–3606, 1989.

[18] M. Satkowski, "The crystallization and morphology of polyethylene and its blends," 1990.

[19] H. Sato *et al.*, “Raman spectra of high-density, low-density, and linear low-density polyethylene pellets and prediction of their physical properties by multivariate data analysis,” *J. Appl. Polym. Sci.*, vol. 86, no. 2, pp. 443–448, 2002.

[20] W. Lin, M. Cossar, V. Dang, and J. Teh, “The application of Raman spectroscopy to three-phase characterization of polyethylene crystallinity,” *Polym. Test.*, vol. 26, no. 6, pp. 814–821, 2007.

[21] B. H. Stuart, “Polymer crystallinity studied using Raman spectroscopy,” *Vib. Spectrosc.*, vol. 10, no. 2, pp. 79–87, 1996.

[22] F. J. Boerio and J. L. Koenig, “Roman scattering in crystalline polyethylene,” *J. Chem. Phys.*, vol. 52, no. 7, pp. 3425–3431, 1970.

[23] G. R. Strobl and W. Hagedorn, “Raman Spectroscopic Method for Determining the Crystallinity of Polyethylene.,” *AIP Conf Proc*, vol. 16, no. 7, pp. 1181–1193, 1978.

[24] C. Conti *et al.*, “Stability and transformation mechanism of weddellite nanocrystals studied by X-ray diffraction and infrared spectroscopy,” *Phys. Chem. Chem. Phys.*, vol. 12, no. 43, p. 14560, Oct. 2010.

[25] L. Rampazzi, A. Andreotti, I. Bonaduce, M. . Colombini, C. Colombo, and L. Toniolo, “Analytical investigation of calcium oxalate films on marble monuments,” *Talanta*, vol. 63, no. 4, pp. 967–977, Jul. 2004.

[26] M. V. Dutton and C. S. Evans, “Oxalate production by fungi: its role in pathogenicity and ecology in the soil environment,” *Can. J. Microbiol.*, vol. 42, no. 9, pp. 881–895, Sep. 1996.

[27] M. T. Madigan, M. T. Madigan, and T. D. Brock, *Brock biology of microorganisms*. Pearson/Benjamin Cummings, 2009.

[28] N. Auer, J. N. Hedger, and C. S. Evans, “Degradation of nitrocellulose by fungi,” *Biodegradation*, vol. 16, no. 3, pp. 229–236, 2005.

[29] A. Pfeil, “Microbial Degradation of Nitrocellulose in a Composting Environment,” *Propellants, Explos. Pyrotech.*, vol. 24, no. 3, pp. 156–158, Jun. 1999.

[30] F. Cappitelli *et al.*, “Investigation of fungal deterioration of synthetic paint binders using vibrational spectroscopic techniques,” *Macromol. Biosci.*, vol. 5, no. 1, pp. 49–57, 2005.

[31] G. Buxbaum and G. Pfaff, *Industrial Inorganic Pigments: Third Edition*. 2005.

[32] M. Gilbert, *Brydson’s Plastics Materials*, William An. 2016.

Chapter 5. Polyurethanes (PURs)

Polyurethanes are a class of synthetic polymers characterized by the presence of the urethane group (R-HN-C(=O)-O-R^{I}) in their structure. Nowadays polyurethanes represent one of the most widespread family of plastics thanks to their intrinsic versatility. Some of the most common applications for these polymers are, in fact, as fibers, soft and hard elastomers, adhesive and binders for varnishes. However, even if the initial development of polyurethanes was focused on the production of fibers and elastomers, at the current time the foams compartment is surely the most important [1].

The synthesis of polyurethanes involves the reaction between polyfunctional isocyanates and polyols through rearrangement polymerization, involving hydrogen transfer according to the following:

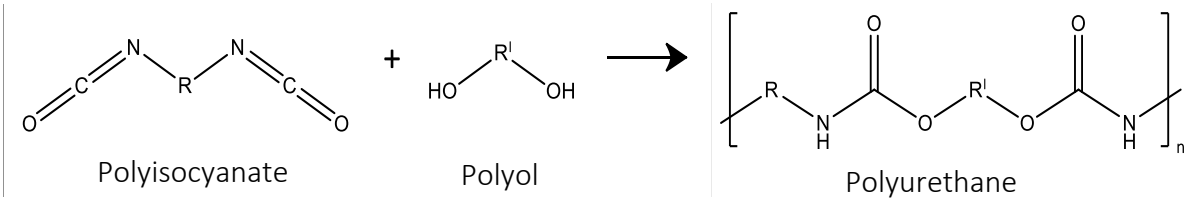

Figure 1: simplified polyurethane synthesis

The synthesis of polyurethane is complex and normally based on different steps: initially the polyisocyanate reacts with the polyol to produce a prepolymer. The prepolymer reacts with more polyol acting as a chain extender to give the final product [1], [2], [3].

5.1. PUR Foams

The first urethanes were synthetized in 1849 by Würtz reacting aliphatic monofunctional isocyanates and alcohols according the following reaction:

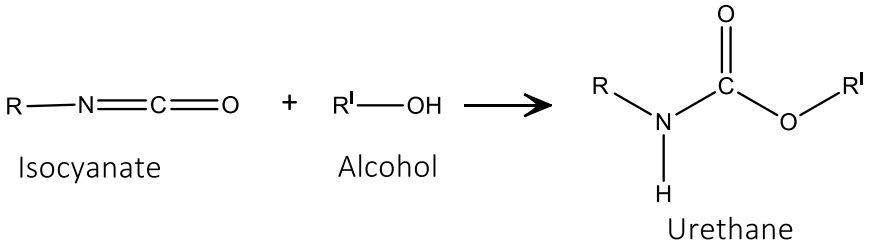

Figure 2: simplified first synthesis of urethanes by Würtz reacting monofunctional isocyanates and alchohols

As mentioned in the introduction, between 1930-40s the whole world was fully living the "Plastic Era", developing and investigating many synthetic polymers such as polystyrene, polyvinyl chloride, polyethylene, polypropylene and polymethylmethacrylate [1]. At the same time, three different research teams[1] were independently studying polyurethanes (reacting polyisocyanates with polyols) and polyureas (using polyisocyanates and aliphatic polyamines).

The first efforts were put mostly in the production of fibers, but in 1942 Zaunbrecher and Barth patented the first flexible polyurethane [3]. The production of this foam involved a one-step reaction, mixing together toluene diisocyanate, polyester based polyol and water (Figure 3). This process allows contemporarily to form the polyurethane and generate gaseous carbon dioxide, but it's highly exothermic and not easily applicable to mass industrial productions.

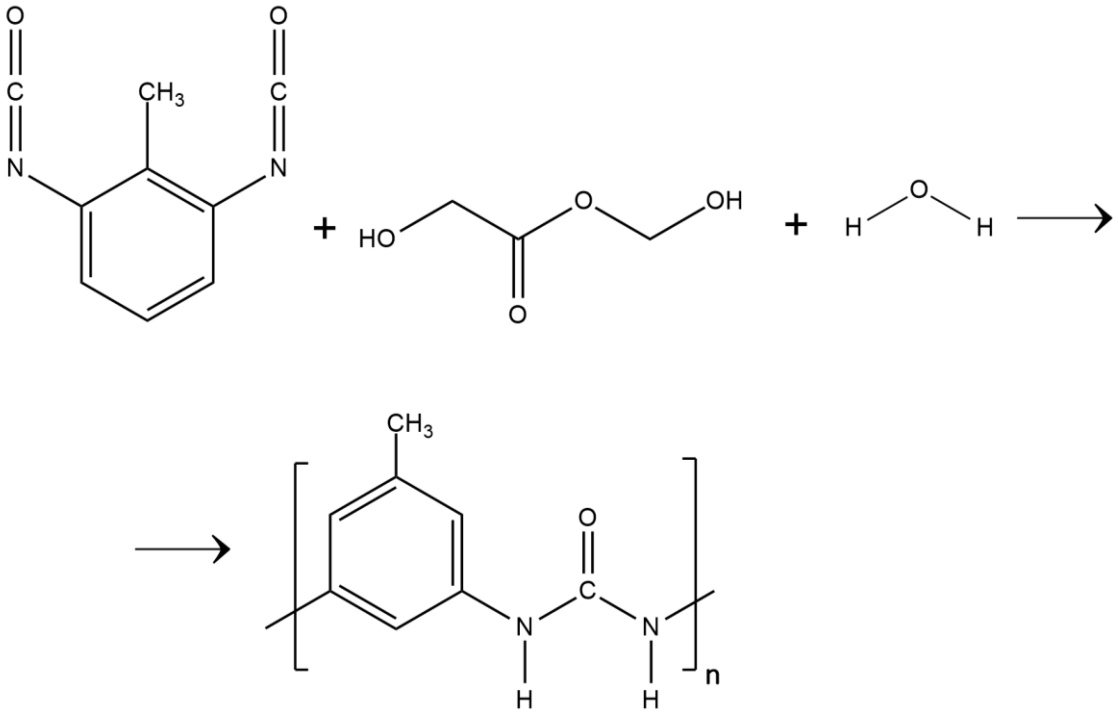

Figure 3: single step process to produce expanded polyurethane

To avoid excessive rise of temperature, often resulting in spontaneous ignitions and fires, a two-step process was introduced. Such pathway involved the formation of a pre-polymer which, after further reaction with water, lead to the formation of the foam. Nowadays, polyurethane foams can be rigid, semi-rigid or flexible and produced with a large variety of

[1] Otto Bayer's team (I.G Farbenindustrie A.G in Germany), T. Hoshino and Y. Iwakura (Tokyo Institute of Technology in Japan) and E.I Dupont Co. In USA

reactants [1]. Polyether polyols are mainly used, in conjunction with molecules such as 1,4-diazabicyclo [2,2,2] octane (DABCO) to accelerate the reaction between secondary OH in polyols and NCO groups in isocyanates [3]. However, polyester polyols or natural oils containing hydroxyls (such as castor oil) may be used too. Silicone based surfactants are also used to promote foaming stability and to increase insulation property in rigid foams. The combination of different processes and reactants leads to the production of 27 commercial forms of expanded polyurethane, making these polymers extremely hard to study as the structural diversities have a great influence on the final products [1].

5.1.1. Isocyanates

An important step in the production of polyurethanes was probably the discovery of the first isocyanates by Würtz in 1849, reacting organic sulphates and cyanic acid salts.

$R_2SO_4 + 2KCNO \rightarrow 2RNCO + K_2SO_4$

Another common reaction is the one described in 1884 by Hentschel, based on the phosgenation of amines and their salts. Nowadays the most widely commercially used polyisocyanates are the following:

- Toluene diisocyanate (TDI)
- Diphenylmethane diisocyanate (MDI)
- Napthylene diisocyanate
- Hexamethylene diisocyanate
- Triphenylmethane-*pp'pp''*-triyl triisocyanate
- p-Phenylene diisocyanate

The major employed are TDI and MDI oligomers Figure 4 [3].

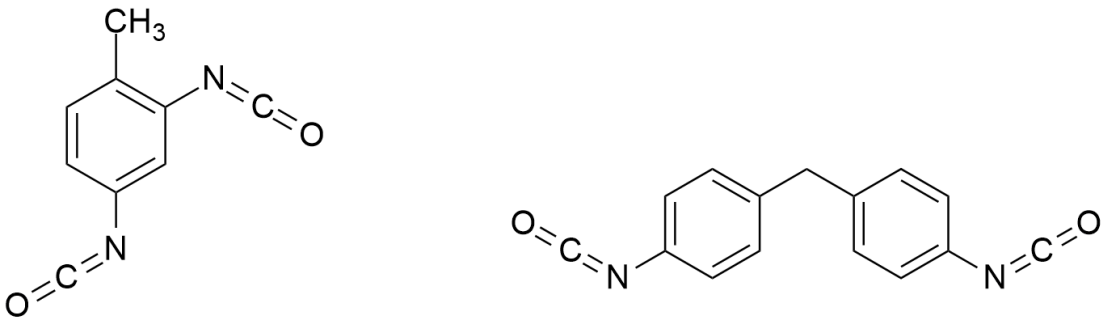

Toluene diisocyanate (TDI) Methylene diphenyl diisocyanate (MDI)

Figure 4: on the left 2,4 toluene diisocyanate, on the right 4,4'-Methylene diphenyl diisocyanate

5.2. Degradation mechanisms

Polyurethanes are usually described as a repeating sequence composed by a hard (derived from the starting isocyanate) and a soft segment (from the polyols used during synthesis and chain extension) [2]. Such a complex structure may be affected by different degradation phenomena interesting each segment of the polymeric chain [4].

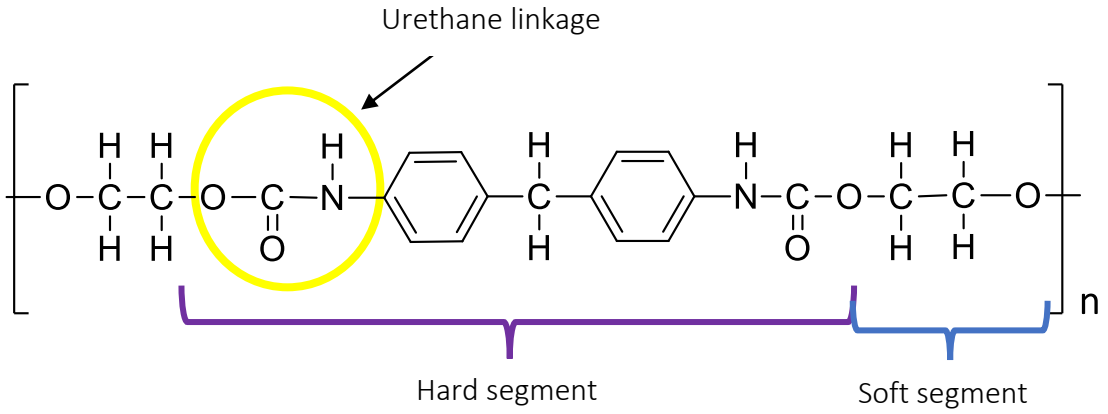

Figure 5: simplified molecular structure of a polyurethane

5.2.1. Urethane segment

Both polyurethanes based on TDI and MDI when exposed to light, decompose to some extent, following photo-Fries rearrangement[2], forming amines and aminobenzoates (both ortho and para substituted) [4].

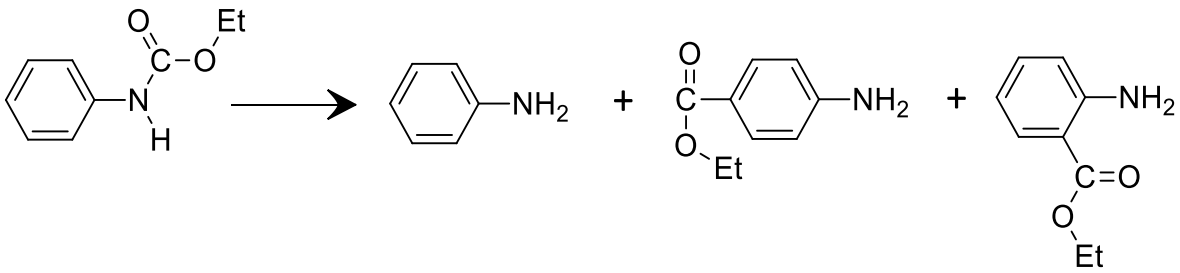

Figure 6: simplified photo-Fries rearrangement

[2] IUPAC golden book definition of photo-Fries rearrangement: A photorearrangement of aryl or acyl esters to give the [1,3]-rearranged product (as well as the [1,5]-rearranged product)
PAC, 1996, 68, 2223 (Glossary of terms used in photochemistry (IUPAC Recommendations 1996)) on page 2261

Beachell & Chang [5] suggested a further step, leading to the formation of azo compounds and water from coupling of aminobenzoates in presence of oxygen.

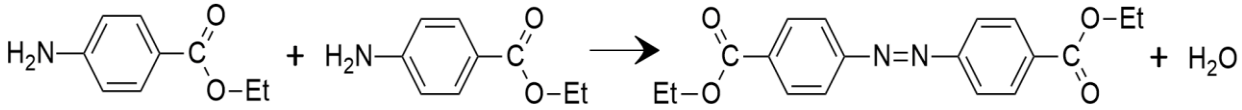

Figure 7: coupling mechanism suggested by Beachell and Chang

These mechanisms are able to explain the progressive yellowing and discolouration of aromatic polyurethanes, considering the high delocalization of π electrons in azo compounds. Schollenberger [6] [7] identified another possible photo-oxidation mechanism, which might be responsible for color changes, involving the formation of quinones-imides moieties according to:

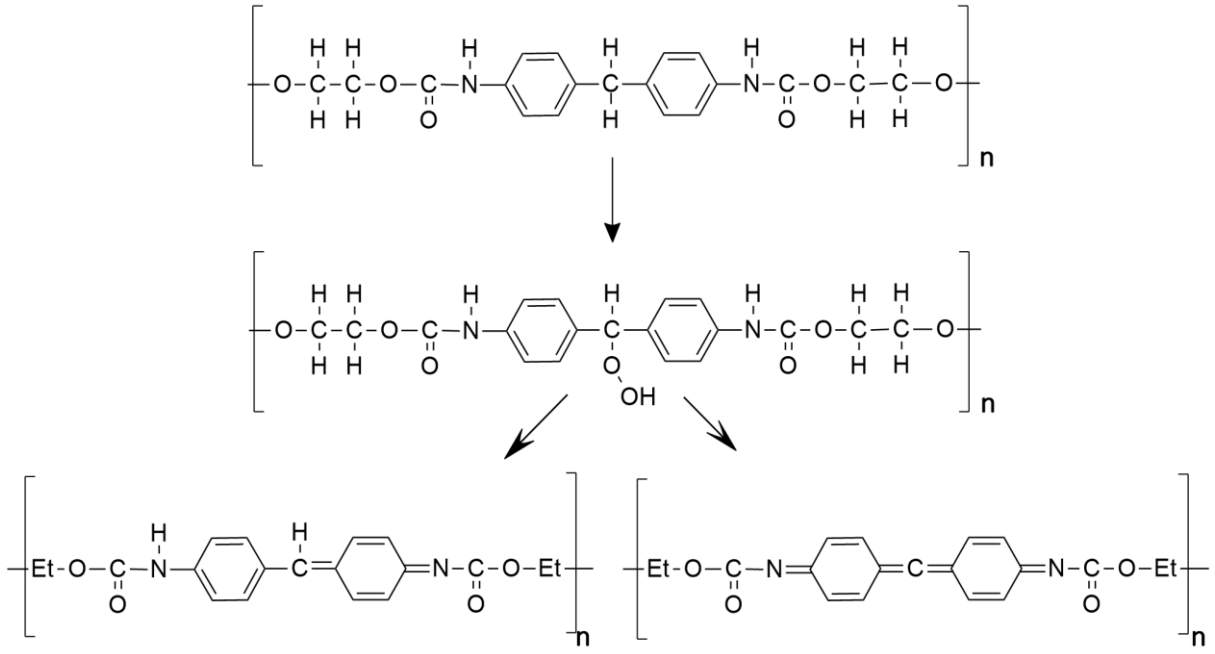

Figure 8: mechanism of formation of quinone imides suggested by Schollenberger

5.2.2. Polyol segment

Polyols may be interested by different degradation pathways according to the chemical nature of them. Once part of the polymeric chain, polyether polyols are usually affected by oxidation while polyester polyols are more prone to undergo hydrolysis [4] according to:

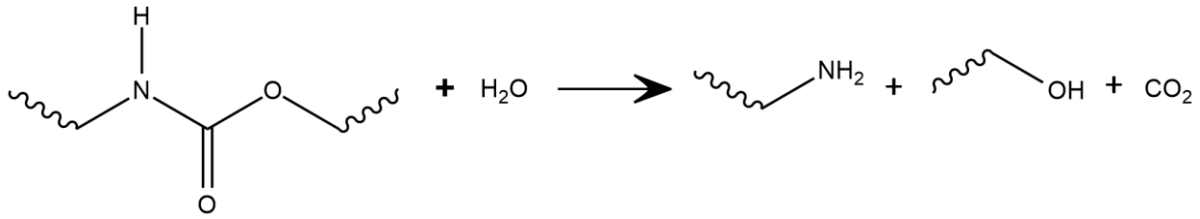

Figure 9: hydrolysis mechanism for polyester polyol based PURs

Oxidation of the polyether polyol can follow different mechanisms such as the one reported by Wypich [4].

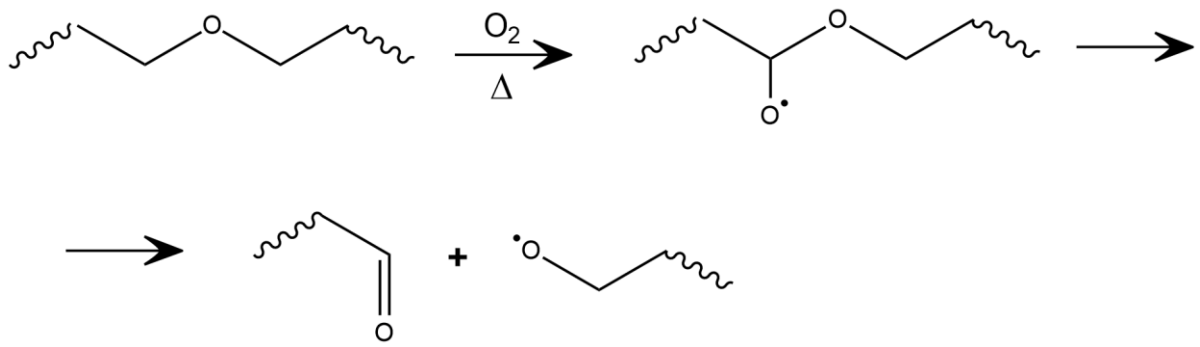

Figure 10: one of the oxidation mechanisms for polyether PURs

Other pathways are the ones described by Mahajan and Gupta [8] regarding oxidative biodegradation and involving hydrogen abstraction from the α-methylene. The reaction frees water and leads to different final products depending on the termination: coupling of polymer macroradicals causes formation of crosslinking (stiffening the material) while further reaction with hydroxyl radicals may produce terminal carboxylic acids and alcohols (fragmenting the polymer chains) (Figure 11).

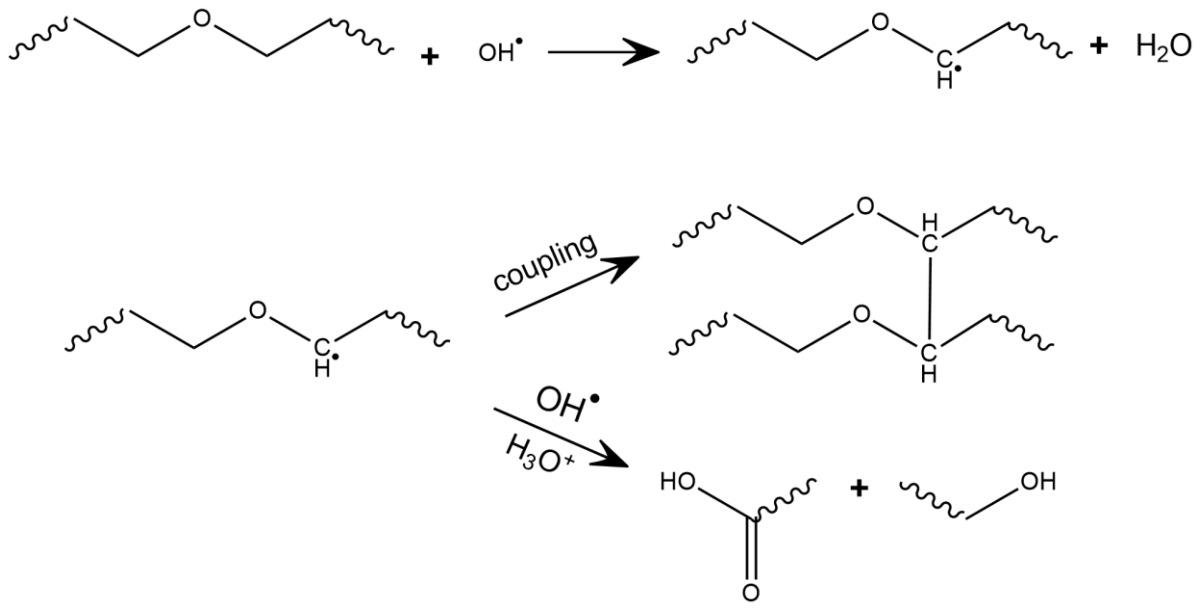

Figure 11: Oxidative mechanism of a polyether PUR soft segment biodegradation.

References

[1] J. A. Brydson, *Plastics materials*. Butterworth-Heinemann, 1999.

[2] T. van Oosten, A. Lorne, and O. Béringuer, *PUR Facts*. 2019.

[3] K. Ashida, *Polyurethane and Related Foams*. 2006.

[4] G. Wypych, *Handbook of material weathering*. .

[5] H. C. Beachell and I. L. Chang, "Photodegradation of urethane model systems," *J. Polym. Sci. Part A-1 Polym. Chem.*, vol. 10, no. 2, pp. 503–520, 1972.

[6] C. S. Schollenberger and F. D. Stewart, "Thermoplastic Urethane Structure and Ultraviolet Stability," *J. Elastoplast.*, vol. 4, no. 4, pp. 294–331, Oct. 1972.

[7] C. S. Schollenberger and F. D. Stewart, "Thermoplastic Polyurethane Hydrolysis Stability," *J. Elastoplast.*, vol. 3, no. 1, pp. 28–56, Jan. 1971.

[8] N. Mahajan and P. Gupta, "New insights into the microbial degradation of polyurethanes," *RSC Adv.*, vol. 5, no. 52, pp. 41839–41854, 2015.

Chapter 6. Piero Gilardi, two artworks

6.1. *La Grotta*, 1981

La Grotta ("*The Cave*") is an installation conserved at the Modern art museum of Bologna (MAMBo) and as the name suggests, represents a cave. As other *Nature Carpets*, the artist reproduced nature elements such as stone, grass and soil using foam rubber and paint.

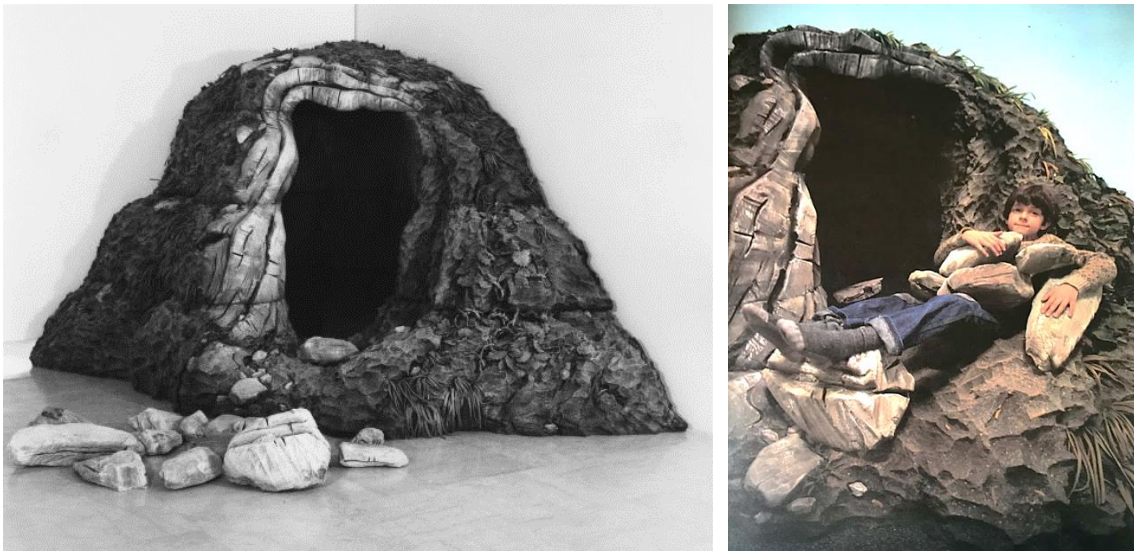

Figure 1: "La Grotta" in 1984

The artwork was meant to offer a complete sensory experience, not merely for eyes but allowing the visitor to touch it or, as the kid visible in Figure 1, to lay on it. In 1987, returning from an exposition, the artwork showed important signs of degradation, loss of the paint in the 60% of the total surface and missing parts in the foam rubber core. Two years later the artist decided to restore *La Grotta* reintegrating the lost vegetal elements, retouching the external paint layer and recommending not to expose the artwork to direct sunlight, as he was conscious of the damage caused by ultraviolet radiation.

The installation was originally conceived to be formed by thirteen blocks of rubber foam, five of which were supposed to compose the principal structure of the cave while the remaining formed small stones meant to be placed in front of the entrance as movable decorations. This work focused on the upper unit, visible in Figure 2, which is approximately 0.47 m height, 1.41 m wide, 1.26 m long.

This unit was meant to be placed in a corner of the exposition room. The whole installation underwent serious physical damages not only due to the public fruition but also to the peculiar association of soft rubber foam and thick paint layer. In fact, the external layer showed extensive cracking (Figure 3), in particular on the corners and on the bearing surfaces, often slightly dragged to place the artwork.

Figure 2: the upper part of the artwork, object of this study

Figure 3: pictures taken at the beginning of this study to assess the conservation conditions of the artwork

6.2. *Scoglio sonoro interattivo*, 1997

Scoglio sonoro interattivo ("Interactive voiced rock"), today conserved in the Art Museum of Gallarate (MAGA), is an interactive installation, made to resemble a big rock surrounded by smaller units. The artist's design was to offer an enjoyable misunderstanding to the public, representing, once again, something that looks like a natural element but using the soft and malleable textures of flexible paint and foam rubber. The public was encouraged to touch the artwork which is 1.45 x 0.67 x 0.65 m big. In fact, when moved and rolled, the central stone was designed to reproduce the sound of waves breaking on the rocks providing a complete sensorial experience to the auditory.

6.3. Sampling

Some small samples were collected from both the artworks to be analyzed through optical microscopy, micro-FTIR and SEM-EDS. The list of the samples and the provenance are listed in Table 1.

Sample	Provenance (artwork)	Description
1	La Grotta	Erratic fragment of rubber foam
2	La Grotta	Paint layer + rubber foam
3	Scoglio sonoro interattivo	Rubber foam
4	Scoglio sonoro interattivo	Paint layer + rubber foam
5	Scoglio sonoro interattivo	Paint layer + rubber foam
6	Scoglio sonoro interattivo	Paint layer + rubber foam

Table 1: samples taken from both artworks

The first sample (1) is a rubber foam fallen vegetal element, visible in Figure 4 highlighted by a yellow circle, while the second sample (2) is a fragment containing both the paint layer and the rubber foam. Considering the short lifespan expanded foams often exhibit, and the severe chemical transformation they usually undergo [1], [2] we selected the sample (2) to characterize the rubber foam composing *La Grotta*, and the sample (1) to look for possible structural alterations. As a matter of fact, being the sample (1) originally located on the external surface of the installation, the rubber foam was exposed to environmental conditions more than the one in the sample (2), protected by the paint layer.

Other three samples (Figure 5) were collected from *Scoglio sonoro interattivo*, again with the purpose of characterizing both the rubber foam and the paint layer.

Figure 4: sampling from "La Grotta", sampling points are highlighted by yellow circles

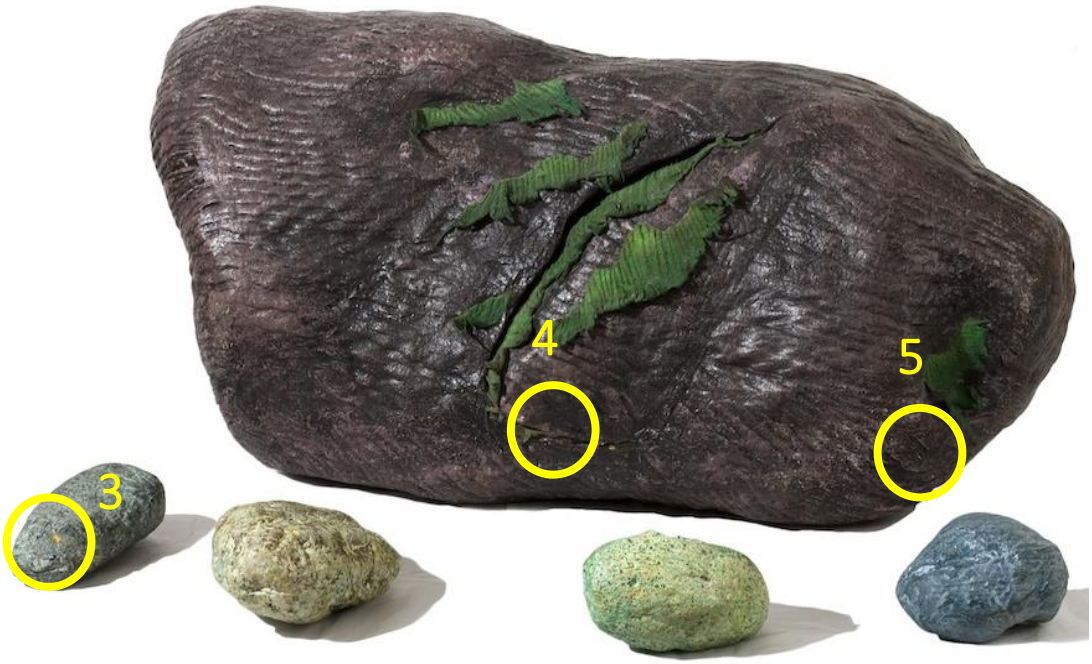

Figure 5: "Scoglio sonoro interattivo", the sampling points are highlighted by yellow circles

6.4. Expanded polymer characterization

6.4.1. La Grotta

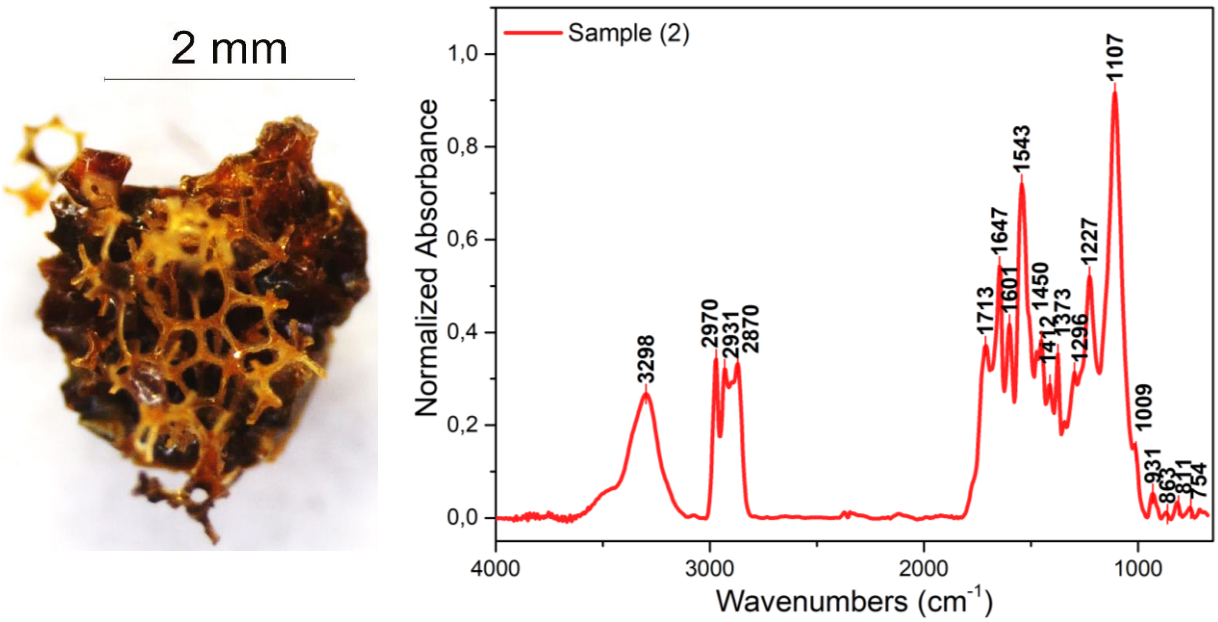

Figure 6: on the left sample (2) from la Grotta. On the right FTIR spectrum of the rubber foam from sample (2)

The infrared spectrum (Figure 6) of the rubber foam from the bulk sample (2) shows typical features of an aromatic expanded polyurethane (Figure 6), in particular the (non-hydrogen bonded) N-H stretching at 3298 cm^{-1}, the O=C-N-H stretching at 1543 cm^{-1}, the aromatic C=C stretching at 1601 cm^{-1} and the bending modes of aromatic C-H at 863, 811 and 754 cm^{-1} [3], [4]. The strong absorption at 1107 cm^{-1}, due to asymmetric C-O-C stretching, is typical of polyurethanes produced from polyether-based polyols [5], [6]. The nature of the reactants used during the preparation of the polymer plays an important role in the resistance of the final product against environmental factors. For example, polyurethanes produced using aromatic polyisocyanates are particularly prone to yellowing, undergoing photo-Fries rearrangement and forming extended conjugated systems, hence colored [7]. At the same time aromatic polyurethanes are normally

Wavenumber (cm^{-1})	Assignment
3298	ν N-H
2970	ν C-H (CH_3)
2931	ν C-H (CH_2)
2870	ν C-H (CH_3)
1713	ν C=O (urethane)
1647	ν C=O (urea)
1601	C=C aromatic
1543	ν O=C-N-H
1450	δ C-H (CH_3)
1412	trimer band isocyanate
1373	δ C-H (CH_3)
1296	ν C-N
1227	ν C-N
1107	ν C-O-C
1009	ν C-O-H
931	ν C-H (CH_3) rocking
863	δ C-H (aromatic ω)
811	δ C-H (aromatic ω)
754	δ C-H (aromatic ω)

Table 2: expanded polyurethane typical IR absorptions

more resistant to chain scission phenomena than aliphatic ones [2]. Finally, polyurethanes containing polyether-based polyols residues are more suitable to undergo radical oxidation than the ones synthetized starting from polyester-based polyols [2], [8].

The sample (1), which appeared inelastic and rigid, was then analyzed via micro-FTIR to study possible degradation signs.

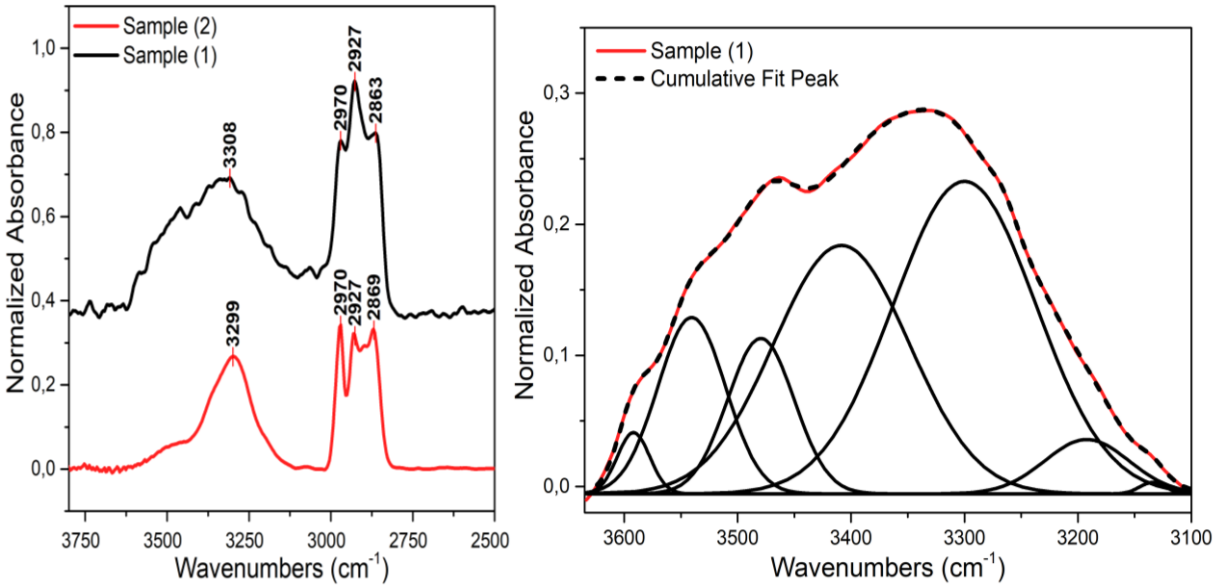

Figure 7: on the left detail on N-H, O-H and C-H stretching spectral region, on the right spectral deconvolution of N-H and O-H stretching modes

Observing the spectral comparison in Figure 7 it is indeed possible to notice a reduction in the signals at 2970 and 2869 cm^{-1} due to CH_3 asymmetrical and symmetrical stretching. At the same time, the absorption at 2927 cm^{-1} (CH_2 asymmetrical stretching) appears increased. These evidences are attributable to crosslinking phenomena of the polymer during ageing [2], [4]. The peak deconvolution in the spectral region at 3600-3100 cm^{-1}, relative both to N-H and O-H stretching modes, shows a complex juxtaposition of different signals, related to the formation of amines (according to photo-Fries mechanism) and hydroxylated photoproducts as result of radical oxidation of the polyether segment [9]. In 1972 Beachell [10] theorized that one possible photochemical process for polyurethanes implies photo-Fries rearrangement forming, in addition to amines, both ortho and para aminoethyl benzoates which, in presence of oxygen, may produce respectively ortho and para substituted azo compounds and water. This mechanism provides a possible explanation for the severe changes in color typical of aromatic expanded polyurethanes.

Observing the fingerprint spectral region (Figure 8), the major changes between the two samples are the shift of the C=O stretching, joined by the appearance of an absorption at 1730 cm^{-1}. The decrease

of the signal at 1650 cm^{-1} may be due to chain scission phenomena of the hard segment, considering that the urea linkage is less stable than the urethane one [2].

The C-O-C stretching at 1107 cm^{-1} appears broadened but not lowered in intensity, suggesting the chain scission phenomena of the polyol segment may not be one of the primary effects of weathering of the polymer. The doublet at 760 and 700 cm^{-1} can be plausibly identified as C-H bending modes of aromatic ring in aminobenzoates [5].

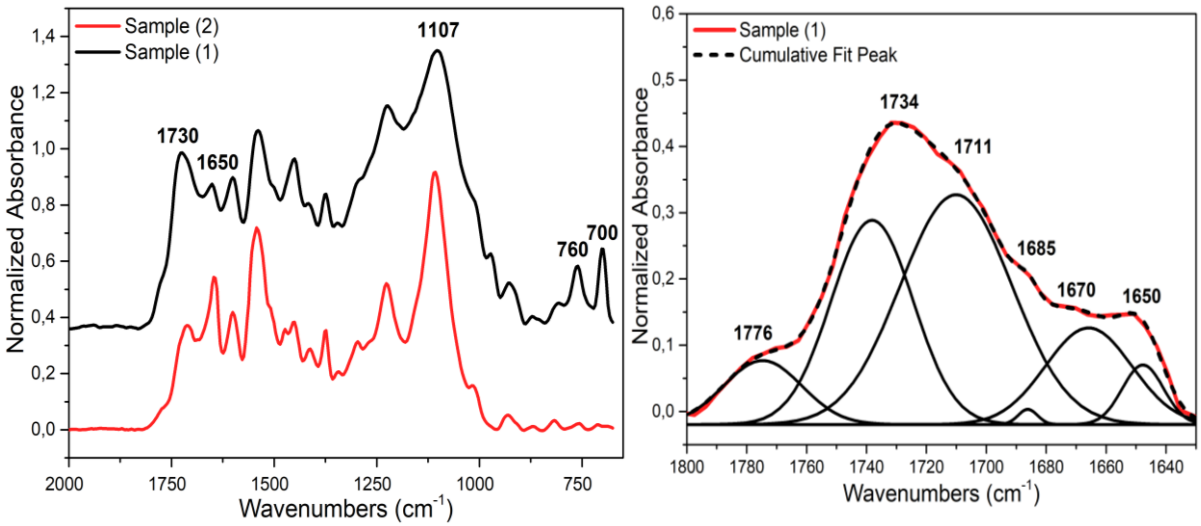

Figure 8:on the left fingerprint comparison between sample (1) and (2), on the right spectral deconvolution of the carbonyl region for sample (1)

Looking with more attention to the carbonyl stretching region (1800-1640 cm^{-1}) is it possible to notice the presence of multiple absorptions (Figure 8). Aside from the urethane C=O stretching at 1711 cm^{-1} and the hydrogen-bond bidentate urea one at 1650 cm^{-1}, characteristic of expanded polyurethane, other signals seem to be due to degradation products. The strong absorption at 1734 cm^{-1} is most likely related to the formation of esters as result of oxidation of the polyol segment. The shoulder at 1685 cm^{-1} could be due to the benzoate carbonyl stretching [10] or to the presence of free urea [4]. The signal at 1670 cm^{-1} may be attributable to hydrogen-bond monodentate urea carbonyl stretching. The shoulder at 1776 cm^{-1}, possibly due to peroxy esters or carboxylic acids [11], is present in both samples.

6.4.2. Scoglio sonoro interattivo

The infrared spectrum registered from the sample (3), collected from an exposed portion of the artwork (visible in Figure 5) shows spectral features very similar to the rubber foam from *La Grotta* (sample (2)). However, some difference between the spectra may be worth a closer observation. The relative intensity of the carbonyl absorptions appears to be different between the two samples: in sample (3) the urethane C=O stretching (1713 cm^{-1}) is more intense than the urea one (1647 cm^{-1}) possibly indicating the less abundant presence of urea linkages following the foaming reaction.

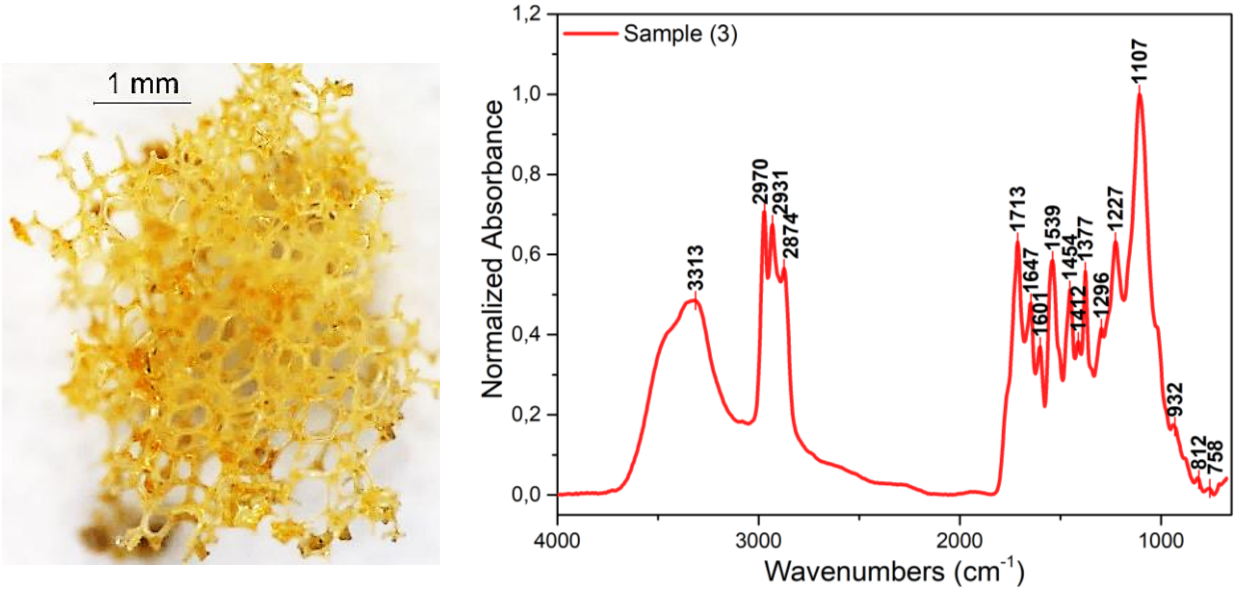

Figure 10: on the left Sample (3), on the right FTIR spectrum of the same.

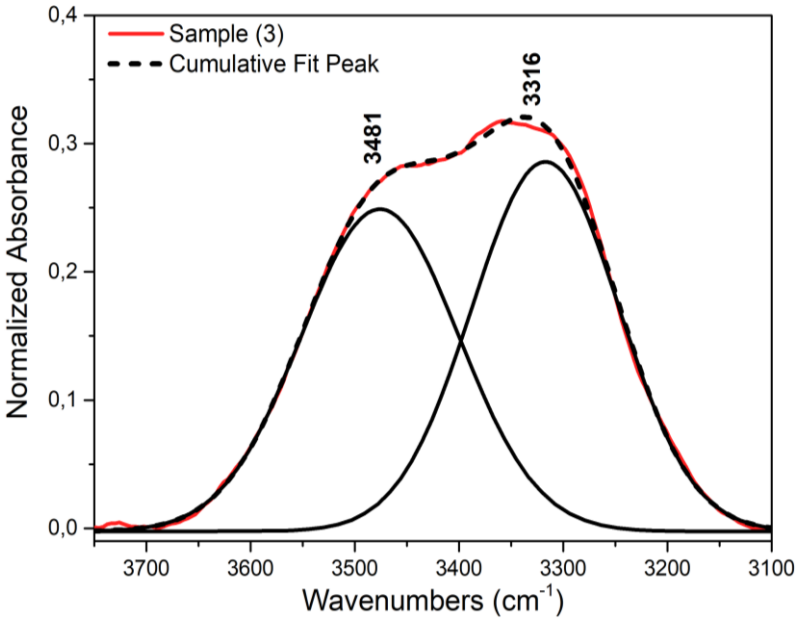

Figure 9: Spectral deconvolution of O-H and N-H stretching region

The spectral region between 3600-3100 cm^{-1} (Figure 10) appears less complex than the sample (1) but still shows the appearance of a shoulder at 3481 cm^{-1}, possibly related to the formation of oxidation products in the polyol residues of the polymer chain.

6.5. Paint Layer characterization

The samples (2), (4) and (5) contained parts of the paint layer which appeared to be extremely rigid (as visible in Figure 13 and Figure 15) and fragile, having lost completely its original flexibility. FTIR analysis showed how the paint layer realized by Gilardi was made using natural rubber (cis-1,4-polyisoprene), which appeared to be extremely degraded (comparison in Figure 11).

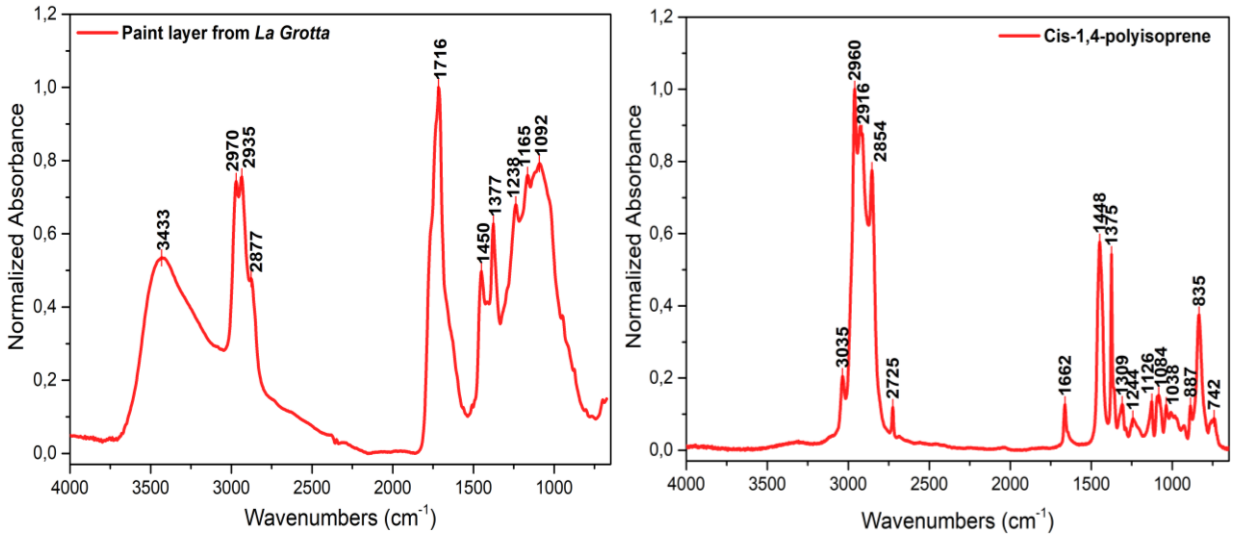

Figure 11: on the left FTIR spectra of the paint layer from the artworks, on the right, Cis-1,4 polyisoprene spectrum

Natural rubber is produced tapping the bark of different trees like *Hevea brasilensis*, *Hancornia speciosa* and *Mumusops globosa* [12]. Polyisoprene, as other natural elastomers, is particularly sensitive to oxidative degradation [12]. Even if the polymer itself is not supposed to absorb UV radiation, the presence of imperfections and impurities in polyisoprene structure induces fast photo-oxidation at environmental conditions [13]. When exposed to ultraviolet radiation the autoxidation proceeds fast through formations of hydroperoxides most likely on methylene groups adjacent to the unsaturation [14]. Hydroperoxides decompose giving free radicals which propagate through the polymer chain, and this process involves the simultaneous decrease of double bonds as the formation of oxidation products increases [11], [15], [16]. Normally, the first stage of the degradative processes of polyisoprene is characterized by a fast decrease of C=C groups, joined by the high rate formation of tertiary hydroperoxides which lead to chain scission phenomena, lowering the molecular weight of the polymer. However, after some time, crosslinking reactions prevail leading to the hardening and stiffening of the rubber [2]. Even though in all the samples analyzed the polymer constituting the paint has been proven to be

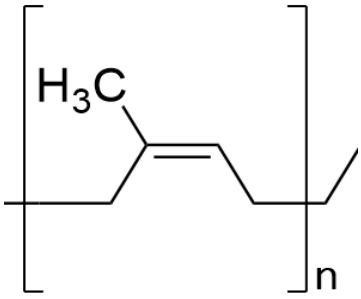

Figure 12: cis-1,4-polyisoprene

the same, portions taken from different artworks, and from different layers of paint, showed slight dissimilarities that may be addressed to different compositions and/or conservation conditions. The sample (2), taken from *La Grotta*, observed through optical microscopy revealed a stratigraphy formed by three different layers (Figure 13), the upper two being opaque while the lower one looking transparent with a glassy appearance. The layers A and B are characterized by same FTIR features, while the layer C exhibits some differences that may be linked to the different state of preservation of the polyisoprene. In fact, according to the more internal position of the layer C, it was reasonable to expect this portion to show less extended signs of degradation.

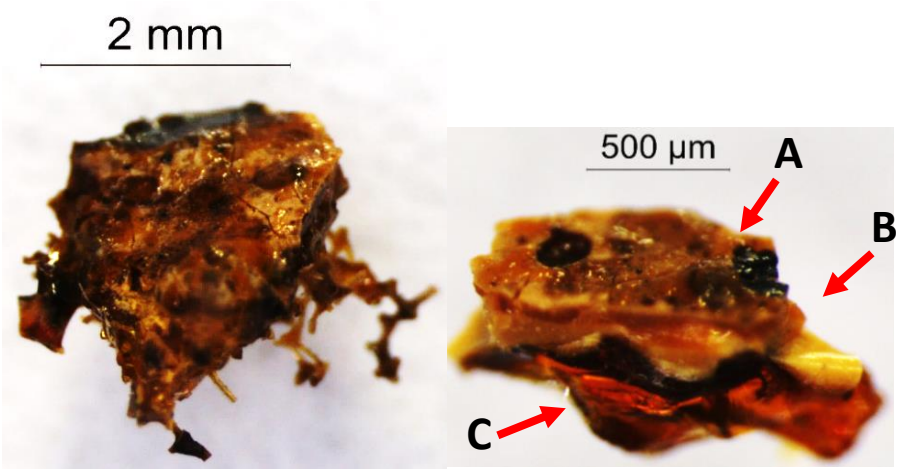

Figure 13: Paint layer sample taken from La Grotta, presenting three different layers

Indeed, in the C-H stretching spectral area, the layer C shows a shoulder at 3060 cm^{-1} due to presence of unsaturation in the polymer structure [3], no longer visible in the more exposed A layer. Moreover, the relative intensities of asymmetric and symmetric stretching of methylene (2935 cm^{-1} and 2854 cm^{-1}) and methyl (2965 and 2877 cm^{-1}) show an increase in methyl absorptions in the layer C, most likely as neo-formed ending groups as a result of chain scission [17].

Observing the fingerprint is possible to notice, in the C layer spectrum, a shoulder at 1640 cm^{-1} (due to H-C=C bending) confirms the presence of residual C=C groups. The carbonyl area shows different absorptions: the C layer is characterized by two distinct strong signals: one at 1733 cm^{-1} and the other at 1715 cm^{-1}. While the band at 1715 cm^{-1}, typical of ketones [3], [12], is present in both layers, the one at 1733 cm^{-1} is visible only in the C layer. This evidence, in conjunction with the peaks at 1240 cm^{-1} (C-C-O stretching) and 1099 cm^{-1} (O-C-C stretching) suggest the formations of esters from carboxylic acids [3], [11]. The shoulder at 1760 cm^{-1}, more evident in layer A, is attributed to C=O stretching of carboxylic acids. In the same layer, the decrease of the band at 1450 cm^{-1} (CH_2 bending)

joined by the increase of the one at 1375 cm^{-1} (CH_3 bending) confirms the chain scission previous evidences. The weak absorption at 874 cm^{-1} in the C layer could be due to the formation of epoxides as oxidation products.

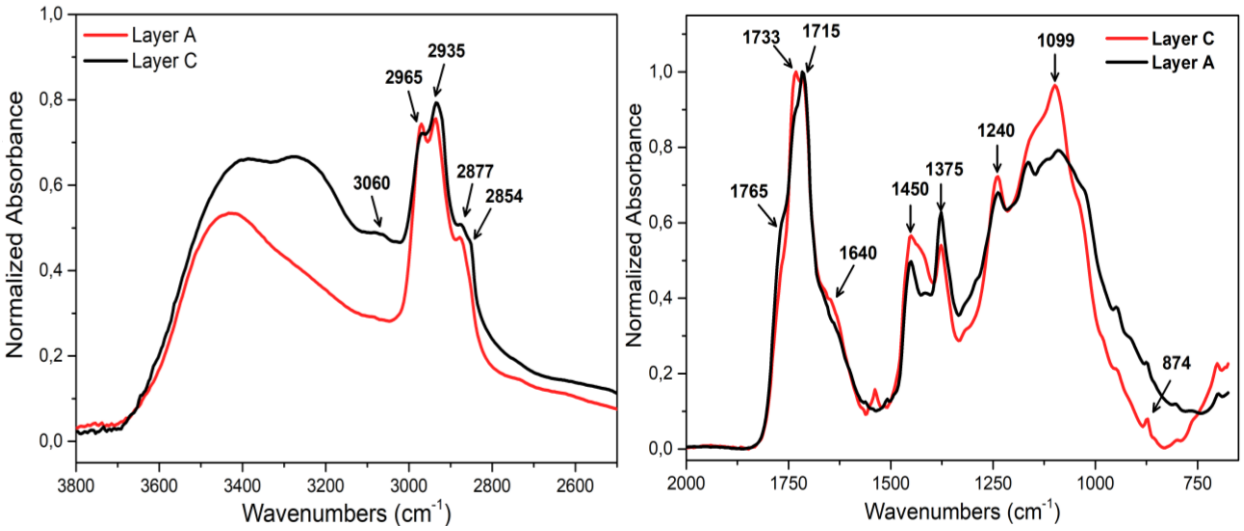

Figure 14: spectral comparisons of layers C and A of the paint layer from La Grotta

The samples taken from "*Scoglio sonoro interattivo*" showed similar spectral features, suggesting the artist used the same products. However, some slight differences are visible comparing the paint layers of the two artworks, as visible in the comparison in Figure 16.

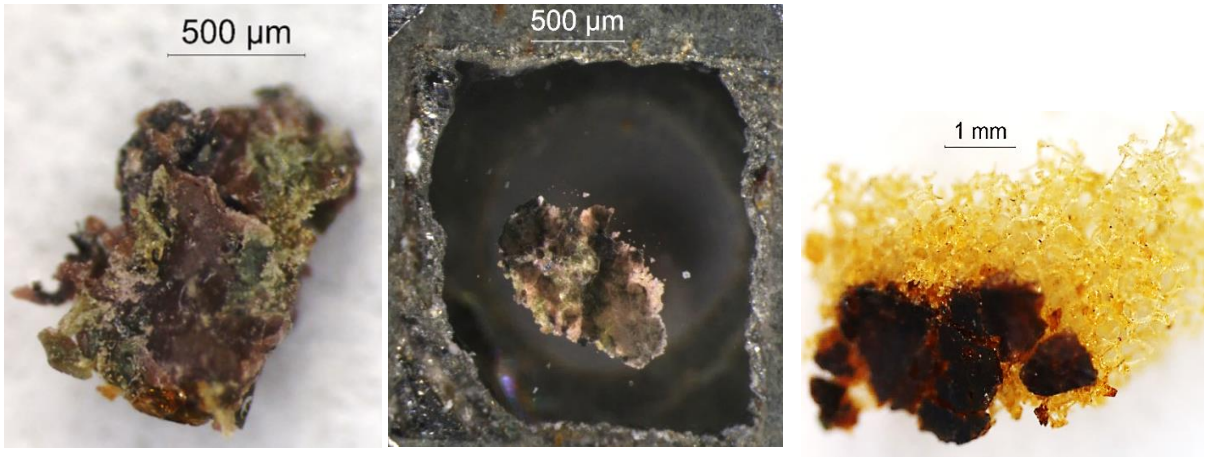

Figure 15: paint layer samples from Scoglio sonoro interattivo

For instance, the peaks at 2514, 877 and 713 cm^{-1}, in conjunction with the shoulder at 1418 cm^{-1} are significative of the presence of calcium carbonate, most likely used as a filler in the paint mixture. Such absorptions have been found only in the samples taken from *Scoglio sonoro interattivo*, suggesting that the artist changed his formula.

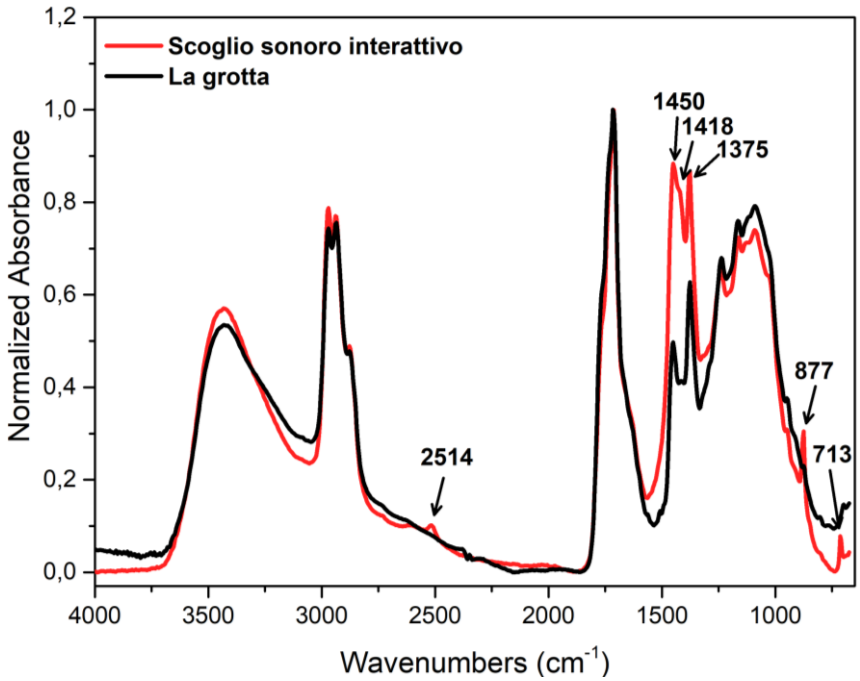

Figure 16: spectral comparison of paint layers taken from both the artworks

6.6. SEM characterization of polyurethane foam

Expanded polyurethanes are generally produced by reacting water with isocyanates, producing instable carbamic acid which easily decomposes giving amines and evolving to volatile carbon dioxide.

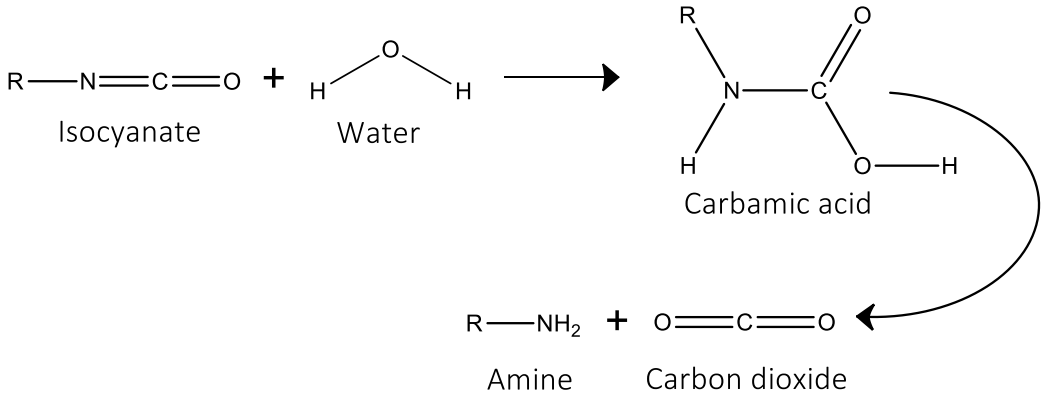

Figure 17: first step in the polyurethanes foaming reaction

The reaction is exothermic, the newly formed amines can react further with other isocyanates producing more carbon dioxide which remains trapped in the structure of the polymer giving rise to the typical cellular structure [18], [1].

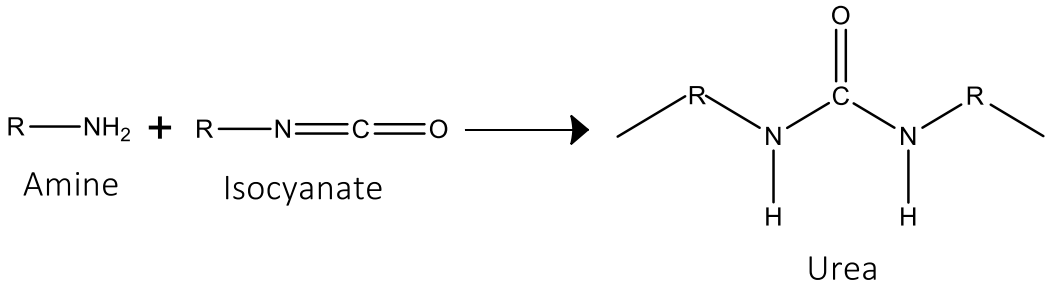

Figure 18: step 2, further reaction of amine with isocyanate to give urea bond

Scanning electron microscopy can provide important information in the study of expanded polymers, expecially in assessing the microstructure of the foam, with higher resolution compared to optical microscopy. As visible in the images below, the sample (1) collected from *La Grotta* appeared extensively yellowed and fragmented under optical microscope. The sample was observed through SEM in variable pressure, methodology which allows to study organic samples without requiring sputtering or any further preparation. Fully functioning expanded polyurethanes should react to compression exhibiting an elastic-perfectly plastic behavior followed by what is usually defined "densification phase" in which the material returns to its starting dimensions [19]. Of course, the behavior of a foam varies according to the microstructure [20] and it is well known how the cellular walls after repeated compression, progressively bend leading to irreversible deformation [21]. As visible in Figure 19, the expanded polyurethane collected from *La Grotta* showed an extensively cracked micro-structure, most likely caused by the degradation phenomena above highlighted by infrared spectroscopy. Both oxidation and crosslinking can indeed be responsible of the progressive stiffening of the polymer, leading to the loss of resilience and elasticity. These processes can finally lead to the complete loss of mechanical properties and the collapse of the microcellular structure [1].

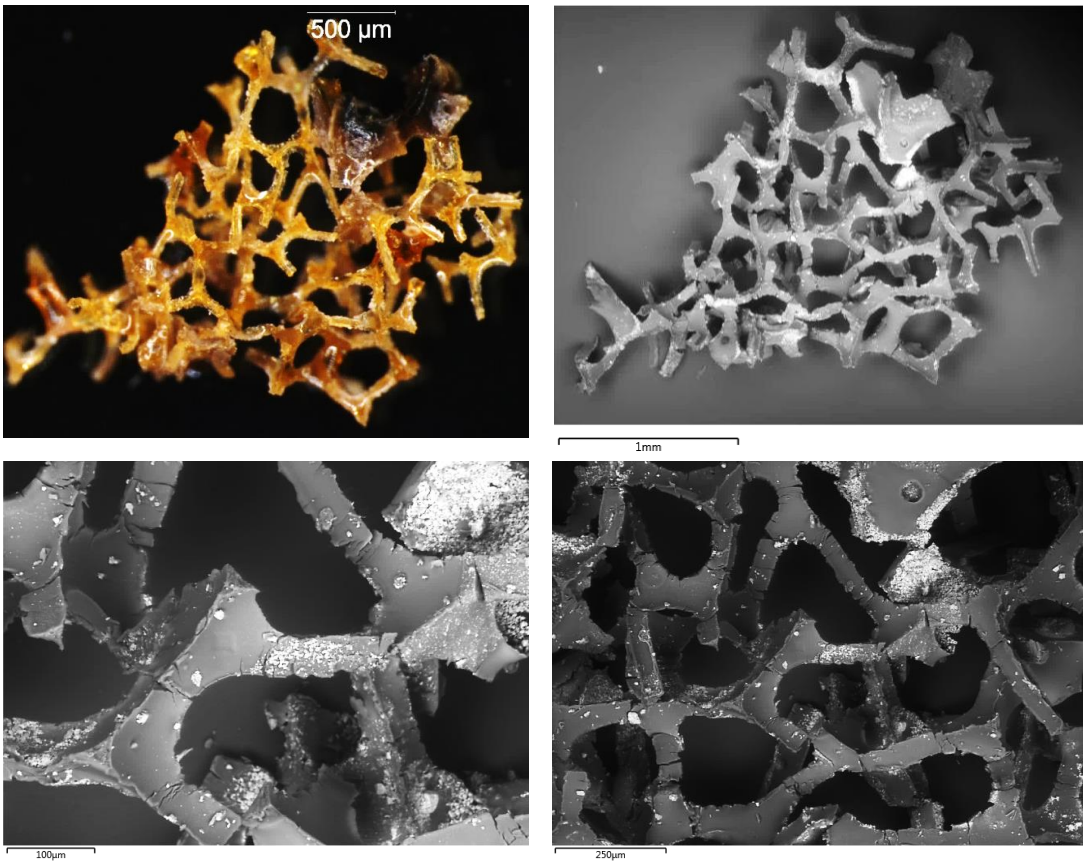

Figure 19: on the left OM image of expanded PUR taken from La Grotta, the others are SEM BDS images of the same sample

6.7. SEM-EDS characterization of the paint layer

The paint layer appeared cracked and extensively degraded, while EDS maps revealed the presence of elements compatible with the use of industrial modern products (Figure 21). Sulfur is uniformly present, reasonably due to vulcanization processes of polyisoprene [22], while titanium and zinc were most likely added as white pigments. Calcium, sparsely associated with sulfur, was plausibly added mostly as carbonate to the mixture. Silicon and aluminum are associated in aluminosilicates. Considering the uniform presence of a top layer of sulfur is it possible to assume the artist used the latex binder to cover the painted surface.

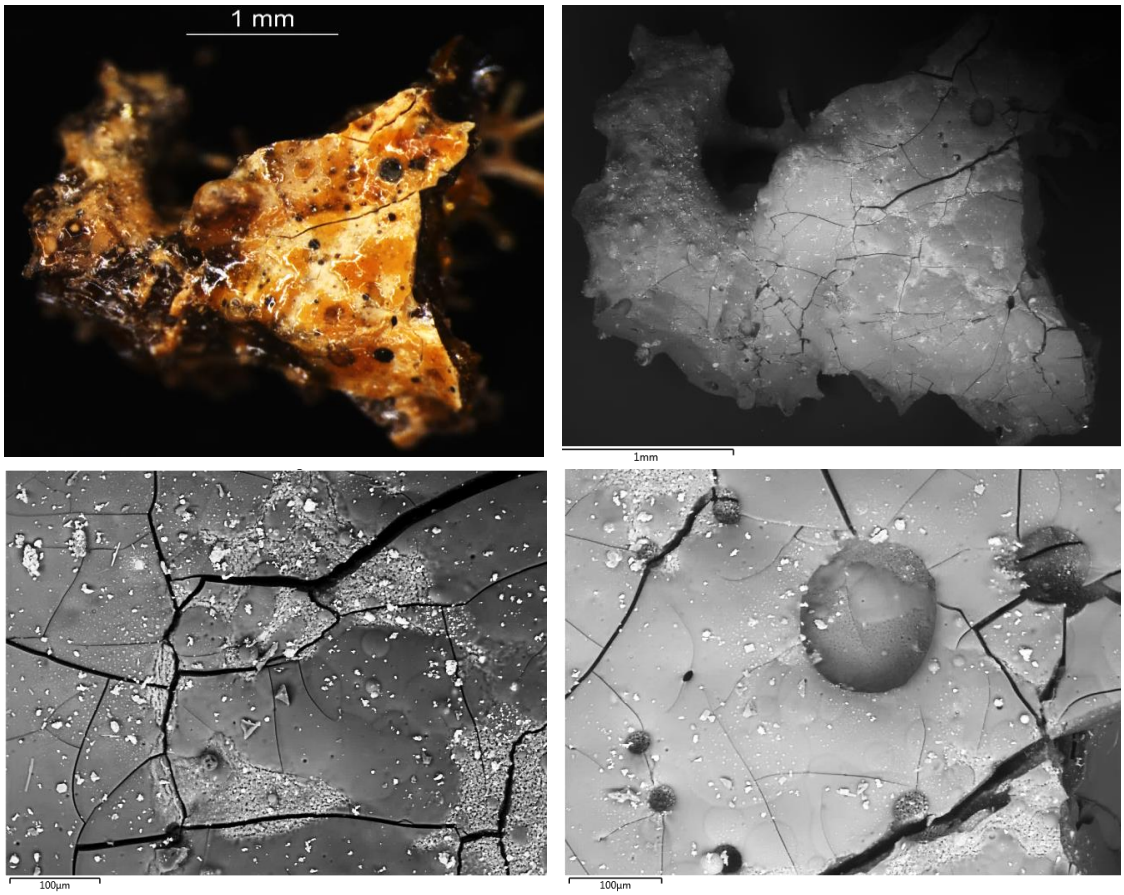

Figure 20: on the left OM image of paint layer taken from La Grotta, the others are SEM BDS images of the same sample

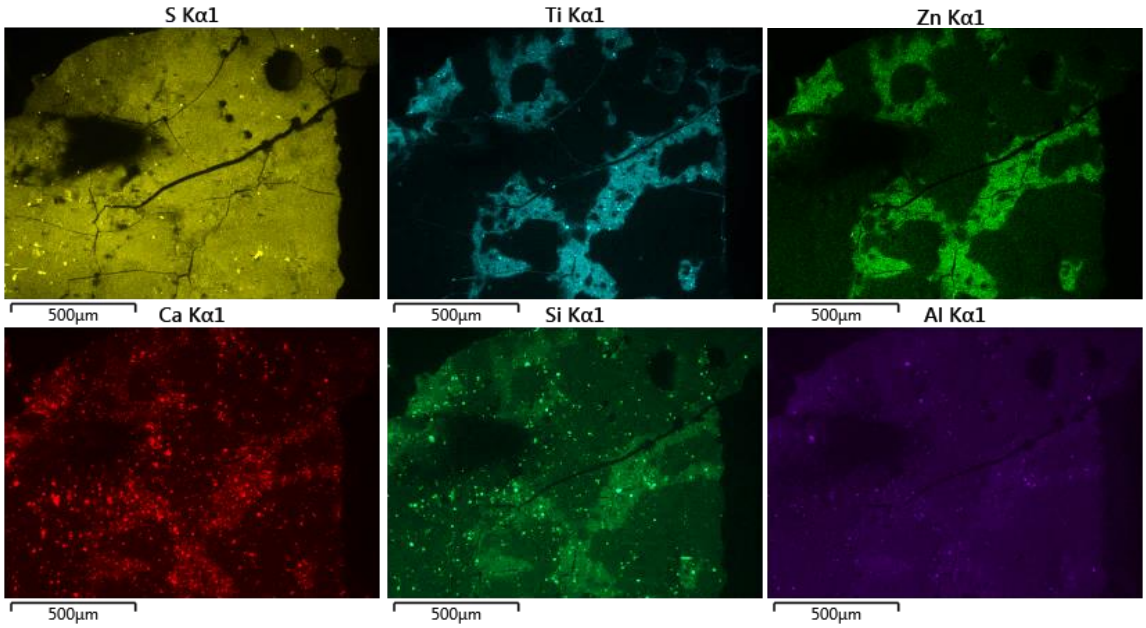

Figure 21: EDS maps of the paint layer from "La Grotta"

6.8. Conclusions

Polyurethanes are complex polymers whose structure is characterized by the presence of a soft segment (residual of the polyols used during the synthesis and as chain extenders) and a hard segment (originated from the polyisocyanate). The reactants used during the synthesis, as well as the chemical pathways followed during the foaming reaction, have great influence in the chemical and physical resistance of the final products. Samples taken from two Piero Gilardi's artworks, La Grotta (1981) and Scoglio Sonoro Interattivo (1997) were studied in order to investigate the materials used by the artist and to assess their conservation conditions. Both La Grotta and Scoglio Sonoro Interattivo are characterized by the use of expanded rubber foam covered by different layers of paint. The materials were chosen by the artist thanks to their extreme flexibility and easy mouldability, which made them perfect to shape natural resembling objects. However, both the rubber foam (characterized as polyether polyurethane) and the paint (recognized as polyisoprene) are materials particularly susceptible of fast degradation. To study the degradation products, a more internal portion of the expanded polyurethane sampled from *La Grotta* (supposedly less degraded) was selected, as well as a more exposed part (plausibly more weathered). FTIR spectra acquired from these two samples were compared, highlighting the presence of complex bands due to ageing phenomena of the rubber foam. In particular, carbonyl bands due to oxidation both of the polyol and the isocyanate residues were observed. Oxidation is one of the causes of yellowing in expanded polyether polyurethane. At the same time, increased methylene stretching (in conjunction with decreased CH_3 stretching) are most likely due to crosslinking phenomena which are plausibly responsible of the hardening of the foam. The paint layers of both artworks were characterized as vulcanized polyisoprene, or natural latex. The presence of C=C groups in the chemical structure of polyisoprene makes the polymer susceptible of extremely fast autoxidation, once exposed to UV radiation. The presence of multiple degradation products made it possible to follow the stages of oxidation studying different micro-layers of the paint identified in a sample taken from *La Grotta*. In particular, the presence of residual C=C groups was detected in the more protected layer, as well as ketone carbonyl band (typical of the early stages of oxidation). As the oxidation proceeds, it is typical to notice disappearance of unsaturation absorptions, while the carbonyl band becomes more complex (as different kind of oxidation products are formed) and the methyl stretching increases (because of chain scissions). All these phenomena are responsible of the dramatic stiffening of polyisoprene, as well as the extreme color change.

References

[1] T. van. Oosten, A. Lorne, and O. Béringuer, *PUR facts : conservation of polyurethane foam in art and design*. .

[2] G. Wypych, *Handbook of material weathering*. .

[3] R. M. Silverstein and G. C. Bassler, *Spectrometric identification of organic compounds*, vol. 39, no. 11. 1962.

[4] J. La Nasa, G. Biale, B. Ferriani, M. P. Colombini, and F. Modugno, "A pyrolysis approach for characterizing and assessing degradation of polyurethane foam in cultural heritage objects," *J. Anal. Appl. Pyrolysis*, vol. 134, no. July, pp. 562–572, 2018.

[5] H. Lobo and J. V. Bonilla, *Handbook of plastics analysis*. Marcel Dekker, 2003.

[6] M. Lazzari, A. Ledo-Suárez, T. López, D. Scalarone, and M. A. López-Quintela, "Plastic matters: an analytical procedure to evaluate the degradability of contemporary works of art," *Anal. Bioanal. Chem.*, vol. 399, no. 9, pp. 2939–2948, Mar. 2011.

[7] D. Rosu, L. Rosu, and C. N. Cascaval, "IR-change and yellowing of polyurethane as a result of UV irradiation," *Polym. Degrad. Stab.*, vol. 94, no. 4, pp. 591–596, 2009.

[8] T. van Oosten, A. Lorne, and O. Béringuer, *PUR Facts*. 2019.

[9] R. P. Singh, N. S. Tomer, and S. V. Bhadraiah, "Photo-oxidation studies on polyurethane coating: Effect of additives on yellowing of polyurethane," *Polym. Degrad. Stab.*, vol. 73, no. 3, pp. 443–446, 2001.

[10] H. C. Beachell and I. L. Chang, "Photodegradation of urethane model systems," *J. Polym. Sci. Part A-1 Polym. Chem.*, vol. 10, no. 2, pp. 503–520, Feb. 1972.

[11] C. Adam, J. Lacoste, and J. Lemaire, "Photo-oxidation of polyisoprene," *Polym. Degrad. Stab.*, vol. 32, no. 1, pp. 51–69, 1991.

[12] K. A. M. Dos Santos, P. A. Z. Suarez, and J. C. Rubim, "Photo-degradation of synthetic and natural polyisoprenes at specific UV radiations," *Polym. Degrad. Stab.*, vol. 90, no. 1, pp. 34–43, 2005.

[13] J. Lacoste, D. J. Carlsson, S. Falicki, and D. M. Wiles, "Polyethylene hydroperoxide decomposition products," *Polym. Degrad. Stab.*, vol. 34, no. 1–3, pp. 309–323, 1991.

[14] J. L. Morand, "Chain Scission in the Oxidation of Polyisoprene," *Rubber Chem. Technol.*, vol. 50, no. 2, pp. 373–396, May 1977.

[15] J. L. Bolland and G. Gee, "Kinetic studies in the chemistry of rubber and related materials. II. The kinetics of oxidation of unconjugated olefins," *Trans. Faraday Soc.*, vol. 42, no. 0, p. 236, Jan. 1946.

[16] J. L. Morand, "Chain Scission in the Oxidation of Polyisoprene.," *Rubber Chemistry and Technology*, vol. 50, no. 2. pp. 373–396, 1977.

[17] K. L. Devries, M. Igarashi, and F. Chao, "Molecular degradation of polymers," *J. Polym. Sci. Polym. Symp.*, vol. 72, no. 1, pp. 111–129, Mar. 2007.

[18] K. Ashida, *Polyurethane and Related Foams*. 2006.

[19] O. Buzzi, S. Fityus, Y. Sasaki, and S. Sloan, "Structure and properties of expanding polyurethane foam in the context of foundation remediation in expansive soil," *Mech. Mater.*, vol. 40, no. 12, pp. 1012–1021, 2008.

[20] P. Barma, M. B. Rhodes, and R. Salovey, "Mechanical properties of particulate-filled polyurethane foams," *J. Appl. Phys.*, vol. 49, no. 10, pp. 4985–4991, Oct. 1978.

[21] S. Youssef, E. Maire, and R. Gaertner, "Finite element modelling of the actual structure of cellular materials determined by X-ray tomography," *Acta Mater.*, vol. 53, no. 3, pp. 719–730, Feb. 2005.

[22] J. A. Brydson, *Plastics materials*. Butterworth-Heinemann, 1999.

Chapter 7. Sante Monachesi, *Composizione Astratta*, 1966

Composizione Astratta (literally “Abstract Composition”), was realized in 1966 by the Futurist Italian artist Sante Monachesi (Macerata, 10 January 1910 – Rome, 28 February 1991).

Figure 1: "Composizione Astratta" and on the left the missing portion from which the samples were taken

Monachesi is famous for his action-sculptures, mostly made of Perspex (polymethylmethacrylate) and rubber foam (polyurethane). Plastic materials were for Monachesi tools to create new shapes, or, for *Composizione Astratta*, to model the conceptual idea of a 3D object. The nucleus of the artwork is made of rubber foam, covered by a layer of white plaster. This external layer was showing evident signs of degradation, such as darkened surface and extended cracks culminating in the missing portion visible in Figure 1.

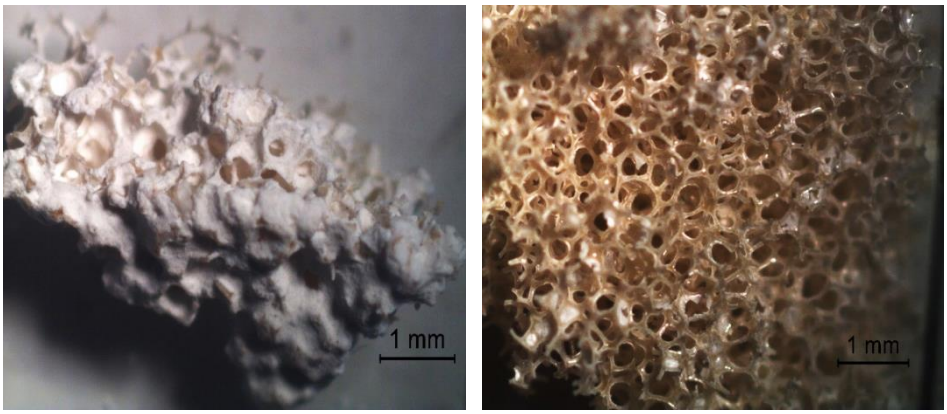

Figure 2: samples taken from "Composizione Astratta", on the left the external layer, on the right the rubber foam

From this *lacuna* two small samples were taken in order to investigate the materials used by the artist both for the internal and the external surfaces of the artwork (Figure 2).

Before the restoration, the lower part of *Composizione Astratta* was showing the results of a bad conservation intervention, performed using a product which most likely darkened after some time, to fix in place a detached part. A small sample of this adhesive was sampled and analyzed via FTIR to better understand the nature of the substance and to help the conservators with the removal of it.

Figure 3: bottom of the artwork, showing the dark adhesive and in the yellow circle the sampling area, on the right a sample of the substance

The samples taken from the artwork are listed in Table 1.

Sample	Provenance (artwork)	Description
1	External layer	External white plaster
2	Rubber foam nucleus	Rubber foam
3	Brown adhesive	Adhesive taken from the bottom

Table 1: samples taken from both artworks

7.1. Materials characterization

7.1.1. Sample 1: External layer

FTIR analysis on the external layer (sample 1 in Figure 4) allowed to recognize the presence of calcium carbonate ($CaCO_3$) by the sharp absorptions at 2514, 1803, 875 and 712 cm^{-1} and the broad one at 1466 cm^{-1} [1]. In addition, the appearance of the peak at 875 cm^{-1} as a singlet allows to recognize calcite above all the calcium carbonate polymorphs [2].

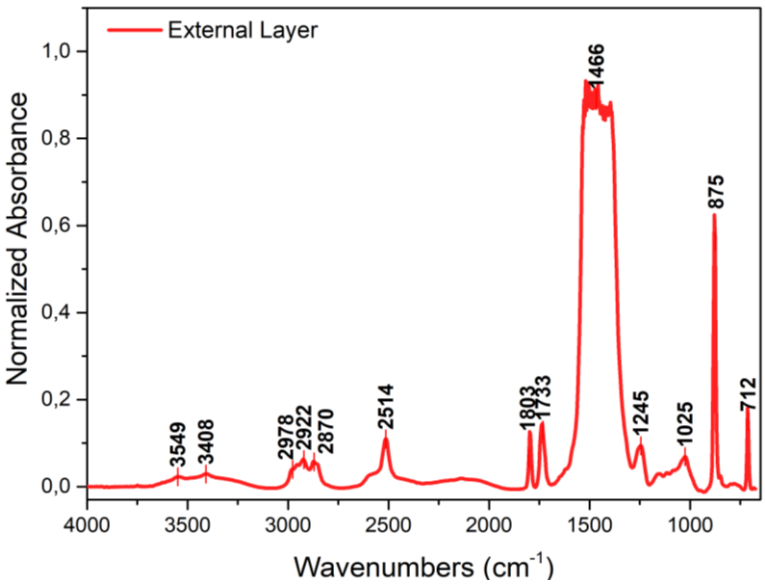

Figure 4: FTIR spectrum of the external layer

The absorptions at 1733 cm^{-1} (C=O stretching), 1245 and 1025 cm^{-1} (C-O stretching) are typical of polyvinyl acetate (PVAc) [3], [4]. Polyvinyl acetate is widely used as paint binder and adhesive, mostly in emulsion [5]. Polyvinyl acetate emulsions are often referred to as "white latex" or "white glue" and usually composed by the monomer vinyl acetate, water, an emulsifier and a polymerization starter, as PVAc can be polymerized while dispersed in water [6]. Other components are stabilizers and preservatives [7]. The carbonate broad absorption centered at 1466 cm^{-1} appears to cover the possible presence of the C-H bending at 1375 cm^{-1} which is useful to identify PVAc. According to these evidences, the artist plausibly mixed together grinded calcium carbonate with PVAc to obtain a plaster with which he covered the internal nucleus.

7.1.2. Sample 2: Rubber foam

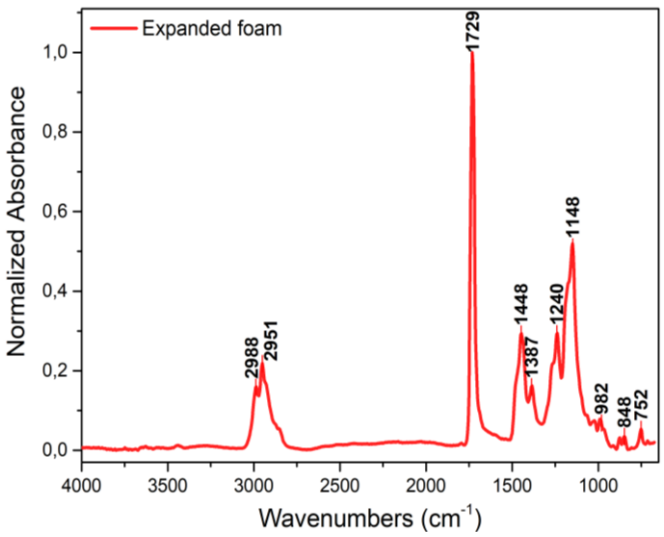

Figure 5: FTIR spectrum of the rubber foam

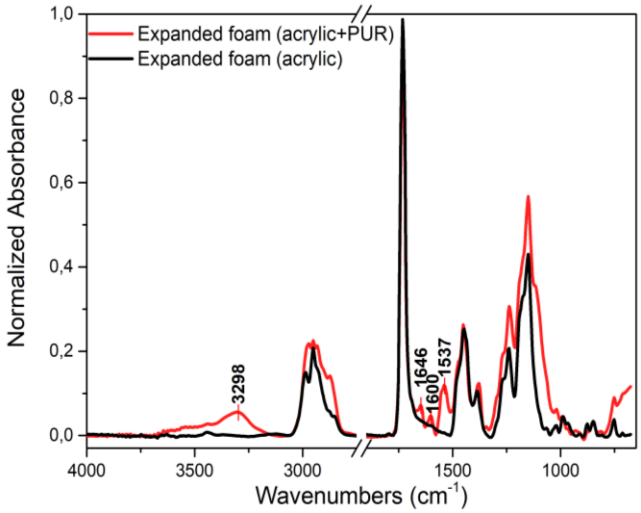

Figure 6: spectral comparison of the first FTIR spectra with a portion containing PUR

The qualitative characterization of the rubber foam core of the artwork (sample 2) through infrared spectroscopy allowed to recognize (Figure 5) vibrational modes of C-H stretching (2988 and 2951 cm^{-1}) and bending (1448 and 1387 cm^{-1}), carbonyl stretching at 1729 cm^{-1}, C-O stretching in the range 1300-1100 cm^{-1} typical of copolymers of ethyl acrylate and methyl methacrylate [8].

Further observations, analyzing a more internal portion of the expanded foam sample, suggested that the rubber foam is an expanded polyurethane covered by a layer of an acrylic polymer, probably used in emulsion by the artist to increase the adhesion of the plaster. Signals typical of aromatic polyurethane foam are the N-H stretching at 3298 cm^{-1}, the urea carbonyl at 1646 cm^{-1}, the C=C stretching of aromatic ring at 1600 cm^{-1} and the stretching of O=C=N-H group at 1537 cm^{-1} (Figure 6).

7.1.3. Sample 3: Brown adhesive

The infrared spectrum of sample 3 shows features specifically associated with proteins such as collagen, typically present in animal glues such as rabbit-skin glue or bone glue. However, the lack of absorptions due to the phosphate group suggest that it is probably not bone glue. Characteristic of proteinaceous adhesives are the absorptions at 3347 cm^{-1} (amide A, mostly due to N-H stretching), the one at 1649 cm^{-1} (amide I, associated with C=O and C-N stretching modes) and the one at 1552 cm^{-1} (amide II, combination of N-H bending and C-N and C-C stretching modes) [9].

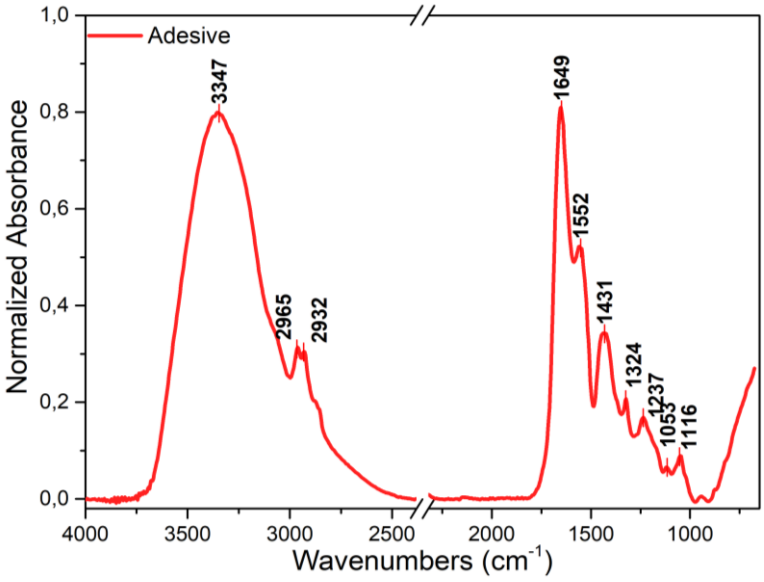

Figure 7: FTIR spectrum of the brown adhesive sampled from the artwork

7.2. Conclusions

Material characterization of the samples taken from *Composizione Astratta* allowed, through FTIR analysis, to recognize in the external layer of the artwork calcium carbonate and polyvinyl acetate. The internal nucleus is made of expanded polyurethane most likely covered by the artist with an acrylic polymer in order to improve the adhesion of the white plaster applied externally. On the bottom side of the artwork it was found a brown substance, part of a previous conservation intervention. FTIR analysis showed signals due to a proteinaceous adhesive, plausibly rabbit glue or skin glue. Such information helped the conservator during the -not easy- removal of this adhesive layer, as this dark substance was initially erroneously recognized as a synthetic adhesive.

References

[1] F. A. Andersen and L. Brecevic, “Infrared spectra of amorphous and crystalline calcium carbonate,” *Acta Chem. Scand*, vol. 45.10, no. 1018-1024., 1991.

[2] M. B. Toffolo, L. Regev, S. Dubernet, Y. Lefrais, and E. Boaretto, “FTIR-Based crystallinity assessment of aragonite-calcite mixtures in archaeological lime binders altered by diagenesis,” *Minerals*, vol. 9, no. 2, 2019.

[3] H. Lobo and J. V. Bonilla, *Handbook of plastics analysis*. Marcel Dekker, 2003.

[4] R. P. D. Amelia, S. Gentile, W. F. Nirode, and L. Huang, “Quantitative Analysis of Copolymers and Blends of Polyvinyl Acetate (PVAc) Using Fourier Transform Infrared Spectroscopy (FTIR) and Elemental Analysis (EA),” *World J. Chem. Educ.*, vol. 4, no. 2, pp. 25–31, 2016.

[5] J. A. Brydson, *Plastics materials*. Butterworth-Heinemann, 1999.

[6] Y. Li and S. Ren, *Building decorative materials*. Woodhead Pub Ltd, 2011.

[7] J. Murphy, *Additives for plastics handbooks*. Elsevier Science Ltd, 2001.

[8] O. Chiantore and M. Lazzari, “Characterization of acrylic resins,” *Int. J. Polym. Anal. Charact.*, vol. 2, no. 4, pp. 395–408, 1996.

[9] S. Krimm and J. Bandekar, “Vibrational Spectroscopy and Conformation of Peptides, Polypeptides, and Proteins,” *Adv. Protein Chem.*, vol. 38, pp. 181–364, Jan. 1986.

Chapter 8. Melamine formaldehyde (MF)

Melamine formaldehyde is part of the family of aminoplastics: thermosetting resins produced reacting amines (or amides) with formaldehyde. The first record about aminoplastics is a patent from 1918 on resinous materials prepared heating urea with formaldehyde to get a viscous material usable as adhesive or as impregnant for fabrics. The production of thermosetting resins based on melamine was patented in 1935 by Henkel. Nowadays, thanks to its superior physical properties and chemical resistance, MF is used for many industrial applications, such as molding compounds, adhesives, coatings, tableware and decorative laminates [1],[2]. MF is synthetized from melamine (1,3,5-Triazine-2,4,6-triamine) and formaldehyde through condensation under alkaline conditions in water or organic solvents (i.e. tetrahydrofuran). The reaction is multi-step: the first involves heating at 80-100°C a mixture of melamine with formaldehyde producing a mixture of methylolmelamines, soluble in water.

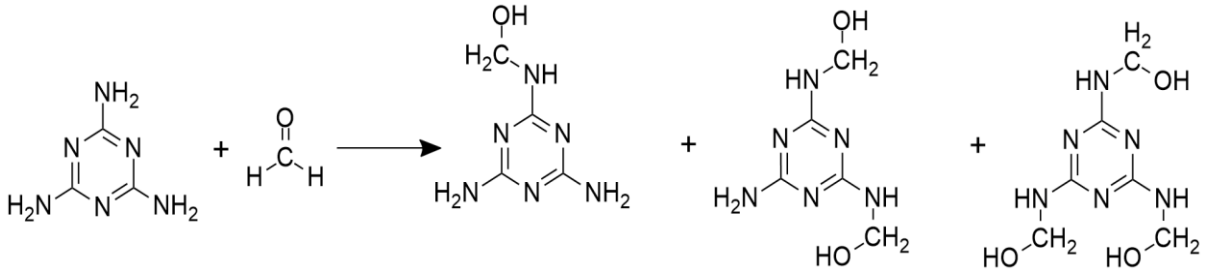

Figure 1: First step in the preparation of MF

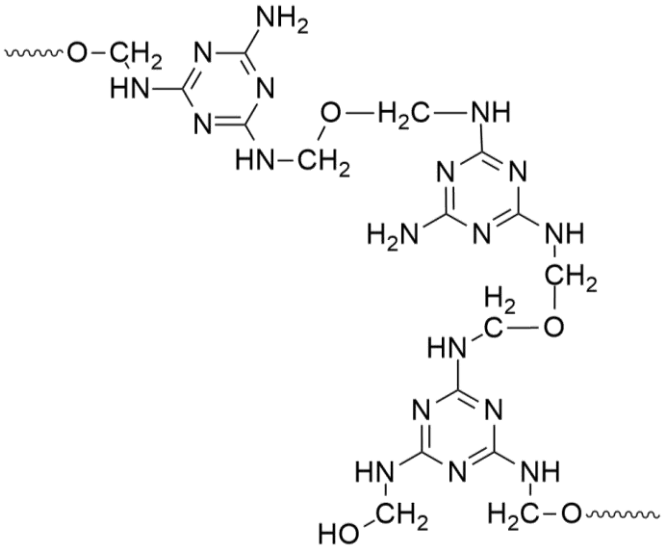

Figure 2: formation of a crosslinked resin after further heating

Changes in reaction conditions and melamine/formaldehyde ratio influences the methylol content of the mixture and the final product. Further heating causes condensation of the methylolmelamines with production of a highly crosslinked resin (Figure 2). Unproper cure of MF may lead to inadequate resistance to hydrolysis and chemical agents [3].

8.1. Decorative laminates

Laminates are composite materials produced combining a liquid thermosetting resin with reinforcing materials and bonding them together through heat and pressure. Plywood is a common example of a laminate, produced combining wood sheets and phenolic resin [4]. Decorative laminates are durable and generally inexpensive materials used to cover furnishings and industrial surfaces. These materials are characterized by high water-repellence as well as superior chemical and physical resistance. Another important feature of decorative laminates is that they can be produced in a wide variety of colors and patterns, often reproducing natural materials such as wood and stones. Nowadays, the most important producer is the Formica Corporation while other important manufacturers are Premark Corporation and DuPont. Commercially available laminates are usually composed by multiple layers of different materials, the bottom one is usually pressed Kraft paper, normally impregnated with phenolic resin; the decorative layer is made of paper and melamine resin and can have different colors and patterns (commonly reproducing natural materials such as stones or wood) while the finish layer is normally composed of paper and clear melamine resin [5].

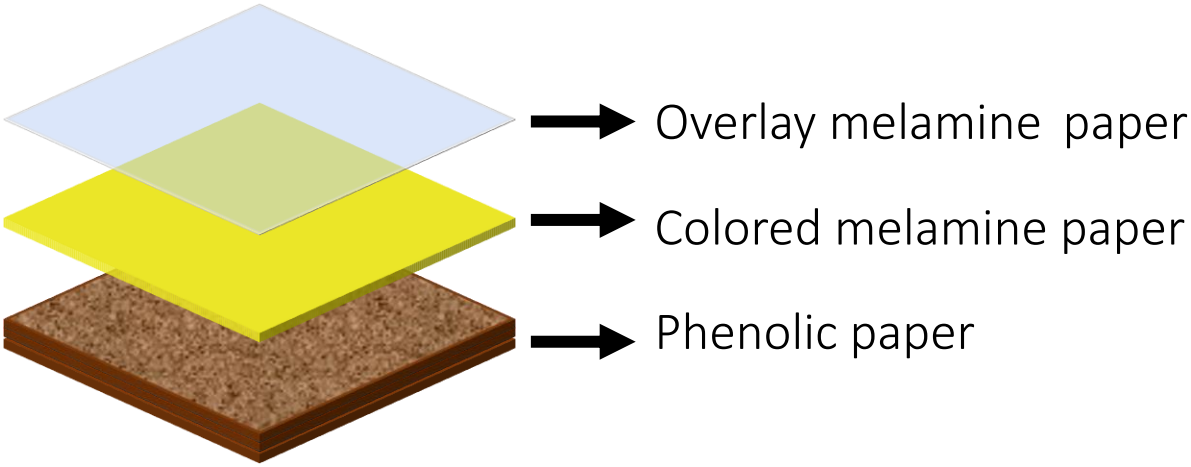

Figure 3: Schematic representation of a decorative laminate

The use of melamine formaldehyde, instead of the dark colored phenolic resins, enables giving to the final products a wide range of color shades [6]. It is possible to distinguish between low-pressure laminates (LPLs) and high-pressure laminates (HPLs) according to some specific manufacture conditions. In the production of decorative laminates based on melamine formaldehyde resin the most common procedure involves the preparation of a low molecular weight prepolymer (a statistical mixture of different oligomers, still soluble in water) to maintain a certain degree of fluidity while impregnating the paper. Such impregnated paper sheets are

dried and stored to be then cured with acid catalysts and sealed through heat and pressure to produce laminates [7].

8.2. Degradation phenomena

MF structural unit can be represented as in Figure 4, although considering that ether bridges can predominate over methylene ones (and vice versa) and residual methylol groups can still be present [8]. The triazine ring has been proven to be particularly stable and resistant, while ether bridges can decompose freeing formaldehyde and giving methylene bridges. Oxidation is said to happen on methylene groups forming carbonyl containing moieties [8].

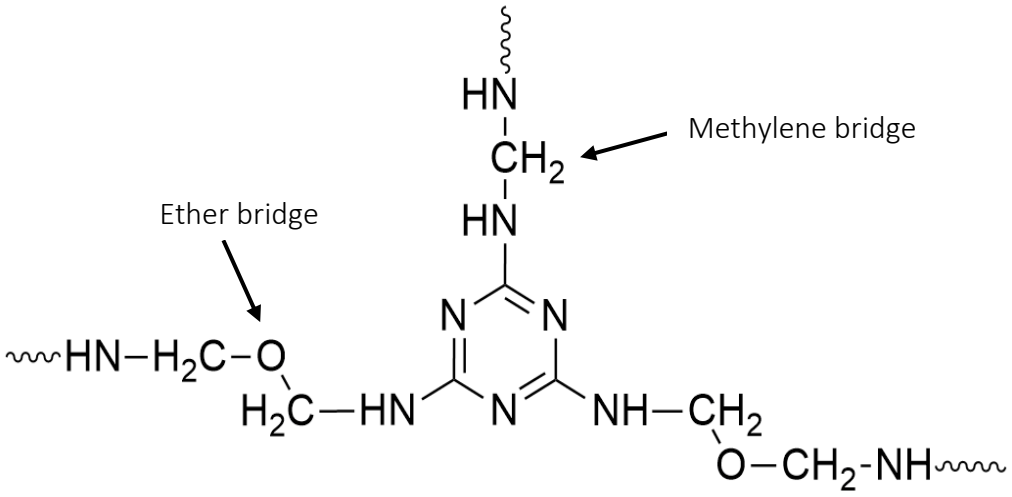

Figure 4: Conventional representation of a MF structural unit

References

[1] J. A. Brydson, *Plastics materials*. Butterworth-Heinemann, 1999.

[2] D. J. Merline, S. Vukusic, and A. A. Abdala, “Melamine formaldehyde: Curing studies and reaction mechanism,” *Polym. J.*, vol. 45, no. 4, pp. 413–419, 2013.

[3] A. Kandelbauer, G. Wuzella, A. Mahendran, I. Taudes, and P. Widsten, “Model-free kinetic analysis of melamine–formaldehyde resin cure,” *Chem. Eng. J.*, vol. 152, no. 2–3, pp. 556–565, Oct. 2009.

[4] C. A. Harper, *Handbook of plastics, elastomers, and composites*. McGraw-Hill, 2002.

[5] S. G. Lewin, *Formica & design : from the counter top to high art*. Rizzoli, 1991.

[6] J. M. G. (John M. G. Cowie and V. (Valeria) Arrighi, *Polymers : chemistry and physics of modern materials*. CRC Press, 2008.

[7] M. Kohlmayr, J. Stultschnik, A. Teischinger, and A. Kandelbauer, “Drying and curing

behaviour of melamine formaldehyde resin impregnated papers," *J. Appl. Polym. Sci.*, vol. 131, no. 3, p. n/a-n/a, Feb. 2014.

[8] W. R. Moore and E. Donnelly, "Thermal degradation of melamine-formaldehyde resins," *J. Appl. Chem.*, vol. 13, no. 12, pp. 537–543, 2007.

[9] J. Murphy, *Additives for plastics handbooks*. Elsevier Science Ltd, 2001.

[10] V. Arjunan, S. Subramanian, and S. Mohan, "Vibrational Spectroscopy Studies on Trans-1,4-Polychloroprene," *Turkish J. Chem.*, vol. 27, no. 4, pp. 423–432, Aug. 2002.

[11] E. Ferrage *et al.*, "Evaluation of talc morphology using FTIR and H/D substitution," *Clay Miner.*, vol. 38, no. 2, pp. 141–150, Jun. 2003.

[12] J. A. Brydson, *Rubber chemistry*. Applied Science Publishers, 1978.

[13] H. Lobo and J. V. Bonilla, *Handbook of plastics analysis*. Marcel Dekker, 2003.

[14] G. Cárdenas, G. Cabrera, E. Taboada, and S. P. Miranda, "Chitin characterization by SEM, FTIR, XRD, and ^{13}C cross polarization/mass angle spinning NMR," *J. Appl. Polym. Sci.*, vol. 93, no. 4, pp. 1876–1885, Aug. 2004.

[15] S. Bajia, R. Sharma, and B. Bajia, "Solid-state microwave synthesis of melamine-formaldehyde resin," *E-Journal Chem.*, vol. 6, no. 1, pp. 120–124, 2009.

[16] K. Fackler, J. S. Stevanic, T. Ters, B. Hinterstoisser, M. Schwanninger, and L. Salmén, "FT-IR imaging microscopy to localise and characterise simultaneous and selective white-rot decay within spruce wood cells," *Holzforschung*, vol. 65, no. 3, pp. 411–420, 2011.

[17] F. Xu, J. Yu, T. Tesso, F. Dowell, and D. Wang, "Qualitative and quantitative analysis of lignocellulosic biomass using infrared techniques: A mini-review," *Appl. Energy*, vol. 104, pp. 801–809, 2013.

[18] A. Pizzi and A. Stephanou, "On the chemistry, behavior, and cure acceleration of phenol–formaldehyde resins under very alkaline conditions," *J. Appl. Polym. Sci.*, vol. 49, no. 12, pp. 2157–2170, Sep. 1993.

[19] X. F. Mo, D. B. Fan, T. F. Qin, and F. X. Chu, "Curing characteristics and adhesion performance of phenol-formaldehyde resins with composite additives," *J. Trop. For. Sci.*, vol. 27, no. 2, pp. 248–254, 2015.

[20] B. Yin and M. Hakkarainen, "Green Plasticizers from Liquefied Wood," *Waste and Biomass Valorization*, vol. 5, no. 4, pp. 651–659, 2014.

[21] M. Farsi, "Thermoplastic Matrix Reinforced with Natural Fibers: A Study on Interfacial Behavior," *Some Crit. Issues Inject. Molding*, no. March 2012, 2012.

[22] V. Hospodarova, E. Singovszka, and N. Stevulova, "Characterization of Cellulosic Fibers by FTIR Spectroscopy for Their Further Implementation to Building Materials," *Am. J. Anal. Chem.*, vol. 09, no. 06, pp. 303–310, 2018.

Chapter 9. Sergio Lombardo, *Supercomponibile ´67*, 1967

Italian artist and psychologist Sergio Lombardo, well known in roman Pop art contexts, is famous for his rejection of artist-as-genius concept, proposing instead to approach to art with a non-artistical point of view. As part of a bigger and more complex project based on "expressive abstinence" *Supercomponibile '67* represents at the best his attitude; as other *Supercomponibili*, this one was meant to be assembled by visitors, without any help from the artist. *Supercomponibile ´67* is, in fact, an installation composed by several wood panels covered in laminates, both red and yellow. As mentioned before, the artist's original design was to leave the position and the whole arrangement of the pieces to the public, although the heavy weight of each of the panel made possible only one public disposal at "*La Salita*" Gallery in Rome (as visible in Figure 1). Since then, the artwork has been conserved as part of the GNAM (*Galleria Nazionale di Arte Moderna*-National Gallery of Modern Art) of Rome collection.

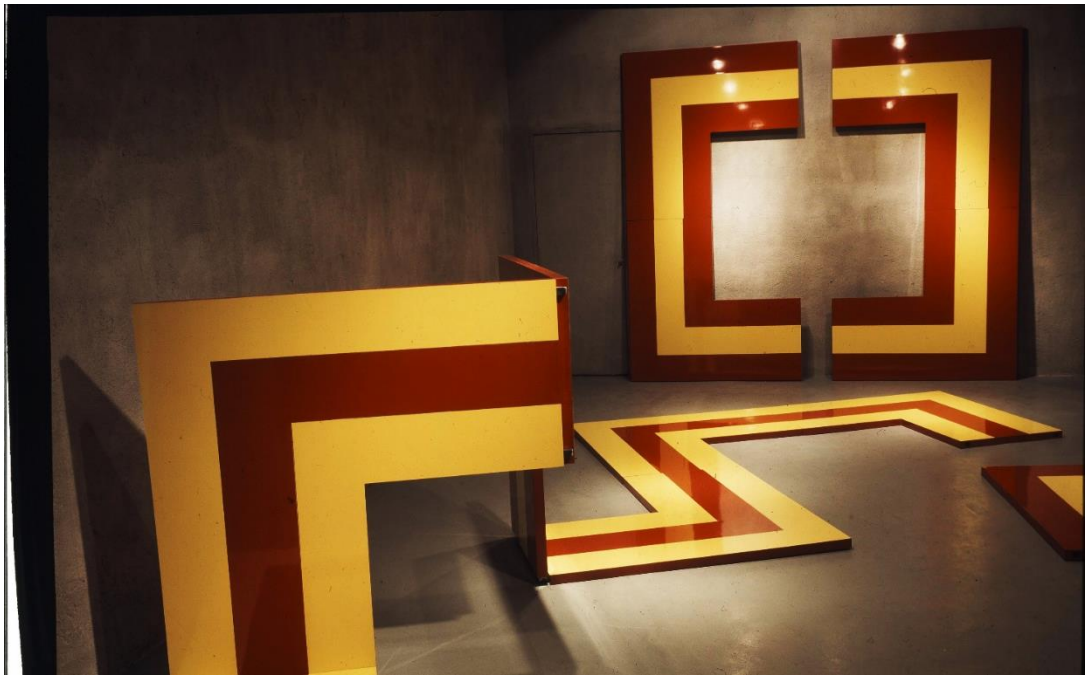

Figure 1:The artwork as installed in 1968 at "La Salita" Gallery

In 2018 Supercomponibile '67 was object of the conservation thesis of Elena Zaccagnini[1] under the supervision of Grazia de Cesare (conservator) and Marcella Ioele (chemist), at the ISCR of Rome. Some

[1] *E. Zaccagnini: "Il Supercomponibile 1967 di Sergio Lombardo. Laminati plastici decorativi a base di fenolo e melammina-formaldeide: storia, morfologie di degrado e restauro" PFP2, 64° Course, ISCR*

results on the scientific analysis performed to support the conservation intervention were presented in October 2019 at XVII IGIIC-National Congress "Lo Stato dell'Arte" with the title *Approccio al restauro di un'opera in "Fòrmica": indagini scientifiche applicate allo studio di un materiale industriale*

A good restoration always requires to deeply investigate materials and techniques and to assess the conservative conditions of the artwork prior to start working on it. As said before, *Supercomponibile '67* is composed by several wood panels covered in decorative laminates and the juxtaposition of these different elements, in conjunction with unsuitable storage conditions, appeared to have a very negative effect on the conservative status of the artwork. In fact, as soon as it arrived to the ISCR, *Supercomponibile '67* showed extended signs of degradation, both of the wood supports and of the laminates. The conservators noticed tiny holes on the wood supports, plausibly due to xylophagous insects; such holes fortunately were quite sparse and seemed not to influence significatively the physical resistance of the artwork. Several parts of the decorative laminates were detached, as visible in Figure 2, for the combined action of two factors: the biological attack by the cellulolytic Basidiomycete fungus *Serpula lacrymans*[2] and the lack of resistance of the adhesive system used by the artist. *Serpula lacrymans* produces filamentous structures called rhizomorphs (long strands of hyphae joined together) which have the function of exploring the environment in order to provide nutrients to the fungus. Growing on the wood supports of the artwork, the rhizomorphs had a strong detaching action, pushing from the inside the laminate surfaces. Some examples of these "root like" structures are visible in Figure 3. Furthermore, the observation through portable optical microscopy allowed the conservators to assume the presence of different kinds of adhesive, exhibiting different degrees of adherence.

[2] The identification of the fungal strain was cured by the Biology department of the ISCR in Rome, thanks to Dr. Marco Bartolini

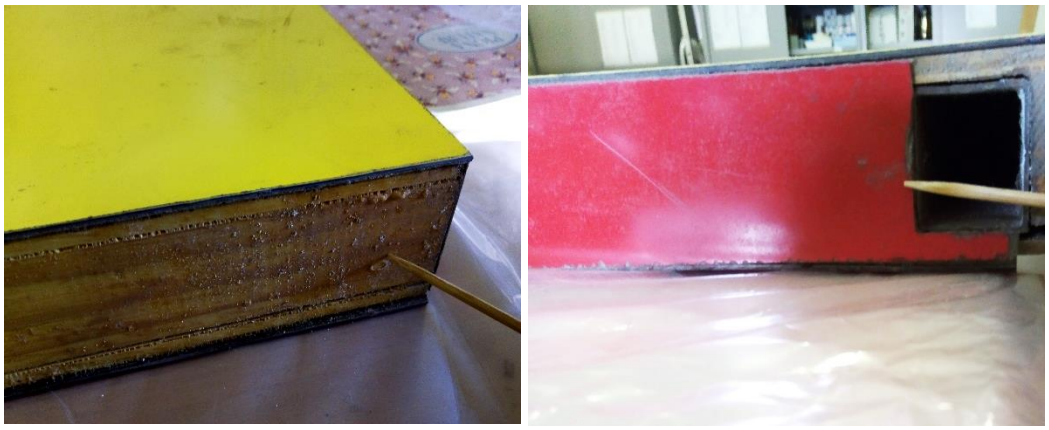

Figure 2:detachment of the decorative laminates in different parts of the artwork

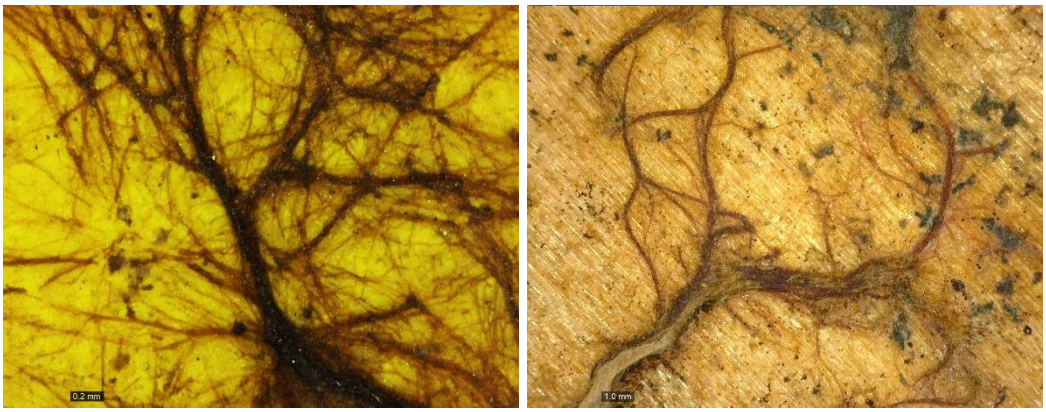

Figure 3:Serpula lacrymans rhizomorphs covering both the laminate (on the left) and the wood support (on the right)

Dealing with such complicated situation, it was absolutely mandatory to study the materials and the techniques chosen by Sergio Lombardo creating *Supercomponibile '67*. The analytical results showed below provided a fundamental tool for the conservative intervention.

9.1. Material characterization: non-destructive approach

The preliminary approach involved the use of portable, non-invasive instruments, namely portable microscopy (DINO-lite) and XRF. Two fragments, one for each colored portion, were then sampled (samples are listed in Table 1Figure 8) in order to analyze them through optical microscopy, micro-FTIR and SEM-EDS to characterize the organic and the inorganic components and to study the microscopic morphology of the laminates.

9.1.1. XRF analysis

Portable XRF analysis was performed at 8kV and 40kV (excitation energy) in order to investigate the inorganic components of the artwork prior to the sampling. XRF analysis is not easily suitable for quantitative analysis since it requires accurate calibrations and to work only with homogeneous samples. The data shown below must be considered only as qualitative since many factors can play a relevant role influencing the intensity of the registered peaks. Figure 4 and 5 show spectra acquired on the red and yellow portions of the artwork.

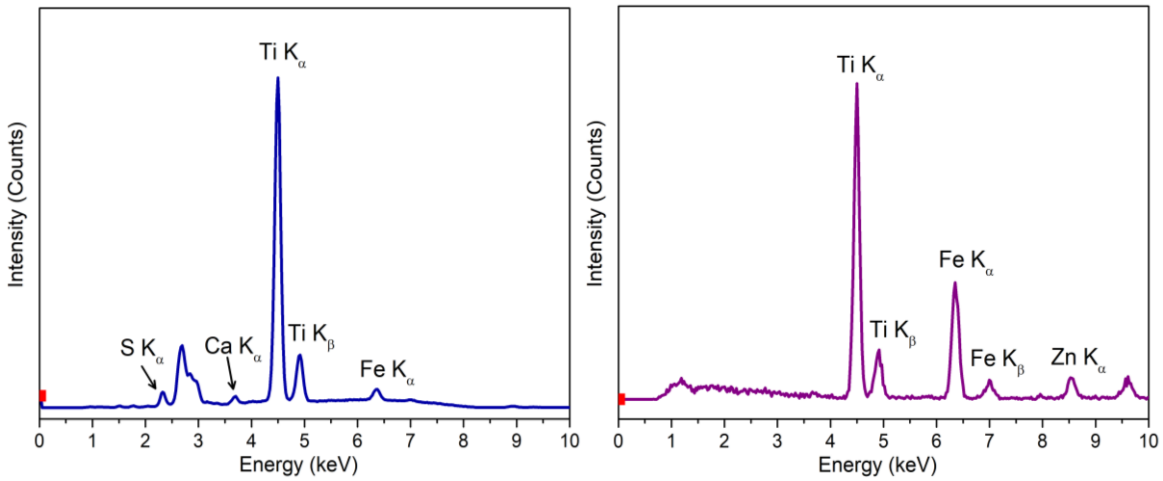

Figure 4: XRF spectra acquired on the red portion of the artwork. On the left 8kV excitation, on the right at 40kV

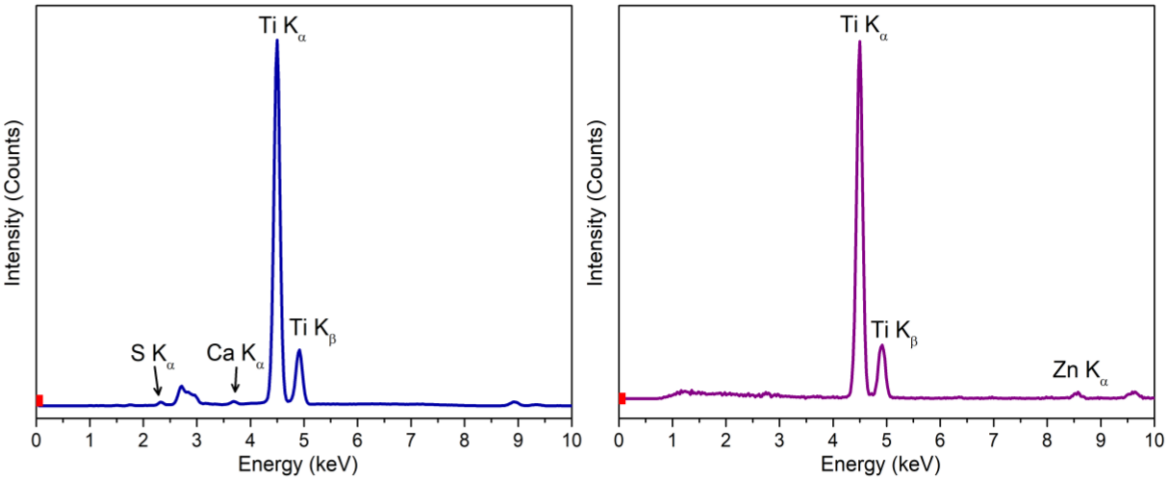

Figure 5: XRF spectra acquired on the yellow portion of the artwork. On the left 8kV excitation, on the right at 40kV

Elements found through XRF analysis are coherent with modern industrial formulations: the most intense peak is in both cases due to titanium, reasonably dioxide, frequently used as white pigment and/or to improve UV resistance in the formulation [1]. Other elements such as sulfur, calcium and

zinc contribute to the spectra to a lesser extent. The most evident difference between the two portions is the presence of iron in the red one, normally used as inorganic red pigment [1]. In this case, however, the relatively low intensity of the peaks associated with iron (in comparison with the titanium ones) suggests the vivid red color of the laminate is due to an organic dye rather than to iron oxides. The occurrence of the red detached piece, visible in Figure 8, made also possible to study the adhesives used by the artist to glue the laminates to the wood supports. XRF analysis registered, (Figure 6) presence of chlorine and, to a lesser extent, zinc, calcium and iron.

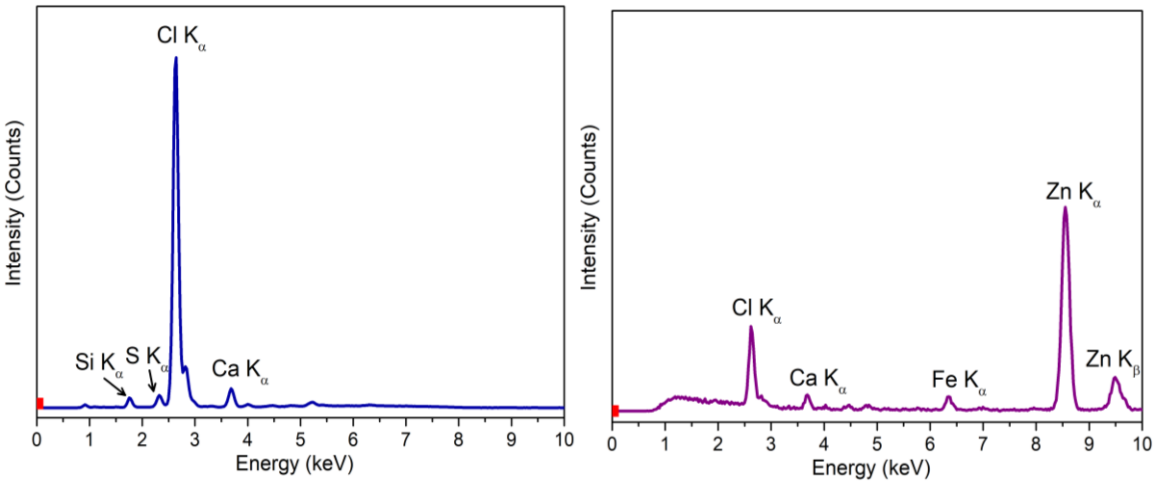

Figure 6: XRF spectra acquired on the back of the red sample. On the left 8kV excitation, on the right at 40kV

9.2. Sampling

Two samples were taken from the artwork in order to study the constituent materials (Table 1).

Sample	Techniques	Description	Results
1L	OM, FTIR, SEM-EDS	Red laminate	melamine formaldehyde-based laminate + 2 adhesives
2L	OM, FTIR, SEM-EDS	Yellow laminate	melamine formaldehyde-based laminate + 2 adhesives

Table 1:samples taken from "Supercomponibile '67"

The observation through optical microscopy of the fragment confirmed the presence of two different kind of adhesives, one more widespread on the laminate (letter A) and the other found only on the corners (B).

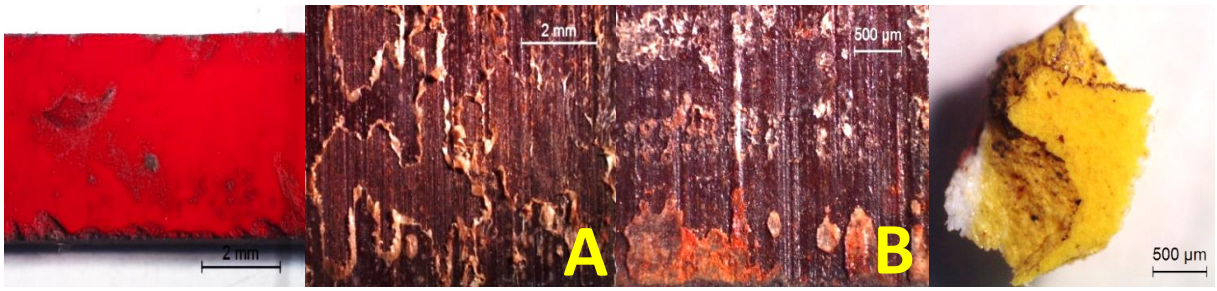

Figure 8: Samples taken from Supercomponibile '67, the red one on the left and the yellow one on the right. The yellow letters A and B distinguish two different adhesives on the back of the red sample

9.3. Adhesives characterization

FTIR analysis allowed to distinguish the chemical composition of both adhesives, as shown below.

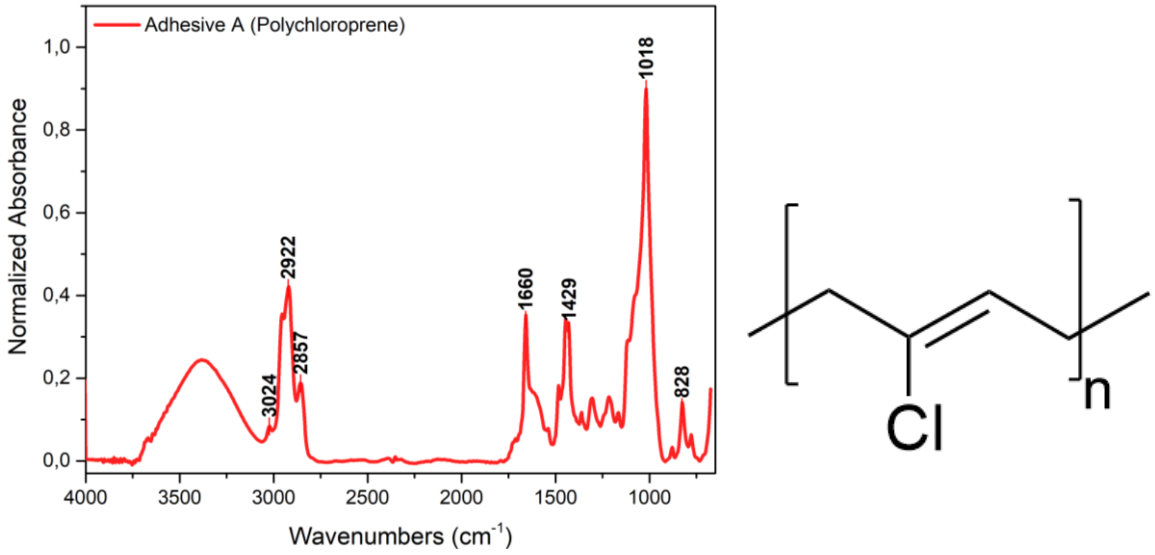

Figure 9: Infrared spectra of adhesive A, recognized as polychloroprene, and the chemical structure of the polymer

The A adhesive appeared more elastic and uniform than the other; as visible in Figure 9 the infrared spectrum shows absorptions typical of polychloroprene, which explains the significative presence of chlorine detected by XRF. Particularly significative for polychloroprene are the absorptions at 3024 cm^{-1} (C=C-H stretching), 1660 cm^{-1} (stretching C=C), 1429 and 828 cm^{-1} (bending CH_2) [2], while the strong peak at 1018 cm^{-1} is plausibly due to the presence of an inorganic filler, namely talc [1], [3]. The spectral comparison with a well-known commercial product in Figure 10 confirms the chemical nature of the adhesive. Polychloroprene, one of the most produced synthetic rubbers, exhibits a high crystallization degree compared to other elastomers. This feature influences some physical properties such as tensile strength, explaining why polychloroprene (commercially known as Neoprene) is nowadays widely used as adhesive and rubber for a wide range of purposes.

Furthermore, the vinylic chlorine atom in the polymer chain stabilizes the double bond resulting in better oxidation resistance compared to other unsaturated elastomers such as polyisoprene [4].

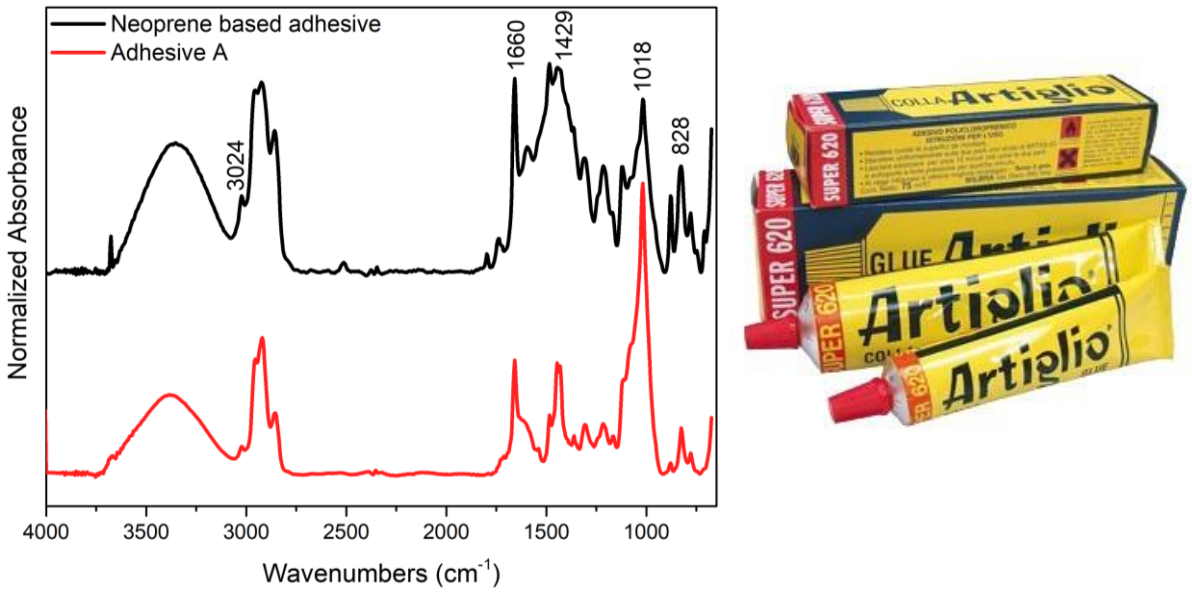

Figure 10: On the left spectral comparison between the adhesive A and a Neoprene commercial adhesive, on the right, the commercial product

Neoprene is a contact adhesive, it must be applied uniformly on two surfaces, then, after the solvent is evaporated and the product is almost completely dry, the two surfaces must be joined together pressing them for a certain amount of time. Bonding too soon the surfaces or applying a weak pressure may result in lack of adhesion and detachment of the two parts.

FTIR analysis (Figure 11) showed for B adhesive features specifically associated with polyvinyl acetate.

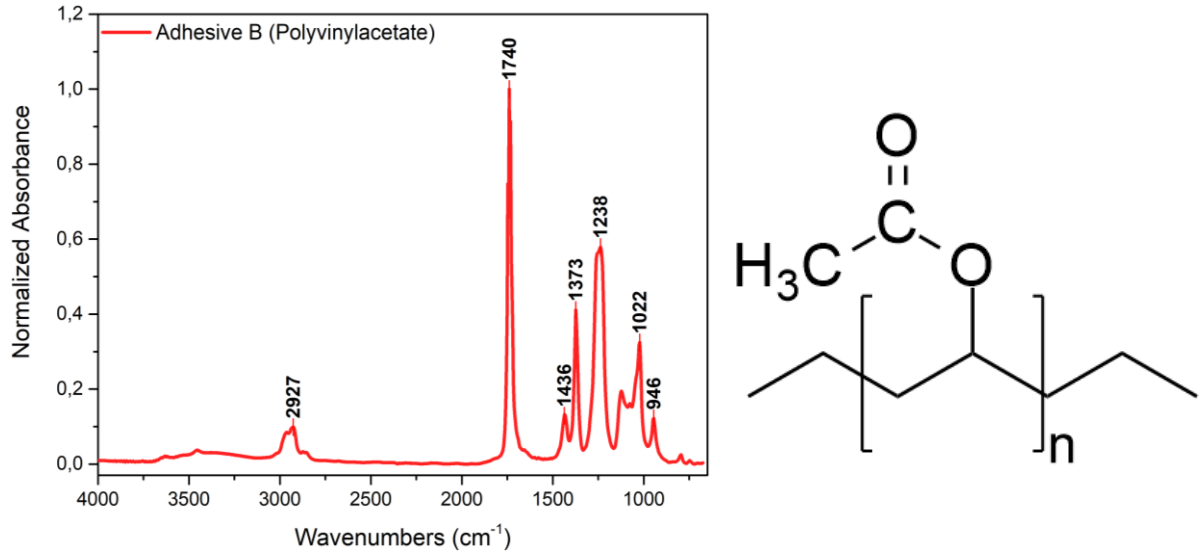

Figure 11: Infrared spectra of adhesive B, recognized as polyvinyl acetate, and the chemical structure of the polymer

Significative for polyvinyl acetate are ester bands, namely carbonyl at 1740 cm^{-1} and C-O-C symmetrical and asymmetrical stretching modes at 1238 and 1022 cm^{-1} in conjunction with both CH_2 and CH_3 bending (1440 cm^{-1} and 1375 cm^{-1}) [5]

9.4. Superficial biological attack

Portable microscopy evidenced the presence of different superficial deposits on both the yellow and the red surface of the panels. Some of them (Figure 12) appeared dark in color and with a thick hard consistency, whilst some others (Figure 13) were more uniformly diffused on the surface, forming a homogeneous net. Shape and diffusion of these deposits required further investigations in order to identify their nature and exclude a biological attack on the laminates' surface.

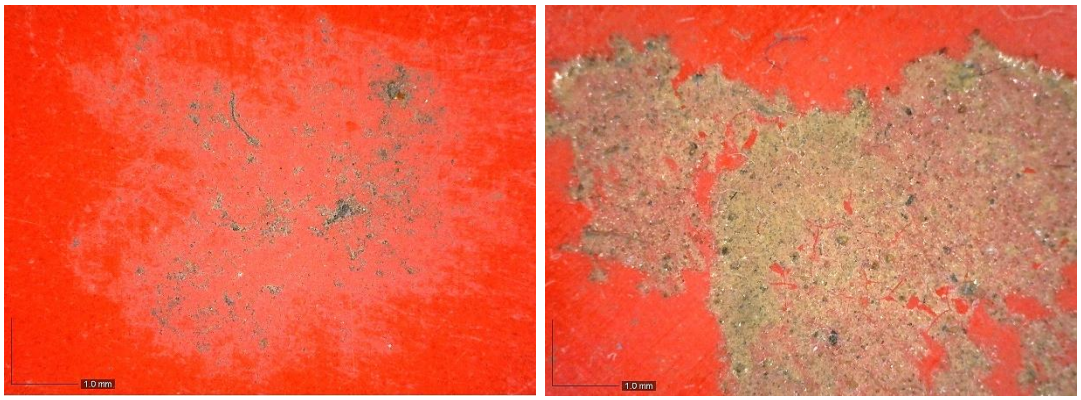

Figure 12: Superficial layers of dirt on the red surface

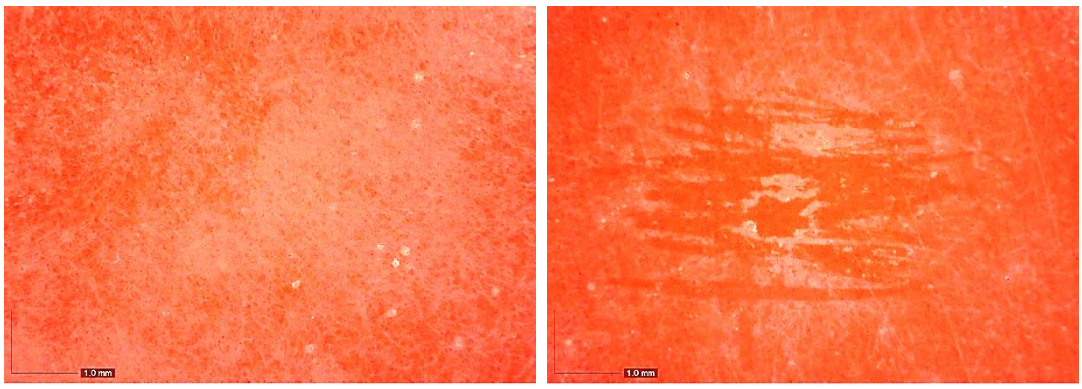

Figure 13: Superficial white contaminant on the red surface of the panels

The FTIR spectrum in Figure 14, obtained sampling a small amount of the dark substance in Figure 12, shows a complex pattern of absorptions linked to the presence of organic components, characterized by an oily fraction (CH_2 and CH_3 stretching modes at 2924 and 2854 cm^{-1} but also the ester carbonyl at 1736 cm^{-1}) in conjunction with signals typical of proteins (amide I and II at 1647 and 1566 cm^{-1}). In this organic matrix are embedded different inorganic components such as gypsum (3537 cm-1, 1117 cm^{-1}), calcium carbonate (1431 cm^{-1}, 876 cm^{-1}) and aluminum silicates, plausibly clay materials (3560 cm^{-1} and 1041 cm^{-1}).

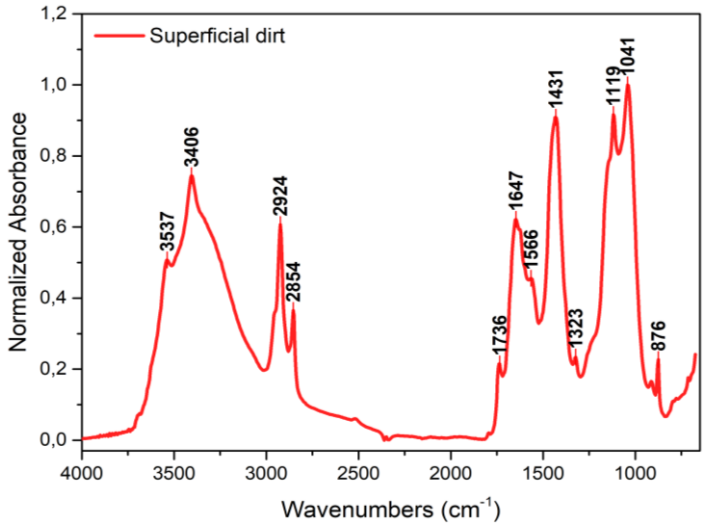

Figure 14: FTIR spectrum of the superficial dirt on the red surface

The peculiar appearance of the white spots in Figure 13 strongly suggested the presence of a biological attack. In fact, the spectrum in Figure 15, shows some characteristic spectral features of chitin (primary component of cell walls in fungi). The most important ones are at 3401 cm^{-1} (stretching O-H), 2929 cm^{-1} (stretching CH_2) 1652 cm^{-1} (amide I band due to carbonyl stretching) 1557 cm^{-1} (amide II, combination of C-N-H stretching and N-H bending). Other significative bands are CH_2 bending at 1424 cm^{-1}, the amide III combination of C-H stretching and N-H bending at 1324 cm^{-1} and finally the asymmetrical and symmetrical C-O stretching modes at 1117 and 1037 cm^{-1} [6]. Laminates are normally characterized by a high water-repellency and a very compact structure, so it is more plausible to assume the biological attack found an ideal culture medium on the superficial dirt rather than on the laminates themselves.

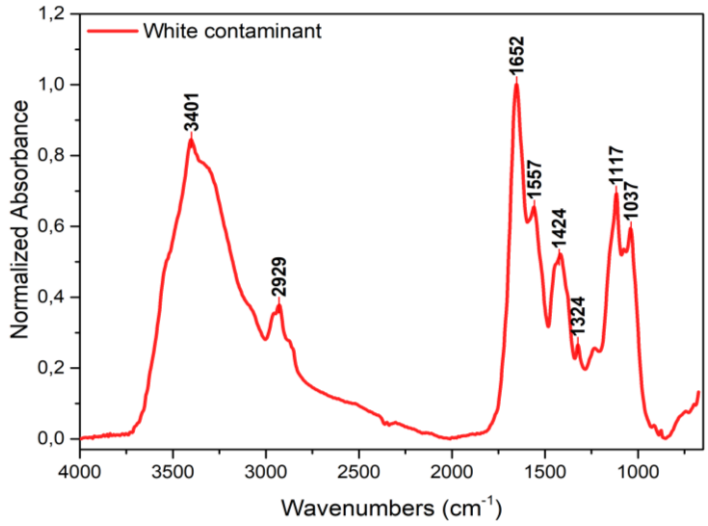

Figure 15: FTIR spectrum of the white contaminant

9.5. Laminates characterization

Small portions of both samples were selected to be analyzed via FTIR and SEM-EDS to clarify the nature of the different layers composing the laminates. The most important observed difference between the two samples was a white layer found between the bottom pressed paper and the top colored thermosetting resin one in the yellow sample. This layer was not visible in the red laminate, which showed one single colored layer above the pressed paper one (Figure 16).

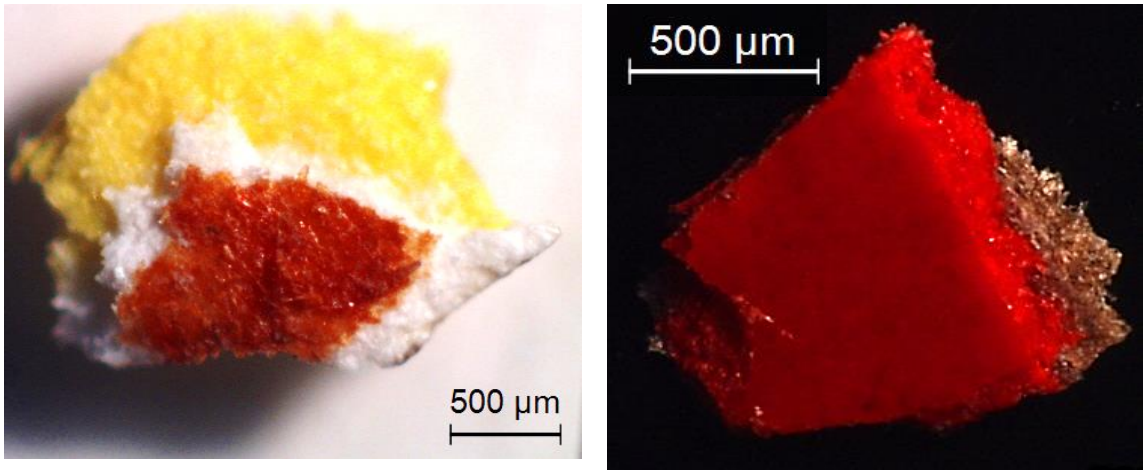

Figure 16: On the left the yellow sample, on the right the red one for FTIR and SEM-EDS analysis

9.5.1. External layer

FTIR analysis of the most external, colored, layer of both samples confirmed the presence of melamine formaldehyde (MF) resin, widely used in the production of laminates thanks to its superior physical properties and resistance to chemicals [7]. Melamine formaldehyde typical spectral features are the N-H and C-H stretching modes (respectively around 3350 and 2925 cm^{-1}), in conjunction with methylene bending modes around 1490 and 1340 cm^{-1}, with the triazine ring absorptions at 1560 cm^{-1} (C=N stretching) and skeletal deformation at 809 cm^{-1}.

The bands at 1160 and 1060 cm^{-1} may be due to the combination of C-O-C asymmetric stretching of cellulose and to ether bridges in melamine formaldehyde structure [8], while the bands at 1112 and 896 cm^{-1} are specifically associated to skeletal vibrations of the cellulose ring [9][10].

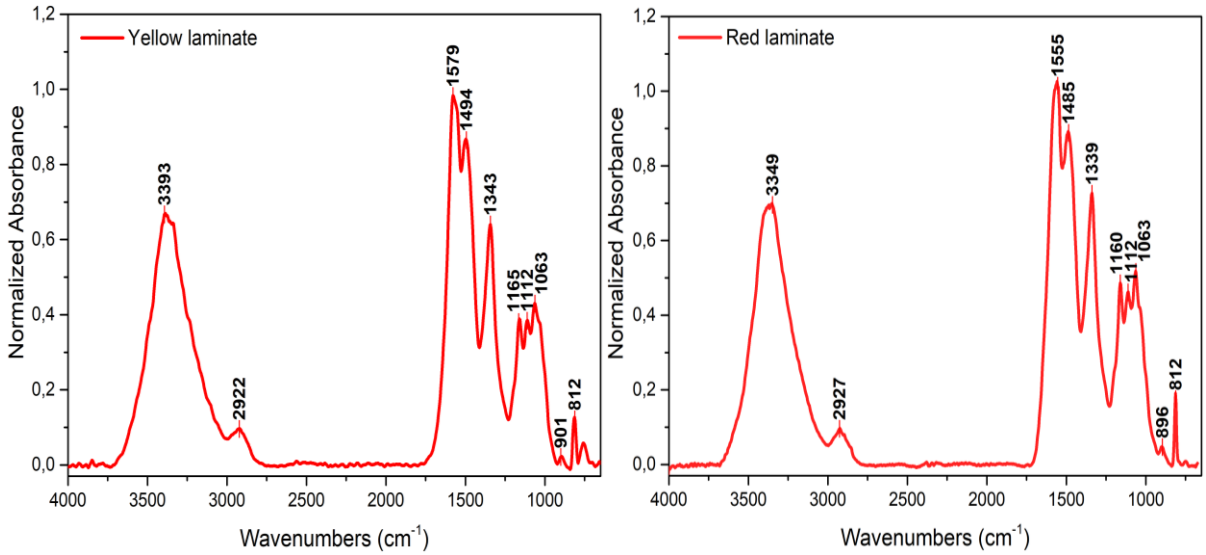

Figure 17: FTIR spectra of the thermosetting resin from the two samples

9.5.2. White intermediate layer

Infrared spectrum of the white layer is shown in Figure 18. Aside from melamine formaldehyde typical absorptions, is it possible to notice an increase in the spectral region related to C-O-C stretching modes, which could be due to a higher content of cellulose in the formulation. The carbonyl band is coherent with the presence of an ester moiety. Esters such as triacetin (glycerin triacetate) are nowadays widely used as accelerating agents during the cure of phenol formaldehyde resins [11],[12].

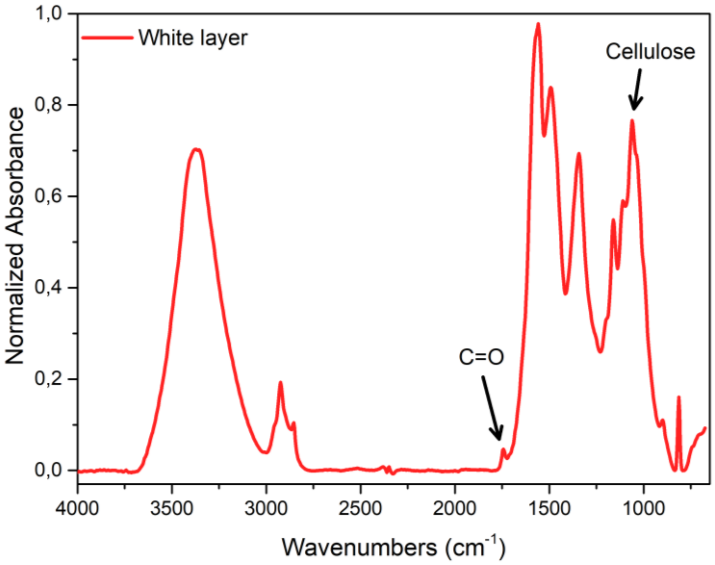

However, the use this kind of accelerants started in the early 1970s [11] while the artwork is dated 1967. Therefore, the carbonyl absorption must be addressed to other additives which may be part of the laminate formulation.

Figure 18: FTIR spectrum of the white layer in the yellow sample

9.5.3. Paper layer

Paper layers spectra obtained from both samples showed comparable spectral features, shown in Figure 19.

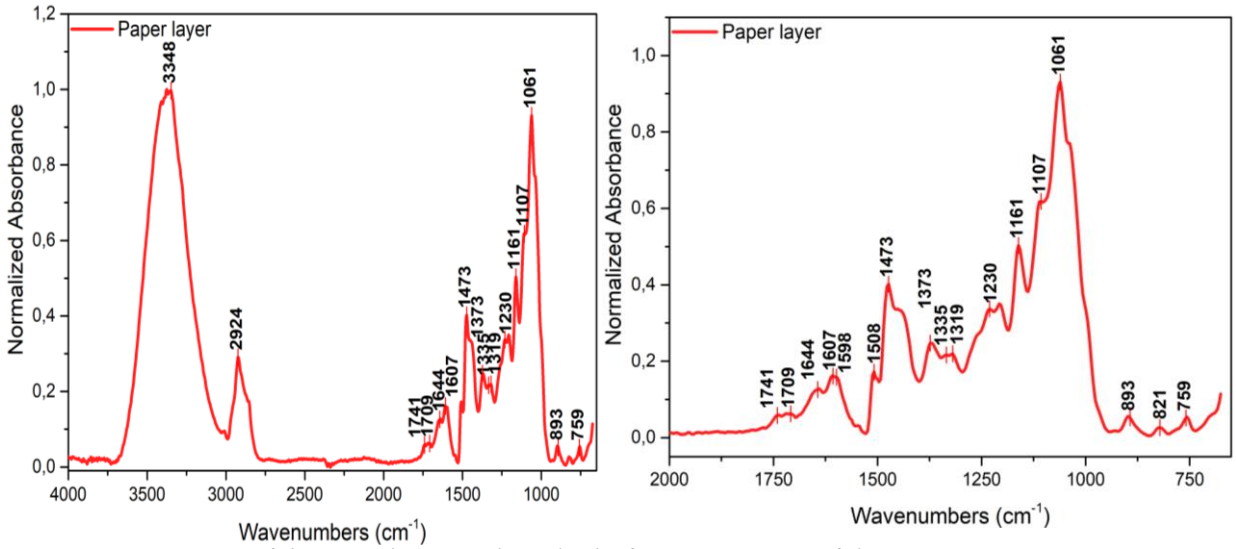

Figure 19: FTIR spectra of the paper layer, on the right the fingerprint region of the same spectrum

Aside from signals typical of cellulose[3], it is possible to notice the presence of absorptions plausibly characteristic of phenol formaldehyde, such as the aromatic ring related ones (1508, 1598, 1607 cm^{-1}) and the phenoxy C-O at 1230 cm^{-1}. Peaks at 821 and 759 cm^{-1} may be attributed to *m*- substituted and *p*-substituted phenols [5]. The carbonyl peak at 1740 cm^{-1}, in conjunction with the strong peak at 1061 cm^{-1} suggests wood flour may be present as a filler both in the paper and in the white layers [13], [14]. However, since some of the typical wood flour spectral features are not easily detectable because of the presence of the phenol resin[4], this assumption cannot be validated. Wood flour is one of the first additives used in synthetic polymers manufacture, initially used as inexpensive filler to improve some physical properties in Bakelite (phenol formaldehyde) made objects [1].

[3] Some cellulose diagnostic absorptions are the O-H stretching of polysaccharides at 3348 cm^{-1}, the O-H bending of water absorbed in cellulose at 1644, 1473 , 1373, 1335, 1061 and 8933 cm^{-1} attributable to vibrational modes of CH_2, CH OH and C-O in β(1→4) linked D-glucose [16]

[4] Some of the most characteristic spectral features of wood flour are related to the aromatic structure of lignin [14]

9.6. SEM-EDS characterization

SEM-EDS analysis was performed analyzing directly a small fragment from each sample on the aluminum stub and working in variable pressure. The red sample, shown in Figure 20, was inspected in order to better understand the microscopic morphology of the laminate.

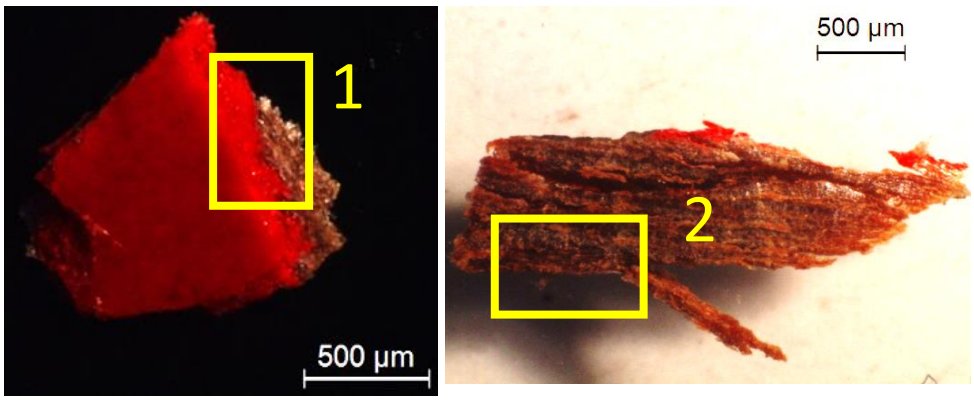

Figure 20: red sample of laminate prepared for SEM-EDS analysis. In the yellow squares the analyzed portions

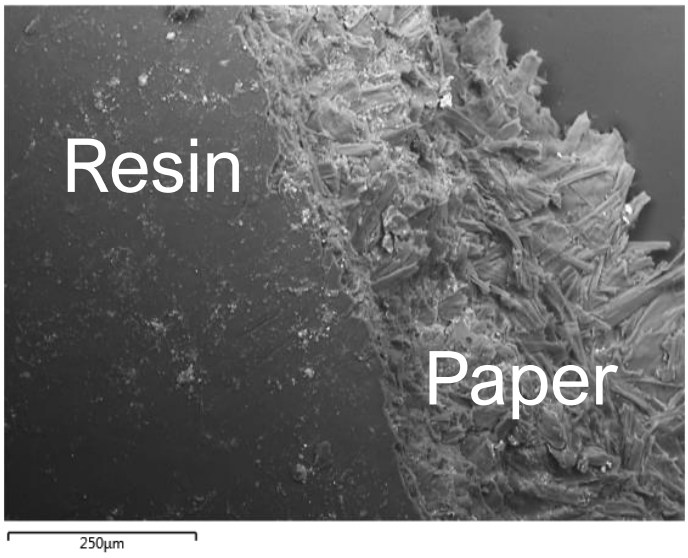

Figure 21: SEM BSD image of the red sample

SEM image in Figure 21, evidences the presence of thick paper fibers both in the bottom layer and in the middle one, while the top layer appears smooth and flat, confirming the manifacture data [15]. EDS results on the area corresponding to the point 1 (Figure 20) are shown in Figure 22. For both areas EDS analysis confirmed XRF and FTIR results, highlighting on area 1 presence of nitrogen (as component of the melamine resin) and titanium, concentrated in the middle layer, which appears to be formed by paper fibers soaked in resin. Aluminum is also present in the formulation, plausibly as additive in form of oxide, with traces of silicon and calcium.

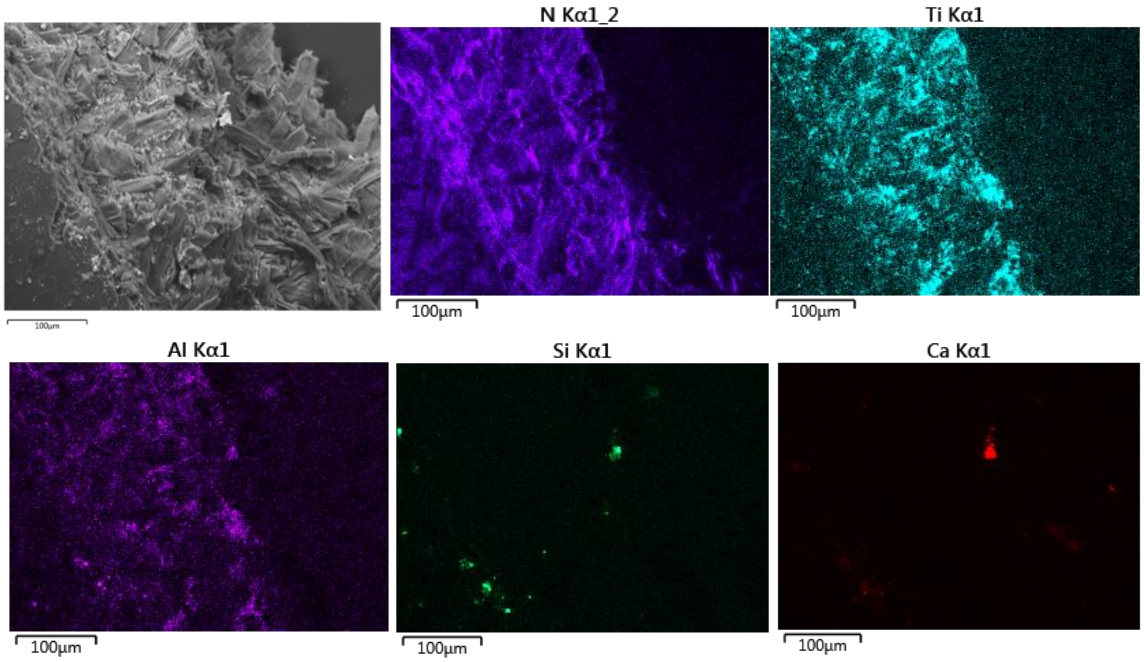

Figure 22: On the right SEM BSD image of a portion of the red sample (area 1), the others are EDS maps of elements on the same area

Area 2, corresponding to the paper layer with traces of adhesive is characterized by a thin layer containing chlorine and silicon (Figure 23), addressable to polychloroprene adhesive mixed with talc, as identified by FTIR.

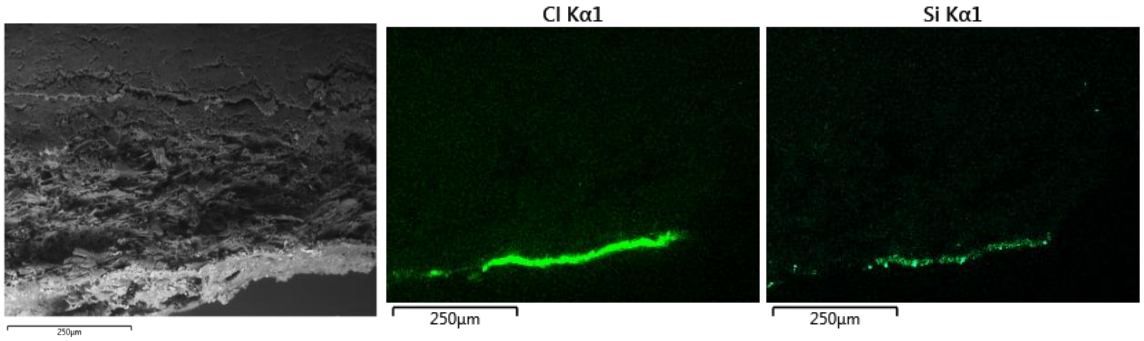

Figure 23:On the right SEM BSD image of a portion of the red sample (area 2), the others are EDS maps of elements on the same area

The yellow sample, observed through SEM, showed a peculiar morphology, as visible in Figure 24 and 25. Paper fibers are less visible, as they look smaller and shorter compared to the red sample. As visible in Figure 26, the external surface appears as flat as the red one but containing titanium.

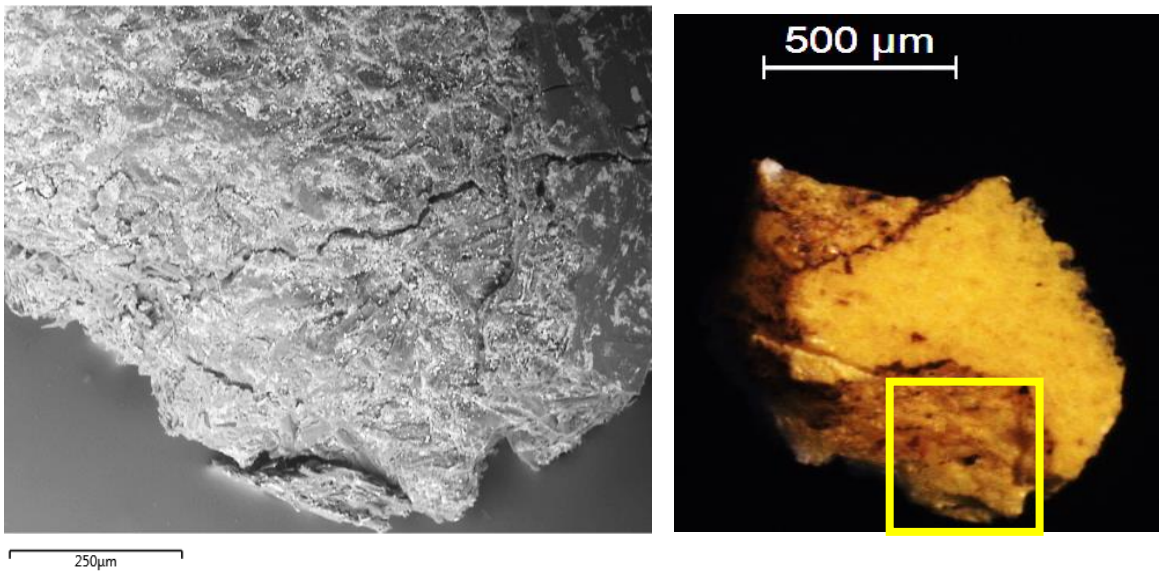

Figure 24: On the left SEM BSD image of a portion of the yellow sample, on the right same portion highlighted by the square

Under this last layer, which probably is a finish, the composition appears to be varied, with aluminum and silicon associated plausibly in aluminosilicates (possibly containing magnesium and potassium as well).

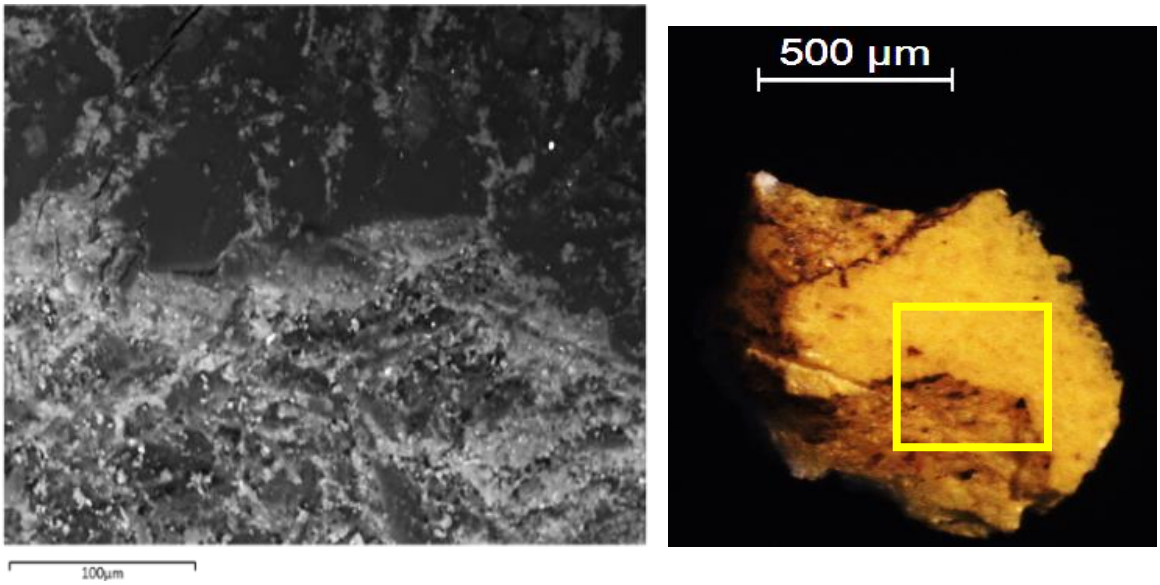

Figure 25: On the left SEM BSD image of a portion of the yellow sample, on the right same portion highlighted by the square

Calcium is associated with Sulfur most likely in gypsum, and magnesium could be also present as carbonate (dolomite) [1].

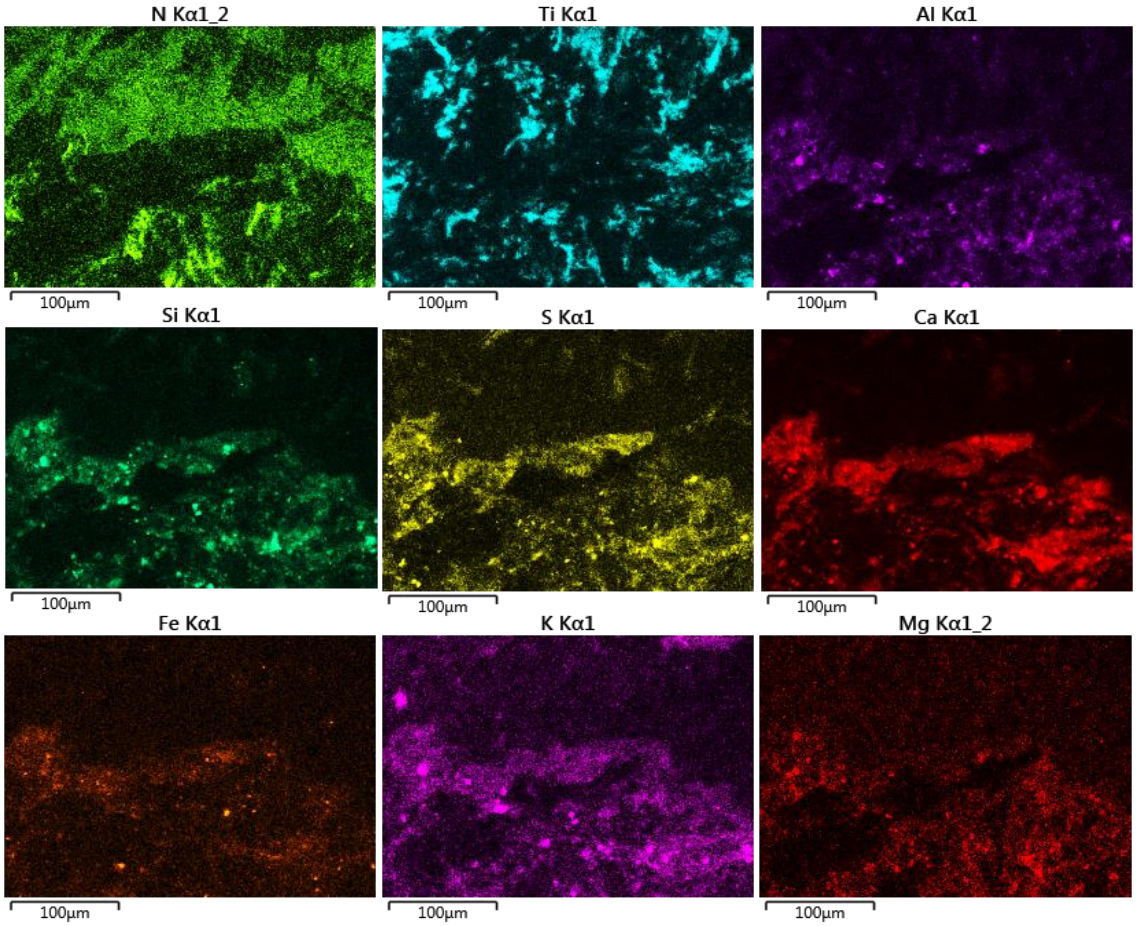

Figure 26: EDS maps of elements on the yellow sample (area in Figure 22)

9.7. Conclusions

Material characterization of two samples taken from *Supercomponibile '67* provided fundamental information to the conservative intervention and offered the possibility to study structure and morphology of decorative laminates. Decorative laminates are composed by different layers of thermosetting resins reinforced with fibers (this kind of polymers are usually called “fiber reinforced polymers” or FRP). The analyses performed on our samples allowed to highlight the structural differences between them. In particular, the sample yellow was composed by four different layers, while the red only by three (as visible in Figure 27).

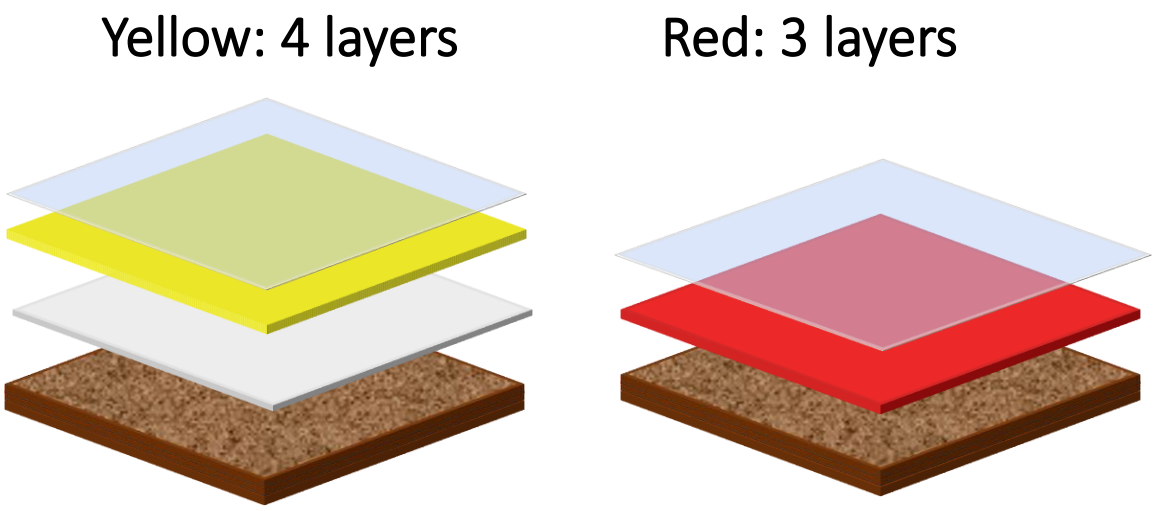

Figure 27: schematic representation of the two samples taken from "Supercomponibile '67", showing the stratigraphy

Red sample, coming from a detached fragment, allowed the study of the whole stratigraphy, included two different kind of adhesive used by the artist to glue the laminates to the plywood support. Through infrared spectroscopy and SEM-EDS analyses, it was possible to discover that one of the adhesives is polychloroprene mixed with talc. Polychloroprene is a commercially widespread rubber well known with the name of neoprene. Since polychloroprene is a contact adhesive, it is plausible to assume the adhesion with the substrate was not perfect, so the artist decided to use a second adhesive (polyvinyl acetate) to secure the detached parts. The identification of the different kinds of adhesives used by the artists was part of a wider experimentation on different products selected for the restoration, in order to identify the most suitable one to secure in place the detached laminates. The laminates are both composed by a top layer of melamine formaldehyde and paper, while the white layer present only in the yellow sample also contain an ester moiety which may be due to the addition of wood flour, as reinforcing fiber. Same additives might be present in the paper layer, although the complexity of the infrared spectra does not allow the sure identification of all components. Observation through portable microscopy highlighted some rounded brown/greyish deposits on the surface of the artwork. Small amounts of these were sampled and analyzed through FTIR revealing a complex pattern of absorptions linked to the presence of organic components, characterized by an oily and a protein fractions, with calcium carbonate and aluminum silicates. Such patina at some point constituted the perfect growth medium for fungal attack, as testified by the presence of white deposits composed by chitin, the most important constituent of fungal cell wall. However, there were no signs that the biological attack damaged the laminates' surface, suggesting that reasonably the fungal growth interested only the superficial patina.

Finally, SEM-EDS on red sample showed in the middle layer thick paper fibers with titanium most likely as dioxide. A different structure was revealed by SEM-EDS on yellow sample: titanium is present in the top layer while in the middle one other elements such as calcium associated with sulfur (plausibly gypsum) and aluminum associated with silicon (aluminosilicates) were found. Paper fibers do not appear to be as thick and long as the red sample.

References

[1] J. Murphy, *Additives for plastics handbooks*. Elsevier Science Ltd, 2001.

[2] V. Arjunan, S. Subramanian, and S. Mohan, "Vibrational Spectroscopy Studies on Trans-1,4-Polychloroprene," *Turkish J. Chem.*, vol. 27, no. 4, pp. 423–432, Aug. 2002.

[3] E. Ferrage *et al.*, "Evaluation of talc morphology using FTIR and H/D substitution," *Clay Miner.*, vol. 38, no. 2, pp. 141–150, Jun. 2003.

[4] J. A. Brydson, *Rubber chemistry*. Applied Science Publishers, 1978.

[5] H. Lobo and J. V. Bonilla, *Handbook of plastics analysis*. Marcel Dekker, 2003.

[6] G. Cárdenas, G. Cabrera, E. Taboada, and S. P. Miranda, "Chitin characterization by SEM, FTIR, XRD, and ^{13}C cross polarization/mass angle spinning NMR," *J. Appl. Polym. Sci.*, vol. 93, no. 4, pp. 1876–1885, Aug. 2004.

[7] S. Bajia, R. Sharma, and B. Bajia, "Solid-state microwave synthesis of melamine-formaldehyde resin," *E-Journal Chem.*, vol. 6, no. 1, pp. 120–124, 2009.

[8] D. J. Merline, S. Vukusic, and A. A. Abdala, "Melamine formaldehyde: Curing studies and reaction mechanism," *Polym. J.*, vol. 45, no. 4, pp. 413–419, 2013.

[9] K. Fackler, J. S. Stevanic, T. Ters, B. Hinterstoisser, M. Schwanninger, and L. Salmén, "FT-IR imaging microscopy to localise and characterise simultaneous and selective white-rot decay within spruce wood cells," *Holzforschung*, vol. 65, no. 3, pp. 411–420, 2011.

[10] F. Xu, J. Yu, T. Tesso, F. Dowell, and D. Wang, "Qualitative and quantitative analysis of lignocellulosic biomass using infrared techniques: A mini-review," *Appl. Energy*, vol. 104, pp. 801–809, 2013.

[11] A. Pizzi and A. Stephanou, "On the chemistry, behavior, and cure acceleration of phenol–formaldehyde resins under very alkaline conditions," *J. Appl. Polym. Sci.*, vol. 49, no. 12, pp. 2157–2170, Sep. 1993.

[12] X. F. Mo, D. B. Fan, T. F. Qin, and F. X. Chu, "Curing characteristics and adhesion performance of phenol-formaldehyde resins with composite additives," *J. Trop. For. Sci.*, vol. 27, no. 2, pp. 248–254, 2015.

[13] B. Yin and M. Hakkarainen, "Green Plasticizers from Liquefied Wood," *Waste and Biomass Valorization*, vol. 5, no. 4, pp. 651–659, 2014.

[14] M. Farsi, "Thermoplastic Matrix Reinforced with Natural Fibers: A Study on Interfacial Behavior," *Some Crit. Issues Inject. Molding*, no. March 2012, 2012.

[15] S. G. Lewin, *Formica & design : from the counter top to high art*. Rizzoli, 1991.

[16] V. Hospodarova, E. Singovszka, and N. Stevulova, “Characterization of Cellulosic Fibers by FTIR Spectroscopy for Their Further Implementation to Building Materials,” *Am. J. Anal. Chem.*, vol. 09, no. 06, pp. 303–310, 2018.

Chapter 10. Experimental work on decorative laminates

Melamine formaldehyde laminates used by Sergio Lombardo for *Supercomponibile '67* have been extensively studied proving that their structure is attributable to the so called HPL (high pressure laminates), "molded and cured at pressures not lower than 1,000 psi (70 kg/cm^2) and more commonly in the range of 1,200 to 2,000 psi (80 to 140 kg/cm^2)"[1]. This kind of laminates is produced using thermosetting impregnated paper layers (of variable number) consolidated under heat (above 70°C) and pressure (5Mpa). Application of heat and pressure allows the resin to fully flow into the paper and to cure, increasing the crosslinks and the physical and chemical resistance while decreasing elasticity and flexibility of the end product [1], hence producing very stiff and resistant end products. However, as seen in the previous chapter, the juxtaposition of different materials such as phenolic resin and melamine formaldehyde impregnated paper could expose the laminates to different degradation phenomena. Even if the analytical study on the samples taken from the *Supercomponibile '67* has not highlighted any sign of chemical degradation in the melamine formaldehyde layers, it pointed out how the ageing behavior of decorative laminates as art materials had not been intensively studied. In an effort to fill this gap, part of this PhD work was dedicated to the study of these materials, carrying on artifical ageing in order to investigate their structural and chemical response. Since the decorative layer is the one carrying the artist's message and also the more exposed to environmental factor, we decided to use a modern product which is produced without the brown phenolic resin Kraft paper layer. The chosen product is Formica ColorCore® CC7940 spectrum yellow matte 58[2], showed in Figure 1.

[1] Harris, Cyril (2000). Dictionary of Architecture & Construction. New York: McGraw-Hill. p. 472. ISBN 0071351787.

[2] http://www.formica.com/~/media/emea/documents/knowledge/brochures/formica-pocket-directory-2015-en.pdf

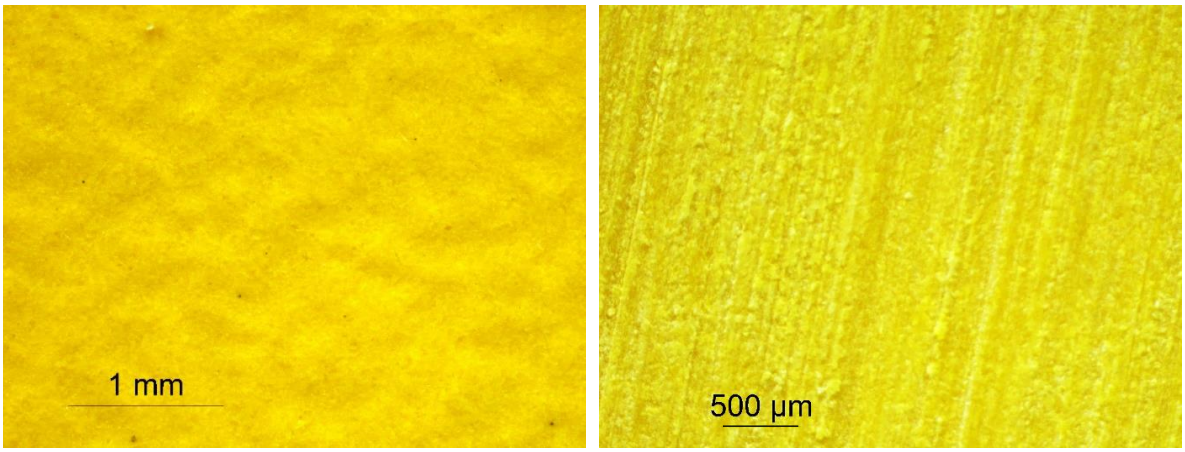

Figure 1: Optical microscopy Formica ColorCore CC7940 spectrum yellow matte 58, on the left the upper part, on the right the bottom

10.1. Material characterization

In the first step of this experimental work, carried out at the ISCR of Rome, small portions of the sample were analyzed through optical microscopy, XRF and SEM-EDS to investigate the inorganic components and the microscopic morphology of the laminate. XRF analysis (Figure 2) detected elements similar to the ones found on *Supercomponibile '67*. The most intense peak is due to titanium K_α, but sulfur, iron, silicon and aluminum are also present.

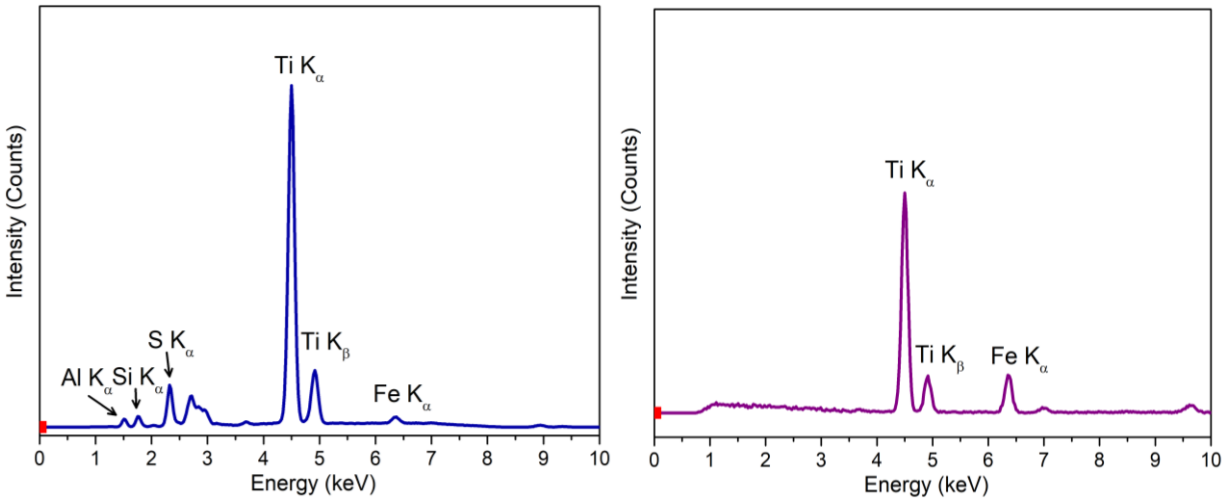

Figure 2: XRF spectra acquired on the reference laminate sample. On the left 8kV excitation, on the right at 40kV

Since it was possible for the sample to have a transparent overlay layer, a portion of the external surface was removed by scalpel to investigate the internal morphology of the product (Figure 3).

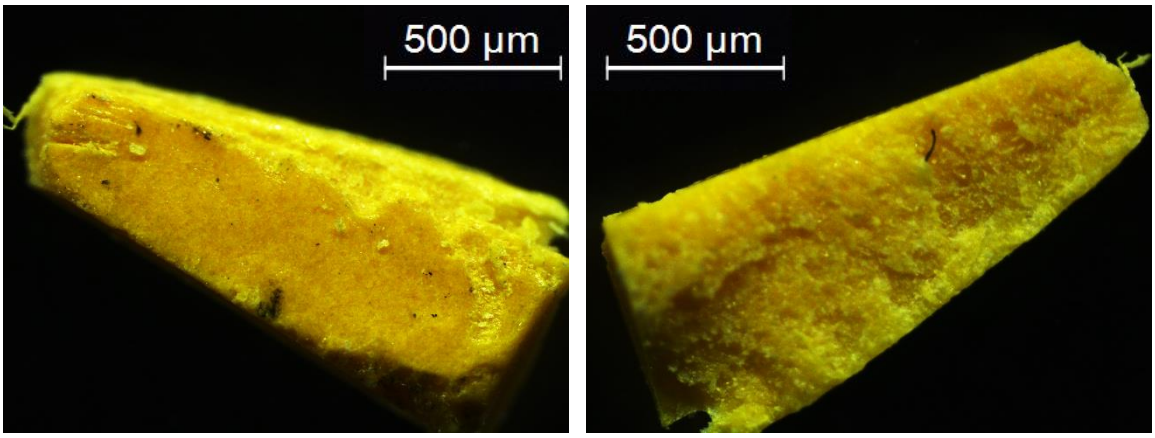

Figure 3: Fragments of the reference laminate sample for SEM analysis, on the left the front, on the right the internal surface

SEM-EDS analysis revealed there is indeed a top layer which appears to be uniform and smooth (Figure 4 on the left). As the yellow sample taken from *Supercomponibile '67* this layer contains titanium (EDS maps in Figure 5). The main difference is the significative presence of silicon associated with magnesium, plausibly in hydrated magnesium silicate (talc), most likely added to improve physical properties to the resin [2]. Silicon is also associated with aluminum, and it is reasonable to suppose as an aluminosilicate like kaolinite, usually added in polymers formulations to increase impact strength and heat resistance [2].

SEM investigation in the middle layer, below the uniform top one, showed long and thick paper fibers (approximately 50-150 µm), similar to the ones found in the red sample taken from *Supercomponibile '67*.

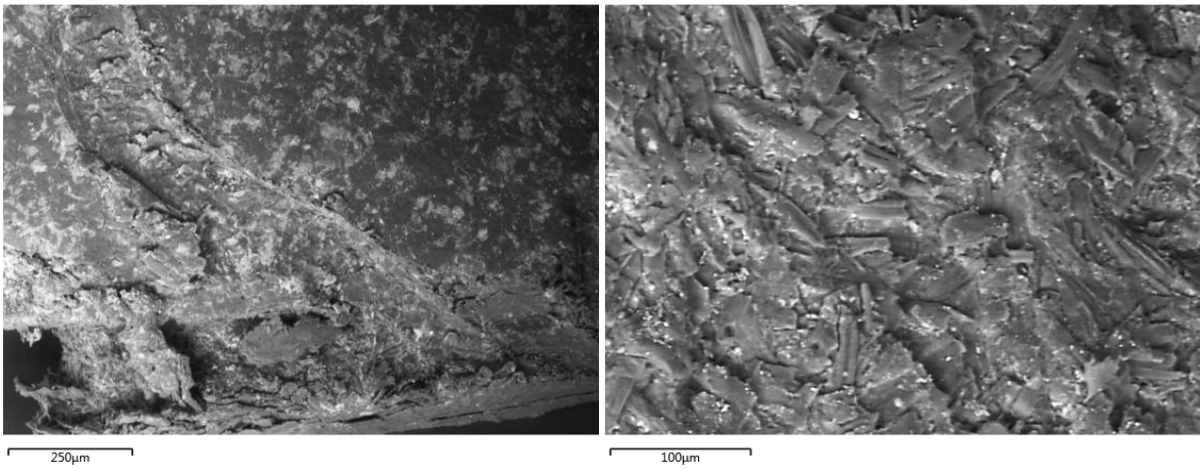

Figure 4: SEM BSD pictures of a small fragment of the sample, left on the front, right on the internal surface

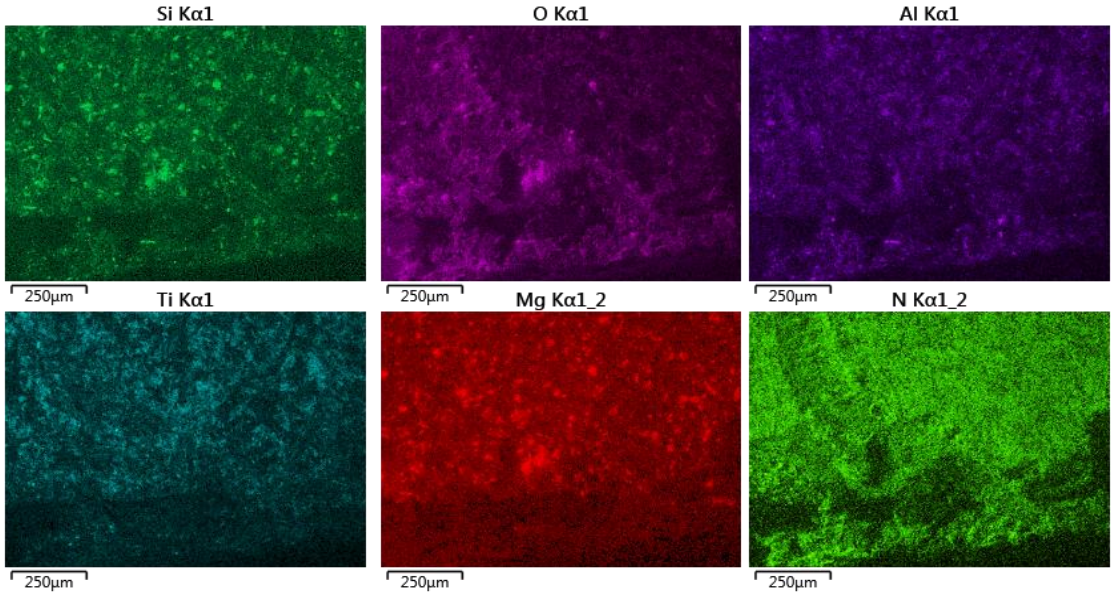

Figure 5: EDS maps of elements on the external surface of the sample

To characterize the organic fraction of the laminate, a small portion was sampled, reduced to a thin film and analyzed through infrared spectroscopy on a diamond cell. FTIR of the sample spectrum yellow is fully comparable with the ones obtained from both laminates taken from the artwork, confirming the use of melamine formaldehyde resin and paper.

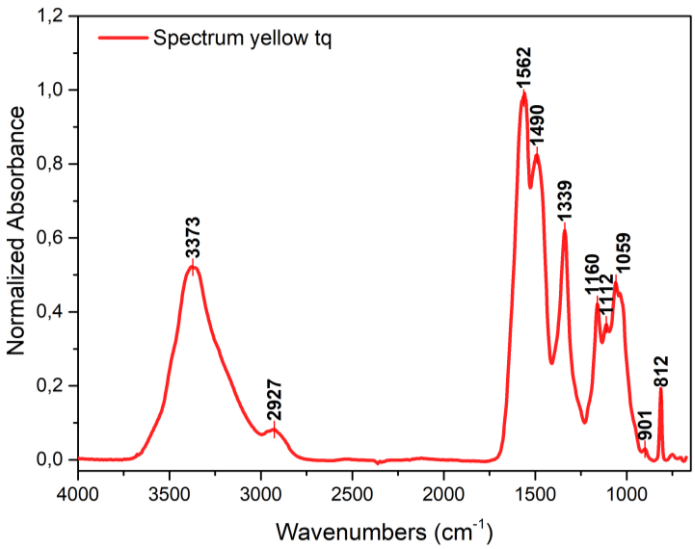

Figure 6: FTIR spectrum of the sample spectrum yellow

10.2. Artificial ageing

The second step of this study was performed at CIQUS in Santiago de Compostela and involved the ageing of the Formica sample in static oven at 145°C to accelerate oxidative degradation processes of the polymer. Eventual changes in type and or/intensity of functional groups were

studied by infrared spectroscopy (which provides a fast and reliable tool for the detection of chemical modifications) while also monitoring by performing colorimetric measurements, thermogravimetric analysis (TGA) and monitoring weight loss (using an analytical balance).

10.2.1. Weight loss

The weight loss of samples of approximately 1x1 cm was monitored throughout the first 260 hours of artificial ageing. After that point no significant change could be measured. Weight loss % data plotted against time are presented in Figure 7, the curve shows fast weight loss during the first 100 hours, most likely due to the evaporation of volatile compounds such as water and formaldehyde [3].

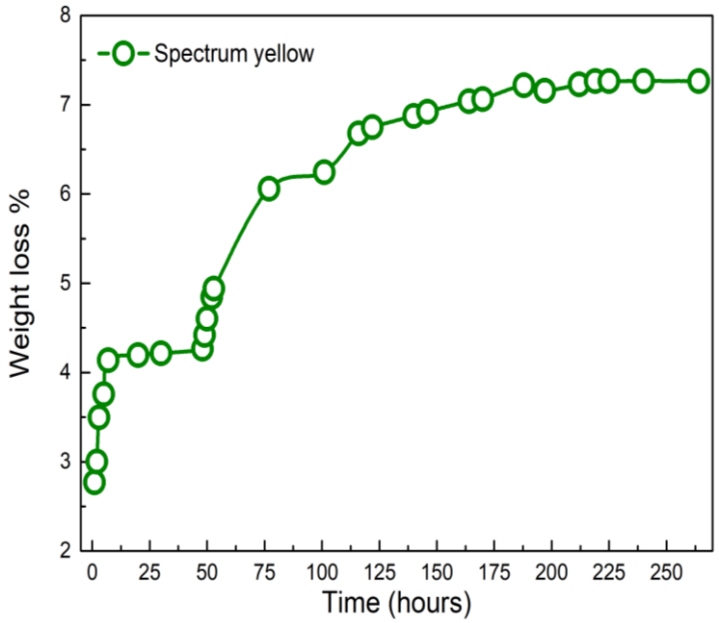

Figure 7: Weight loss curve for Spectrum yellow at 145°C

10.2.2. FTIR spectroscopy

Since, as recalled in Materials and Methods (Chapter 2) comparisons between FTIR spectra obtained in transmission and ART are not recommended, during artificial ageing all the samples were measured using the same apparatus and the same work conditions. Moreover, since ATR requires a good contact between the sample and the crystal surface, laminate samples were reduced in powder in order to overcome its intrinsic hardness and stiffness. As visible in Figure 8 after more than 1000 hours of artificial ageing, the appearance of a carbonyl band was detected.

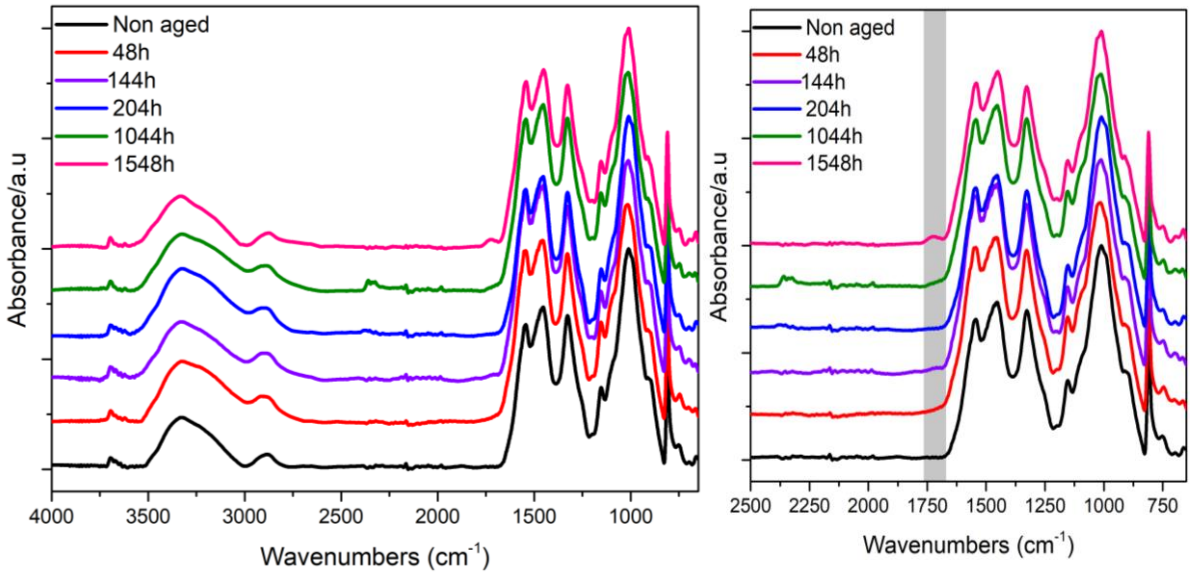

Figure 8: Spectral comparison between non aged and aged Formica samples

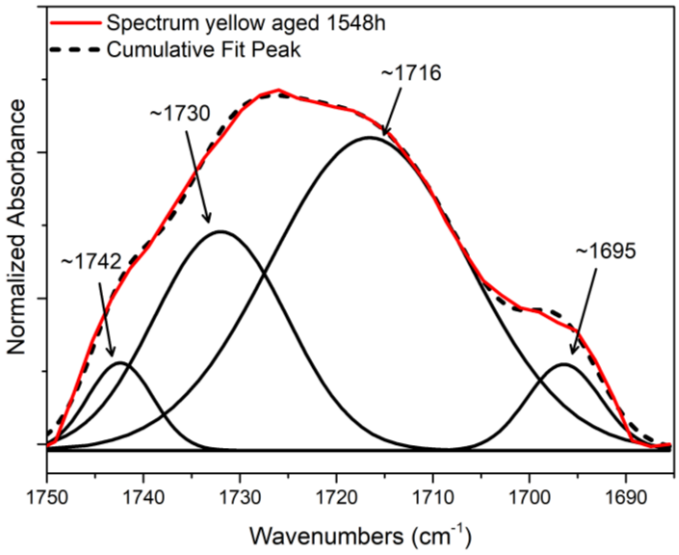

Figure 9: spectral deconvolution of carbonyl stretching

Spectral deconvolution revealed the presence of different contribution in C=O stretching spectral area. The absorption centered at 1695 cm^{-1} could be significative of hydroperoxides [4], while 1716, 1730 and 1740 cm^{-1} may be respectively addressable to the appearance of ketones (or carboxylic acids), aldehydes and esters moieties [5].

10.2.3. Colorimetry

The measured ΔE^*_{ab} for aged Formica Spectrum yellow samples are 8.91 (SCE) and 8.96 (SCI), while pseudo color simulations, given by the instrument as a tool to visually express color

coordinates, are visible in Figure 10. ΔE^*_{ab} values between 2 and 10 are defined as color differences perceptible at a glance [6].

However, since ΔE^*_{ab} formula includes contributions of all three factors (L^*, a^* and b^*) low values of it do not always represent little color changes. In this case, for instance, while the

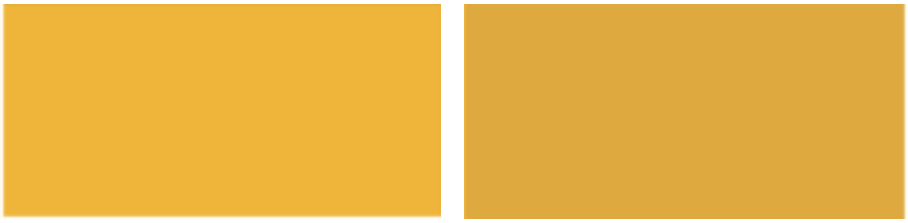

Figure 10: Pseudo color simulations of non-aged (left) and aged (right) Formica samples

SCE measured Δa* is only -1.93, ΔL* is -4.34 and Δb* is -7.54 (all Δ values are reported in Table 1).

Value	Δ(SCE)	Δ(SCI)
L*	-4.34	-4.14
a*	-1.93	-1.94
b*	-7.54	-7.71

Table 1: CIELAB Δ values

L* and b* values against time are reported in Figure 11. Decreasing b* indicates the yellowness reduced, tending to more blue values. At the same time, the decrease of L* suggest the final color is darker than the original one.

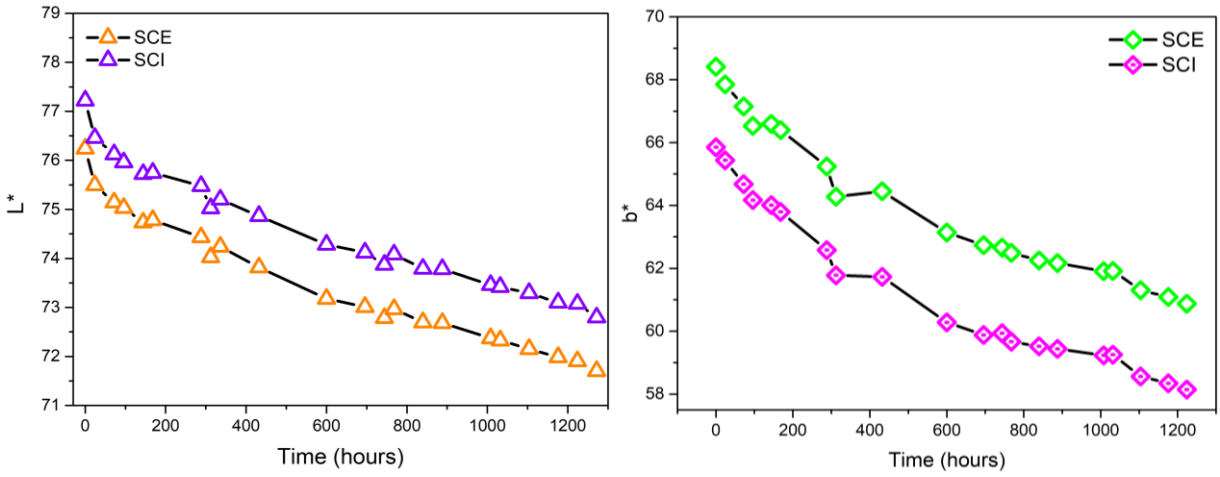

Figure 11: L values (on the left) and b* values plotted against time*

Reflectance % curves of non-aged and aged samples show a decrease at λ <500 nm. Considering absorbance is related to reflectance as A=log(1/R), is it possible to convert reflectance % data in pseudo-absorbance (since reflectance is a surface phenomenon while absorbance is a bulk one). Such conversion allows easy comparisons between before and after ageing. As visible in Figure 12, spectral subtraction curve (aged minus non-aged) shows two pseudo-absorbance negative peaks at 500 nm (blue) and 560 (green) which indicate how the aged sample reflects more in those colors, in accordance with decreasing values of b* and a*.

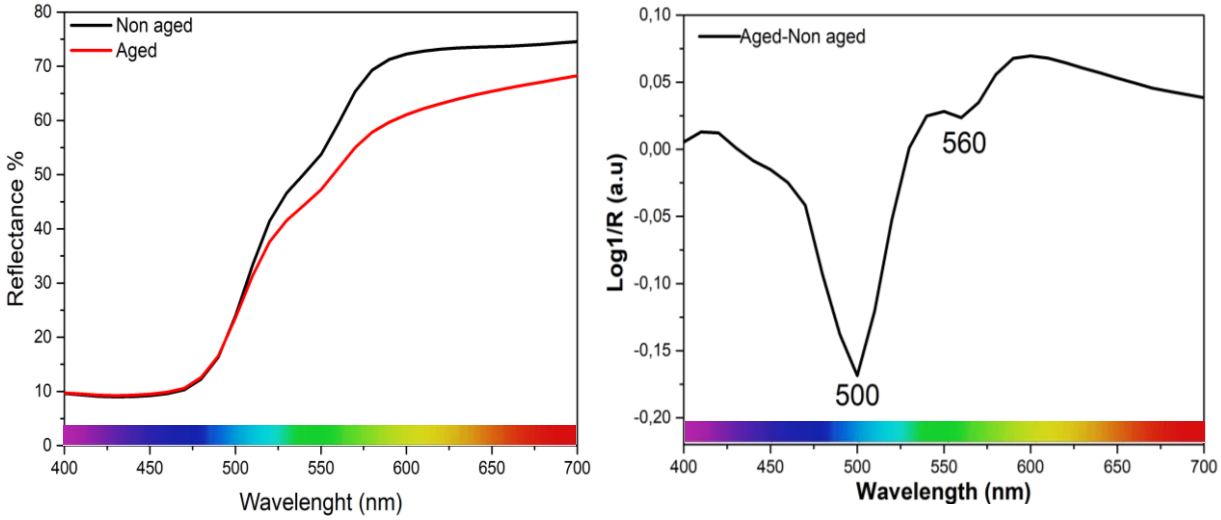

Figure 12: on the left reflectance % curves of aged and non-aged samples, on the right pseudo-absorbance converted spectral subtraction data

10.2.4. Thermogravimetric analysis

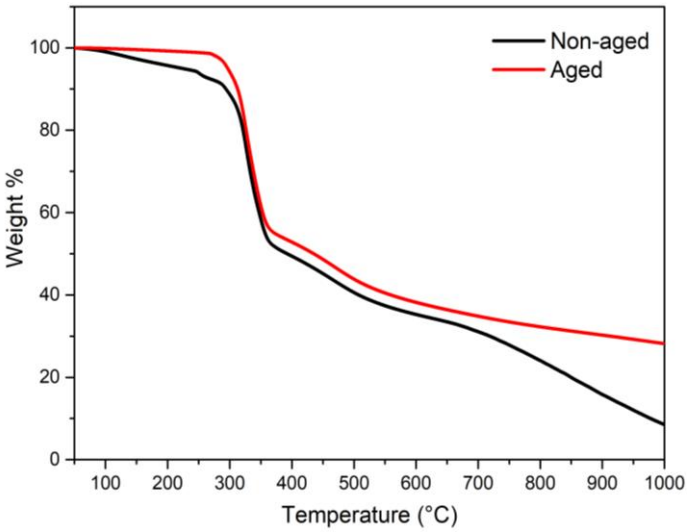

Figure 13: TGA curves of non-aged and aged samples of spectrum yellow laminate

Thermogravimetric analyses were carried out from 500 to 1000°C in N_2 atmosphere (flow rate 25 mL/min) with a heating rate of 10°C/min. TGA curves are shown in Figure 13, while derivative curves are reported in Figure 14 and major weight losses are listed in Table 2.

Sample	Non aged	Aged
T (°C)	110, 280, 294, 326, 472	273, 294, 326, 472

Table 2: samples and corresponding weight losses

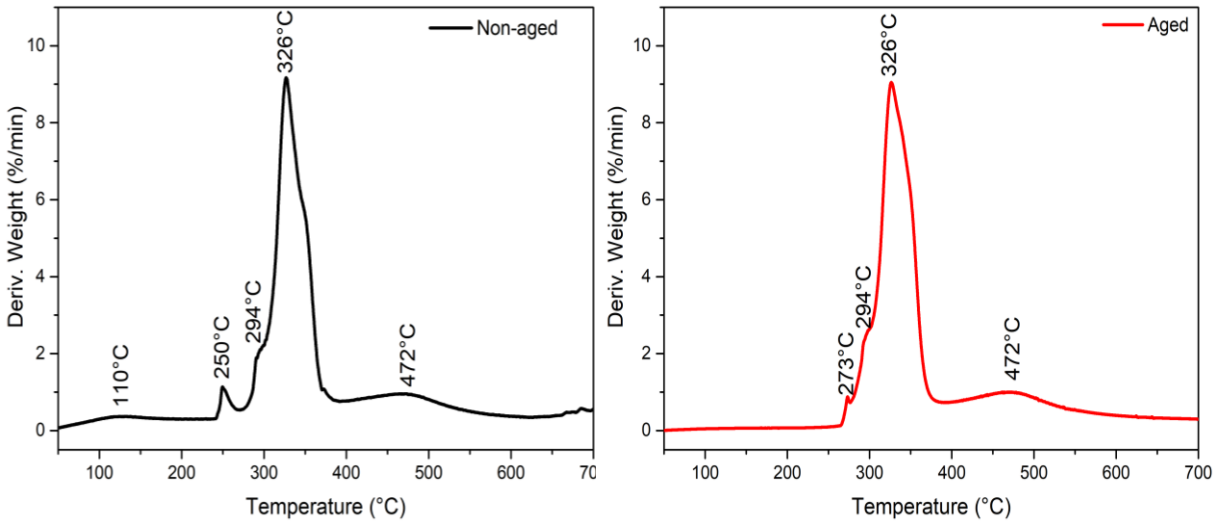

Figure 14: TGA derivative curves of non-aged and aged samples of spectrum yellow laminate

The wide shoulder observed at 110°C in non-aged sample is most likely due to evaporation of water from both paper and melamine resin components [7],[1]. The drying process of resin impregnated paper sheets influences the thermal behaviour of the final product; in general, the presence of a single peak located at T>100°C is related to long drying times at high temperatures (up to 130°C) [1]. The water loss peak is not present in derivative TGA curve of aged samples, and it has been observed how residual weights at 1000°C increased with ageing (from 8.45% for non-aged sample to 28.15% for 1548 hours aged) most likely because of the loss of water during ageing. Most important weight losses for both samples were registered between 300 and 500°C and could be addressable to structural decomposition of melamine. The major weigh loss is at 326°C, coherently with release of low molecular weight compounds such as formaldehyde, methanol, and amine [8]. At T>450°C melamine resin gradually forms condensed structures (heptazines) [8], [9]. Thermal degradation of cellulose is attested to start above 300°C so it is reasonable to assume the losses at 250°C (273°C for the aged sample) and 294°C may be addressable to paper fraction [7].

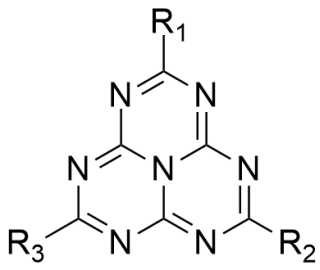

Figure 15: generic heptazine structure

10.3. Conclusions

This experimental work was carried on with the purpose of studying the degradation behavior of melamine-formaldehyde based laminates, structurally similar to the ones used in *Supercomponibile '67*. A modern material, Formica ColorCore® CC7940 spectrum yellow matte 58 was therefore first fully characterized to ensure that structure and materials used to produce it were similar to the ones of *Supercomponibile '67*. XRF and EDS confirmed similar inorganics composition, while SEM allowed to verify the cellulose fibers were dimensionally comparable to the ones observed in the samples taken from *Supercomponibile '67*. FTIR spectroscopy showed the use of melamine-formaldehyde in the laminate.

The further step was to artificially age the Formica spectrum yellow sample in order to accelerate oxidative degradation of the material, at 145° in static oven. Several parameters were monitored during and after the artificial ageing. Weight loss % was more intense in the first 100 hours, probably due do the evaporation of water and formaldehyde. After 1500 hours FTIR spectroscopy detected a newly formed carbonyl band ascribable to oxidation phenomena, plausibly of both the cellulose and the melamine-formaldehyde fractions. Color changes were monitored to show severe decrease of L* and b* parameters, coherent with the progressive darkening of the sample during artificial ageing.

Finally, thermogravimetric analysis did not show particularly significant changes aside from the loss of adsorbed water in the aged samples.

All these results confirm the superior resistance of melamine formaldehyde based laminates, while offering an interesting insight on the ageing behavior of these materials.

References

[1] M. Kohlmayr, J. Stultschnik, A. Teischinger, and A. Kandelbauer, “Drying and curing behaviour of melamine formaldehyde resin impregnated papers,” *J. Appl. Polym. Sci.*, vol. 131, no. 3, p. n/a-n/a, Feb. 2014.

[2] J. Murphy, *Additives for plastics handbooks*. Elsevier Science Ltd, 2001.

[3] W. R. Moore and E. Donnelly, “Thermal degradation of melamine-formaldehyde resins,” *J. Appl. Chem.*, vol. 13, no. 12, pp. 537–543, 2007.

[4] J. H. Lady, R. E. Adams, and I. Kesse, “A study of thermal degradation and oxidation of polymers by infrared spectroscopy. Part I. Experimental technique and butylated melamine formaldehyde and urea formaldehyde,” *J. Appl. Polym. Sci.*, vol. 3, no. 7, pp. 65–70, 1960.

[5] R. M. Silverstein and G. C. Bassler, “Spectrometric identification of organic compounds,” *J. Chem. Educ.*, vol. 39, no. 11, p. 546, Nov. 1962.

[6] S. K. Shevell and Optical Society of America., *The science of color*. Elsevier, 2003.

[7] M. Nuruddin *et al.*, “Extraction and characterization of cellulose microfibrils from agricultural wastes in an integrated biorefinery initiative,” *Cellul. Chem. Technol.*, vol. 45, no. 5–6, pp. 347–354, 2011.

[8] S. Ullah, M. A. Bustam, M. Nadeem, M. Y. Naz, W. L. Tan, and A. M. Shariff, “Synthesis and thermal degradation studies of melamine formaldehyde resins,” *Sci. World J.*, vol. 2014, 2014.

[9] J. M. M. Ferra, M. Ohlmeyer, A. M. Mendes, M. R. N. Costa, L. H. Carvalho, and F. D. Magalhães, “Evaluation of urea-formaldehyde adhesives performance by recently developed mechanical tests,” *Int. J. Adhes. Adhes.*, vol. 31, no. 3, pp. 127–134, Apr. 2011.

Chapter 11. Photochemistry of photographic films

A black and white photographic film is typically characterized by a multilayer structure containing silver halide salts (namely AgBr, AgCl or AgI) of little dimension, generally named "grains". Silver halide crystals are suspended in an animal gelatin matrix commonly called "emulsion"[1]. The emulsion, in liquid state, is applied in a thin layer on a polymer base (commonly cellulose acetate or polyester). At least one protective layer called “supercoat” is added to the film. This layer has the purpose of protecting the sensitive silver halide emulsion from physical stresses during the use, and it is realized in hardened (crosslinked) gelatin. Finally, the backing (usually called anti-halation backing) has the function of avoiding the light to be reflected or scattered back through the emulsion lowering definition and quality of the final image. Between each layer some adhesive may be added in order to bind the layers [1], [2].

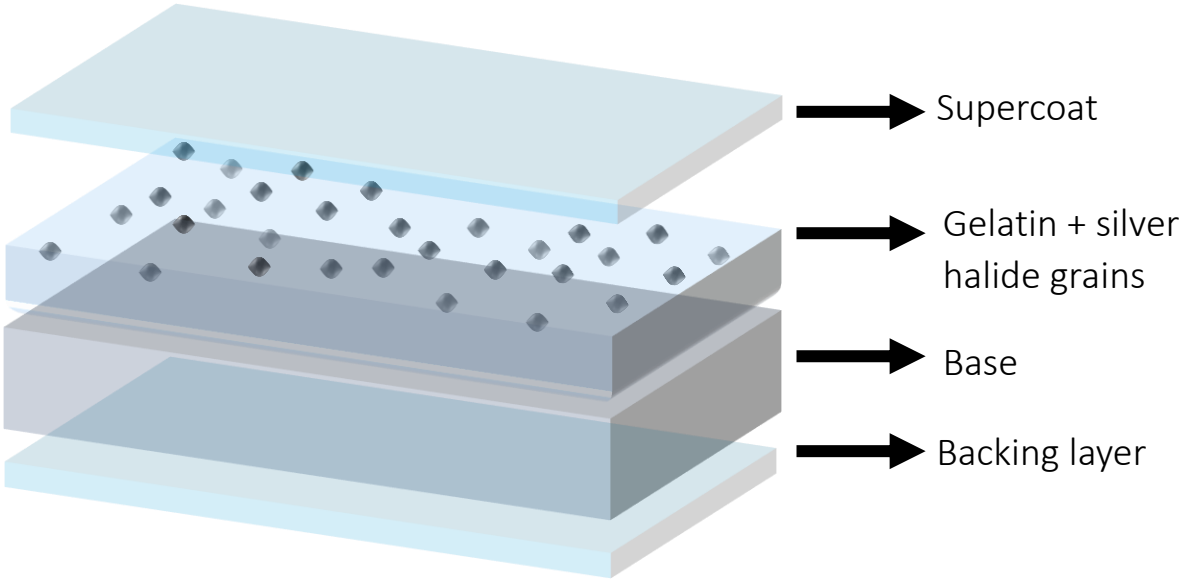

Figure 1: simplified photographic film structure

Further details about the structure and the formulation of photographic films are usually

[1] The definition of emulsion is actually incorrect, since the silver halide grains form a dispersion in the liquid gelatine during production

protected by patent and industrial secrecy, which makes extremely hard to deeply investigate single components and additives.

Silver halide grains are prepared from metallic silver, stored in ingots. Silver reacts with HNO_3 to give silver nitrate ($AgNO_3$). The solution obtained is cooled to precipitate silver nitrate crystals which reacts with appropriate alkali halides (NaCl, NaBr, NaI or KBr, KCl, KI) using gelatine as a protective colloid. The resulting dispersion, kept in a fluid state at about 40°C, to maintain in suspension the silver halide grains, is then applied on the base, where it cools, hardening. Successively, the accessory protective layers are added to the film.

When the photographic film is exposed to an appropriate light source (such as sunlight) it starts a series of chemical reactions which lead to the formation of metallic silver:

$Ag^+ Br^- + hv \rightarrow Ag^+ + Br + e^-$

$Ag^+ + e^- \rightarrow Ag^0$

The impact of photons on a photographic film generates nuclei of metallic silver, which are responsible for the formation of the so called “latent image”. The process of formation of the latent image is called “impression”.

Size and shape of silver halide grains have great influence in the latent image formation and they can be influenced by several factors during the preparation, such as the temperature, the viscosity of the solution, concentration of the reactants (halide and nitrate but also gelatin), rates and sequence of addition of them [2]. Once impressed, the photographic film undergoes a process called “development” as it is treated with appropriate chemical products (such as hydroquinone) which act reducing the halide grains close to the metallic silver nuclei. The increase of metallic silver is responsible for the black portions in black and white photographic films. The reductant does not react with non-impressed silver halide grains, which have to be removed by washings to avoid further exposure to light and stabilize the image [1], [2].

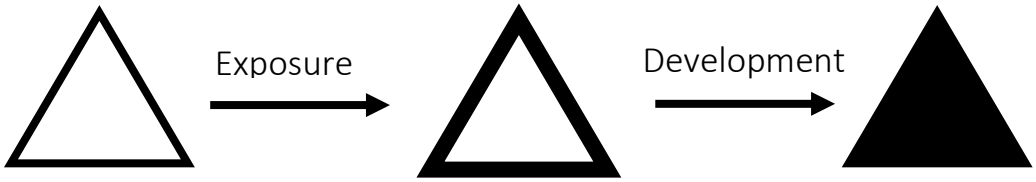

Figure 2: schematic passage from silver halide to metallic silver during photographic process

Since silver halides are generally not soluble in water (except for silver fluoride, which is not commonly used), products such as sodium thiosulfate are used to obtain complexes that are easily washable away:

$AgX + 2Na_2S_2O_3 \rightarrow Na_3Ag(S_2O_3)_2$ [soluble] + NaX

X being the halogen: Br, Cl, I

11.1. Polymeric bases

The polymeric base plays an important role in the quality of the final photographic film and it has to possess specific characteristics such as elevated transparency and the right balance between flexibility and toughness [3]. Since 1950s, different kinds of polymers have been exploited for the production of photographic films, the most important being cellulose nitrate, polystyrene, cellulose acetate and polyester (namely polyethylene terephthalate) [4]. Thickness and width may vary according to different purposes, in general polyethylene terephthalate is preferred when working with big dimensions of photographic films thanks to its good dimensional stability [2]. This introductive part will regard both cellulose acetate and polyethylene terephthalate, materials used by Paola Levi Montalcini in the two artworks studied for this thesis work.

11.1.1. Cellulose acetate (CA)

Cellulose acetate was synthetized in 1869 by the German chemist Schutzenberger, but first produced as molding powder only in 1919. It progressively started to replace the highly flammable cellulose nitrate during the 30's, with the discovery of suitable plasticizers [5]. Cellulose acetate may be produced with different degrees of acetylation, according to the degree of substitution of the hydroxyl groups. Acetylation of all OH groups produces cellulose triacetate (Figure 3) which is insoluble in the majority of organic solvents. Partial deacetylation to reach a degree of substitution of 2.6 leads to the production of a product soluble in

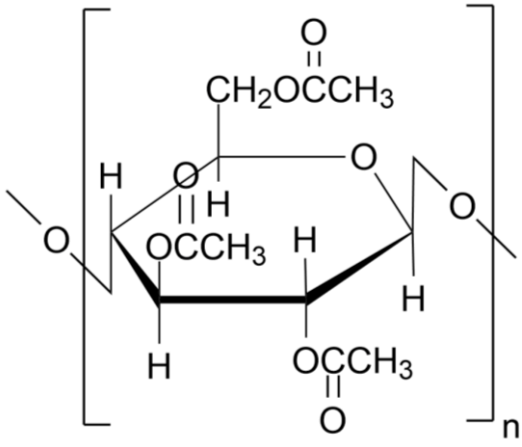

Figure 3:chemical structure of cellulose triacetate

acetone [6] hence suitable for casting from a solution, which is the regular way to produce films [5].

Degradation phenomena

Studies on photographic films showed how the loss of plasticizer may lead to shrinkage of the material increasing its brittleness [7] while at the same time deterioration of the polymer causes further loss of plasticizer in a vicious cycle strictly connected [8].

To complicate the situation, cellulose acetate spontaneously undergoes hydrolysis (eased by high temperatures and relative humidity) losing acetic acid and virtually going back to cellulose (Figure 4). The whole process is called deacetylation, or "vinegar syndrome" for the strong smell of acetic acid coming from aged cellulose acetate samples. The reaction is autocatalytic as the further production of acetic acid lowers the pH accelerating additional deacetylation (the reaction is pH dependent and cellulose diacetate is less stable than the triacetate) [9].

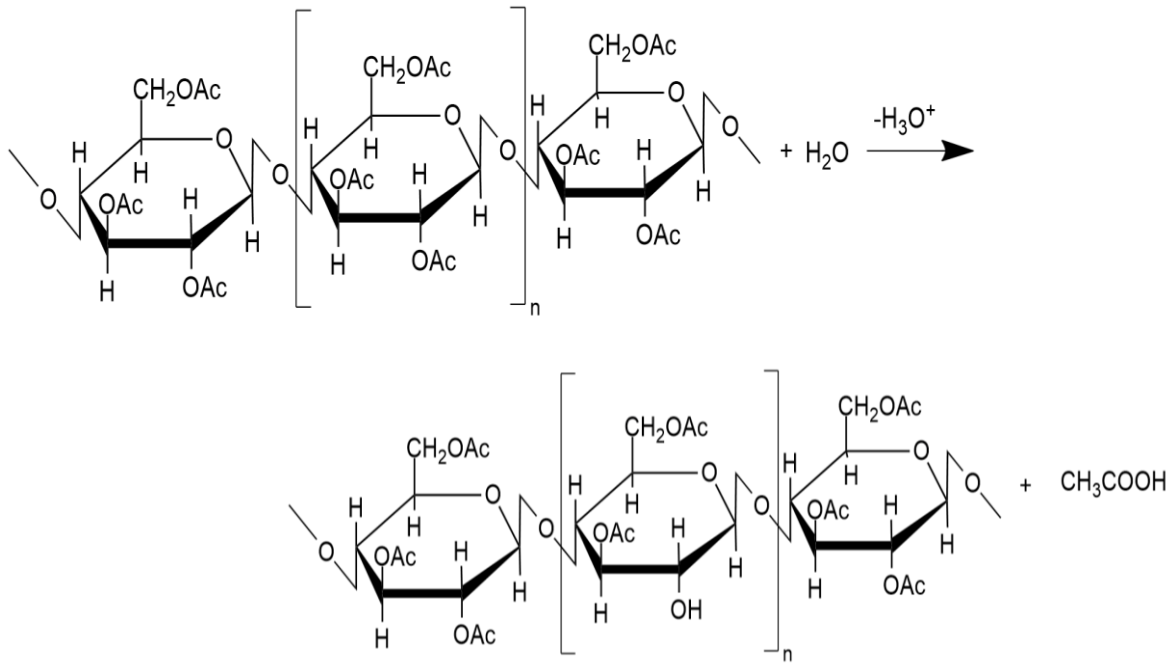

Figure 4: deacetylation of cellulose acetate (Ac is the acetate group)

11.1.2. Polyethylene terephthalate (PET)

Polyethylene terephthalate is the most common aromatic polyester, produced from terephthalic acid and ethylene glycol through esterification.

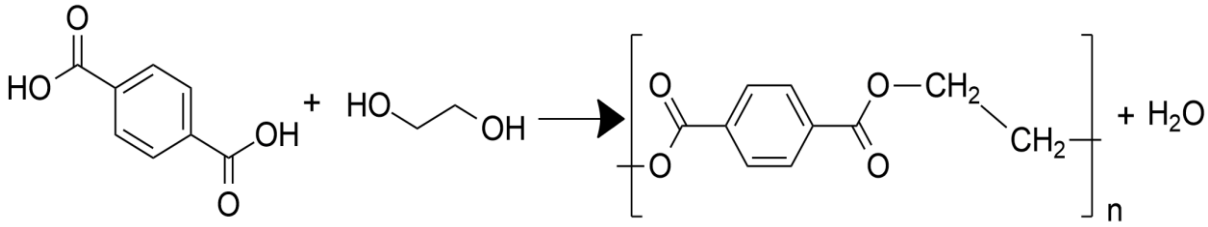

Figure 5: synthesis of polyethylene terephthalate

Since the first patent in 1941, PET had been intensively used during 40s to produce fibers and from 50s to make films, while its probably most famous application in beverage bottles followed the patent in 1973 by Dupont engineer Nathaniel Wyeth [10]. Replacing the ethylene glycol with different diols allows to prepare different polymers such as PTT (polytrimethylene terephthalate) or PBT (polybutylene terephthalate), produced, respectively, using 1,3-propanediol and 1,4-butanediol [11]. The great versatility of this polymer, in conjunction with the high melting point and glass transition temperature (respectively about 255°C and 70°C) [12] makes polyethylene terephthalate, initially created for specific applications as engineering polymer, one of the most used plastic nowadays, enough to earn the number one in the ASTM International Resin Identification Coding System (RIC) [13].

Degradation phenomena

The degree of crystallization may have a great influence in polyethylene terephthalate degradation behavior [12]. In fact, more crystalline materials exhibit higher resistance to temperature and humidity than more amorphous ones [8]. As transparency and flexibility are fundamental requirements the varieties of PET used to produce photographic films cannot be particularly crystalline, which influences the fragility of the end products.

One of the most important degradation pathways of polyethylene terephthalate is the homolytic scission around the ester linkage following a Norrish I mechanism [8]:

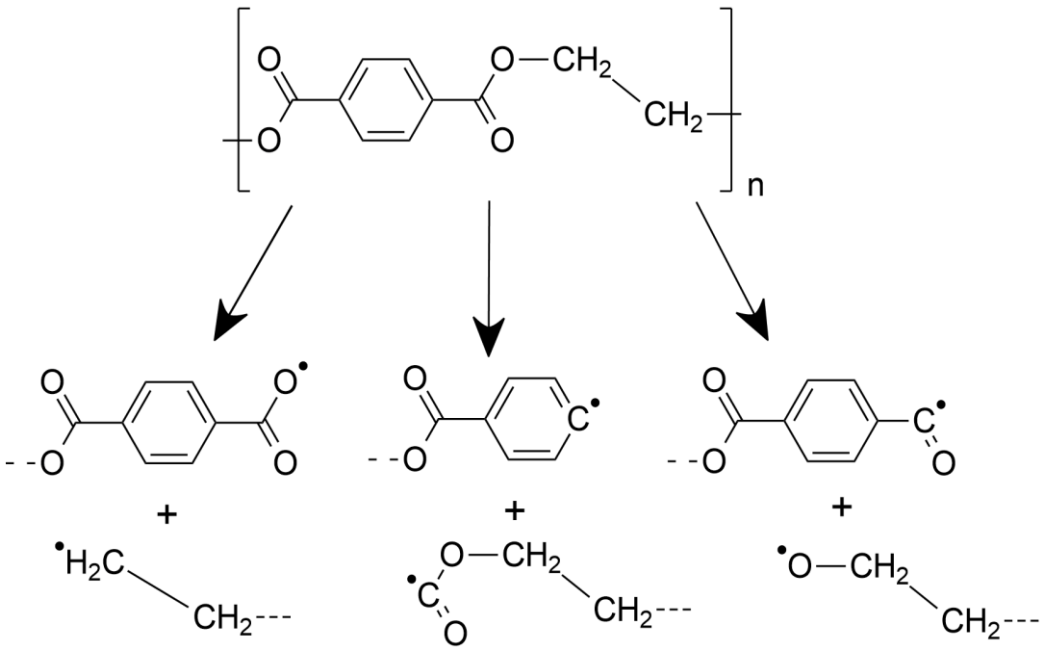

Figure 6: Norrish I scission of polyethylene terephthalate

The radical species formed can abstract inter or intra-molecular hydrogens or undergo coupling giving rise to crosslinking and consequent stiffening of the material. Hydrogen abstraction leads to the production of carbonyl containing terminal groups which are responsible for the progressive yellowing of the material.

References

[1] S. Fujita, *Organic Chemistry of Photography*. Springer Berlin Heidelberg, 2004.

[2] D. Rogers, *The chemistry of photography : from classical to digital technologies*. Royal Society of Chemistry, 2007.

[3] B.Cattaneo, *Il restauro della fotografia: Materiali fotografici e cinematografici, analogici e digitali*. 2017.

[4] M. R. P. De Gregorio, R. Falciani, A. Righini, "Studio comparato di alcune emulsioni fotomeccaniche e di alcuni rivelatori in relazione alle applicazioni nell'isodensitometria fotografica," 1967.

[5] J. A. Brydson, *Plastics materials*. Butterworth-Heinemann, 1999.

[6] S. PÉrez and D. Samain, "Structure and Engineering of Celluloses," *Adv. Carbohydr. Chem. Biochem.*, vol. 64, pp. 25–116, Jan. 2010.

[7] Y. Shashoua, *Conservation of Plastics 1st Edition*. 2008.

[8] G. Wypych, *Handbook of material weathering*. .

[9] M. Edge, N. S. Allen, T. S. Jewitt, and C. V. Horie, "Fundamental aspects of the degradation of cellulose triacetate base cinematograph film," *Polym. Degrad. Stab.*, vol. 25, no. 2–4, pp. 345–362, 1989.

[10] N. C. Wyeth and R. N. Roseveare, "Biaxially oriented poly(ethylene terephthalate) bottle," US3733309.

[11] M. Gilbert, *Brydson's Plastics Materials*, William An. 2016.

[12] J. P. Jog, "Crystallization of Polyethyleneterephthalate," *J. Macromol. Sci. Part C Polym. Rev.*, vol. 35, no. 3, pp. 531–553, Aug. 1995.

[13] "ASTM D7611 / D7611M - 19 Standard Practice for Coding Plastic Manufactured Articles for Resin Identification." .

Chapter 12. Paola Levi Montalcini: *Nel Deserto*, 1966

In 2018 two artworks from the Italian artist Paola Levi Montalcini were object of the conservation thesis of the students Micaela Storari e Fabiana Di Lorenzo under the supervision of Grazia de Cesare and Marcella Ioele[1]. Both *Nel Deserto* and *Vortice e Figura* are part of the *Net* series, composed by eight pieces property of the MART (Modern and Contemporary art museum of Trento and Rovereto). Some results of the multidisciplinary teamwork on this project were presented in October 2019 at XVII IGIIC-National Congress *Lo Stato dell'Arte* with the title "*Vortice e Figura" di Paola Levi Montalcini: intervento su un'opera polimaterica costituita da supporti fotografici affetti da sindrome acetica*[2]*.* Unique features of this series are the use by the artist of big (approximately 119x88 cm) transparent photographic films placed on panels painted with vibrant colors (both metallic and matte). When this study started in *Nel Deserto* and *Vortice e Figura* were immediately recognizable the effects of completely different conservation conditions. In particular, while *Nel Deserto* was not showing particularly evident signs of degradation, *Vortice e Figura* immediately caught the attention for the dramatic condition of the whole artwork. This surprising difference between two -apparently- similar artworks suggested each of them should be treated in different chapters, starting with *Nel Deserto* (visible in Figure 1), which results are shown below.

Figure 1: "Nel Deserto"

[1] F. Di Lorenzo and M. Storari "*Il restauro delle Reti di Paola Levi Montalcini: supporti plastici trasparenti dipinti o emulsionati fotograficamente*" PFP2, 64° Course, ISCR

[2] Authors: Micaela Storari, Fabiana Di Lorenzo, Barbara Cattaneo, Matteo Collina, Grazia De Cesare, Marcella Ioele, Natalia Macro, Angelo Raffaele Rubino, Mauro Torre

Nel Deserto (1966) is a multi-material artwork realized by the Italian artist Paola Levi Montalcini (Turin, 1909 - Rome, 2000). In occasion of the restoration, the artwork was disassembled offering the possibility to study the materials used by the artist and the nature and extension of the degradation phenomena regarding them. As visible from the scheme in Figure 2, the artwork is composed by a transparent photographic film (B), placed on a polymethylmethacrylate support painted in two different color, brilliant yellow and metallic gold (C). The whole artwork is framed (D) and sealed under a transparent plastic sheet (A).

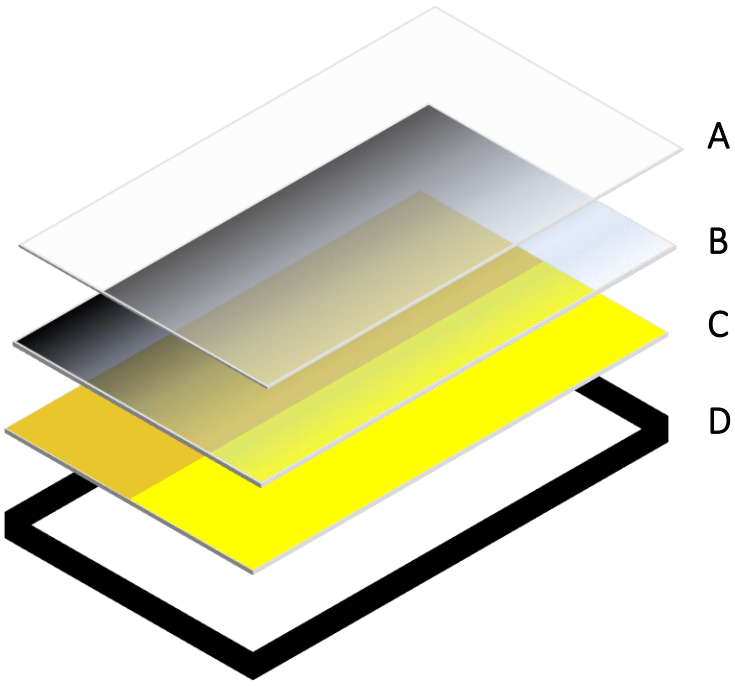

Figure 2: schematic representation of the artwork

12.1. Material characterization: non-destructive approach

For this study, the first approach involved the use of portable instrumentation such as x-ray fluorescence spectroscopy (XRF), and digital microscopy (DINO-Lite). Then, to better characterize the chemical nature of the constituent materials, some small samples have been analyzed via micro Fourier transformed infrared spectroscopy (micro-FTIR) and Scanning electron microscopy coupled with dispersive energy spectroscopy (SEM-EDS). The scientific investigation was supported by the precious contribution of Angelo Ientile, Paola Levi Montalcini's assistant during the realization of *Nel Deserto*.

12.1.1. XRF

The portable XRF technique allowed a preliminary and non-destructive screening both of painted support and photographic film to study the inorganic components. The yellow painted zone (Figure 3) contains chromium and lead (probably lead chromate, also called chrome yellow [1], titanium (likely as oxide, as white pigment) (Figure 4).

Figure 3: PMMA support painted in golden and yellow colors

The golden painted portion contains zinc and copper with small amounts of lead (most likely used to produce metallic pigment called “golden bronze” [1], but the most significative peak is the chlorine one (Figure 5).

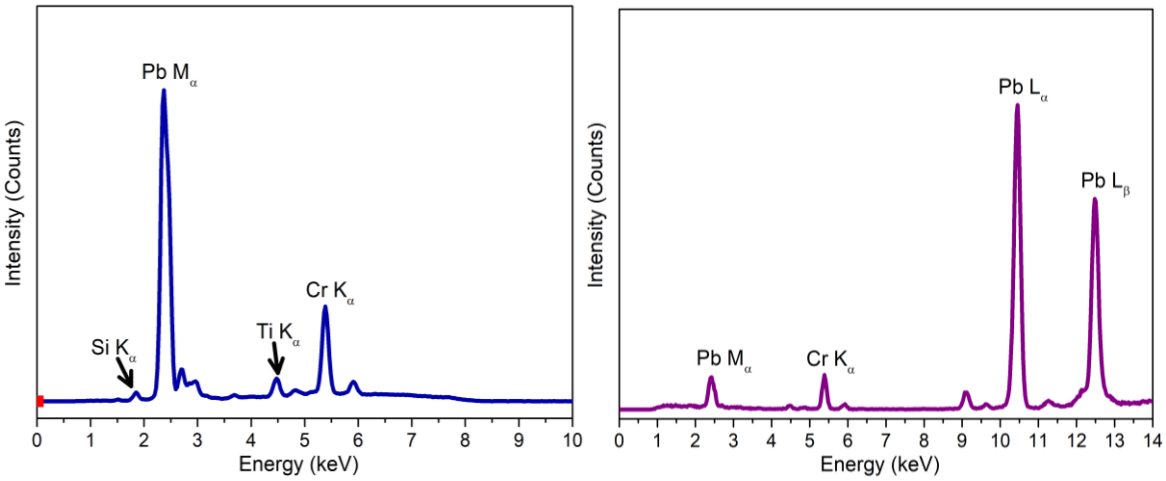

Figure 4: XRF spectra acquired on the yellow portion of the artwork. On the left 8kV excitation, on the right at 40kV

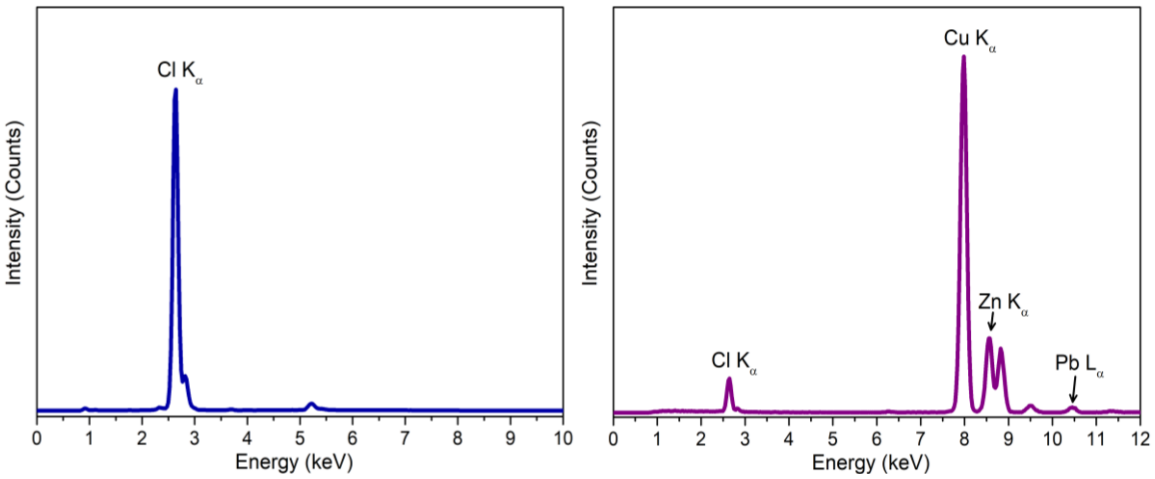

Figure 5: XRF spectra acquired on the golden portion of the artwork. On the left 8kV excitation, on the right at 40kV

The XRF measurements, carried also on some touched up zones showing different shades of golden, revealed a Zn/Cu ratio being almost constant for the different zones, suggesting the artist used the same product to fix some minor imperfections[3]. XRF measurements on the photographic film revealed the presence of small amounts (given the low counts compared to others) of silicon, sulfur, chlorine, and calcium. Silver is present only on the impressed, black colored, portions. Signals other than the K_α and K_β in Figure 6 are due to scattering of the X-ray by the sample, namely Compton and Rayleigh [2].

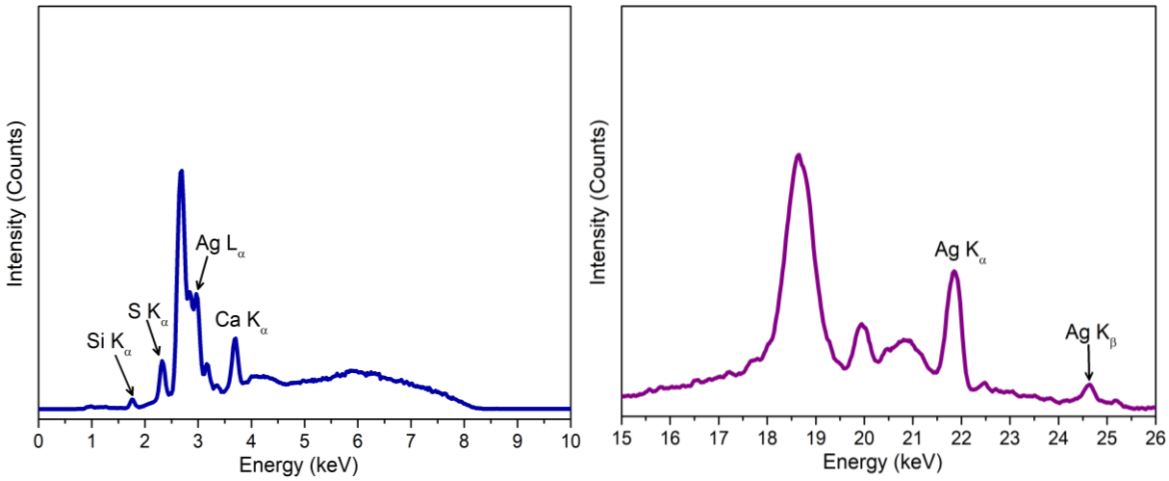

Figure 6: XRF spectra acquired on photographic film. On the left 8kV excitation, on the right at 40kV

[3] Angelo Ientile confirmed the artist provided to fill some areas of the support where the color was missing, XRF analysis clarified the product used was the same.

12.2. Sampling

All the collected sample, together with a brief description and short results for each of them, are listed in Table 1.

Sample	Techniques	Description	Results
1ND	OM, FTIR	Adhesive closing the frame	PMMA
2ND	OM, FTIR	Portion of golden paint	Brass (Cu, Zn alloy) in nitrocellulose and plasticizer
3ND	OM, FTIR	Portion of yellow paint	Lead chromate in nitrocellulose and alkyd resin
4ND	OM, FTIR, SEM-EDS	Fragment of adhesive film on the golden portion	PVC plasticized with phthalates
5ND	OM, FTIR, SEM-EDS	2 Fragments of photographic film, one for CS	PET, gelatin, silver

Table 1: samples taken from "Nel Deserto"

12.3. Adhesive characterization: sample 1ND

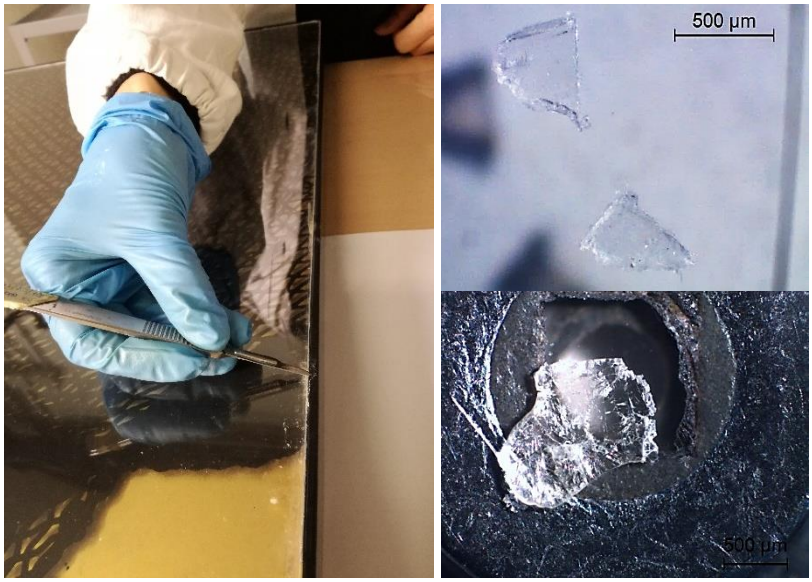

Figure 7: sampling of the adhesive from the artwork, on the right the adhesive in OM and on the diamond cell

The artist used a synthetic transparent adhesive to seal the transparent PMMA sheet to the frame and keep in place all the layers. Some of this adhesive was sampled to better understand how to remove it (Figure 7). As visible in Figure 8, the infrared spectrum shows characteristic bands of methacrylates, in particular the two doublets in the ester region at 1300-1150 cm^{-1}. The absorptions at 1269, 1242, 1192, 1149 cm^{-1} are typical of polymethylmethacrylate (PMMA) [3].

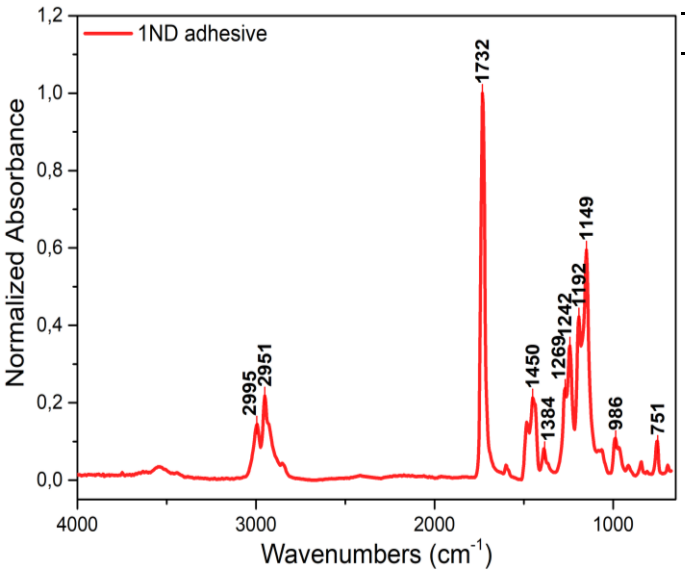

Wavenumber (cm^{-1})	Assignment
2995	ν C-H (CH_3)
2951	ν C-H (CH_2)
1732	ν C=O (acrylate ester)
1450	δ C-H (CH_3)
1384	δ C-H (CH_3)
1269	ν C-O-C
1242	ν C-O-C
1192	δ O-CH_3
1149	ρ C-H (CH_3)
986	δ O-CH_3
751	ρ C-H (α CH_3)

Figure 8: on the left FTIR spectrum of the adhesive, on the right tables with IR absorptions

12.4. Paint characterization: samples 2ND and 3ND

The polymethylmetacrylate support was, as said before, painted in two different colors, metallic golden and brilliant yellow.

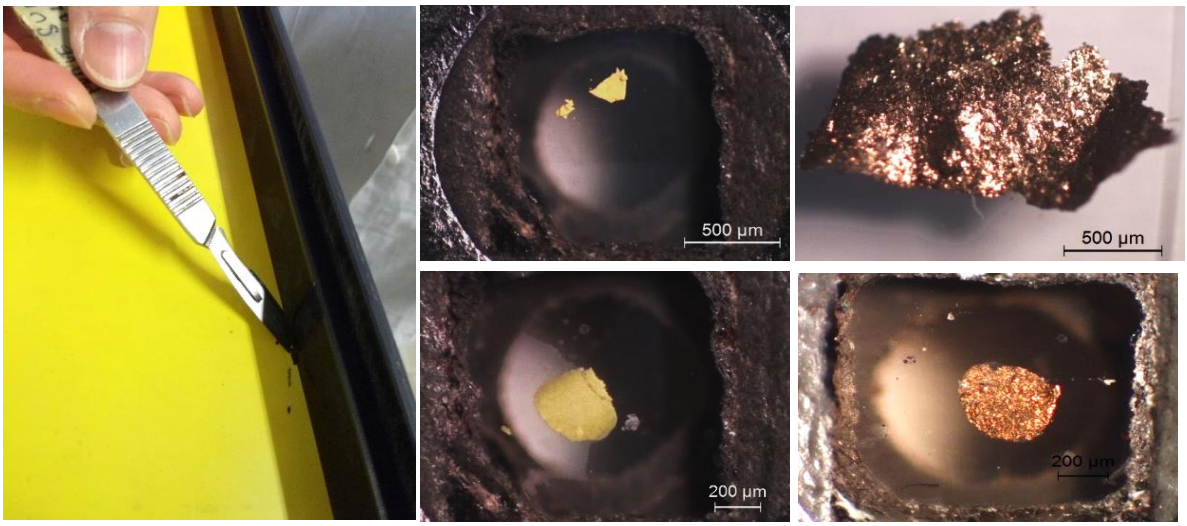

Figure 9: sampling of the yellow from the artwork, on the right yellow and golden paint in OM and on the diamond cell

Both the samples 2ND and 3ND showed very similar spectral features, suggesting that the binders may be the same for both products used. Figure 10 shows the infrared spectrum for the sample 3D (yellow paint) and the identified absorptions.

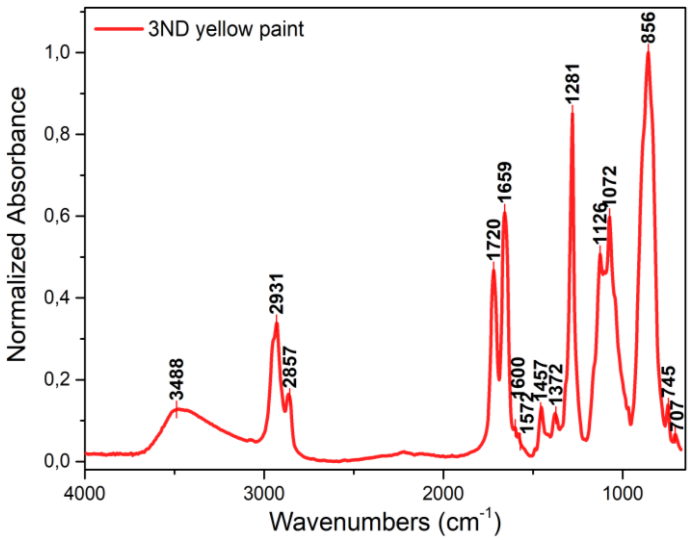

Wavenumber (cm^{-1})	Assignment
3488	ν O-H
2931	ν C-H (CH_2) alkyd
2857	ν C-H (CH_2) alkyd
1720	ν C=O alkyd
1659	ν NO_2 nitrocellulose
1600	ν C=C aromatic
1572	ν C=C aromatic
1457	δ C-H (CH_2 alkyd)
1372	δ C-H
1281	ν NO_2
1126	ν C-O-C alkyd ester
1072	ν C-O-C alkyd ester
856	ν NO_2
745	γ NO_2 + δ C-H aromatic
707	δ C-H aromatic

Figure 10: on the left FTIR spectrum of the yellow paint, on the right tables with IR absorptions

FTIR analysis clarified the binders of both yellow and golden paint are composed by a mixture of nitrocellulose and aromatic alkyd resin. As other cellulose derivates, the IR spectrum of cellulose nitrate presents, as peculiar features, absorptions associated both with hydroxy (strong signal of the stretching at 3488 cm^{-1} and bending at 1457 cm^{-1}) and ether groups (C-O at 1072 cm^{-1}) [3]. In addition, what uniquely identifiy cellulose nitrate are the absorptions linked to the nitro group, especially the NO_2 stretching (asymmetric at 1659 cm^{-1} and symmetric at 1281 cm^{-1}) and the wagging at 745 cm^{-1} (this last band may result from a combination of nitro and aromatic C-H bending) [4]. Due mostly to its property of rapid drying and smooth finish, nitrocellulose has been widely used as a binding medium in paint formulation commercially available during '50 and '60. Nowadays, the use of nitrocellulose is limited to some specific spray formulations. [5].

To be used as binding medium, nitrocellulose must be blended with other polymers to improve some of its poor physical properties (adherence, resistance, hardness). Alkyd resins were often used as second components in industrially diffused paints [6]. As seen before (Chapter 4), alkyds are unsaturated polyester resins, produced reacting polyols with di-carboxylic acids or anhydrides (usually phthalic acid or maleic anhydride [7], [8] and modified adding monobasic fatty acids in order to decrease the degree of cross-linking, improving flexibility and acting as drying agents [8], [5], [9].

The most important absorptions related to alkyd resin in the spectrum in Figure 10 are the asymmetric and symmetric C-H methylene stretching (2931 and 2857 cm^{-1}) due to the long chain derived from the fatty acid and the ester carbonyl at 1720 cm^{-1}. Peaks at 1600 and 1572 cm^{-1} (C=C stretching) and 745 and 707 cm^{-1} (C-H bending) are attributable to the aromatic fraction.

12.5. Transparent film characterization: sample 4ND

The XRF *in-situ* measurement showed the presence of an important amount of chlorine on the surface of the golden painted portion of the support, in addition it was also possible to observe the presence of swallowed zones (Figure 11), on what appeared to be a plastic film layer. The interview with Angelo Ientile, Montalcini's personal assistant, confirmed the choice of the artist to protect the golden painted portion with an adhesive transparent film to overcome the lack of adherence of the paint itself on the plastic support. This evidence, in conjunction with the presence of chlorine detected by XRF analysis, lead to the hypothesis that the film was made of a chlorinated synthetic polymer, such as polyvinylchloride (PVC).

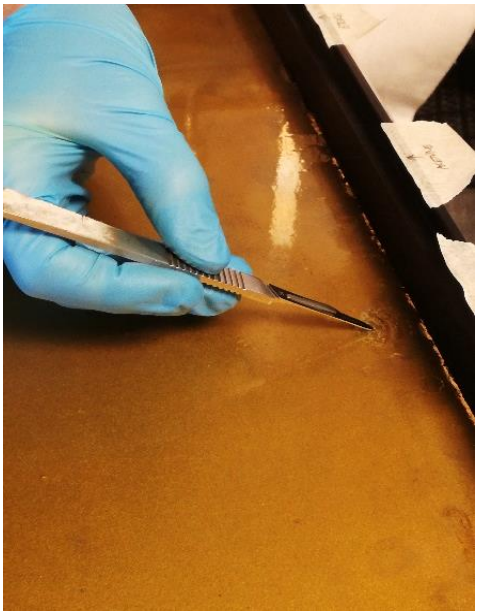

Figure 11: transparent plastic film on the golden paint

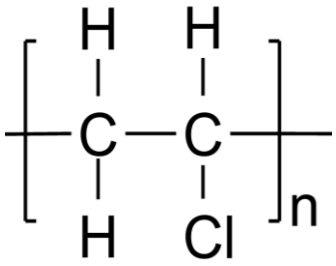

Figure 12: chemical structure of PVC

FTIR analysis (Figure 13) confirmed this assumption, as clearly visible from the presence of C-Cl stretching bands (690 and 617 cm^{-1}) [10]. Other important features of PVC are methylene (CH_2) absorptions (scissoring at 1431 and rocking at 969 cm^{-1}), C-H bending (-CH-Cl-group) at 1327 cm^{-1} and 1254 cm^{-1} and the slight signal at 1076 cm^{-1} related to C-C stretching [3]. Unplasticized PVC is a brittle and rigid material, thanks to the presence of the chlorine atom in the aliphatic chain [7]. To overcome this problem, plasticizers are usually added to the polymer in order to decrease the glass transition temperature and increase the flexibility of the final product. Phthalic acid esters are commonly used as plasticizers for PVC because of their similar solubility parameters to the polymer [11]. Plasticizers can make harder the identification of PVC because of their usually dominant spectral features [3], such as the ester carbonyl absorption (1732 cm^{-1}) or the C=C aromatic stretching (1583 cm^{-1}). The absorptions at 1176 and 1138 cm^{-1} could be due to the presence of non-

drying alkyd resins, nowadays often added as plasticizers thanks to their lower toxicity towards humans and their superior compatibility with PVC [12].

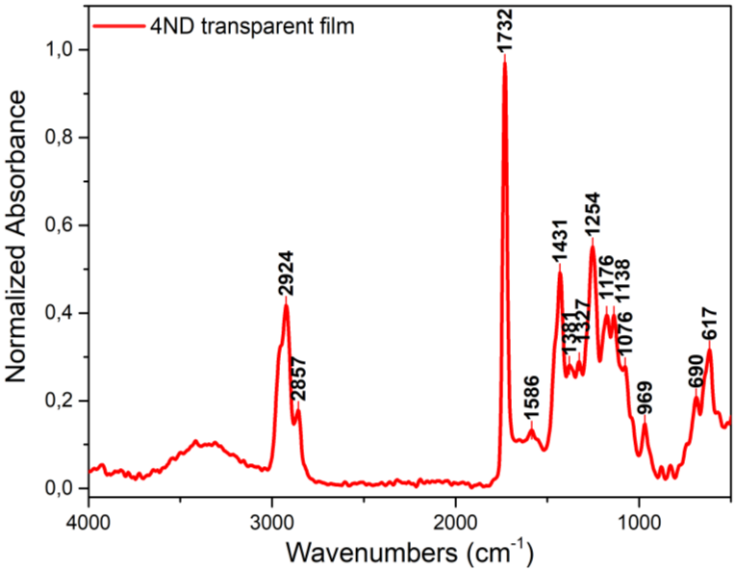

Wavenumber (cm^{-1})	Assignment
2924	ν C-H (CH_2)
2857	ν C-H (CH_2)
1732	ν C=O phthalate
1586	ν C=C (aromatic)
1431	δ CH_2 PVC
1381	δ C-H
1327	δ CH -CHCl-
1254	δ CH -CHCl-
1176	ν C-O-C (alkyd)
1138	ν C-O-C (alkyd)
1076	ν C-C PVC
969	ρ C-H (CH_2) PVC
690	ν C-Cl PVC
617	ν C-Cl PVC

Figure 13: on the left FTIR spectrum of the plastic film, on the right tables with IR absorptions

Adhesive under PVC

The adhesive, sampled from the interface between the PVC film and the golden paint, showed (Figure 14) typical acrylic polymers absorptions, such as methylene and methyl bending at 1450 and 1388 cm^{-1}, carbonyl stretching at 1732 cm^{-1}, the C-O-C asymmetrical and symmetrical stretching at 1246 and 1153 cm^{-1} [13].

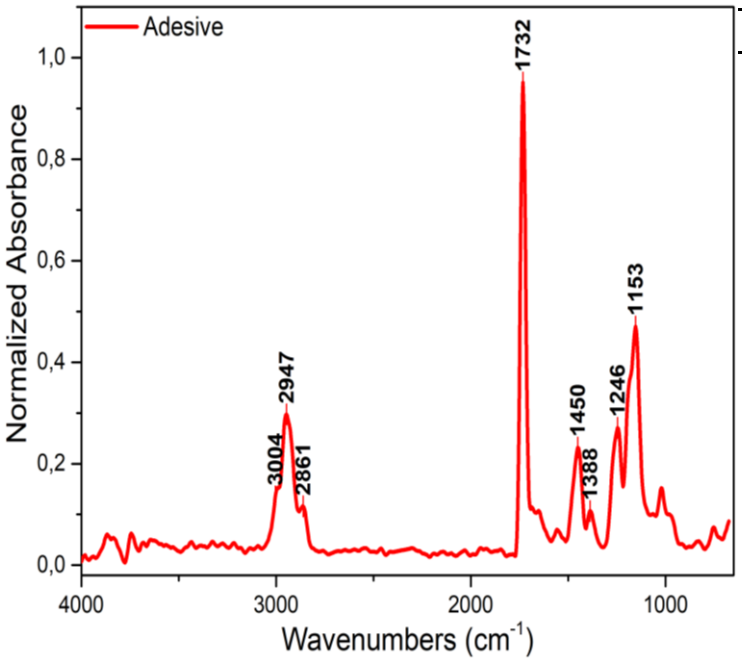

Wavenumber (cm^{-1})	Assignment
3004	ν CH_3
2947	ν CH_2
2861	ν CH_3
1732	ν C=O
1450	δ CH_2
1388	δ CH_3
1246	ν C-O-C
1153	ν C-O-C

Figure 14: on the left FTIR spectrum of the adhesive under PVC film, on the right tables with IR absorptions

The presence of a single peak at 1243 cm^{-1} may help with the discrimination between acrylates and methacrylates, considering that the seconds usually exhibit a doublet in that spectral region [14].

12.6. Degradation phenomena

Observing the golden paint sample under optical microscope, it was possible to notice the presence of a greenish deposit (visible in Figure 15) in the portion of the paint right under the PVC plastic film.

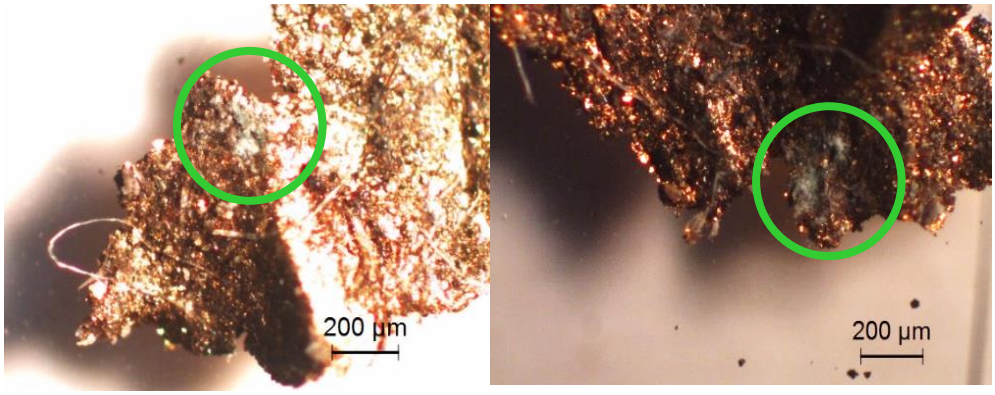

Figure 15: sample of golden paint showing grey/green salts

Once selectively removed using a scalpel, the substance was analyzed via FTIR (Figure 16) revealing the occurrence of a copper halide, namely atacamite $Cu_2Cl(OH)_3$. The copper oxychloride atacamite is usually found as degradation product on bronze object exposed to chlorine rich (such as marine) environments. Atacamite was also found to be an important component of the patina on the Statue of Liberty [15], [16], [17]. Copper chlorides are easily washed away by rains, which clearly did not represent a problem in the formation of atacamite by reaction of the copper in the bronze paint and the chlorine released by the PVC transparent film. It is well known [18], [19], [20] how dehydrochlorination is the most important chemical degradation pattern for polyvinylchloride.

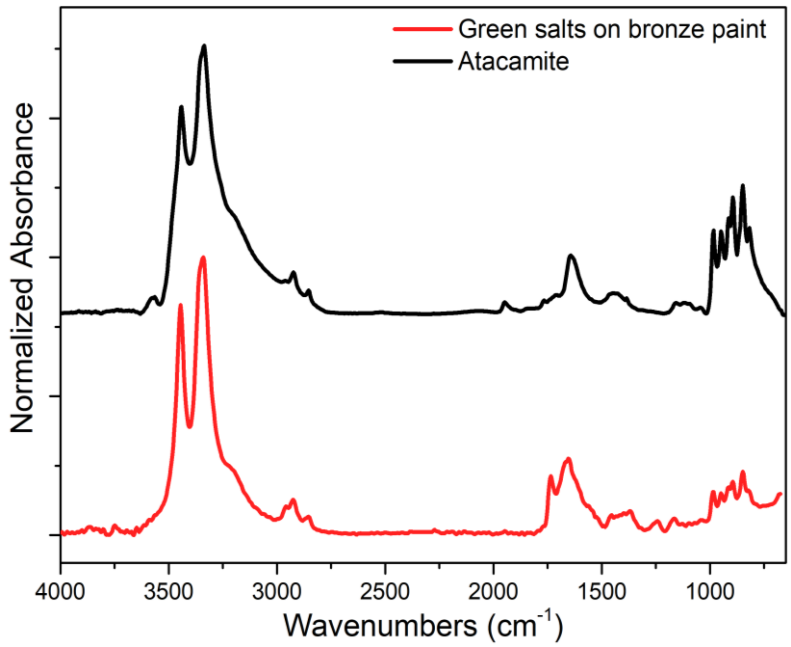

Figure 16: spectral comparison between the green salts on the bronze paint and atacamite

12.7. Photographic film characterization: sample 5ND

12.7.1. Base

The preliminary observation of the photographic film through portable optical microscopy allowed to find a small portion of a corner, plausibly free from any external layer other than the polymeric base. A small fragment was sampled from this portion and analyzed via FTIR (Figure 17); the spectrum obtained exhibits absorption characteristic of a saturated polyester, namely polyethylene terephthalate (Figure 18). More specifically, it is possible to recognize absorptions due to the aromatic ring vibrational modes (C-H stretching at 3067 cm^{-1}, C=C bending at 1577 and 1505 cm^{-1}, out-of-plane C-H bending in the region 900-675 cm^{-1} [21]. The absorption at 729 cm^{-1} is diagnostic for PET and it is due to the interaction of the C=O ester group with the aromatic ring [22].

Figure 17: sampling of small fragment of photographic film, on the right the sample in OM and on the diamond cell

Compared to other plastic polymers commonly used in photographic films (such as cellulose nitrate and acetate) PET exhibits superior physical properties such as dimensional stability [23], resistance to hydrolysis [24]. Such reasons contributed to make PET a material commonly used to produce photographic supports.

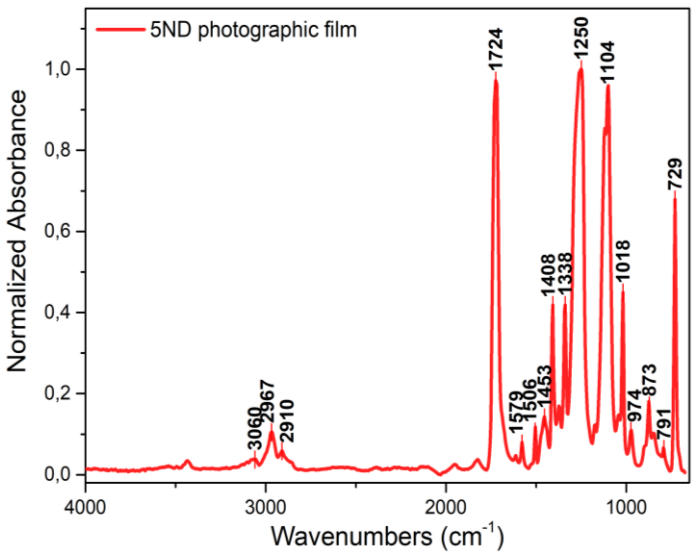

Wavenumber (cm^{-1})	Assignment
3060	ν C-H aromatic
2967	ν C-H (CH_2)
2910	ν C-H (CH_2)
1724	ν C=O
1579	δ C=C aromatic
1506	δ C=C aromatic
1453	ν C-O + ω C-H (CH_2)
1408	ν C-O + ω C-H (CH_2)
1338	ν C-O + ω C-H (CH_2)
1250	ν C-O-C
1104	ν C-O-C
1018	δ C-H aromatic
974	δ C-H aromatic ring + δ C-O-C
873	δ C-H aromatic
791	δ C-C out of plane
729	δ C-H aromatic

Figure 18: on the left FTIR spectrum of base from the photographic film, on the right tables with IR absorptions

12.7.2. Supercoat & Backing

Another small fragment from another corner of the film was sampled in order to study the superficial gelatin coating (supercoat), which was recognized thanks to observation through portable microscopy. The first approach was to scrape the surface of the fragment using a scalpel and to analyze the residue via FTIR.

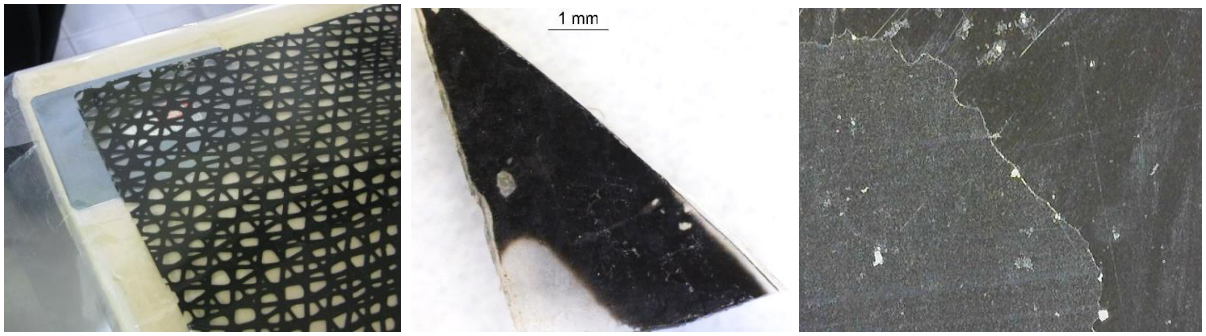

Figure 19: on the left the corner of photographic film from which the fragment was sampled on the right a detail in portable microscopy

The FTIR spectrum, showed in Figure 20 appears extremely complex, due to the contribution of different chemical species, most likely animal gelatin, calcium carbonate and a silicone polymer. The presence of the carbonyl peak at 1737 cm^{-1} has not been identified but could be due to the addition of a wax ester (such as carnauba, candelilla or beeswax) as reported [25]. It is possible to recognize absorptions typical of gelatin, such as the amide A and B (respectively at 3279 and 3069 cm^{-1}), the amide I and II (1651 and 1543 cm^{-1}) [26], [27].

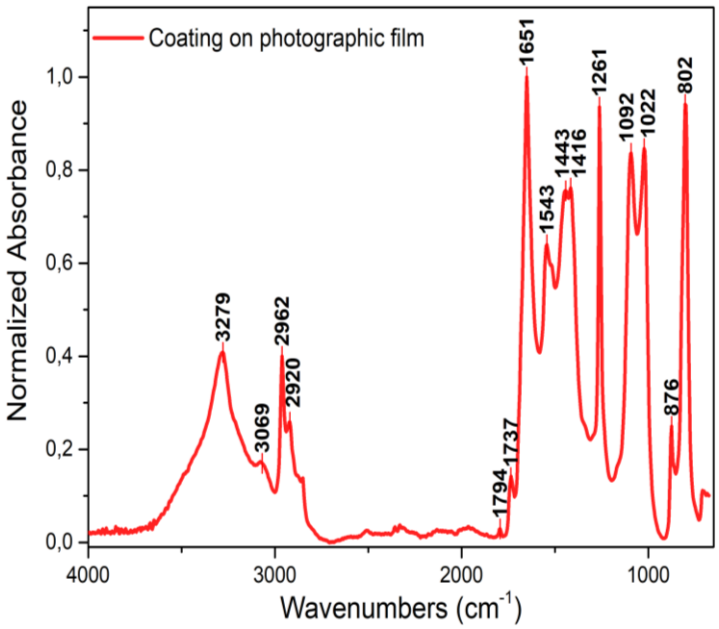

Wavenumber (cm^{-1})	Assignment
3279	ν N-H (gelatin)
3069	ν N-H (gelatin)
2962	ν C-H (CH_3)
2920	ν C-H (CH_2)
1794	ν CO_3 ($CaCO_3$)
1737	ν C=O (ester)
1651	ν C=O (gelatin)
1543	δ N-H (gelatin)
1443	δ C-H (CH_2) (gelatin)
1416	ν CO_3 ($CaCO_3$)
1261	δ Si-C-H (siloxane)
1092	ν Si-O-Si (siloxane)
1022	ν Si-O-Si (siloxane)
876	ν CO_3 ($CaCO_3$)
802	δ Si-C-H (CH_3 siloxane)

Figure 20: on the left FTIR spectrum coating on the photographic film, on the right tables with IR absorptions

Absorptions at 1794, 1416, 876 cm^{-1} are attributable to calcium carbonate vibrational modes. The presence of a silicon-based polymer (namely polysiloxane) is deducible from the signals at 1261 and 802 cm^{-1} (bending of Si-CH_3) in conjunction with 1092 and 1022 cm^{-1} (stretching Si-O-Si).

Silicones are synthetic polymers characterized by the siloxane backbone (Figure 21) which, in conjunction with the presence of different organic groups attached to the silicon atom, make this class of polymers extremely versatile. Some outstanding properties of silicones are their high temperature and oxidative stability and the low surface tension, which make them capable of wetting a large variety of surfaces [28],[29].

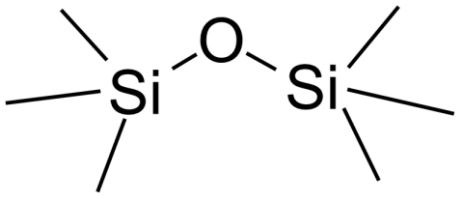

Figure 21: siloxane linkage

Polydimethylsiloxane (PDMS, also called dimethicone) is nowadays one of the most used silicones also thanks to its chemical and physical properties. The low elastic modulus allows PDMS to work as a rubber [30] and the presence of non-polar methyl groups helps shielding the polar Si-O backbone and forming very hydrophobic films while maintaining a high permeability to oxygen and water vapor. The presence of a particularly strong peak at 2962 cm^{-1} (due to methyl stretching) and the relative intensities of Si-O-Si and Si-CH_3 absorptions lead to the

hypothesis the silicone present in the supercoat is, indeed, polydimethylsiloxane [30]. However, the lack of information about the industrial formulas used in the production of photographic films does not allow to get to a definitive interpretation. Both supercoat and backing are expected to be thin compared to base and emulsion layer, hence the traditional preparation methodology, based on separating under optical microscopy the components of a sample, could lead to errors. Therefore, to better study the stratigraphy of supercoat and backing layers, a fragment of the sample in Figure 19 was analyzed via FTIR using the ATR accessory (equipped with a germanium crystal). The small tip of the ATR allows to vary the applied pressure increasing penetration and so measuring deeper layers without damaging the sample. The analyzed portions are highlighted by a yellow circle in the following figures.

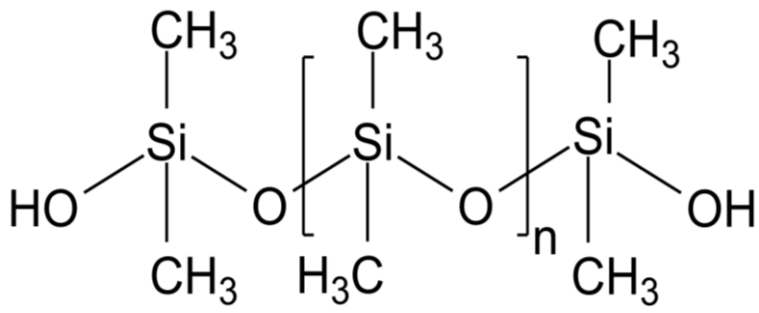

Figure 22: chemical structure of polydimethylsiloxane

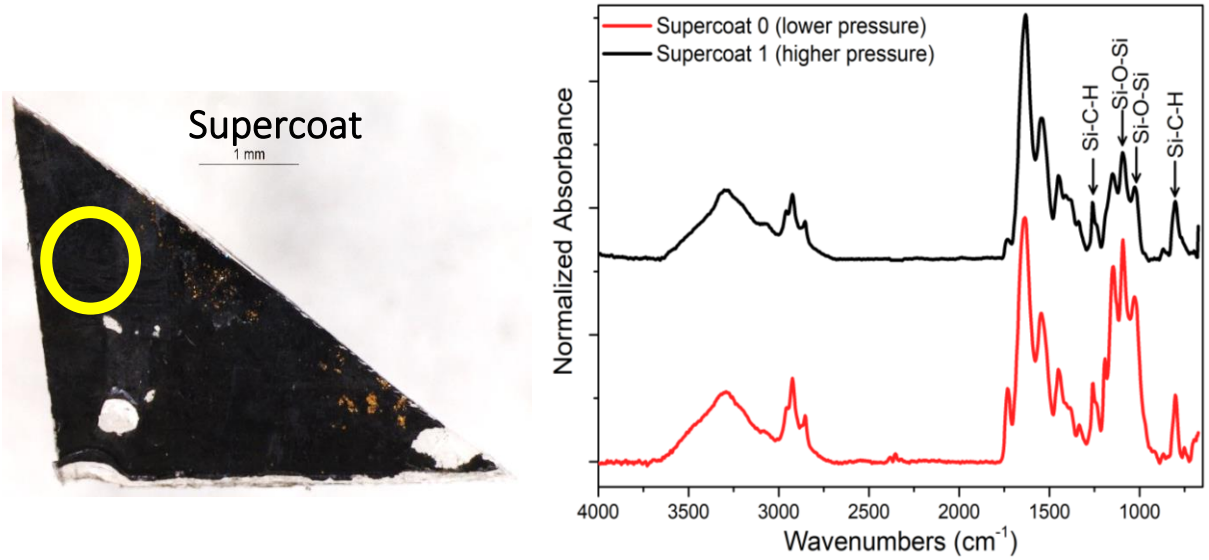

Figure 23: on the left a fragment of photographic film on the supercoat side, on the right comparison between spectra registered at different pressure of the ATR tip

As visible in the spectral comparison in Figure 23, increasing the pressure of the tip the signals linked to the presence of a polysiloxane decrease, suggesting the silicone is present only on the most superficial layer. The same analysis on the backing layer showed increasing amounts of what appears to be a long chain acrylate, in particular considering the methylene and ester modes (Figure 24). Typical of acrylates (differently from methacrylates) is the appearance of a doublet of peaks in the C-O stretching area [3]. Once again, the lack of detailed information about photographic films

components makes harder to interpret this information, but it is plausible to link it to the presence of an acrylic adhesive

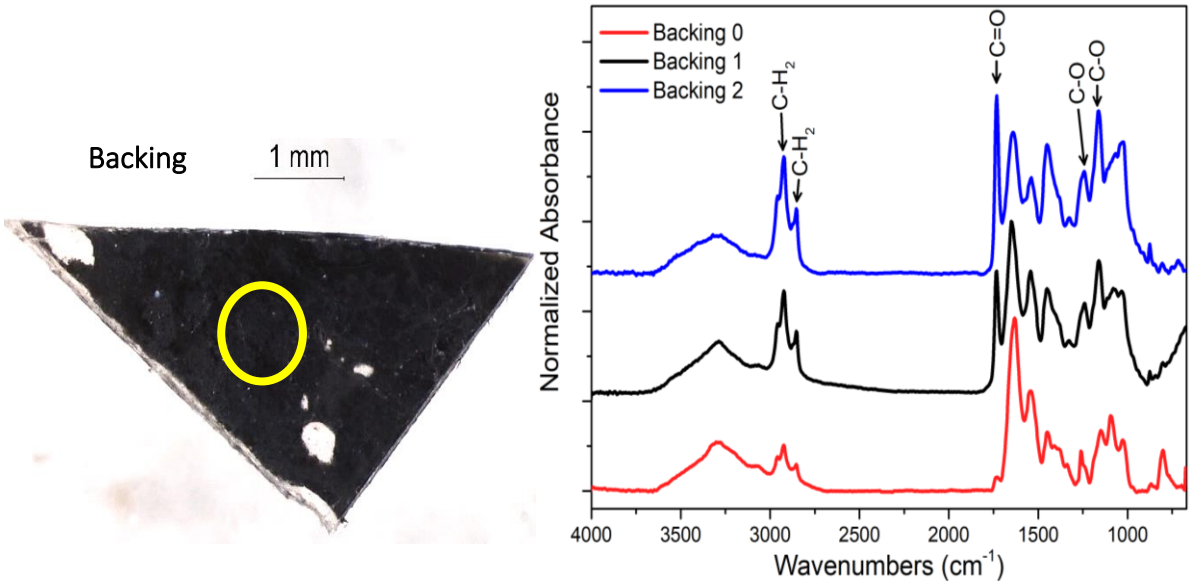

Figure 24: on the left a fragment of photographic film on the backing side, on the right comparison between spectra registered at different pressure of the ATR tip. Pressure of the tip increased from Backing 0 to 2.

The same sample was then embedded in resin and prepared in cross section to be studied through optical microscopy (in UV light) and SEM-EDS.

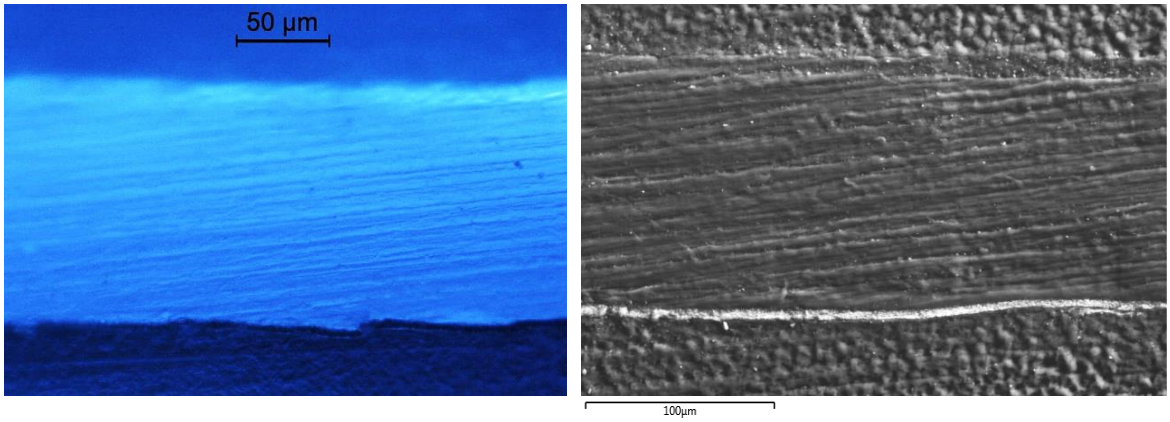

Figure 25: cross section of the photographic film, on the left in OM under UV light, on the right in SEM BDS

Under UV light the photographic film cross section showed fluorescence, particularly intense on the backing layer, while in backscattered electrons the impressed layer appeared more light in color, according to the relatively higher atomic weight of the silver contained in this portion (Figure 25). SEM-EDS analysis provided information on the thickness and the elemental composition of each layer. In particular, while the first layer (supercoat and silver gelatin) is 5 µm thick, the base is 120 µm and the backing is approximately 10-15 µm. EDS maps of elements (Figure 26) confirmed results

obtained through portable XRF, in particular the presence of silver (on the silver gelatin), potassium, sulfur, chlorine, calcium and silicon. The lack of a more defined layer of silicon suggests the polysiloxane was not uniformly spread on the supercoat, and only sporadically present, perhaps as a contaminant. The higher concentration of sulfur on the silver gelatin may be related to tarnish of silver forming Ag_2S (mineral acanthite).

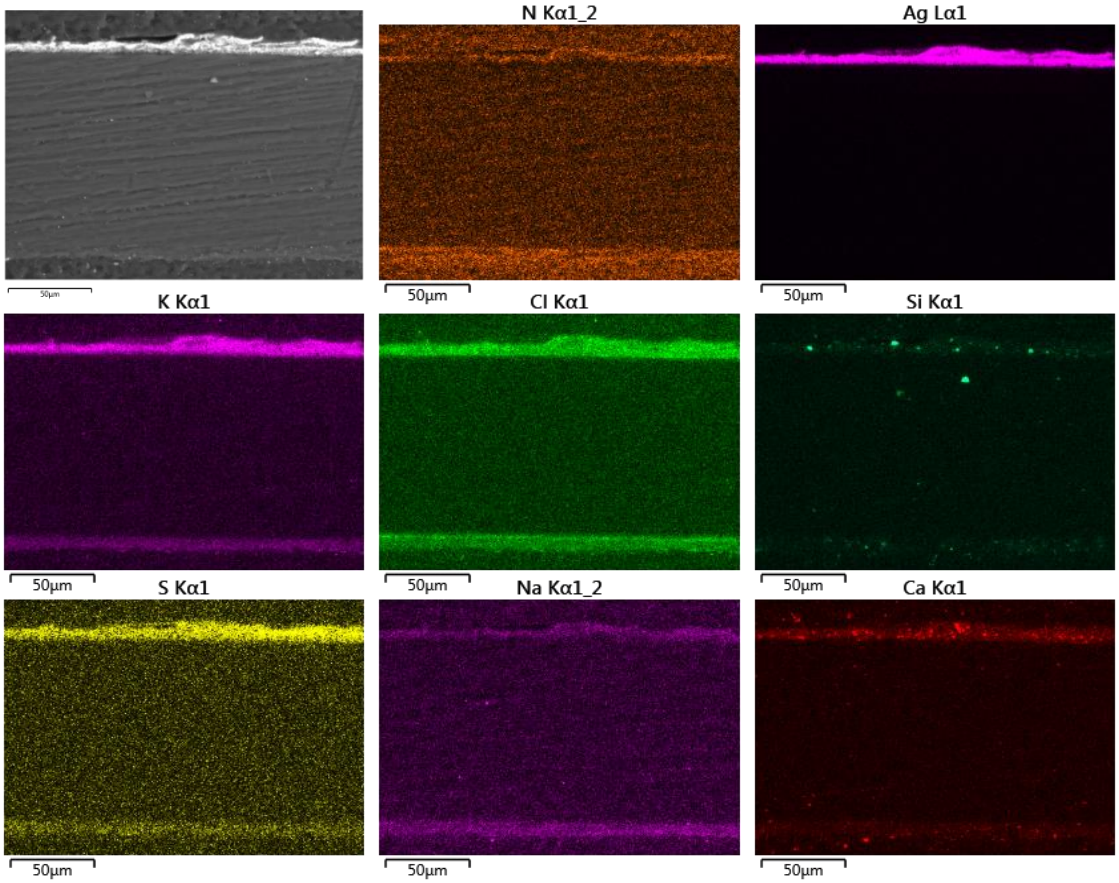

Figure 26: On the left top corner SEM BSD image of a portion of the photographic film cross section, the others are EDS maps of elements on the same area

12.8. Conclusions

The study of Paola Levi Montalcini's artworks, *Nel Deserto* and *Vortice e Figura*, represented a priceless opportunity both for the large variety of synthetic materials associated together, and for the possibility to actively communicate with Angelo Ientile, Montalcini's assistant. Ientile provided important information which helped characterizing the materials and understanding the artist's intentions.

The preliminary characterization of the materials through portable XRF revealed the yellow paint used on the PMMA support plausibly contains lead chromate and titanium dioxide as white pigment. On the golden portion XRF detected zinc and copper, associated in a brass alloy (industrial pigment usually called "golden bronze"). However, the significant presence of chlorine on the golden portion required further investigations. Observing closely the artwork it was possible to notice the occurrence of a transparent film on the golden portion, which also contained signs of touching-up. Ientile confirmed the artist first personally touched up some zones as the PMMA support was not providing good adhesion to the golden paint, and then decided to seal in place the paint applying an adhesive transparent film on the whole golden surface. A small portion of this transparent film was characterized via FTIR as polyvinylchloride, glued using an acrylic adhesive. Binders of both paint colors were characterized as composed by nitrocellulose and alkyd resin. Seeing the artwork after a long time, Ientile noticed a deep change in the golden paint, which appeared darkened. Observation through optical microscopy revealed the presence, on a paint sample taken under the PVC film, of green/greyish salts, characterized as copper chloride (atacamite). It is plausible to assume the PVC film lost hydrogen chloride (through dehydrochlorination) which reacted with the copper of the golden paint forming green colored atacamite.

Nel Deserto contains a single photographic film, made of PET and covered by a silver halide-based (silver was detected both with XRF and SEM-EDS) emulsion (containing animal gelatin). FTIR analysis revealed the presence of siloxane and calcium carbonate in the supercoat layer, although since SEM-EDS did not detect a uniform layer of silicon on the same surface, it is reasonable to assume such elements are contaminants.

References

[1] G. Buxbaum and G. Pfaff, *Industrial Inorganic Pigments: Third Edition*. 2005.

[2] P. Brouwer, *Theory of XRF*. 2010.

[3] H. Lobo and J. V. Bonilla, *Handbook of plastics analysis*. Marcel Dekker, 2003.

[4] V. I. Kovalenko, R. M. Mukhamadeeva, L. N. Maklakova, and N. G. Gustova, “Interpretation of the IR spectrum and structure of cellulose nitrate,” *J. Struct. Chem.*, vol. 34, no. 4, pp. 540–547, 1994.

[5] T. Learner and Getty Conservation Institute., *Analysis of modern paints*. Getty Conservation Institute, 2004.

[6] J. H. Stoner, “Conservation of Easel Paintings,” *Conserv. Easel Paint.*, 2013.

[7] J. A. Brydson, *Plastics materials*. Butterworth-Heinemann, 1999.

[8] M. Gilbert, *Brydson's Plastics Materials*, William An. 2016.

[9] R. Ploeger and O. Chiantore, "Characterization and Stability Issues of Artists' Alkyd Paints," *New*, no. November 2010, pp. 89–95, 2013.

[10] S. Narita, S. Ichinohe, and S. Enomoto, "Infrared spectrum of polyvinyl chloride. II," *J. Polym. Sci.*, vol. 37, no. 131, pp. 281–294, 1959.

[11] G. Wypych, *Handbook of plasticizers*. ChemTec Pub., 2004.

[12] K. Lim, Y. Ching, and S. Gan, "Effect of Palm Oil Bio-Based Plasticizer on the Morphological, Thermal and Mechanical Properties of Poly(Vinyl Chloride)," *Polymers (Basel).*, vol. 7, no. 10, pp. 2031–2043, Oct. 2015.

[13] J. Zięba-Palus, "The usefulness of infrared spectroscopy in examinations of adhesive tapes for forensic purposes," *Forensic Sci. Criminol.*, vol. 2, no. 2, pp. 1–9, 2017.

[14] O. Chiantore and M. Lazzari, "Characterization of acrylic resins," *Int. J. Polym. Anal. Charact.*, vol. 2, no. 4, pp. 395–408, 1996.

[15] I. Peterson, "Lessons Learned from a Lady," *Sci. News*, vol. 130, no. 25–26, pp. 392–395, 1986.

[16] W. H. J. Vernon and L. Whitby, "The open-air corrosion of copper: a chemical study of the surface patina," *J. Inst. Met.*, vol. 42, no. 2, pp. 181–202, 1929.

[17] R. L. Opila, "Copper patinas: an investigation by Auger electron spectroscopy," *Corros. Sci.*, vol. 27, no. 7, pp. 685–694, Jan. 1987.

[18] C. S. Marvel, J. H. Sample, and M. F. Roy, "The Structure of Vinyl Polymers. VI. [1] Polyvinyl Halides," *J. Am. Chem. Soc.*, vol. 61, no. 12, pp. 3241–3244, Dec. 1939.

[19] G. Wypych, *Handbook of material weathering*. .

[20] G. Wypych, *PVC Degradation and Stabilization.* Elsevier Science, 2015.

[21] R. M. Silverstein and G. C. Bassler, *Spectrometric identification of organic compounds*, vol. 39, no. 11. 1962.

[22] M. Edge, R. Wiles, N. S. Allen, W. A. McDonald, and S. V. Mortlock, "Characterisation of the species responsible for yellowing in melt degraded aromatic polyesters - I: Yellowing of poly(ethylene terephthalate)," *Polym. Degrad. Stab.*, vol. 53, no. 2, pp. 141–151, 1996.

[23] J. M. Calhoun, P. Z. Adelstein, and J. T. Parker, "Physical properties of estar polyester base aerial films for topographic mapping," *Photogramm. Eng.*, vol. 27, pp. 461–470, 1961.

[24] M. C. Fischer and A. Robb, "Guidelines for care and identification of film-base photographic materials," 1993, pp. 117–123.

[25] D. Stulik and A. Kaplan, *The Atlas of Analytical Signatures of Photographic Processes*. 2013.

[26] S. Krimm and J. Bandekar, "Vibrational Spectroscopy and Conformation of Peptides, Polypeptides, and Proteins," *Adv. Protein Chem.*, vol. 38, pp. 181–364, Jan. 1986.

[27] T. Riaz *et al.*, "FTIR analysis of natural and synthetic collagen," *Appl. Spectrosc. Rev.*, vol. 53, no. 9, pp. 703–746, Oct. 2018.

[28] W. Noll, *Chemistry and Technology of Silicones.* Elsevier Science, 1968.

[29] J. E. Mark, D. W. Schaefer, and G. (Scientist) Lin, *The polysiloxanes*. .

[30] L. M. Johnson *et al.*, “Elastomeric microparticles for acoustic mediated bioseparations,” *J. Nanobiotechnology*, vol. 11, no. 1, 2013.

Chapter 13. Paola Levi Montalcini, *Vortice e Figura*, 1967

As *Nel deserto*, *Vortice e figura* (1967) is a multi-material artwork composed layering different materials, protected by a PMMA sheet and framed. In spite of the many similarities with *Nel Deserto*, in *Vortice e figura* the artist decided to combine two different photographic films (B and C in Figure 1), placed onto a plywood support (D) partially painted with fluorescent red paint and partially covered with a silver plastic film. Once again, the whole artwork is protected by a PMMA sheet (A) and framed (E).

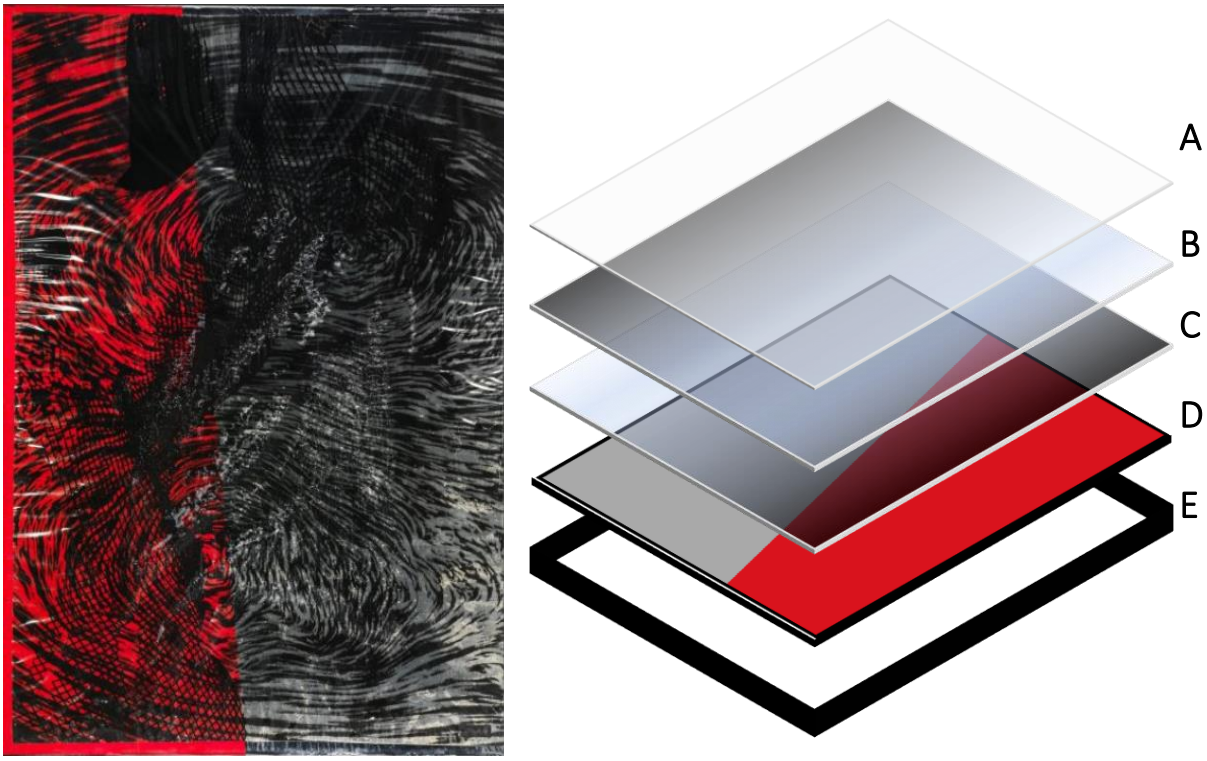

Figure 1: on the left "Vortice e figura", on the right a schematic representation of the artwork

13.1. Material characterization: non-destructive approach

The approach chosen to investigate the artwork was the same as for *Nel Deserto*, so, after a preliminary observation through portable optical microscopy and XRF analysis, some samples were taken to be analyzed through FTIR and SEM-EDS.

13.1.1. XRF

Portable XRF analysis was carried out both on the painted wood panel and on the photographic films. Aside from an initial resemblance, the silver surface appeared substantially different from the golden one in *Nel Deserto*, which was in fact obtained painting the support with golden paint and then covering it with a transparent plastic film. The silver one, as Angelo Ientile confirmed, was instead realized sticking a lucid silver film ("mirror effect") onto the wooden support, which was initially entirely painted in black (as visible on the back side of the artwork in Figure 3). XRF analysis on the silver surface (Figure 2) did not show presence of silver, coherently with the use modern metallic products, rarely containing rare (and expensive) metals. As with the golden paint, made using a copper/zinc alloy, silver pigments are usually produced using aluminum-based

Figure 3: back side of the artwork

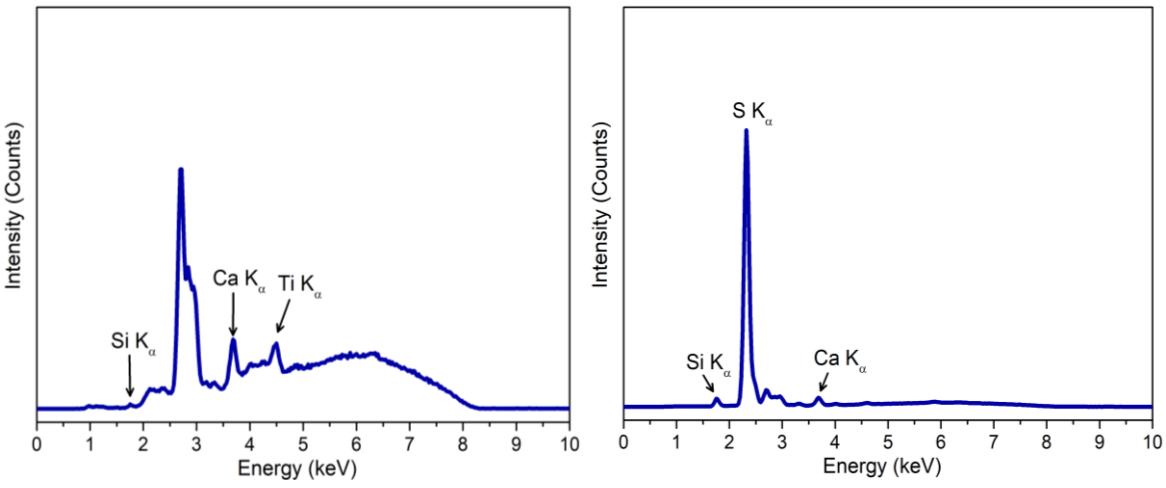

Figure 2: XRF spectra acquired on the silver (left) and red (right) portions of the artwork, with 8kV excitation.

powders [1]. Anyway, the appearance of the silver layer, suggests the use of a thin foil (rather than a powder) of aluminum plausibly wrapped between two layers of a flexible plastic polymer. On the red paint, which appeared to be fluorescent under UV light, the most significative XRF peak is due to sulfur.

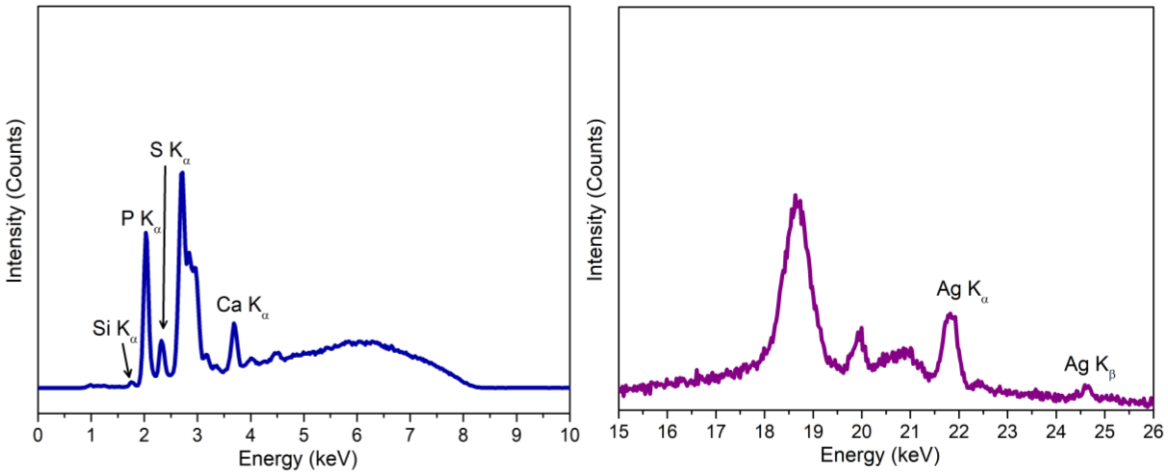

Figure 4: XRF spectra acquired on photographic film. On the left 8kV excitation, on the right at 40kV

XRF on the photographic film, aside from silver on the impressed portion, revealed the presence of phosphorous (Figure 4), the nature of which was subsequently cleared by infrared spectroscopy analysis.

13.2. Sampling

All the collected samples, together with a brief description and short results for each of them, are listed in Table 1.

Sample	Techniques	Description	Results
1VF	OM, FTIR	Deposits on PMMA	triphenyl phosphate
2VF	OM, FTIR	Portion of red paint	melamine formaldehyde sulfonamide + alkyd resin
3VF	OM, FTIR	Silver adhesive sheet	Polyethylene terephthalate + acrylic adhesive
4VF	OM, FTIR, SEM-EDS	2 Fragments of photographic film, one for CS	Cellulose acetate, gelatin, triphenyl phosphate

Table 1: samples taken from "Vortice e Figura"

13.3. Deposits on PMMA characterization: sample 1VF

Looking at the artwork, it was possible to notice the presence of diffused white circular dots on the polymethyl methacrylate sheet (Figure 5), plausibly coming from the photographic films underneath the PMMA. Observed through optical portable microscopy, these dots appeared to be mostly rayed, diffusing from a center to various directions, as visible in Figure 6. A small amount of these deposits was sampled and analyzed through FTIR.

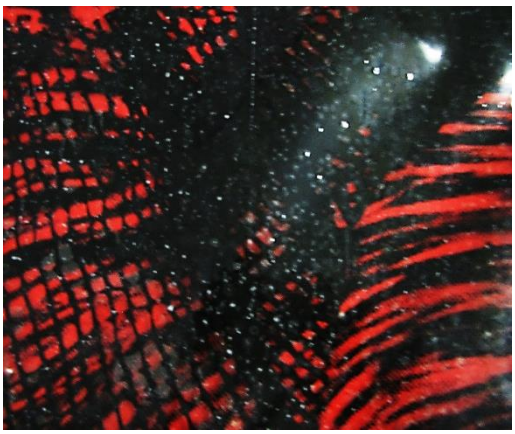

Figure 5: PMMA with white dots

Figure 6: portable OM pictures of the deposits on PMMA

FTIR analysis revealed typical spectral features of triphenyl phosphate, frequently used as plasticizer and flame retardant in highly flammable plastics such as cellulose nitrate and acetate [2].

Particularly significant are the P=O and P-O vibrational modes at 1292, 1011 and 957 cm^{-1}, while the aromatic component contributes to the spectra mainly with C-H stretching at 3057 cm^{-1} and out of plane bending at 771 and 690 cm^{-1} [3]

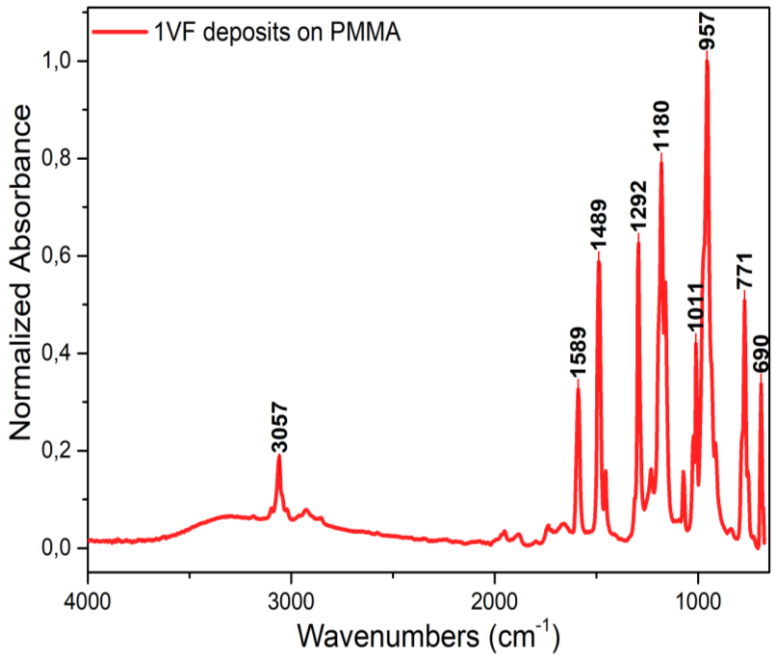

Wavenumber (cm^{-1})	Assignment
3057	ν C-H
1589	ν C=C
1489	ν C=C
1292	ν P=O
1180	δ C-H
1011	ν P-O
957	ν P-O
771	δ C-H
690	δ C-H

Figure 7:on the left FTIR spectrum of the adhesive, on the right tables with IR absorptions

Triphenyl phosphate (TPhP) is produced reacting a phenol with phosphorus oxychloride [4],[5]. As other plasticizers, TPhP, once added to a polymer, acts reducing the glass transition temperature and increasing flexibility of the final product (reducing hardness and tensile strength). The flame-retardant action is carried out during the combustion first giving phosphoric acid. Successively, phosphoric acid spontaneously forms pyrophosphoric acid which acts to block heat transfer [6], [7]. While one of the first use of TPhP was as plasticizer and flame retardant for cellulose acetate safety films, currently, its main applications are in cable and wire insulation, vinyl foams and automotive interiors [8].

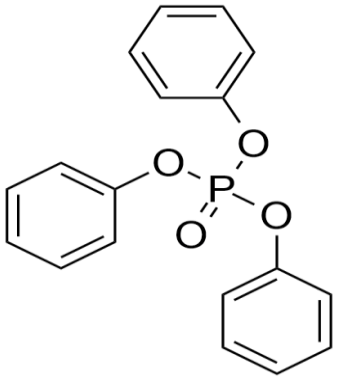

Figure 8: chemical structure of triphenyl phosphate

13.4. Red paint characterization: sample 2VF

The red painted portion, clearly visible in Figure 3 appeared to be realized using a fluorescent paint, with a deep and vibrant purplish red shade.

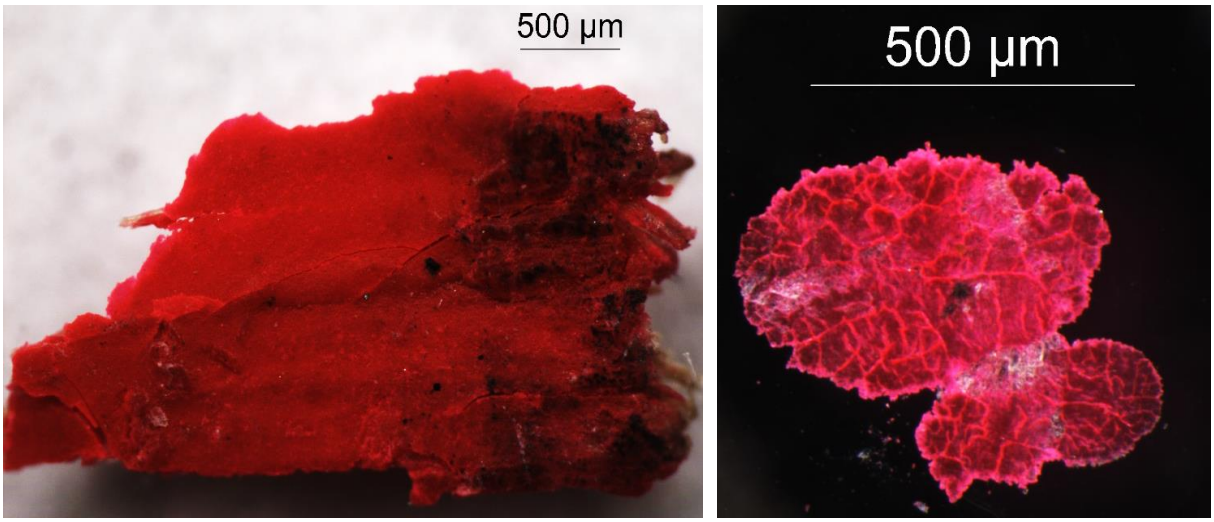

Figure 9: sample or the red paint from the artwork, on the right sample on the diamond cell

FTIR spectrum appeared to be extremely complex, as result of different contributions. In general, fluorescent paints often are characterized by complex formulations due to the necessity of adding numerous additives and stabilizers to the final product. In fact, fluorescent dyes often exhibit poor fade resistance in comparison with regular pigments [9]. The spectrum in Figure 11 contains contributions from a melamine formaldehyde sulfonamide (the latter being *ortho* or *para* toluene sulfonamide) resin, plausibly mixed with an alkyd resin to improve flexibility. Copolymers of toluene sulfonamide and melamine formaldehyde are often used as carrier in the production of fluorescent dyes [10] and the presence of sulfonamides may explain the significative signal of sulfur detected through portable XRF. Typical of the toluene sulfonamide component are the absorptions at 1331 cm^{-1} (combination of C-H bending of melamine formaldehyde and S=O stretching), 1151 cm^{-1} (S=O stretching) and the C-H aromatic bending at 761 cm^{-1} [11].

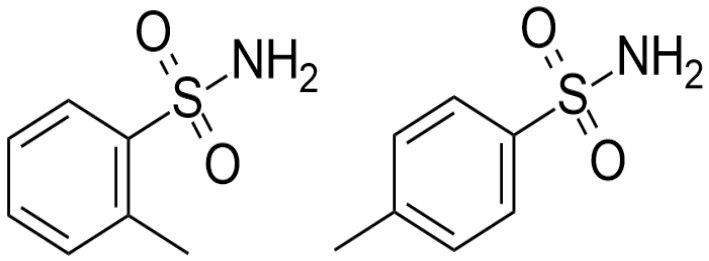

Figure 10: ortho and para toluene sulfonamide

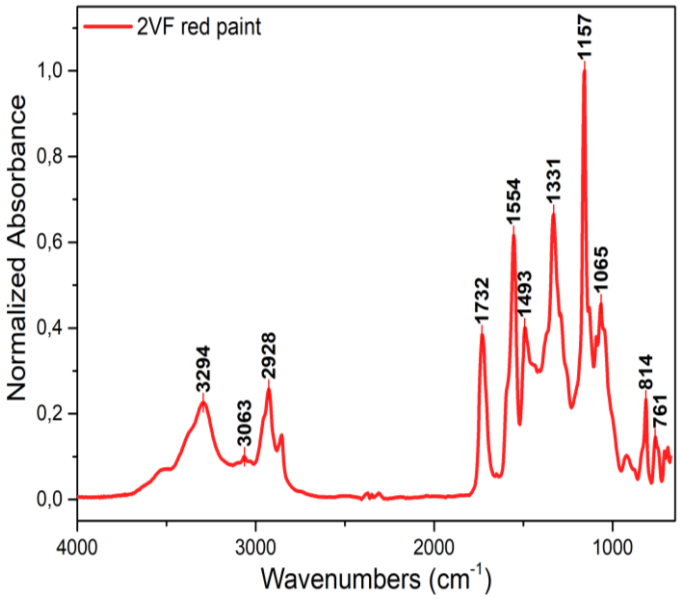

Wavenumber (cm^{-1})	Assignment
3294	ν N-H melamine
3063	ν C-H aromatic alkyd
2928	ν C-H (CH_2) alkyd
1732	ν C=O alkyd
1554	ν C=N melamine
1493	δ C-H melamine
1331	δ C-H + ν S=O sulfonamide
1157	ν S=O sulfonamide
1065	ν C-O-C alkyd ester
814	triazine skeletal
761	δ C-H aromatic

Figure 11: on the left FTIR spectrum of the red paint, on the right tables with IR absorptions

13.5. Silver adhesive sheet characterization: sample 3VF

As said before, Angelo Ientile confirmed the use of a self-adhesive silver sheet on the wooden panel (sample in Figure 12). Both optical microscopy observation and FTIR analysis confirmed the presence of a plastic polymer (namely polyethylene terephthalate, Figure 13) covering what appeared to be a thin foil of aluminum. The whole sheet was attached to the wooden support using an acrylic adhesive.

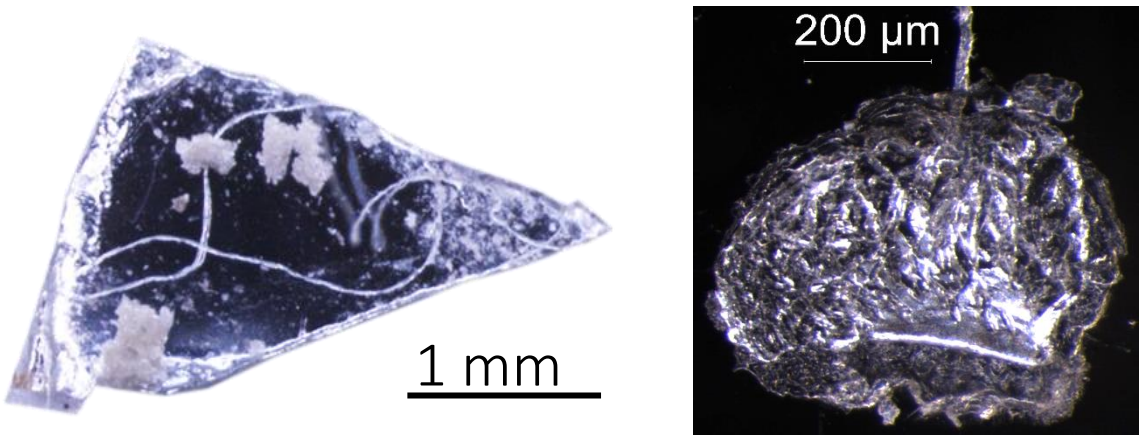

Figure 12: sample or the silver adhesive sheet from the artwork, on the right sample on the diamond cell

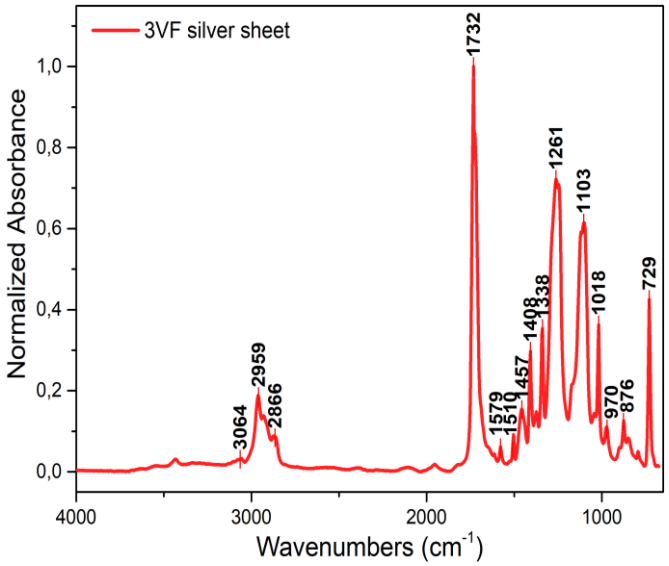

Wavenumber (cm^{-1})	Assignment
3064	ν C-H aromatic
2959	ν C-H (CH_2)
2866	ν C-H (CH_2)
1732	ν C=O
1579	δ C=C aromatic
1510	δ C=C aromatic
1457	ν C-O + ω C-H (CH_2)
1408	ν C-O + ω C-H (CH_2)
1338	ν C-O + ω C-H (CH_2)
1261	ν C-O-C
1103	ν C-O-C
1018	δ C-H aromatic
970	δ C-H aromatic + δ C-O-C
876	δ C-H aromatic
729	δ C-H aromatic

Figure 13:on the left FTIR spectrum of the silver sheet covering polymer, on the right tables with IR absorptions

In particular, FTIR results (Figure 14) suggest the acrylic used may be poly(2-ethylexyl acrylate), often applied alone or in blend with other acrylics in the production of pressure sensitive adhesives (PSAs), polymeric materials which can adhere to solid surfaces under light pressure for short amount of time [12].

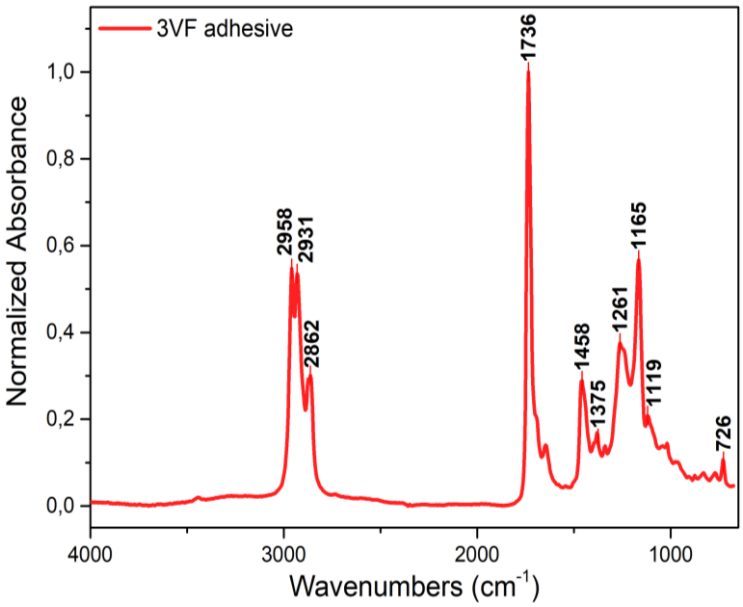

Wavenumber (cm^{-1})	Assignment
2958	ν C-H (CH_3)
2931	ν C-H (CH_2)
2862	ν C-H (CH_3)
1736	ν C=O
1458	δ C-H (CH_2)
1375	δ C-H (CH_3)
1261	ν C-C-O
1165	ν C-O-C
1119	ν C-O-C
726	δ C-H

Figure 14: on the left FTIR spectrum of the adhesive of the silver sheet, on the right tables with IR absorptions

SEM-EDS analysis did not detect any element which may be responsible of the silver color, other than aluminum, allowing to validate the hypothesis that a thin foil of aluminum was used to obtain the mirrored finish (as visible Figure 15).

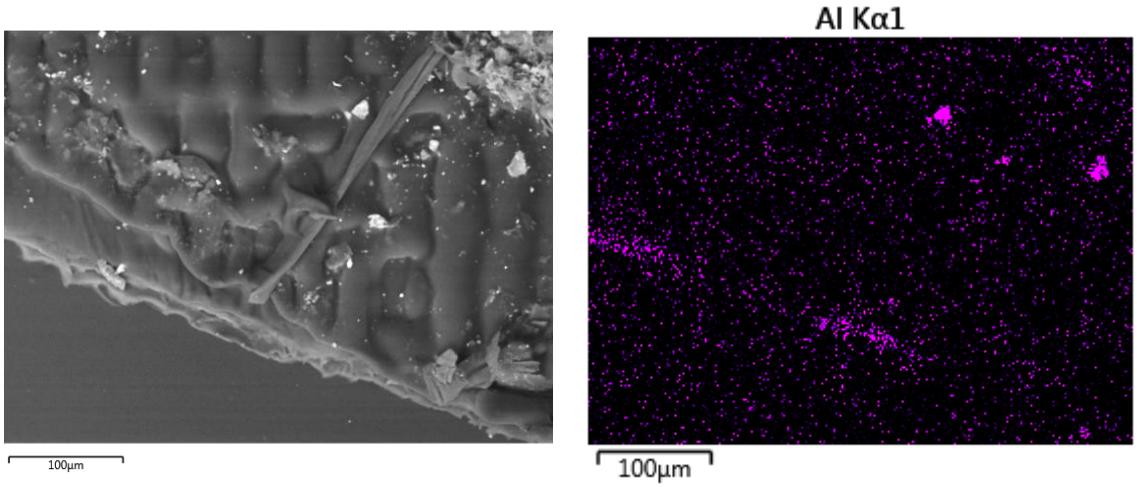

Figure 15: on the left SEM BDS image of the silver adhesive sheet, on the right EDS Map of aluminum

13.6. Photographic films characterization: sample 4VF

Differently from *Nel deserto*, *Vortice e figura* is composed by two photographic films (called, according to the pattern on each or them, "net" and "sand", as showed in Figure 17) placed by the artist one on top of the other. When the conservators opened the case to start working on the artwork, a strong smell of acetic acid came from it, and the photographic films appeared immediately severely damaged. In fact, as visible in Figure 16, the superior sheet ("net") was missing some parts and both the films were seriously deformed.

Figure 16: photographic films on Vortice e Figura showing degradation signs

Figure 17: the two photographic films, on the left "net" and on the right "sand"

Observation through optical microscopy clarified how the stratigraphy of the photographic films was completely comparable to the one used in *Nel Deserto*, exhibiting a base and at least two different layers of gelatin (one on top and one on the bottom of the base).

FTIR analysis revealed the base is made of cellulose acetate, plasticized with triphenyl phosphate (as already detected analyzing the deposits on the PMMA sheet), covered with animal gelatin.

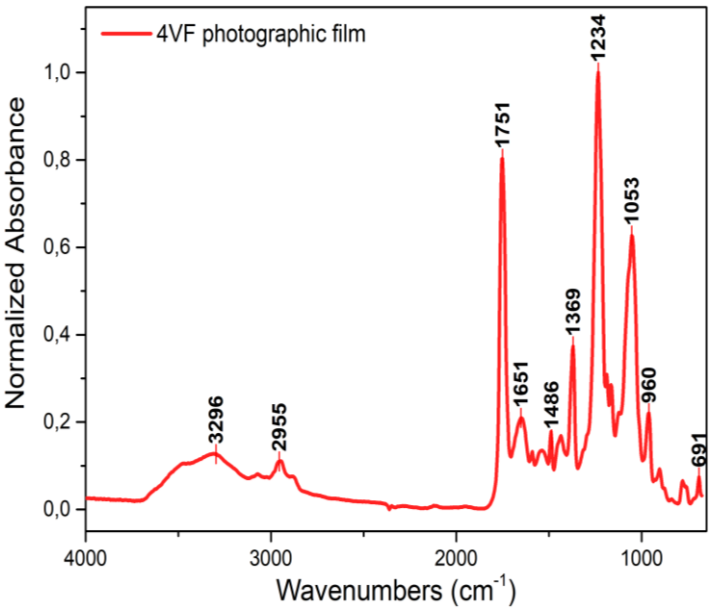

Wavenumber (cm^{-1})	Assignment
3296	ν O-H cellulose acetate
2955	ν C-H (CH_2)
1751	ν C=O cellulose acetate
1651	ν C=O gelatin
1486	δ C-H TPhP
1369	δ C-H
1234	ν C-O-C cellulose acetate
1053	ν C-O-C pyranose ring CA
960	ν P-O TPhP
691	δ C-H TPhP

Figure 18:on the left FTIR spectrum of the base of the photographic film, on the right tables with IR absorptions

Diagnostic of cellulose acetate are the strong ester absorptions, with the carbonyl at 1751 cm^{-1} and C-O-C at 1234 cm^{-1}, while the methyl group on the acetate absorbs at 1369 cm^{-1}.

The impressed gelatin layer was then selectively sampled from the photographic film and analyzed separately. Infrared spectroscopy confirmed the use of animal gelatin with presence of triphenyl phosphate, migrated from the base (Figure 19).

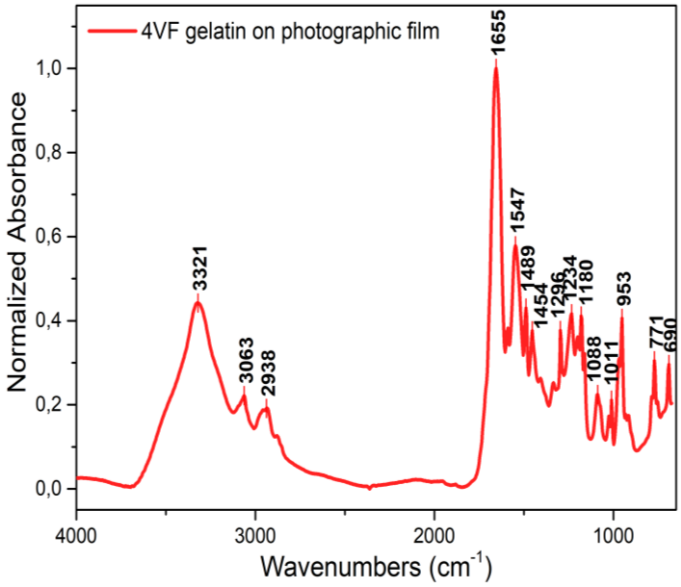

Wavenumber (cm^{-1})	Assignment
3321	ν N-H (gelatin)
3069	ν N-H (gelatin) + ν C-H (TPhP)
2938	ν C-H (CH_2)
1655	ν C=O (gelatin)
1547	δ N-H (gelatin)
1489	ν C=C (TPhP)
1454	δ C-H (CH_2) (gelatin)
1296	ν C-O (gelatin)
1234	ν P=O
1180	δ C-H
1088	δ C-H
953	ν P-O
771	δ C-H
690	δ C-H

Figure 19:on the left FTIR spectrum of the gelatin on the photographic film support, on the right tables with IR absorptions

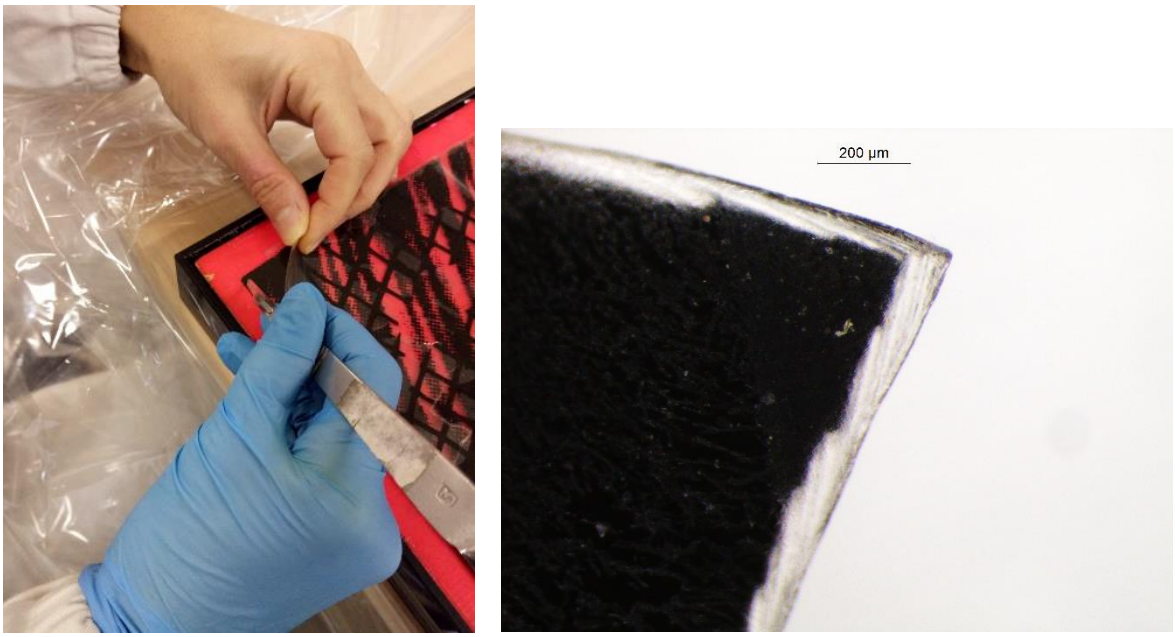

Figure 20: sampling of a portion of the photographic film, on the right a detail of the sample showing the black impressed side

One fragment of photographic film was embedded in resin to prepare a cross section, which was first observed through optical microscopy (under visible and UV light) revealing (Figure 21) an intense fluorescence of the gelatin layer, while the base (differently from the PET one from *Nel Deserto*) did not appear fluorescent.

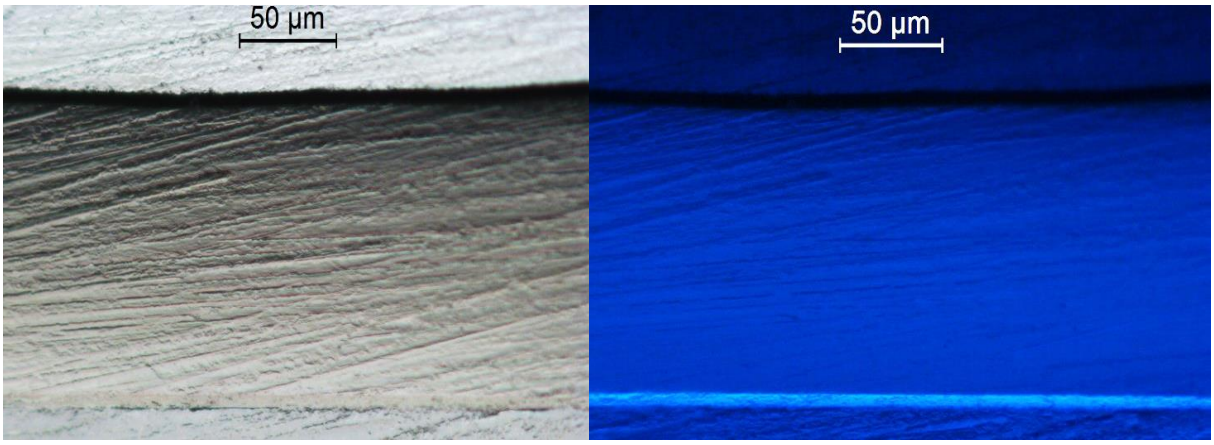

Figure 21: cross section of the photographic film, on the left in OM, on the right under UV light

SEM analysis allowed to define the thickness of the different layers: the base appears to be approximately 130 µm while both inferior and superior layers are 6-7 µm thick.

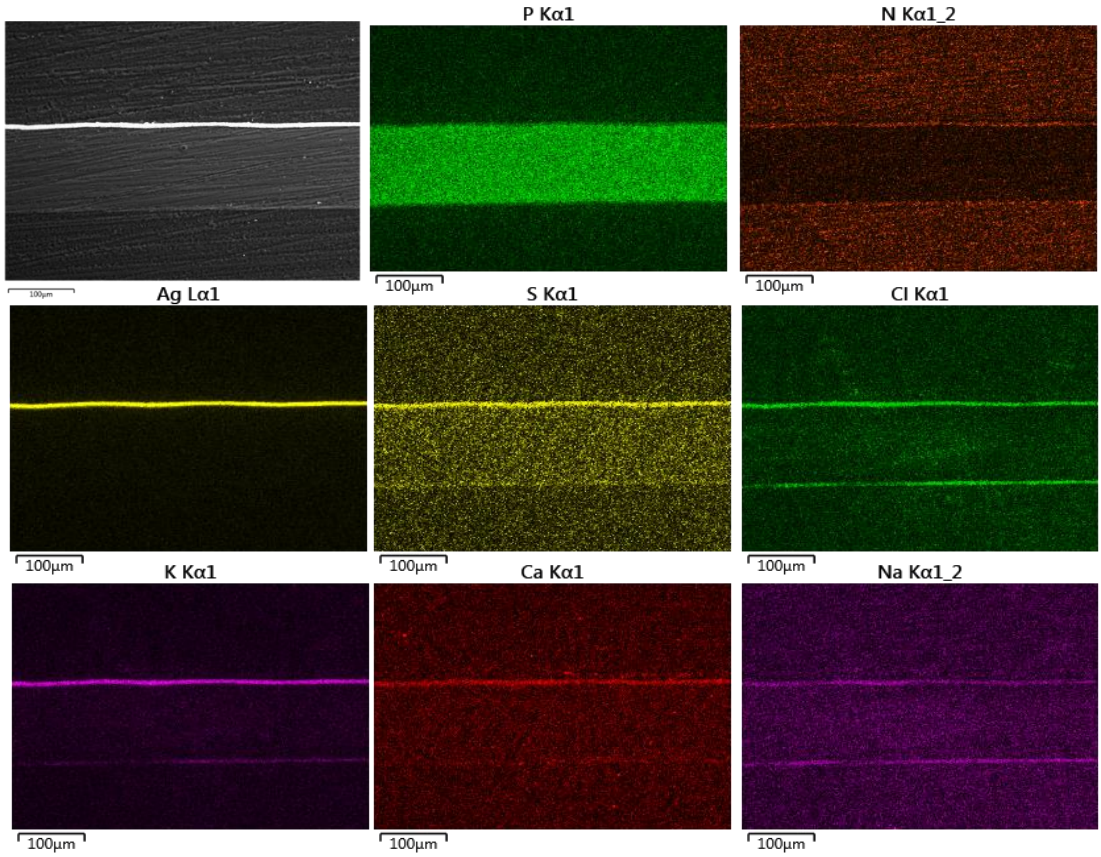

Figure 22: On the left top corner SEM BSD image of a portion of the photographic film cross section, the others are EDS maps of elements on the same area

EDS mapping (Figure 22) showed diffuse presence of phosphorus in the base (due to triphenyl phosphate), nitrogen on the gelatin layers, silver on the emulsion. Presence of sodium and

chlorine on both gelatin layers may be due to the use of sodium chloride baths during the production/development of photographic films.

13.7. Degradation phenomena

The most important degradation signs found on the artwork were surely related to the photographic films condition. Figure 23 shows a simplified scheme of the stratigraphy of the artwork. The superior photographic film ("net") was placed with the emulsion (black in the scheme) layer in contact with the back side of "sand". The hygroscopicity of the gelatin layers, in conjunction with severe degradation phenomena of the cellulose acetate base, caused the attachment of the photographic films together making it almost impossible to separate them.

Figure 23: simplified scheme of the artwork

As briefly explained in Chapter 11, the vinegar syndrome shows very peculiar and evident signs, such as the strong smell of acetic acid coming from the polymer; obviously, the stronger the smell is, the worse the degradation of the material is. In fact, hydrolysis of cellulose acetate evolves progressively from a first stage characterized by the yellowing of the polymer, followed by its shrinking which may cause the detachment of the gelatin layer (phenomenon known as "channeling") [13]. Deacetylation may also have a negative effect on the plasticizers added to the polymer, causing its migration and hence loss of flexibility of the photographic film [13]. Vinegar syndrome can easily lead to dramatic and completely irreversible consequences and nowadays the common conservation practices advice to store cellulose acetate films at low temperatures and relative humidity and almost in absence of light (anyway not above 50 lux and filtering the UV ray) [14].

13.8. Conclusions

Vortice e Figura, in spite of the many similarities shared with *Nel Deserto*, is realized with completely different materials, which are responsible for the dramatic conservative conditions of the artwork. The support panel is realized in plywood, material highly permeable to water vapor, hence exposed to thermo-hygrometric variations and consequences related to them.

Such support is painted in two colors: a fluorescent red and a matte black, this last is covered by a self-adhesive silver plastic film. Portable XRF on the red paint showed presence of sulfur and FTIR analysis suggested the use of a fluorescent paint made of melamine formaldehyde sulfonamide and alkyd resin. The silver film was characterized as formed by two layers of polyethylene terephthalate enclosing a thin film of aluminum (detected by SEM-EDS). The adhesive used to attach the film to the support is an acrylic (plausibly poly(2-ethylexyl acrylate)).

Another difference in comparison with *Nel Deserto* is the use, in *Vortice e Figura*, of two overlapped photographic films. At the opening of the frame, a strong smell of vinegar came from it, and both the photographic films appeared extremely warped and deformed, as well as strongly attached one to the other.

XRF analysis on them showed presence of silver (on the black impressed parts) and phosphorous; this last was also found on the PMMA sheet used to seal the frame, which was also showing numerous circular white deposits. A small amount of this white substance was sampled and analyzed via FTIR, revealing the presence of triphenyl phosphate, a common plasticizer and flame retardant added to plastics. The base of both photographic films was characterized as cellulose acetate, which is a particularly fragile material, as, when exposed to oxygen and humidity, spontaneously undergoes hydrolysis loosing acetic acid, in an autocatalytic process.

This degradation pathway is called *vinegar syndrome* and causes dramatic consequences as its effects are irreversible and the autocatalytic hydrolysis can be slowed down only dramatically lowering temperature and relative humidity. Often, artworks realized in cellulose acetate have to be removed from museums to be conserved in particular environments, hence depriving the public of their fruition. The analytical results presented in this and in the previous chapter provided fundamental information to the conservator, who had to deal with such unique pieces, often facing particularly hard conservative situations.

References

[1] G. Buxbaum and G. Pfaff, *Industrial Inorganic Pigments: Third Edition*. 2005.

[2] G. Wypych, *Handbook of plasticizers*. ChemTec Pub., 2004.

[3] M. K. Trivedi, A. Branton, D. Trivedi, G. Nayak, K. Bairwa, and S. Jana, "Physicochemical and Spectroscopic Characterization of Biofield Treated Triphenyl Phosphate," Oct. 2015.

[4] R. D. Ashford, *Ashford's dictionary of industrial chemicals : properties, production, uses*. Wavelength, 1994.

[5] WHO, "Environmental Health Criteria 111: Triphenyl phosphate," p. 79, 1991.

[6] I. van der Veen and J. de Boer, "Phosphorus flame retardants: Properties, production, environmental occurrence, toxicity and analysis," *Chemosphere*, vol. 88, no. 10, pp. 1119–1153, Aug. 2012.

[7] H. M. Stapleton *et al.*, "Detection of Organophosphate Flame Retardants in Furniture Foam and U.S. House Dust," *Environ. Sci. Technol.*, vol. 43, no. 19, pp. 7490–7495, Oct. 2009.

[8] D. Brooke, M. Crookes, P. Quarterman, and J. Burns, "Environmental risk evaluation report: Triphenyl phosphate (CAS No. 115-86-6)," no. 115, pp. 1–140, 2009.

[9] P. (Peter) Bamfield and M. G. Hutchings, *Chromic phenomena : technological applications of colour chemistry*. Royal Society of Chemistry, 2010.

[10] W. Fremout, "Characterization of daylight fluorescent pigments in contemporary artists' paints by Raman spectroscopy Investigation," in *11th Infrared and Raman Users Group Conference 5-7 November 2014 Museum of Fine Arts, Bos-ton*, 2014, pp. 39–45.

[11] T.-M. Yang, C.-S. Su, J.-S. Li, K.-T. Lu, and T.-F. Yeh, "Recrystallization and Micronization of p-Toluenesulfonamide Using the Rapid Expansion of Supercritical Solution (RESS) Process," *Crystals*, vol. 9, no. 9, p. 449, Aug. 2019.

[12] S. H. Park, T. H. Lee, Y. Il Park, S. M. Noh, and J. C. Kim, "Effect of the n-butyl acrylate/2-ethylhexyl acrylate weight ratio on the performances of waterborne core–shell PSAs," *J. Ind. Eng. Chem.*, vol. 53, pp. 111–118, 2017.

[13] B.Cattaneo, *Il restauro della fotografia: Materiali fotografici e cinematografici, analogici e digitali*. 2017.

[14] F. Waentig, *Plastics in art : a study from the conservation point of view*. Imhof, 2008.

Chapter 14. Conclusions

This research aimed to study the degradation behaviors of different plastic materials associated together in contemporary artworks, using some common spectroscopic techniques such as FTIR, Raman and XRF, in conjunction with SEM-EDS and thermal analyses like DSC and TGA.

Several factors made this research particularly hard: the extreme variability in structure, formulation and chemical nature typical of synthetic polymers is one of them. Moreover, artists are usually not aware of the composition of the materials they use, which complicates the study of contemporary artworks. Plastics are usually seen as eternals, but in reality, they degrade usually very fast, changing color, consistence and loosing resistance often with dramatical consequences. Since plastics are relatively modern materials it is particularly uneasy to find samples old enough to be considered "aged". Different artificial ageing methodologies are nowadays applied to simulate the natural weathering of materials, but often these methods fail to fully represent the wide spectra of degradation processes. In this context, the study of contemporary artworks dated from the end of the 60s to the end of the 90s, offered the priceless possibility to take a real look into real life "senior" plastics.

Additionally, many polymers age suffering chemical modifications that are so severe that modify dramatically their chemical structure, making it almost impossible to recognize them. A glaring example may be the painted layers of *La Grotta* and *Scoglio Sonoro Interattivo* (Chapter 6). In fact, the artist chose to use natural latex, plausibly thanks to its great flexibility and smooth finish, ignoring (or not fully realizing) how this material is intrinsically fragile and prone to undergo auto-oxidation. Only a few decades after the realization of the artwork, the original material had lost almost completely some of its original physical properties, becoming brittle and rigid. Such marked changes have hardly been seen in traditional art materials such as stone, metals or even canvas.

Considering all these aspects, the correct characterization of the materials is absolutely fundamental to help planning the best conservative intervention possible. In this context, the analytical results on *Teca con Frutta* (Chapter 4) were particularly helpful as they made it possible to identify the materials used as low density polyethylene covered by a spray paint containing nitrocellulose and an alkyd resin. Infrared spectroscopy also highlighted oxidation phenomena and unveiled the presence of a biological attack which was responsible for the severe external alteration of the artwork. All these evidences helped the conservator to plan their intervention, which, as visible in Figure 1, was particularly significative.

Figure 1: "Teca con Frutta" before (on the left) and after (on the right) the restoration. Thanks to Alessia Sturari

Contemporary artworks are usually extremely complex, according to the original design of the artist and the more or less wide variety of materials they combine together. Each of them represents a unique piece and has to be taken care of following specific guidelines which vary every time. In fact, differently from the traditional art, which has been studied extensively and which conservative modalities have been encoded successfully, the peculiar variability observable in modern and contemporary art requires special cares and sensitivities which are impossible to generalize. The conservator has to consider several factors before planning the restoration of contemporary art, according to the specific necessities of each artwork.

In this context, it was particularly interesting to study *Supercomponibile '67* (Chapter 9) as high pressure laminates are not what we usually define a "traditional" art material. Indeed, it offered the possibility to investigate such materials, and to compare them with a modern laminate, studying its artificial ageing behavior with a traditional polymer science approach.

Finally, the study of Paola Levi Montalcini's works, namely *Nel Deserto* and *Vortice e Figura* (Chapter 12 and 13) represented an incredible opportunity to observe how plastic materials behave when juxtaposed and how, in ageing, they influence each other. A particularly significative example is how the PVC transparent film in *Nel Deserto* lost hydrochloric acid and reacted with the copper of the bronze painting, altering irreparably the original color chosen by the artist. The dramatic consequences of the relentless ageing of plastics may be clearly seen on the photographic films in *Vortice e Figura*. In fact, the signs of vinegar syndrome on the cellulose acetate-based films were so severe

that the conservators suggested making a copy of the artwork as the original was no longer in condition to be exposed.

This research was possible only thanks to the collaboration between different institutions[1], which allowed to study some inestimable artworks, working side by side with restorers and chemists in a really productive and multidisciplinary teamwork, while following all the phases of the restoration interventions.

Concluding, only a deep knowledge of modern materials, in particularly synthetic and semi-synthetic polymers, can guide us to comprehend how to preserve and restore the essential heritage of contemporary art.

[1] The *Istituto Superiore per la Conservazione ed il Restauro* di Roma (ISCR) (RM, Italy), the *Scuola di restauro ENAIP of Botticino* (BR, Italy), the *MAMbo - Museo d'Arte Moderna di Bologna* (BO, Italy) and the *MAGA – Museo di Arte di Gallarate* (VA, Italy), the CiQUS-Center for Research in Biological Chemistry and Molecular Materials of Santiago de Compostela.